



**Proceedings  
of the  
4<sup>th</sup> International Workshop  
on  
Polarized Target Materials and Techniques**

**Proceedings  
of the  
4<sup>th</sup> International Workshop  
on  
Polarized Target Materials and Techniques**

*Editor:* W. Meyer

Sponsored by:  
The International Advisory Committee for Symposia on  
High Energy Spin Physics  
TRIUMF  
The Bundesministerium für Forschung und Technologie

Bad Honnef  
Federal Republic of Germany  
September 3-6, 1984

Published  
by  
Physikalisches Institut  
Universität Bonn  
Nussallee 12  
5300 Bonn 1  
F.R. Germany

Printed by  
Druck- und Werbegesellschaft GmbH  
von-Weichs-Straße 23  
5300 Bonn 1  
F.R. Germany

## PREFACE

The fourth International Workshop on Polarized Target Materials and Techniques was held in Bad Honnef in September 1984, with the Physikalisches Institut der Universität Bonn as the host.

This series of workshops was started at the Argonne Laboratory in 1978, with the aim to discuss new concepts which can improve the experimental situation of polarized targets in high or intermediate energy physics experiments. In many cases serious experimental difficulties arise from the target materials, in particular from their relatively low content of polarizable nucleons and their polarization resistance due to radiation damage. Decisive for further developments in this field was the discovery of high polarization in materials prepared for the dynamic nuclear polarization (DNP) process by irradiation (2<sup>nd</sup> Workshop-Abingdon 1979). Since that time most of the activities have been concentrated on polarizing irradiated ammonia as well as chemically doped hydrogen-rich glasses. The first detailed results were presented and discussed at the 3<sup>rd</sup> Workshop (Brookhaven 1982). In the meantime the studies were completed, and irradiated NH<sub>3</sub> and ND<sub>3</sub> were used in high and intermediate energy physics experiments.

In addition, the development of dilution refrigerators with high cooling power, and the development of frozen spin techniques were important. The highest polarization values can be obtained using dilution refrigerators. For this reason they have become more and more the standard equipment of a polarized target system. The present status of polarized deuteron targets allows us to consider experiments with tensor polarized deuteron targets. Progress has also been made for the cleanest target material - atomic hydrogen.

Thus the presentations and discussions on the 4<sup>th</sup> Workshop were focussed on the following topics:

1. Irradiated materials
  - Use in high and intermediate energy physics experiments
  - Radiation resistance studies
  - DNP in irradiated materials

- II. Chemically doped hydrogen-rich materials
- III. Technical developments
  - Irradiation techniques
  - Improvement in cryogenics
  - Frozen spin technology
  - NMR-technology
- IV. Tensor polarization
- V. Atomic hydrogen.

At this Workshop many very interesting and important recent results were presented and reviewed. Thus we hope these proceedings will be valuable to many researchers in the field.

The organizing committee would like to thank the speakers for their stimulating talks, the chairmen for their cooperation and the members of the Bonn Polarized Target Group for their enthusiastic help in preparing and running the Workshop.

The Physikzentrum Bad Honnef provided an ideal venue for the Workshop in pleasant surroundings. We would like to thank all participants, guests and, last but not least, the staff of the Physikzentrum for helping us to create the lively and stimulating atmosphere of a successful workshop.

W. Meyer

## WORKSHOP ORGANIZATION

### ORGANIZING COMMITTEE

K.H. Althoff	(Bonn)	W. Meyer	(Bonn)
		- Chairman -	
G.R. Court	(Liverpool)	T.O. Niinikoski	(CERN)
O. Kaul	(Bonn)	L. Van Rossum	(Saclay)
S. Mango	(SIN)		

### INTERNATIONAL ADVISORY COMMITTEE

A.D. Krisch	(Michigan)	M. Jacob	(CERN)
- Chairman -			
A. Abragam	(Coll.de France)	A. Masaike	(KEK)
O. Chamberlain	(Berkeley)	A.N. Skrinsky	(Novosibirsk)
E.D. Courant	(Brookhaven)	L.D. Soloviev	(Serpukhov)
G.R. Court	(Liverpool)	J. Thirion	(Saturne)
G. Fidecaro	(CERN)	G.A. Voss	(DESY)
V.W. Hughes	(Yale)	C.N. Yang	(Stony Brook)

### SPONSORS

International Advisory Committee for Symposia on  
High Energy Spin Physics

TRIUMF

Bundesministerium für Forschung und Technologie

## CONTENTS

Title	Presented by	Page
PREFACE		
<u>DYNAMIC NUCLEAR POLARIZATION</u>		
On the extension of Provotorov's theory to low spin-temperatures	W.Th. Wenckebach	1
<u>IRRADIATED MATERIALS</u>		
Operational characteristics of radiation doped ammonia in a high intensity proton beam	D.G. Crabb	7
First use of ND <sub>3</sub> in a high energy photon beam	E. Schilling	13
Radiation resistances of ammonia at 1 Kelvin and 2.5 Tesla	U. Hartfiel	23
Dynamic nuclear polarization studies in irradiated ammonia at 1 K	W. Meyer	33
The dynamic polarisation of the nitrogen nuclei in <sup>14</sup> NH <sub>3</sub> , <sup>15</sup> NH <sub>3</sub> and <sup>14</sup> ND <sub>3</sub>	W.G. Heyes	53
An investigation of dynamic polarisation in irradiated borane-ammonia and ammonium borohydride	W.G. Heyes	60

## CONTENTS

Title	Presented by	Page
<u>IRRADIATION TECHNIQUES</u>		
The production of large quantities of irradiated ammonia for use as a polarised target material	S. Brown	66
Preparation and irradiation of ammonia target beads	P.R. Cameron	79
Attempt to polarize a large sample of <sup>7</sup> LiH irradiated with high energy electrons	G. Durand	81
<u>CHEMICALLY DOPED MATERIALS</u>		
Polarization in chemically doped hydrogen-rich glasses	D. Hill	84
Stability of chromium (V) doped target materials containing borane-ammonia and amines	M. Krumpolc	94
Radiation damage in an ethylamine-borane: ammonia target	D.G. Crabb	100

## CONTENTS

Title	Presented by	Page
<u>TARGET AND FROZEN SPIN TECHNOLOGY</u>		
The EMC polarized target	G.R. Court	102
Improvements of the polarized target for nucleon nucleon experiments at Saturne II	J. Ball	112
A vertical dilution refrigerator for the LAMPF polarized target	J.J. Jarmer	119
The Liverpool polarised target material test facility	G.R. Court	122
A brute-force polarised proton target	W. Heeringa	129
<u>IMPROVEMENTS IN CRYOGENICS</u>		
A simple model of bead cooling	P.R. Cameron	136
Operation of a polarized proton target in an intense beam: cooling the beads	P.R. Cameron	143
First experience with a $^3\text{He}/^4\text{He}$ mixture in a $^3\text{He}$ -refrigerator in high intensity electron beams	T. Hewel	149
<u>NMR-TECHNOLOGY</u>		
Microprocessorized NMR measurement	A. Rijllart	155
Hydrogen NMR signal associated with silver	J.J. Jarmer	163

## CONTENTS

Title	Presented by	Page
<u>TENSOR POLARIZATION</u>		
Tensor polarized deuteron targets for intermediate energy physics experiments	W. Meyer	165
<u>HIGH ENERGY PHYSICS EXPERIMENTS</u>		
Polarized proton physics at the AGS	A.D. Krisch	174
The experiments at KEK with polarized beam and polarized target	N. Horikawa	177
Plan for a polarized target for the Fermilab polarized beam	D. Hill	182
<u>ATOMIC HYDROGEN</u>		
Stable atomic hydrogen: polarized atomic beam source	T.O. Niinikoski	183
Polarized atomic beams for targets	W. Gruebler	193
Plans and progress toward an ultra-cold polarized proton jet	R.S. Raymond	202
AUTHOR INDEX		206
LIST OF PARTICIPANTS		208
ACKNOWLEDGMENTS		209

## 2. Historical remarks

Redfield made the first step in what is now called the Provotorov theory of magnetic resonance saturation and relaxation /15/. He proposed that if a saturating rf-field is applied on a spin system, the resulting stationary state can be described by a single spin temperature, but in a frame of reference rotating with the frequency of the rf-field. This idea should be valid at all temperatures, not only the high temperature approximation, so any theory describing the evolution of a spin system under the influence of an rf-field should have stationary solutions of the type proposed by Redfield.

Provotorov /11/ made the bolder assumption, that a spin system should be described by two parameters instead of one single spin temperature: one for the Zeeman interaction and one for the spin-spin interactions. This allowed him to describe the development of the spin system from the moment the rf-field is switched on to the stationary state described by Redfield. Unfortunately, his theory is valid in the high temperature approximation only. Provotorov also applied this theory to the case of cross-relaxation and spin-lattice relaxation /16/. Finally he was the first to introduce the idea of EST for DNP /17/. After him many other groups have worked on the idea of EST. Some very convincing experiments providing the existence of EST are given e.g. in refs. /18/ and /19/.

A useful treatment of Borghini made it possible to describe DNP via EST for the case of general temperatures, if an inhomogeneously broadened ESR-line is assumed /20/. This treatment was extended by Abragam and Goldman to ESR-lines broadened by hyperfine interactions /10/. However, without an extension to general temperatures of Provotorov's theory of magnetic resonance saturation and relaxation, these treatments remain without a satisfactory theoretic-basis.

Kochelaev and Nigmatullin /21/ gave such an extension using the non-equilibrium statistical operator of Zubarev. De Haas et al. /12,13,14/ extended their work and gave their results a rigorous basis by using the Mori-Zwanzig formalism and linear response methods.

## 3. The concept of spin temperature

The basic problem of an extension of Provotorov's theory to general temperatures is due to the fact, that one needs to describe the spin system with two parameters instead of one. Following Provotorov one wishes to describe the spin system by means of the canonical density matrix

$$\sigma = \exp(-\alpha Z - \beta \mathcal{K}_{int}) \quad (1)$$

where  $Z$  is the Zeeman-interaction of the spins, and  $\mathcal{K}_{int}$  the spin-spin interaction, while  $\hbar/k\alpha$  is the so-called Zeeman-temperature and  $\hbar/k\beta$  the interaction temperature. This density matrix replaces the canonical density matrix that was used in pre-Provotorov times:

$$\sigma = \exp(-\beta_s (Z + \mathcal{K}_{int})) \quad (2)$$

where  $\hbar/k\beta_s$  is the spin temperature. In these equations is  $\hbar$  = Planck's constant,  $k$  = Boltzmann constant, while  $Z$  and  $\mathcal{K}_{int}$  are in units of angular frequency.

Instead of using the canonical ensemble to introduce spin-temperatures, one can also use the fluctuation-dissipation theory. This is most easily illustrated in the case of a spin system described by a single spin tempera-

ture, interacting via the direct process with a lattice, which is described by a single temperature also. In that case the energy transfer between the two systems is given by

$$\dot{E} = \int d\omega \{ X_S''(\omega) \Sigma_L(\omega) - X_L''(\omega) \Sigma_S(\omega) \} \quad (3)$$

where  $X_S''(\omega)$  and  $X_L''(\omega)$  are the absorption spectra of respectively the spin system and the lattice, and  $\Sigma_L(\omega)$  and  $\Sigma_S(\omega)$  their respective emission spectra. The fluctuation-dissipation theory gives a relation between the absorption and emission spectra. In the case of a single spin temperature and a single lattice temperature these relations are /22/:

$$\Sigma_S(\omega) = \frac{1}{e^{\beta_s \omega} - 1} X_S''(\omega) \quad (4a)$$

and

$$\Sigma_L(\omega) = \frac{1}{e^{\beta_l \omega} - 1} X_L''(\omega) \quad (4b)$$

where  $\hbar/k\beta_l$  is the lattice temperature. The fluctuation-dissipation theorems (4a) and (4b) can be used to define the spin temperature and the lattice temperature. On the other hand, equation (4a) can also be proven by means of linear response theory if one uses the canonical density matrix (2). Hence the definition of the spin temperature by means of the fluctuation-dissipation theory (4a) is consistent with the definition by means of the canonical ensemble.

In fact, finding the fluctuation-dissipation theories is the most difficult problem in working out an equation like (3). Once these are found, useful results can often be obtained in a straightforward manner. This can be illustrated if one inserts eqs.(4a) and (4b) in eq.(3). Then the energy transfer is given by:

$$\dot{E} = \int d\omega X_S''(\omega) X_L''(\omega) \left\{ \frac{1}{e^{\beta_l \omega} - 1} - \frac{1}{e^{\beta_s \omega} - 1} \right\} \quad (5)$$

In this equation  $X_S''(\omega)$  corresponds to the magnetic resonance line which is a narrow function around the Larmor frequency  $\omega_0$ . On the other hand the absorption spectrum  $X_L''(\omega)$  is a broad function, so we may approximate:

$$\dot{E} = X_L''(\omega_0) \left\{ \frac{1}{e^{\beta_l \omega_0} - 1} - \frac{1}{e^{\beta_s \omega_0} - 1} \right\} \int d\omega X_S''(\omega) \quad (6)$$

The energy absorption spectrum of the lattice is proportional to the density of lattice states multiplied by their energy, so:

$$X_L''(\omega_0) = A \omega_0^3 \quad (7a)$$

The integral of the energy absorption spectrum of the spins over the frequency yields equivalently /23/:

$$\int d\omega X_S''(\omega) = -BN \omega_0 P \quad (7b)$$

where  $P = \tanh(\frac{1}{2}\beta_s \omega_0)$  is the spin polarization and  $N$  the number of spins. Furthermore direct calculation yields:

$$\frac{1}{e^{\beta_l \omega_0} - 1} - \frac{1}{e^{\beta_s \omega_0} - 1} = 2 \left( \frac{1}{P} - \frac{1}{\bar{P}} \right)$$

where  $P_0 = \text{th}(\frac{1}{2}\beta_1\omega_0)$  is the thermal equilibrium value of the spin polarization. If one finally takes into account that the energy transfer  $\dot{E}$  is equal to change in spin energy  $N\omega_0 \dot{P}$ , eq.(6) yields the familiar result for the direct process:

$$\dot{P} = -\frac{1}{T_1} (P - P_0) \quad (8)$$

where:

$$\frac{1}{T_1} = 2AB\omega_0^3 \coth \frac{\beta_L \omega_0}{2} \quad (8a)$$

is the spin-lattice relaxation rate.

Thus we see that once the fluctuation-dissipation theorems (4a) and (4b) are obtained, the equations (8) and (8a) for the direct process follow straightforwardly. This indicates that the time evolution of a spin system described by two spin temperatures can also be obtained, once a fluctuation-dissipation theorem with two spin temperatures is formulated. As was indicated above, the two spin temperatures can be defined by formulating such a fluctuation-dissipation theorem. However, if such a definition is to make sense, one must also prove that the thus formulated fluctuation-dissipation theorem can be derived using the canonical density matrix (1) containing two spin temperatures.

De Haas et al. /12/ formulated a fluctuation-dissipation theorem containing a temperature  $\hbar/k\alpha$  for the Zeeman interactions and a temperature  $\hbar/k\beta$  for the spin-spin interactions:

$$\chi_S''(\omega) = \frac{1}{e^{\alpha\omega_0 + \beta(\omega - \omega_0)} - 1} X_S''(\omega) \quad (9)$$

Furthermore he proved by means of linear response theory that the thus defined spin temperatures are consistent with the spin temperatures defined in the usual way by the canonical ensemble (1). This allows one to write down equations shaped like eq.(5) for the energy transfer between a spin system and an rf-field (rf-saturation), between several spin systems, (cross-relaxation), and between a spin system and a lattice (spin-lattice relaxation). If one is able to work out these equations, one thus obtains the extension of the Provotorov equations to general temperatures.

#### 4. Spin-lattice relaxation

As an example, we will use the fluctuation-dissipation theorem (8) to derive the spin-lattice relaxation behaviour of the spin-spin interactions. In order to do so we insert eq.(9) and eq.(4b) in eq.(3):

$$\dot{E} = - \int d\omega X_S''(\omega) X_L''(\omega) \left( \frac{1}{e^{\alpha\omega_0 + \beta(\omega - \omega_0)} - 1} - \frac{1}{e^{\beta_L \omega} - 1} \right)$$

which can be rewritten as:

$$\begin{aligned} \dot{E} &= - \int d\omega X_S''(\omega) X_L''(\omega) \left( \frac{1}{\text{th}(\frac{1}{2}(\alpha\omega_0 + \beta(\omega - \omega_0)))} - \frac{1}{\text{th}(\frac{1}{2}(\beta_L \omega_0 + \beta_L(\omega - \omega_0)))} \right) \\ &= - \int d\omega X_S''(\omega) X_L''(\omega) \left( \frac{1 + P \text{th}(\frac{1}{2}\beta(\omega - \omega_0))}{P + \text{th}(\frac{1}{2}\beta(\omega - \omega_0))} - \frac{1 + P_0 \text{th}(\frac{1}{2}\beta_L(\omega - \omega_0))}{P_0 + \text{th}(\frac{1}{2}\beta_L(\omega - \omega_0))} \right) \end{aligned} \quad (10)$$

where  $P = \text{th}(\frac{1}{2}\alpha\omega_0)$  and  $P_0 = \text{th}(\frac{1}{2}\beta_L\omega_0)$ . Just as in the case of one single spin temperature, the absorption spectrum of the spins is a narrow function around the Larmor frequency  $\omega_0$ , while the absorption function of the lattice is a broad function. Hence we may expand  $X_L''(\omega)$  about  $\omega_0$ :

$$X_L''(\omega) = X_L''(\omega_0) + \left( \frac{\partial}{\partial \omega} X_L''(\omega) \right)_{\omega=\omega_0} (\omega - \omega_0) + \dots = A\omega_0^3 + 3A\omega_0^2(\omega - \omega_0) + \dots$$

where we used eq.(7a). Then:

$$\begin{aligned} \dot{E} &= -A\omega_0^3 \int d\omega X_S''(\omega) \left( \frac{1 + P \text{th}(\frac{1}{2}\beta(\omega - \omega_0))}{P + \text{th}(\frac{1}{2}\beta(\omega - \omega_0))} - \frac{1 + P_0 \text{th}(\frac{1}{2}\beta_2(\omega - \omega_0))}{P_0 + \text{th}(\frac{1}{2}\beta_2(\omega - \omega_0))} \right) - \\ &\quad - 3A\omega_0^2 \int d\omega X_A''(\omega) (\omega - \omega_0) \left( \frac{1 + P \text{th}(\frac{1}{2}\beta(\omega - \omega_0))}{P_0 + \text{th}(\frac{1}{2}\beta_2(\omega - \omega_0))} \right) - \dots \end{aligned}$$

The first term corresponds to relaxation of the Zeeman interactions. If we take the special case where the spin temperature corresponding to the spin-spin interactions is infinite, so  $\beta = 0$ , then this first term reduces to eq.(8). The second term corresponds to relaxation of the spin-spin interactions. In the special case of pure spin-spin interaction-lattice relaxation we may put  $P = P_0$  if we furthermore assume a high temperature approximation for the spin-spin interactions, so

$$\beta(\omega - \omega_0) \text{ and } \beta_L(\omega - \omega_0) \ll 1$$

we get after some calculations:

$$\dot{E} = -3A\omega_0^2 \left[ \int d\omega X_S''(\omega) (\omega - \omega_0)^2 \right] \frac{1}{P_0} \left( P_0 - \frac{1}{P_0} \frac{1}{2}(\beta - \beta_2) \right) \quad (11)$$

We define the reduced second moment of the absorption spectrum of the spins as:

$$M_2 = \int d\omega X_S''(\omega) (\omega - \omega_0)^2 / \int d\omega X_S''(\omega) \quad (12)$$

and use eq.(7b). Then

$$\begin{aligned} \dot{E} &= -\frac{3}{4} N A B \omega_0^3 \frac{1}{P_0} \cdot M_2 (1 - P_0^2) (\beta - \beta_2) \\ &= -\frac{3N}{4} \frac{1}{T_1} M_2 (1 - P_0^2) (\beta - \beta_2) \end{aligned} \quad (13)$$

where  $T_1$  is defined by eq.(8a). From this result the spin-lattice relaxation of the spin-spin interactions can be calculated.

A familiar case occurs if the above treated spins are  $N_e$  electron spins, and if the spin-spin interaction of these electron spins are coupled to a nuclear spin system of  $N_n$  spins with a Larmor frequency  $\omega_n$ . In the high temperature approximation one then has:

$$E = \frac{N_n}{4} \beta \omega_n^2$$

$$\text{so: } \dot{\beta} = -\frac{3}{T_1} \frac{N_e M_2}{N_n \omega_n^2} (1 - P_0^2) (\beta - \beta_2) \quad (14)$$

giving the nuclear spin-lattice relaxation rate.

## Acknowledgments

The present work is part of the research program of the Stichting Fundamenteel Onderzoek der materie, which is funded by the Stichting Zuiver Wetenschappelijk Onderzoek.

## References

- /1/ A. Abragam, C.R. Acad. Science., Paris 251 (1960), 225.
- /2/ J. Marks, W.Th. Wenckebach, N.J. Poulis, *Physica* 96B (1979), 337.
- /3/ J. Marks, J.C.M. Sprenkels, L.J. de Haas, W.Th. Wenckebach, *Physica* 109 & 110B (1982), 2155.
- /4/ J.C.M. Sprenkels, W.Th. Wenckebach, N.J. Poulis, *J. Phys. C: Solid State Physics* 15 (1982), L941.
- /5/ J.C.M. Sprenkels, W.Th. Wenckebach, N.J. Poulis, *J. Phys. C: Solid State Physics* 16 (1983), 4425.
- /6/ H.W. van Kesteren, W.Th. Wenckebach, J. Schmidt, N.J. Poulis, *Chem. Phys. Lett.* 89 (1982), 67.
- /7/ M. Deimling, H. Brunner, K.P. Dinse, K.H. Hauser, P. Colpa *J. Magn. Reson.* 39 (1980), 185.
- /8/ H. van Kesteren, W.Th. Wenckebach, J. Schmidt, N.J. Poulis, *Proc. XIIth Colloque AMPERE, Zürich 1984*, p. 275.
- /9/ W.Th. Wenckebach, T.J.B. Swanenburg, N.J. Poulis, *Phys. Reports* 14C (1974), 183.
- /10/ A. Abragam, M. Goldman, *Rep. Progr. Phys.* 41 (1978), 395.
- /11/ B.N. Provotorov, *J. Eksptl. Teor. Fiz.* 41 (1961), 1582; *Sov. Phys. JETP* 14 (1962), 1126.
- /12/ L.J. de Haas, W.Th. Wenckebach, N.J. Poulis, *Physica* 103A (1980), 295.
- /13/ L.J. de Haas, W.Th. Wenckebach, N.J. Poulis, *Physica* 111B (1981), 219.
- /14/ L.J. de Haas, C.M.B. van der Zon, W.Th. Wenckebach, N.J. Poulis, *Physica* 123B (1983), 35.
- /15/ A.G. Redfield, *Phys. Rev.* 98 (1955), 1787.
- /16/ B.N. Provotorov, *J. Eksptl. Teor. Fiz.* 42 (1962), 882; *Sov. Phys. JETP* 15 (1963), 611.
- /17/ M.A. Kozhushner, B.N. Provotorov, *Proc. Krasnoyarsk Conf.* 18-26 June 1964.
- /18/ V.A. Atsarkin, M.I. Rodak, *Fiz. Tverd. Tela* 11 (1969), 613; *Sov. Phys. Solid State* 11 (1969), 493.
- /19/ W.Th. Wenckebach, G.M. van den Heuvel, H. Hoogstrate, T.J.B. Swanenburg, N.J. Poulis, *Phys. Rev. Lett.* 22 (1969), 581.
- /20/ M. Borghini, *Phys. Rev. Lett.* 20 (1968), 419.
- /21/ B.I. Kochelaev, R.R. Nigmatullin, *Fiz. Tverd. Tela* 14 (1972), 3413; *Sov. Phys., Solid State* 14 (1973), 2880.
- /22/ R. Kubo, *J. Phys Soc. Japan* 12 (1957), 570.
- /23/ A. Abragam, M. Goldman, *Nuclear magnetism: order and disorder*, Clarendon Press, Oxford (1982), Chapter V.

## OPERATIONAL CHARACTERISTICS OF RADIATION DOPED AMMONIA IN A HIGH INTENSITY PROTON BEAM

D.G. Crabb, P.R. Cameron, A.M.T. Lin and R.S. Raymond

Harrison M. Randall Laboratory  
Physics Department  
University of Michigan  
Ann Arbor, Michigan 48109-1120 U.S.A.

## ABSTRACT

Several radiation doped ammonia targets have been used in a polarized target physics experiment using a 28 GeV/c high intensity proton beam ( $5 \times 10^{10}$  protons/pulse) at the AGS at Brookhaven National Laboratory. After initial radiation doping under liquid argon, using 70 MeV electrons, and subsequent in-cryostat irradiation at 0.5 K, with 28 GeV/c protons, polarizations of ~ 70% have been obtained. Other polarization properties of the ammonia targets, including radiation damage and annealing characteristics, are discussed.

## 1. Introduction

At the Brookhaven Workshop on Polarized Target Materials/1/ in 1982 we reported/2/, along with two other groups/3,4/ on the production of irradiated ammonia and its properties when used in a polarized target. Though there were conflicting data and unanswered questions there was a clear consensus that irradiated ammonia was close to becoming a standard polarized target material, particularly when used with high intensity beams. It is clear from the program at this workshop that indeed it has become a standard material.

In this report we will discuss the properties of irradiated ammonia when used as a target in high energy physics scattering experiments. We have studied radiation damage, annealing, polarization and other parameters during the course of the experiments with a view to minimizing the operational downtime. The experiments were carried out over the past two years on the AGS at Brookhaven National Laboratory in a 28 GeV/c proton beam.

## 2. Conditions

### a) NH<sub>3</sub> Fragment Preparation

The ammonia was "slowly" frozen in bulk and then crushed and sifted for the desired size/5/. In the later target samples there was much better control of the fragment size. The sizes used as targets ranged from 0.4 mm to 2.5 mm.

### b) Initial Irradiation

The selected fragments of frozen NH<sub>3</sub> were placed under liquid Argon (90 K) and irradiated by 70 MeV electrons obtained from the linac at the National Synchrotron Light Source at Brookhaven. The beam flux was

$\sim 2 \cdot 10^{15}$  e-/cm<sup>2</sup>/hour and a typical irradiation run lasted 24 hours.

### c) In Cryostat (In Situ) Irradiation

After loading, the ammonia was subjected to further irradiation during the physics experiment. Typically, the proton beam intensity was  $3-7 \times 10^{10}$  protons/pulse but during some periods was as high as  $1-2 \times 10^{11}$  protons/pulse. In this mode the AGS pulse has a duration of 1 sec every 2.5 sec. The beam spot was 1-1.5 cm diameter FWHM.

### d) Cryostat

We have continued to use our evaporation cryostat but using a <sup>3</sup>He/<sup>4</sup>He mixture rather than pure <sup>3</sup>He as the refrigerant. This has enabled us to obtain much better cooling of the target material/6/. <sup>3</sup>He/<sup>4</sup>He ratios in the range of 40:60 to 60:40 have been used with good results.

### e) NMR and Microwaves

The cavity configuration is shown in Fig. 1. Two NMR coils were used: the small coil is simply a thin wall tube along the axis of the cavity while the large coil consists of three turns of tubing on a 2 cm diameter. The 106.8 MHz rf was swept by  $\pm 250$  KHz and the signal detected by a series tuned Q meter and phase sensitive detector/7/.

The microwaves were provided by a 70 GHz carcinotron.

## 3. Results

### a) Polarization

Shown in Fig. 2 is a polarizing curve for a typical target. The main features are a relatively fast initial rise to  $\sim 40\%$  followed by a much slower rate of increase to 70%. The polarizing time  $T_{0.7}$  to 0.7 of the final value is longer than reported by Bonn/3/ due to a smaller number of polarizing centers. Our initial irradiation dose is considerably less than reported as typical by Bonn.

Fig. 3 shows the polarization after three stages of irradiation; the initial "warm" irradiation and two further doses in situ. They show that at least two radicals contribute to the polarization process; the NH<sub>2</sub> radical, generally accepted as being produced during the warm irradiation/8/ and another species produced in the in situ irradiation. This second species contributes, after very modest doses, to the rapid initial rise but does not affect significantly the level of the maximum achievable polarization. We also note that the NH<sub>2</sub> radical continues to be produced as the maximum achievable polarization rises slowly with in situ irradiation dose and appears to saturate at 70%.

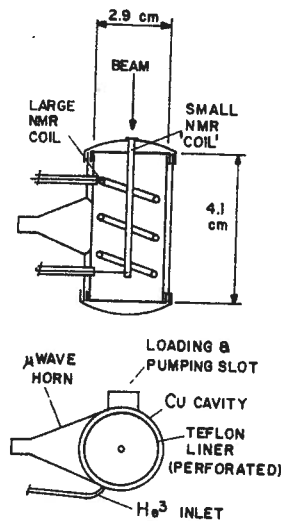


Figure 1  
The Target Cavity

### b) Radiation Damage and Annealing

At the same time that the particle irradiation is producing centers for polarization, the material is being radiation damaged and producing depolarizing centers. Fortunately the depolarizing effects can be annealed away by warming to a temperature which depends on the radical which is producing the polarization./8/

Figure 4 shows the polarizations measured over a series of physics data runs. The polarizations plotted were obtained after about four hours of polarizing and usually were the equilibrium values obtained with beam on target. Also shown are the annealing points and temperatures. Midway through the life of the target some low temperature anneals were made but little improvement in polarization is seen for temperatures less than 70 K.

On the other hand, Fig. 5 shows the evolution of the polarization in a sample in which the original polarization was mostly destroyed by an inadvertent anneal at 135 K. In this sample 50 K anneals are sufficient and in agreement with our earlier data presented at the Brookhaven Workshop/2/. We did not try any lower temperature anneals on this sample. However as the accumulated dose increased 50 K anneals became less efficient and it was necessary to increase the anneal temperature to 80 K.

Anneals were made frequently during the physics run in order to keep the average polarization as high as possible. The rate of radiation damage is shown in Fig. 6. The large and small coils measured the same radiation

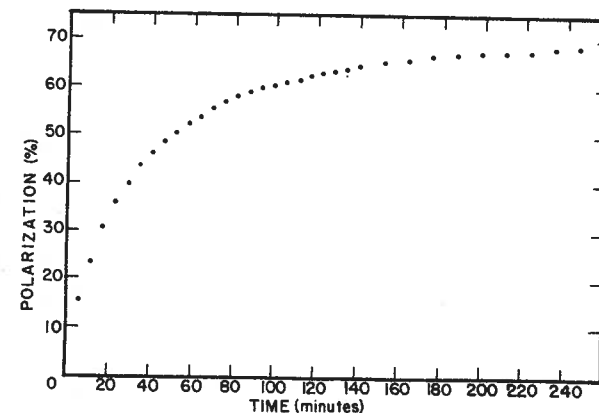


Figure 2  
Polarizing Curve for NH<sub>3</sub> Target after Initial e<sup>-</sup> Warm Irradiation and In Situ Proton Irradiation

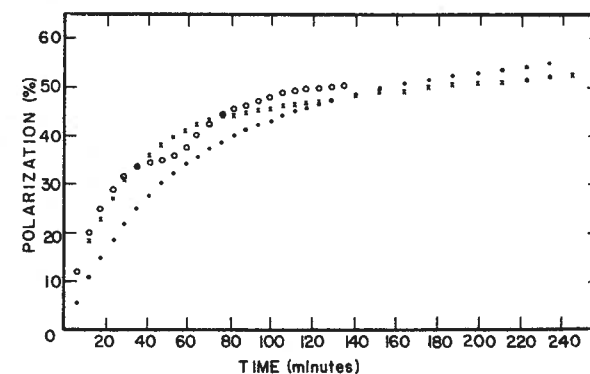


Figure 3  
Polarizing Curve for NH<sub>3</sub> after  
● initial e<sup>-</sup> irradiation  
x e<sup>-</sup> + 10<sup>15</sup> protons in situ  
o e<sup>-</sup> + 2 · 10<sup>15</sup> protons in situ

resistance, and over the range of dose accepted before an anneal, the polarizations fall exponentially. Assuming the simple form of the decay of the polarization

$$P(I) = P_0 \exp(-I/I_0)$$

the characteristic value,  $I_0$ , in total protons through the target is shown in Table 1.

These values show a radiation resistance two to three times greater than for butanol/porphyraxide. For comparison with other chemically doped materials see Ref./9/.

Another important fact is that ammonia can be annealed repeatedly without any apparent long term damage. Figure 4 shows that after  $2.5 \times 10^{16}$  protons through the target and seventeen anneals the polarization maintained at the end is the same as at the beginning. This is in contrast to chemically doped materials where the damage does not anneal away completely. There, after a few anneals the target material must be changed. So far only external factors have influenced the changing of an ammonia target.

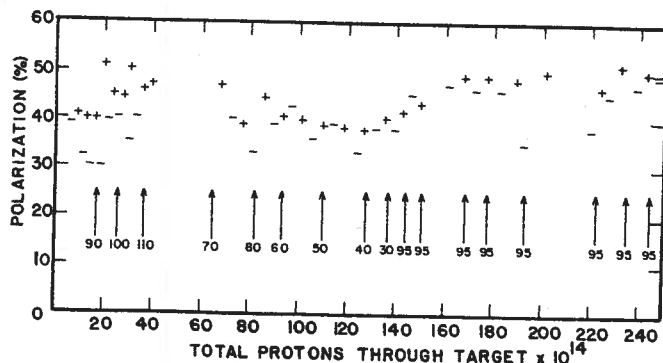


Figure 4  
NH<sub>3</sub> polarizations obtained with a proton beam of  $5 \times 10^{10}$  ppp on target. The target had been previously irradiated with electrons. The arrows show the annealing points and temperatures.

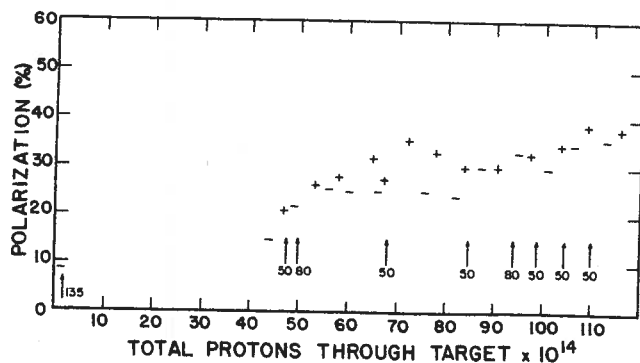


Figure 5  
Evolution of NH<sub>3</sub> polarization with proton beam in situ irradiation. Arrows show the annealing points and temperatures.

Table 1. Radiation Damage Characteristics

Enhancement	$I_0$ (Total Protons)
+	$(6 \pm 1) \times 10^{15}$
-	$(2.5 \pm 0.5) \times 10^{15}$

### c) Fragment Size

Another factor which influences the fragment cooling, and therefore achievable polarizations, is the size of the ammonia fragments. In our case, where we are using a <sup>3</sup>He/<sup>4</sup>He mixture as a coolant, it was felt that the optimum fragment size might be different than the 1-2 mm normally used.

During the course of the experiment targets of different fragment sizes were used and the results are shown in Fig. 7. The polarizations obtained with and without beam are plotted and show that the best results are obtained for the larger size fragments. In Fig. 7 the dashed line around 1.75 mm indicates that a range of sizes were used in this sample. Eventually this sample was further crushed to provide the 0.4 mm sample.

### 4. Conclusions

We compare ammonia with conventional chemically doped targets for doing spin physics with high intensity beams:

#### a) Advantages

- (i) NH<sub>3</sub> contains ~ 17 1/2% hydrogen by weight compared to ~ 10% for the diols.
- (ii) Radiation resistance two to three times better than butanol-porphyraxide.
- (iii) No non-annealable radiation damage. After  $2.5 \times 10^{16}$  protons through a target and many anneals the polarization is the same as at the start. This has the big advantage that the target material does not have to be changed frequently as is

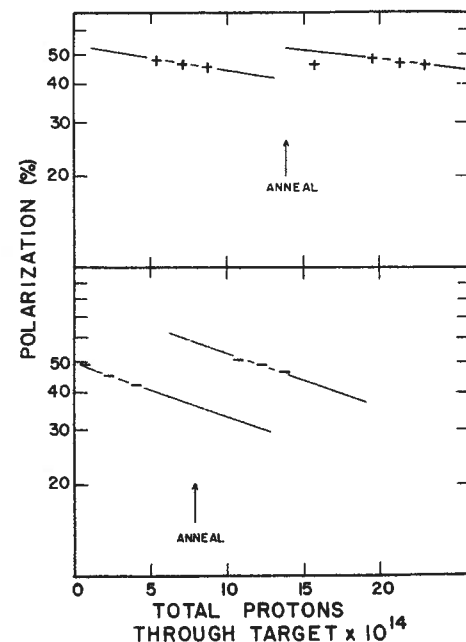


Figure 6  
NH<sub>3</sub> Radiation Damage for Both Enhancements

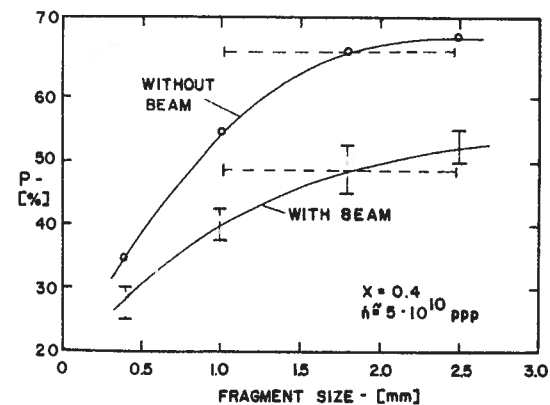


Figure 7  
Polarization achieved with target fragments of different sizes. I polarization with beam on target  
● polarization without beam

the case with chemically doped targets.

(iv) Low annealing temperatures < 90 K. Taken together with (ii) this means considerably less down time for annealing.

(v) A high time-averaged polarization can be maintained.

b) Disadvantages

(i) The target preparation is tedious.

(ii) Up to now our irradiations at 90 K have not been sufficient to produce enough centers for optimum performance. The  $t_{0.7}$  polarizing times are considerably larger than obtained by Bonn/3/.

(iii) The centers tend to disappear at low temperatures. This makes the target loading more difficult as the target temperature should be kept below 80 K.

5. Summary

The advantages of ammonia over chemically doped materials occur mainly because of the inherent properties of the material while the disadvantages are really matters of technique. The use of ammonia as a polarized target material in physics experiments with high intensity beams has thus become established and represents a considerable improvement over the materials used only two or three years ago.

For the future we intend to

a) substantially increase the initial irradiation at 90 K

b) continue investigation of the material

c) investigate ways of improving the target fragment cooling.

We hope this will lead to HIGHER AVERAGE POLARIZATIONS AT HIGHER BEAM INTENSITIES.

6. References

1. High Energy Spin Physics - 1982 (Brookhaven, 1982), ed. G. Bunce, AIP Conference Proceedings No. 95 (AIP, New York, 1983).
2. D.G. Crabb et al., Reference /1/, p. 488.
3. W. Meyer, Reference /1/, p. 526.
4. M.L. Seely et al., Reference /1/, p. 526.
5. P.R. Cameron, this workshop.
6. P.R. Cameron et al., this workshop.
7. G. Court and D. Gifford, Proc. Second Workshop on Polarized Target Materials (Abingdon, 1980), Rutherford Laboratory Report RL-80-080 (1980) p. 76.
8. T.O. Niinikoski, Reference /1/, p. 367.
9. D.G. Crabb, Reference /7/, p. 52.

First Use of ND<sub>3</sub> in a High Energy Photon Beam

R. Dostert, W. Havenith, O. Kaul, E. Kohlgarth, W. Meyer, E. Schilling, G. Sternal, W. Thiel and K.H. Althoff

Physikalisches Institut der Universität Bonn, Germany

1. Abstract

First target asymmetry measurements of the photodisintegration reaction  $\gamma d \rightarrow pn$  with deuterated ammonia (ND<sub>3</sub>) as target material were performed at the Bonn 2.5 GeV electron synchrotron. The deuterons were polarized in a <sup>3</sup>He/<sup>4</sup>He dilution refrigerator at about 200 mK and in a magnetic field of 2.5 T.

The paramagnetic radicals were created by irradiating the material under liquid argon at 90 K ('high temperature' irradiation) with electrons from the 20 MeV injection linac of the Bonn synchrotron. The accumulated flux was measured 'in situ' with a current integrator.

Using this 'high temperature' irradiated material a deuteron polarization of +31% and -29% could be reached at the beginning of the target asymmetry experiment. After additional 'low temperature' irradiation at about 200 mK with the photon beam the deuteron polarization went up to the maximum values of +40% and -44%. The subsequent resistance of the polarization to radiation damage is more than one order of magnitude higher than that of butanol.

2. The Experiment

First measurements of the target asymmetry of the photodisintegration reaction  $\gamma d \rightarrow pn$  are performed in the energy range of 450 - 650 MeV /1,2/.

The target asymmetry is defined by

$$T = \frac{3}{2} \frac{\sigma_{\uparrow} - \sigma_{\downarrow}}{\sigma_{\uparrow} + \sigma_0 + \sigma_{\downarrow}}$$

where  $\sigma_{\uparrow}$ ,  $\sigma_0$  and  $\sigma_{\downarrow}$  represent the differential cross sections for the three states of the deuteron spin, the symbol  $\uparrow$  referring to the direction ( $\vec{k} \times \vec{q}$ ) where  $\vec{k}$  and  $\vec{q}$  are the momenta of the photon and proton, respectively. To obtain T from the counting rate asymmetry  $\epsilon = N_{\uparrow} - N_{\downarrow} / 2N_0$  we must know the polarization P and the quantity K which is the ratio of the number of proton-neutron coincidences from the polarizable deuterons to the number of coincidences coming from the background such as <sup>14</sup>N-nuclei, helium and cryostat walls. Then T is given by  $T = (1/P) \cdot (1/K) \cdot \epsilon$ . The quantity K was determined by comparing the counting rate from the ND<sub>3</sub> target to the rate from a similar target containing NH<sub>3</sub>. This was done for each energy at which we obtained asymmetry data. The values of K varied between 0.5 and 0.8 .

The experimental set-up is shown in fig. 1.

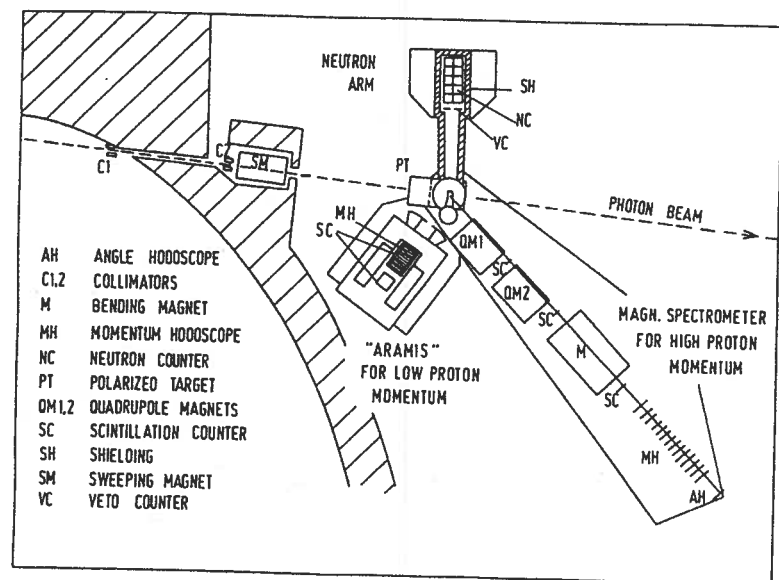


Fig. 1: Experimental set-up

Some features of the Bonn polarized target are given in the following list:

**Cryostat:** Horizontal dilution refrigerator /3/ - based on a  $^3\text{He}$ -cryostat /4,5/ combined with an easily loadable dilution unit /6/ - with appropriate radiation shields for the  $\gamma$ -beam. The lowest temperature without external heat load is 165 mK. At a circulation rate of 6 mmol/sec the cooling power is 5 mW at 200 mK and 20 mW at 300 mK. The cool-down time is 2 hours, using a  $^4\text{He}$ -bypass.

**Magnet:** 2.5 T conventional C-magnet

**NMR:** Polarization measurement accurate to  $\pm 5\%$ , due to the accuracy of the thermal equilibrium (T.E.) calibration signal. Relative accuracy repeating a measurement 0.5%, e.g.  $P = 40 \pm 0.2\%$  /7/.

### 3. Sample Preparation

Compared to the preparation of a butanol/porphyrin sample /8/, the one of ammonia/irradiation doping is more complicated. It is known that radicals are necessary for the Dynamic Nuclear Polarization (DNP) process. At Bonn, the radicals are formed during irradiation in a high intensity electron beam ( $10^{14}$  e/cm $^2$ ) of the 20 MeV injection linac. The  $\text{ND}_3$  is cooled by liquid argon ('high temperature' method, 90 K).

The details of the solid ammonia preparation /9,10/ are given in fig. 2:

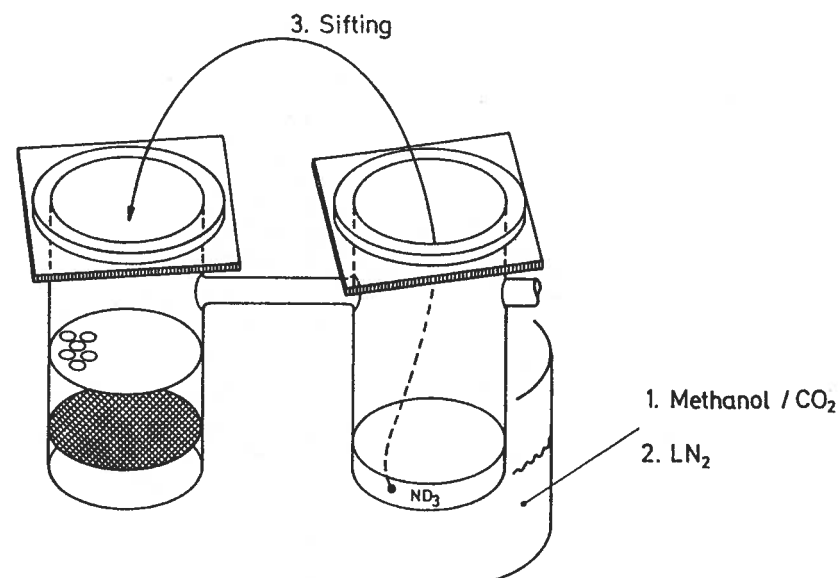


Fig. 2:

Gaseous ammonia ( $\text{ND}_3$ ) is filled into the right glass cylinder, liquified in a bath of methanol/frozen  $\text{CO}_2$  at  $\sim 240$  K, then slowly frozen ( $t > 1$  h) to a block of transparent solid (1). Being shock-frozen to  $\text{LN}_2$  temperature (2) the block can be exposed to atmosphere. It shows cracks which allow to crush it into fragments. After the removal of the glass lids the sample is sifted through a sieve with 3 mm holes in a twin cylinder (3). Beads of ammonia which are too small (powder) fall through a finer sieve ( $\varnothing 1,5$  mm) and can be reliquified in a next cycle of liquification, whereas the fraction above showing the proper size is taken out. The crystalline fragments show a high mechanical stability.

### 4. 'High Temperature' Irradiation

The irradiation was performed at the 20 MeV injection linac of the Bonn 2,5 GeV electron synchrotron. During the irradiation the sample is cooled under liquid argon in a closed argon liquifier /11,12/. The  $\text{ND}_3$  sample was typically exposed to a flux of  $3,6 \times 10^{16}$  electrons/cm $^2$ . The beam intensity was about  $2 \times 10^{14}$  e/sec.

The initial polarization performance of ammonia samples /9,13/ is dependent on the linac irradiation dose. For this, it is necessary to measure the accumulated flux precisely.

## 5. Beam Monitoring and Flux Measurement in the Linac

The irradiation dose is a function of the beam intensity as well as of the beam profile. The Bonn linac is a pulsed machine performing pulse lengths of  $2 \mu$  sec at a rate of 50 Hz, each pulse containing  $\sim 8 \times 10^{13}$  electrons. So it is possible to calibrate the induction signal of the electron bunches in a toroid coil around the beam line with a pulsed electric current of known amplitude. Together with a known beam profile at the beam window of the liquifier, obtained by the degree of blackening of a plastic foil, the first flux measurements were carried out giving a result of  $\sim 10^{17} \text{ e/cm}^2 / 3/$ .

A systematic research of the beam profile and the showering behaviour by using thermoluminescent dosimeters in a block of plastic was carried out to determine the design of the Liverpool argon liquifier /13/.

Nevertheless, the size and the form of the beam changes due to the operational conditions of the linac, as experience shows. The induction signal is unfortunately not a good monitor for the beam quality and, for reasons of defocussing and showering, does not give the number of electrons which actually hit the sample inside the cryostat.

To avoid this, a faraday cup insert for the Liverpool argon liquifier was introduced (Fig. 3).

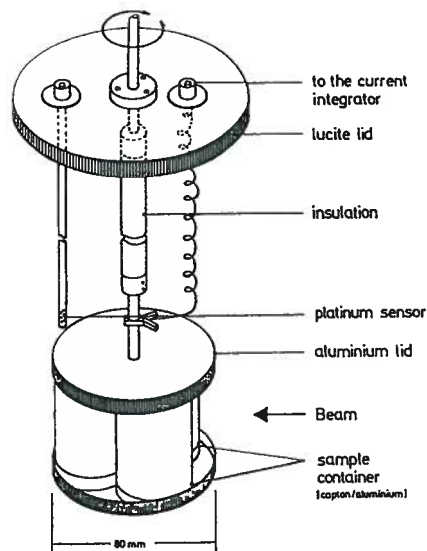


Fig. 3: Faraday cup insert

It is meant to provide a true figure of the absorbed irradiation dose. Another aim was the possibility of steering the beam to the center of the target cell.

Together with a scintillation screen monitor the irradiation time could be shortened by a factor of three.

A test of the performance showed agreeable results. In fig. 4 the sampled charge expressed by the number of electrons is plotted versus the number of electrons in the beam derived from the induction signal.

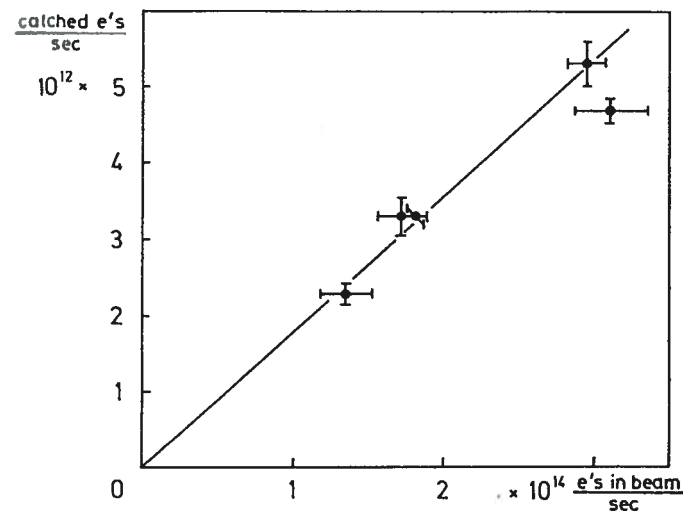


Fig. 4: Performance of the faraday cup

It shows good linearity, no loss of charge by irradiation induced conduction of the liquid argon was observed. The efficiency of collecting electrons is 1.5% for a  $75 \text{ cm}^3 \text{ ND}_3$  sample and a beam size of 10 cm FWHM at the window of the liquifier facing the beam.

Most of the processes taking place during irradiation are ionizing ones. This means that an average sample of 15 g  $\text{ND}_3$  in a 80 g aluminium container, as in our case, only takes 3% of the electrons. Thus, not being much affected by the differing weights of the samples the reproductivity of the irradiation dose is improved.

## 6. 'Low Temperature' Irradiation

To give a rough survey about the behaviour of  $\text{ND}_3$  compared to d-butanol, the polarization achieved during the experiment is plotted against the irradiation dose (fig. 5).

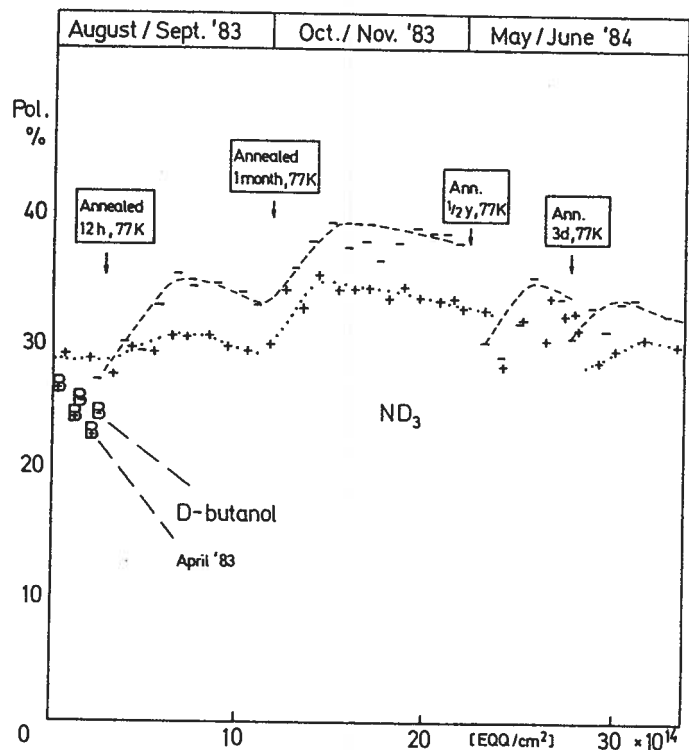


Fig. 5: Polarization of  $\text{ND}_3$  compared to d-butanol in the photodisintegration experiments

D-butanol, measured under the same conditions, shows a quick depolarization with a critical dose of  $1,5 \times 10^{15}$   $\text{EQQ}/\text{cm}^2$ . Like d-butanol,  $\text{NH}_3$  and  $\text{ND}_3$  is annealable [12,15], now revealing that polarization is even growing during the first  $6 \times 10^{14}$  photons/ $\text{cm}^2$  after each annealing.

The maximum polarization turned out to be -44% at a dose of  $1,5 \times 10^{15}$   $\text{EQQ}/\text{cm}^2$  without, and 40% with beam, due to a rise of temperature (depolarizing effects).

The resistance against radiation damage is more than one order of magnitude higher than that of butanol. Another important aspect is the build-up time  $\tau_{0,7}$  of the polarization in which 70% of the maximum polarization is reached. For reasons of less systematical errors, in our experiment the sign of polarization was changed every 6 - 12 h. In this respect d-butanol is the better target material because the polarization build-up time is shorter (fig. 6).

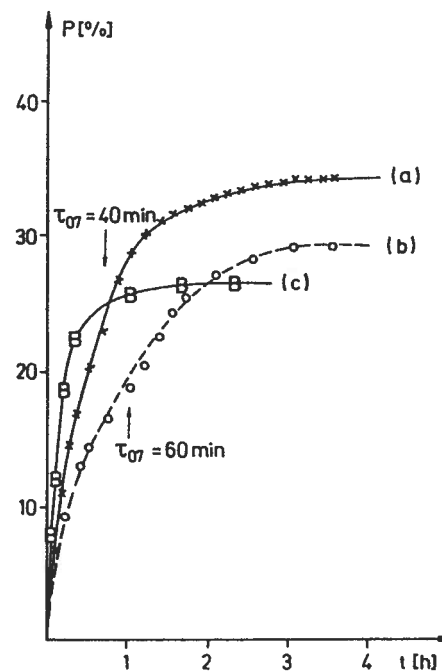


Fig. 6: Build-up time of  $\text{ND}_3$  (a), (b) and d-butanol (c), respectively. (a) Accumulated flux of  $3 \times 10^{15}$   $\text{EQQ}/\text{cm}^2$  and (b)  $1,8 \times 10^{14}$   $\text{EQQ}/\text{cm}^2$ .

During irradiation the polarization build-up in  $\text{ND}_3$  quickens, too. Unfortunately, for lack of time, it was not feasible to measure the relaxation time constant of the  $\text{ND}_3$  sample at 175 mK and 2,5 T during the experimental run. At a break the polarization decreased by 3% in 16 h, showing a frozen spin behaviour. A detailed information of the  $\text{ND}_3$  properties as polarized target material is given in [14,15].

## 7. Depolarizing Effects

Starting from a maximum polarization of -44%, by switching on the beam the polarization went down to a degree of -41%, due to beam heating.

In case of an inhomogeneous beam this may cause a serious error in maintaining the polarization value, since polarization is measured by a NMR coil which is averaging the polarization over the whole sample. A check was done by comparing the depolarization time constant (see fig. 7) with the warming-up time constant of the helium bath.

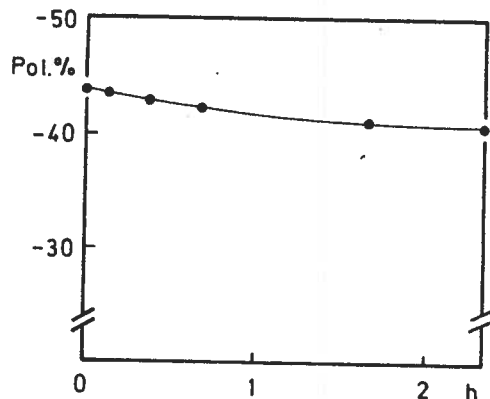


Fig. 7: Depolarization by beam heating

The result was 20 seconds for heating up the helium bath and two hours to depolarize the sample with the beam. The temperature was measured with an encased Speer Carbon resistor (220  $\Omega$ ) outside the beam. The heat input (see table 1) was derived from the temperature rise in comparison with a previous measurement of the cryostat's cooling power using an electric heater /16/.

Table 1: Heat input by the  $\gamma$ -beam

beam intensity [photons/sec]	temperature [mK]	heat input [mW]
-	175	-
$0,55 \times 10^9$	215	5
$1,1 \times 10^9$	240	9
beam on:	175 mK 20 sec	240 mK
beam off:	240 mK 50 sec	175 mK

The quick response to the heat load (tab. 1) is due to a good thermal contact between the  $\text{ND}_3$  fragments and the  $^4\text{He}$ -part in the mixture. This leads to a heating-up of the mixture which is distributing the heat over the whole sample, so that depolarization is homogeneous, not affecting the accuracy of the polarization measurement.

Another problem is the inhomogeneous depolarization of target materials during irradiation with inhomogeneous beam profiles /17/. In our case ( $\text{ND}_3$ ), this is to some degree balanced by the formation of 'low temperature' radicals providing a gain in polarization during the first  $6 \times 10^{14}$  photons/cm<sup>2</sup> (see fig. 5).

## 8. Targetasymmetry Results from D-Butanol/ $\text{ND}_3$ at the Same Kinematics

Fig. 9 shows the target asymmetry plotted against the proton CM angle at a photon energy of 550 MeV. The preliminary results for  $\text{ND}_3$  are in agreement with the previously measured d-butanol ones. In spite of this,  $^{14}\text{N}$  as a constituent of  $\text{ND}_3$  as a spin 1 particle may be polarized and cause trouble. For this reason a subtraction measurement using  $^{14}\text{NH}_3$  is performed in connection with each kinematical setting. The degree of  $^{14}\text{N}$  polarization in  $^{14}\text{NH}_3$  and  $^{15}\text{ND}_3$  is now under investigation /18, 19/. The gain in statistics, due to the new target material  $\text{ND}_3$ , was well recognized during a three weeks' run remeasuring the d-butanol value for  $155^\circ$ .

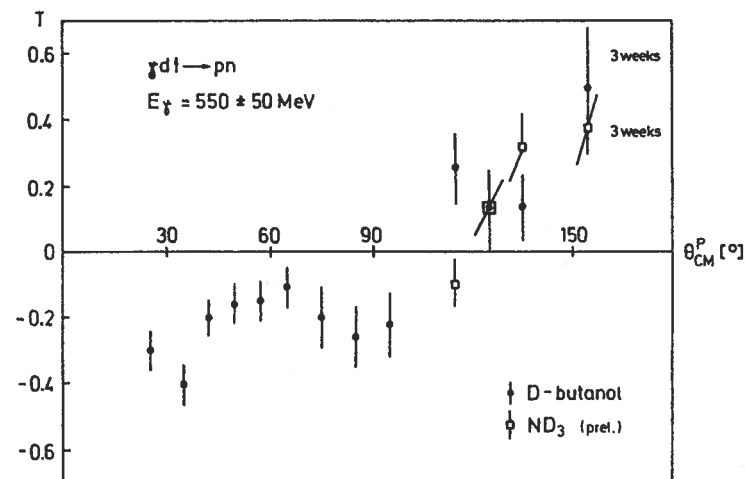


Fig. 9: Targetasymmetry results for  $\gamma d + p \rightarrow n + p$  at 550 MeV. The data at  $115^\circ$ ,  $125^\circ$ ,  $135^\circ$ , obtained with  $\text{ND}_3$ , are preliminary.

## 9. References

- /1/ K.H. Althoff, G. Anton et al, Zeitschrift für Physik C, Particle and Fields 26, 175 - 179 (1984)
- /2/ P. Erbs, E. Schilling, D. Sundermann, Thesis (in preparation)
- /3/ W. Meyer et al, Nucl. Instr. and Methods 204, 59 (1982)
- /4/ H. Herr and V. Kadansky, Nucl. Instr. and Methods 121, 1 (1974)
- /5/ W. Meyer, Thesis, BONN-IR-77-4
- /6/ T.O. Niinikoski and J.-M. Rieubland, Proc. II R Commission A 1 - 2, Zürich (Switzerland) (1978) p. 181
- /7/ O. Kaul, Diplomarbeit, BONN-IR-76-21
- /8/ S. Mango et al, Nucl. Instr. and Methods 72, 45 (1970)
- /9/ G. Sternal, Staatsexamensarbeit, BONN-IR-84-09
- /10/ W. Havenith, Staatsexamensarbeit, BONN-IR-84-08
- /11/ W. Meyer, High Energy Spin Physics (BNL) AIP Conference Proceedings 95, p. 505 (1982)
- /12/ U. Härtel et al, in High Energy Physics with Polarized Beams and Polarized Targets, Birkhäuser Verlag, Basel (1981) p. 447
- /13/ S. Brown, in these proceedings
- /14/ W. Meyer et al, Nucl. Instr. and Methods 227, 35 (1984)
- /15/ U. Hartfiel, in these proceedings
- /16/ E. Schilling, Diplomarbeit, BONN-IR-82-12
- /17/ G.R. Court et al, Nucl. Instr. and Methods 177, 281 (1980)
- /18/ G. Heyes, in these proceedings
- /19/ W. Thiel, Diplomarbeit, Bonn (in preparation)

## RADIATION RESISTANCES OF AMMONIA AT 1 KELVIN AND 2.5 TESLA

K. H. Althoff, V. Burkert, U. Hartfiel, T. Hewel,  
G. Knop, M. Leenen, W. Mehnert, W. Meyer,  
H.D. Schablitzky, E. Schilling, W. Thiel

Physikalisches Institut der Universität Bonn  
Nussallee 12  
D-5300 Bonn 1  
Fed. Rep. of Germany

presented by U. Hartfiel

### ABSTRACT

We have studied the radiation resistance behaviour of Ammonia in an intensive electron beam. After a pre-irradiation at "high temperature" at the 20 MeV electron linac in Bonn the samples were irradiated at "low temperature" conditions (1 Kelvin and 2.5 Tesla) in an external electron beam of the 2.5 GeV electron synchrotron. The proton polarization in  $\text{NH}_3$  asymptotically decreased from 36% to 25%. The deuteron polarization in  $\text{ND}_3$  first of all increased from 3.5% up to more than 7% but after additional irradiation the polarization asymptotically dropped down to 5.5%. The polarization build-up time decreased and the frequency dependence changed. We found good annealing conditions by heating the samples up to 75 K.

### 1. Introduction

All high energy experiments in Bonn, which dealt with a polarized target have been performed in photon beams. Presently experiments are being prepared using polarized targets in an (polarized) electron beam. Butanol or Propandiol as target materials suffer from low resistivity to radiation damage operating in intensive electron beams. Ammonia seems to be more suitable in this respect. We therefore studied extensively the performance of this material in our electron beam.

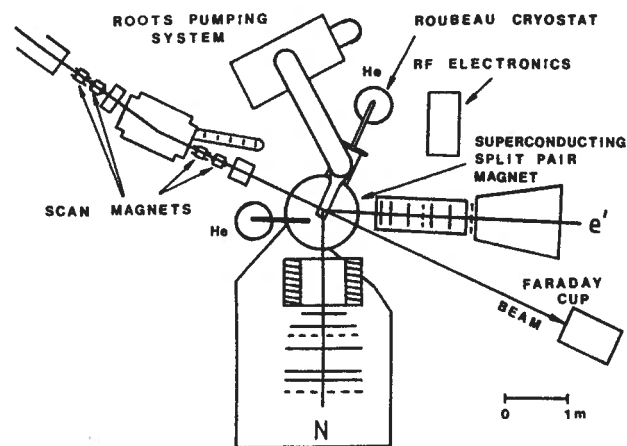


Fig. 1. Top view of the target area

## 2. The Apparatus

We used slowly frozen  $\text{NH}_3$  and  $\text{ND}_3$  /STE/. The samples were irradiated at "high temperature" under liquid Argon at the 20 MeV linac in Bonn. These pre-irradiated samples were transported to the experimental area (see fig. 1) of the external electron beam of the 2.5 GeV electron synchrotron. The beam passes the target and is dumped in a totally absorbing faraday cup, which measures the total charge. The target magnet is a superconducting split pair magnet (see fig. 2).

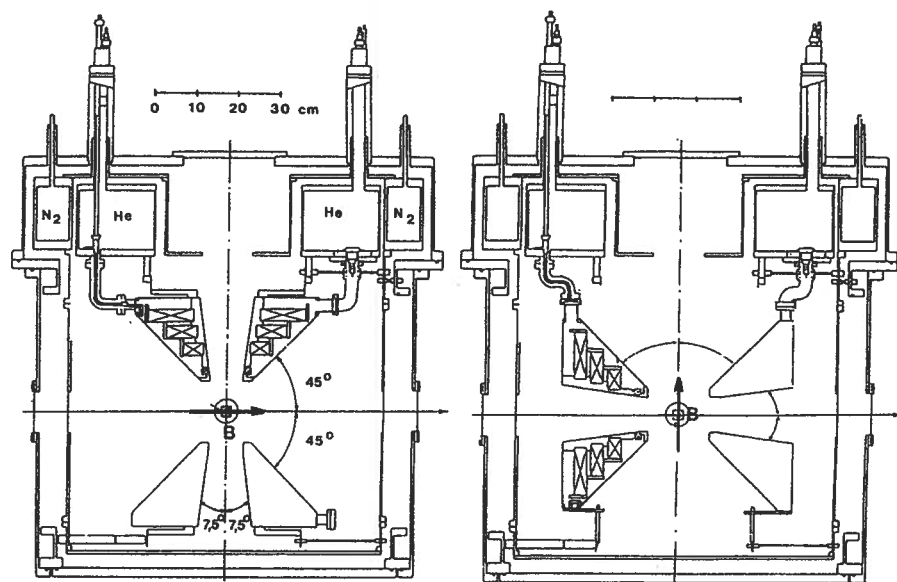


Fig. 2. Cut view of the superconducting split pair magnet

The magnet can reach a maximum field of  $B_{\text{max}} = 4$  Tesla. The homogeneity  $\Delta B/B$  is better than  $\pm 5 \cdot 10^{-5}$  over a volume of more than  $20 \text{ cm}^3$ . The coil system can be disconnected and turned in such a way to produce a horizontal field as well as a vertical field. In our experiments the field was 2.5 Tesla. The temperature was 1 Kelvin produced by a horizontal Roubeau cryostat.

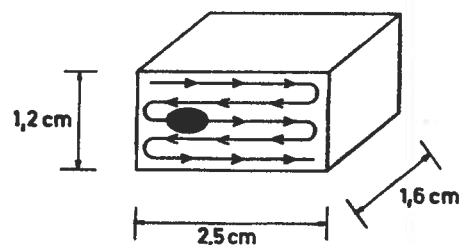


Fig. 3. Target extension

Since the target front face is much larger than the beam (see fig. 3) the beam was scanned by four scanning magnets (see fig. 1). The scanning velocity was proportional to the beam current. The beam intensity was  $< 5 \cdot 10^{10} \text{ e}/(\text{cm}^2 \text{ s})$ .

### 3.1. Comparison Butanol and $\text{NH}_3$

We first of all compared the radiation resistance behaviour of chemically doped Butanol and pre-irradiated Ammonia (see fig. 4).

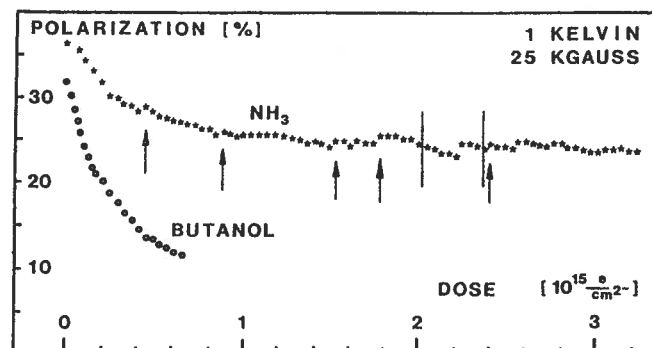


Fig. 4. Radiation damage of Butanol and  $\text{NH}_3$

The starting polarization of  $\text{NH}_3$  (36.3%) is higher than the starting polarization of Butanol (31.8%) and  $\text{NH}_3$  appears to be much more resistant than Butanol. The polarization of Butanol drops down very rapidly whereas the polarization of  $\text{NH}_3$  reaches an asymptotic value of about 25%.

We observed a clear change of the frequency curve depending on the irradiation of the sample. To check on the frequency dependence we therefore had several irradiation breaks. Five times we changed the microwave frequency (arrows in fig. 4).

At a radiation dose of  $2.0$  to  $2.4 \cdot 10^{15} \text{ e}/\text{cm}^2$  we had some problems with the NMR. So there is no real physics in the jump at  $2.2 \cdot 10^{15} \text{ e}/\text{cm}^2$ .

In the literature the statements concerning the radiation resistivity of Ammonia disagree. Earlier studies at Bonn /MEY/ were performed in a photon beam. The resistivity of Ammonia was found to be three times higher than that of Butanol. Other studies were done in an electron beam at SLAC /SEE/. In these studies a factor of thirty was obtained.

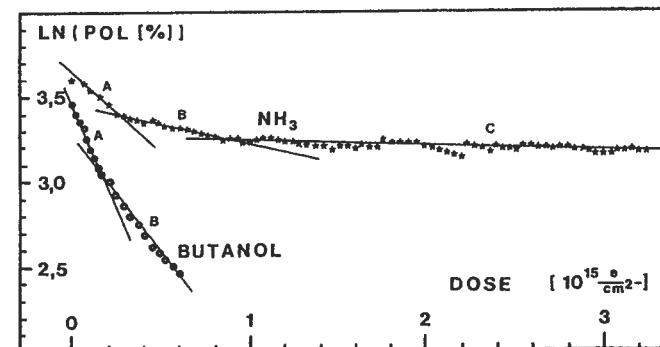


Fig. 5. Radiation damage of Butanol and  $\text{NH}_3$  (log. scale)

For a better comparison we plotted the data (see fig. 4) in a logarithmic scale (see fig. 5). Both curves are clearly not exponential. It is therefore difficult to compare the resistivity by explicit values. Only to get some numbers we made exponential fits of some points using  $P(\phi) = P_0 \exp(-\phi/\phi_0)$ . In table 1 the critical doses  $\phi_0$  of  $\text{NH}_3$  and Butanol are compared.

Table 1. Critical dose of butanol and  $\text{NH}_3$

		$\phi_0$ [ $10^{15} \text{ e/cm}^2$ ]
$\text{NH}_3$	A	1.0
	B	4.1
	C	30.
Butanol	A	.38
	B	.66

At the beginning (part A) the critical dose of  $\text{NH}_3$  is three times larger than that of Butanol. In part B it already is seven times larger and in part C this ratio is probably larger than thirty.

### 3.2. Frequency dependence on the irradiation

During the irradiation we observed a change in the shape of the ESR frequency curve. Figure 6 in detail shows the frequency dependence around the positive maximum polarization.

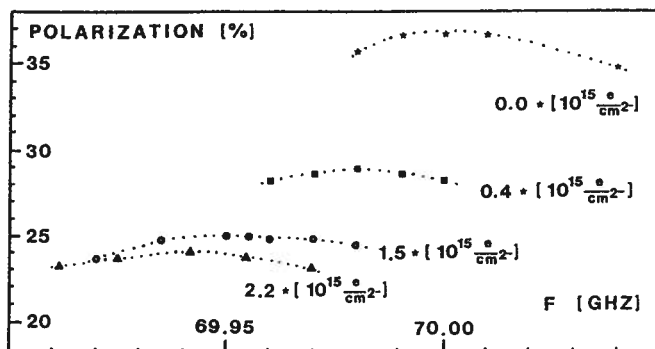


Fig. 6. Change in the frequency curve

The frequency was measured with a digital frequency counter. The systematic error was  $\pm 2$  MHz produced by the instability of the carcinotron. The superconducting magnet was driven in the persistent mode. The field controlled by NMR was exactly 2.5 Tesla. For the experiment practise figure 7 shows how the frequency for the highest positive maximum polarization has to be changed depending on the radiation dose.

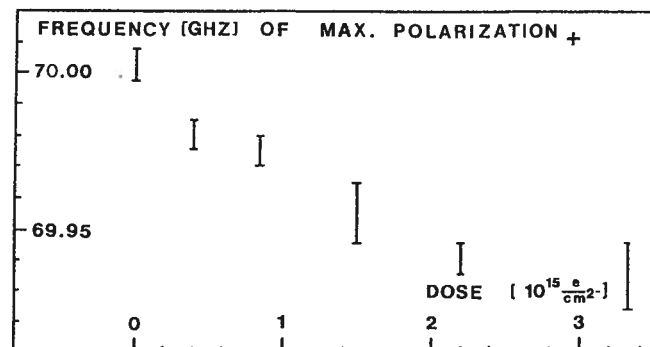


Fig. 7. Frequency dependence on the irradiation

### 3.3. Build-up and relaxation behaviour

Depending on the irradiation we also observed a change in the build-up time and in the relaxation behaviour (see fig. 8 and fig. 9).

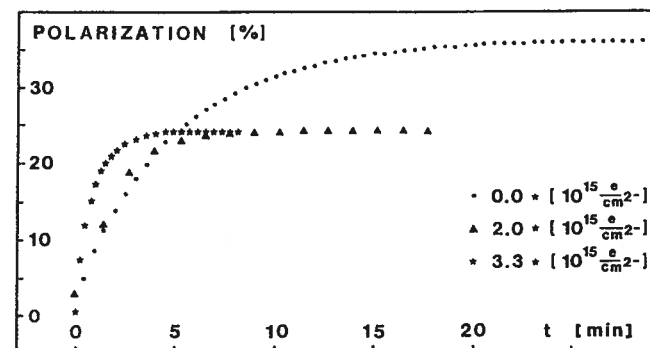


Fig. 8. Polarization build-up

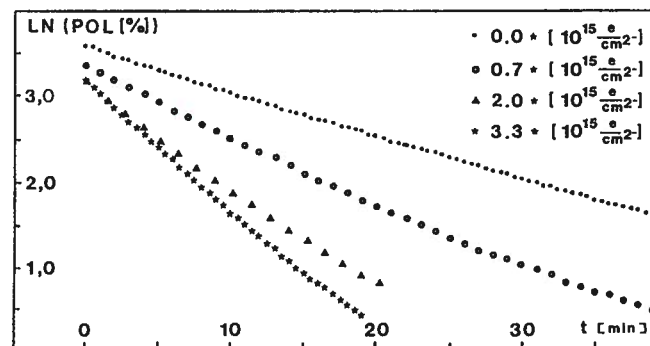


Fig. 9. Relaxation

We also observed that the sample became quicker with the irradiation. In table 2 the 70% build-up time and the relaxation time are summarized. Because the relaxation curves differ from the exponential behaviour two different times are noticed respectively the relaxation to  $1/e$  and  $1/e^2$ .

Table 2. Build-up time and relaxation time

dose [ $10^{15} \text{ e/cm}^2$ ]	$t(0.7)$ [min]	$\tau(1/e)$ [min]	$\tau(1/e^2)$ [min]
0.0	5.8	18.5	39.0
0.7	-	9.8	22.0
2.0	2.5	7.5	16.5
3.3	1.5	6.3	13.3

### 3.4. Annealing of $\text{NH}_3$

Although it seems that the polarization will not drop below 25% we think for the practise it is better to anneal the sample before the polarization will reach the final value. We have performed many annealing tests and figure 10 shows the final tries for the best reproduction of the polarization.

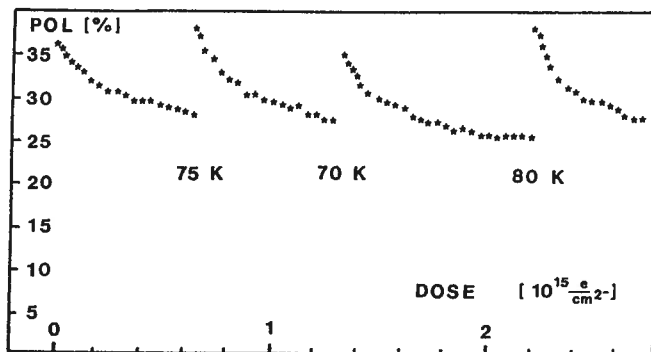


Fig. 10. Annealing of  $\text{NH}_3$

The best annealing temperature was found to 75 K to 80 K. Annealing at lower temperature does not recover the full polarization. Annealing at higher temperature gives more polarization, but the sample gives becomes much slower. Annealing at 75 K does not only recover the polarization, but also the other starting parameters. Figure 11 and 12 show the build-up and relaxation behaviour before and after the 75 K annealing compared to the starting curves.

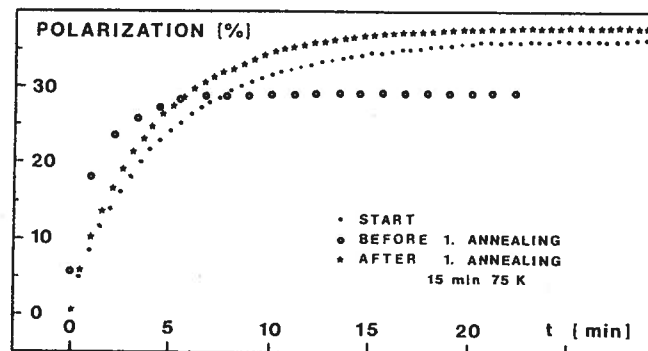


Fig. 11. Polarization build-up

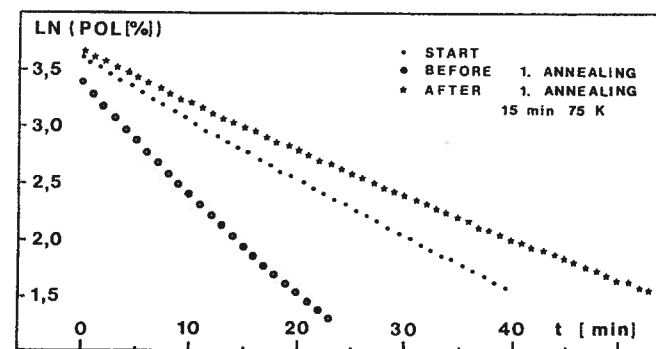


Fig. 12. Relaxation

### 4. $\text{NH}_3$ without pre-irradiation

The next test dealt with an Ammonia sample without any preirradiation. Figure 13 shows the polarization dependence on the irradiation at "low temperature".

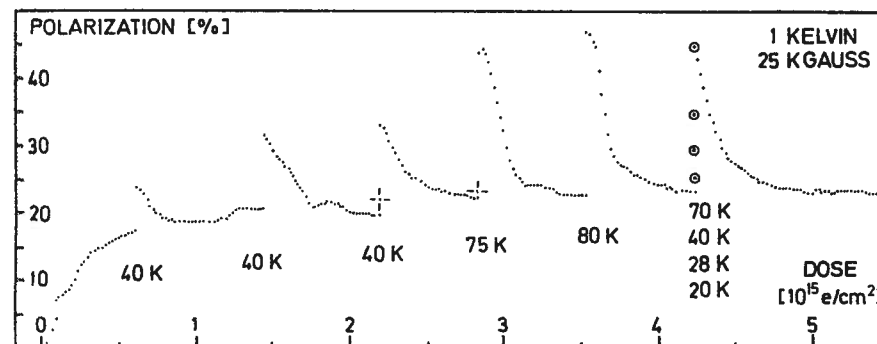


Fig. 13.  $\text{NH}_3$  without any pre-irradiation

Leaking any radicals the polarization starts at zero. A break in the irradiation caused a jump from about 4% to 7%. The sample was annealed three times at 40 K. The frequency check before the last 40 K anneal reveals that we had missed to correct the frequency. The single point shows the real reachable polarization. Annealing at 75 K and 80 K brought high values of polarization. After the 80 K anneal we obtained 47% (at 1 K and 2.5 Tesla !). But continuing the irradiation let the polarization quickly drop down. Before the last period of irradiation we made four annealings with temperatures from 20 K to 70 K. Again the polarization drops down very quickly, but stays at the final value of about 25%.

In fig. 14 the behaviour of the virginal sample is compared to the pre-irradiated sample. Ignoring the annealings both samples reach the same asymptotical value of about 25% !

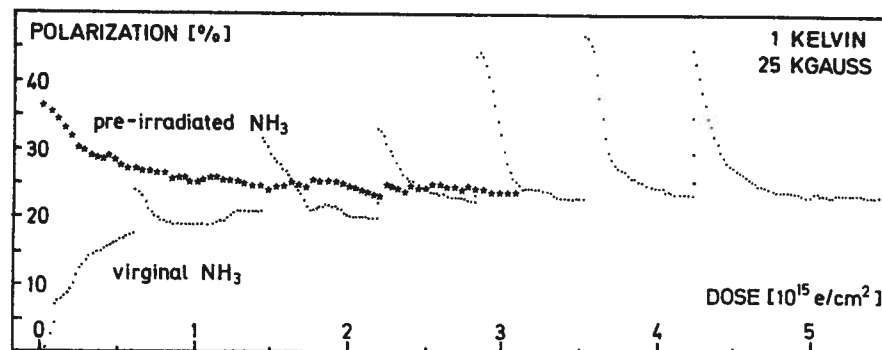


Fig. 14. Pre-irradiated and virginal  $\text{NH}_3$

### 5.1. Irradiation behaviour of $\text{ND}_3$

The  $\text{ND}_3$  sample was pre-irradiated at "high temperature" very similar to the pre-irradiated  $\text{NH}_3$  sample. But the "low temperature" behaviour was absolutely different. Figure 15 shows the polarization dependence on the irradiation at 1 K and 2.5 Tesla. We started at 3.5%. Depending on the irradiation the polarization quickly rose up to more than 7%. Continuing the irradiation the polarization dropped asymptotically down to 5.5%.

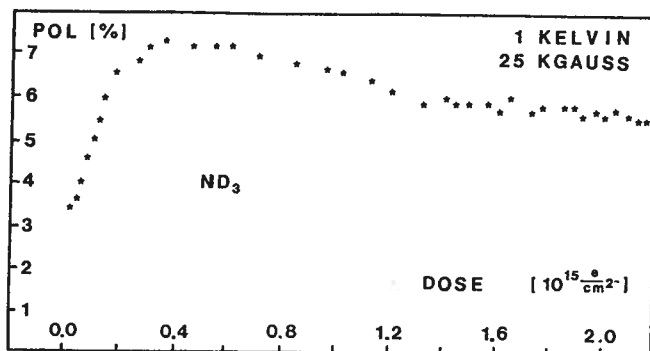


Fig. 15. Irradiation dependence of  $\text{ND}_3$

### 5.2. Frequency dependence on the irradiation

During the irradiation the frequency curve changed quite drastically (see fig. 16). The curve enlarged very much. At the starting point the frequency difference between the positive and the negative maximum of polarization was 125 MHz, after a radiation dose of  $2.2 \cdot 10^{15} \text{ e/cm}^2$  it was 300 MHz.

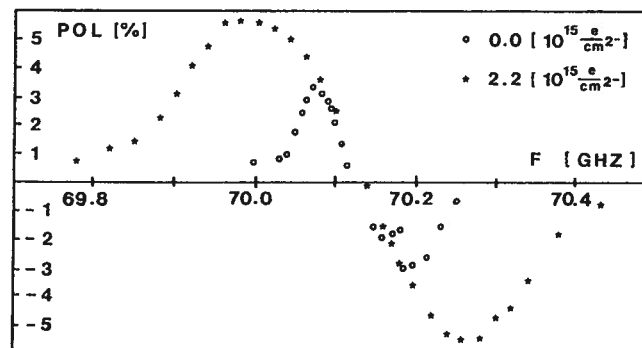


Fig. 16. Enlargement of the frequency curve

### 5.3. Build-up and relaxation behaviour

Depending on the irradiation the sample became quicker. The 70% build-up time was at the start 10 minutes and after  $2.2 \cdot 10^{15} \text{ e/cm}^2$  about 3 minutes. The relaxation time dropped from 38 minutes at the start to 3.8 minutes after the radiation dose.

### 5.4. Annealing of $\text{ND}_3$

Figure 17 shows the annealing behaviour of  $\text{ND}_3$ . The first annealing was done at 40 K, which clearly was too low. The second annealing at 75 K was successful. The starting conditions became reproduced very accurately.

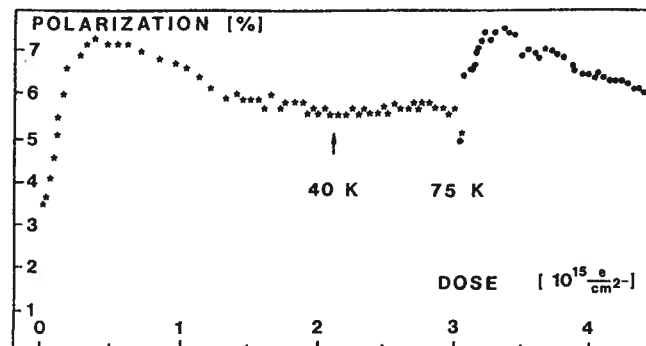


Fig. 17. Annealing of  $\text{ND}_3$

Figure 17 shows the polarization behaviour and figure 18 the frequency dependence after the 75 K anneal compared to the behaviour at the starting point.

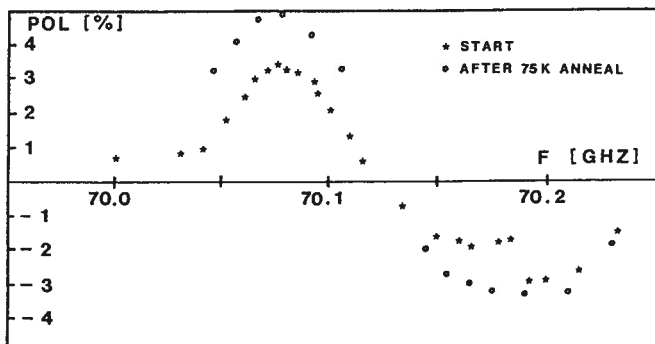


Fig. 18. Frequency curves

After the 75 K anneal the 70% build-up time was about 8 minutes comparable to 10 minutes at the start. The relaxation time after the start was 36 minutes which is close to the 38 minutes at the starting point.

#### 5.5. Frequency change in detail

After the 75 K anneal we studied the enlargement of the frequency curve in detail. Depending on the radiation dose we reached a maximum polarization at  $0.4 \cdot 10^{15} \text{ e/cm}^2$ . The absolute maxima were +7.8% and -8.8%. Continuing the irradiation caused a further enlargement. Figure 19 shows the change in frequency at the highest positive polarization.

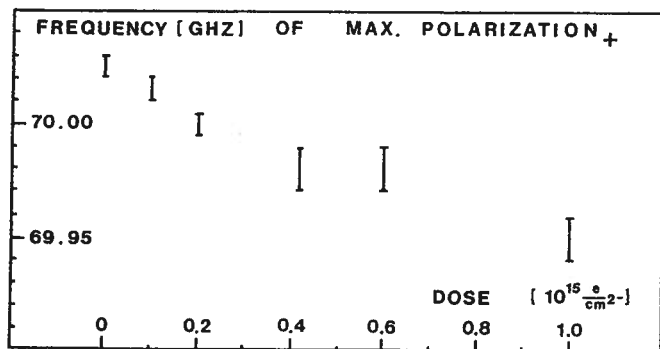


Fig. 19. Frequency dependence on the irradiation

#### 6. References

- /MEY/ MEYER et al., Nucl. Instr. and Meth. 215 (1983) 65  
 /SEE/ SEELY et al., SLAC-PUB-2874  
 /STE/ STERNAL, Staatsexamensarbeit, Bonn IR-84-07

#### DYNAMIC NUCLEAR POLARIZATION STUDIES IN IRRADIATED AMMONIA AT 1 K

R. Dostert, W. Havenith, O. Kaul, E. Kohlgarth, W. Meyer,  
 H. Riechert\*, E. Schilling, G. Sternal, W. Thiel and K.H. Althoff

Physikalisches Institut der Universität Bonn

Nussallee 12

D-5300 Bonn 1

Fed. Rep. of Germany

#### ABSTRACT

Dynamic proton and deuteron polarization measurements in irradiated  $^{14}\text{NH}_3$ ,  $^{14}\text{ND}_3$  and  $^{15}\text{ND}_3$  were performed at 1 K in a magnetic field of 2.5 T. The paramagnetic radicals were created by irradiating the material under liquid argon at 90 K ('high temperature' irradiation) with electrons from the 20 MeV injection linac of the Bonn synchrotron.

These measurements were performed in order to obtain information about the nitrogen polarization as well as to gain insight into the prevailing mechanism of dynamic nuclear polarization (DNP) in these irradiated materials. The polarization results in  $^{14}\text{NH}_3$  give hints that the equal spin temperature (EST) theory is applicable to this material. Thus the nitrogen polarization in  $^{14}\text{NH}_3$  is calculable.

The polarization measurements of the protons and deuterons in  $^{14}\text{ND}_3$  disagree with the EST-theory. They rather give evidence for a more complex behaviour apparently involving more than one polarization mechanism. It is attempted to explain these observations with a differential solid state model. First measurements in  $^{15}\text{ND}_3$  indicate, that  $^{14}\text{ND}_3$  and  $^{15}\text{ND}_3$  are very similar under the aspect of DNP-behaviour.

#### 1. Introduction

Since the discovery of high proton polarization in irradiated ammonia in 1979 /1/, some properties of the hydrogen rich material  $^{14}\text{NH}_3$  were studied. Especially its extremely good polarization resistance to radiation damage, which is mainly a result of the radical formation by irradiation, enables improved polarized target experiments with high intense particle beams. For the first time irradiated  $^{14}\text{NH}_3$  was used in high energy physics experiments, performed in Brookhaven /2/ and at CERN /3/.

\*Now at: Institut für Festkörperforschung, KFA Jülich, Germany

At intermediate energies a lot of interest has been concentrated on the deuteron in the last time. Since some years the photodisintegration reaction  $\gamma d \rightarrow pn$  with the Bonn polarized target is studied. Therefore the main emphasis was put here on  $^{14}\text{ND}_3$  polarization measurements. For the first time  $^{14}\text{ND}_3$  was polarized in Bonn at 1 K and 0.5 K in a magnetic field of 2.5 T /4/. Remarkable was the strong temperature dependence of the deuteron polarization. Polarization values as high as 44% were obtained in a dilution refrigerator during a photodisintegration experiment  $\gamma d \rightarrow pn$ , as reported in ref. 5. Good radiation damage resistance of the polarization and also good polarization values were reported at the Brookhaven workshop by a Yale-Slac group /6/. Detailed radiation resistance studies of  $^{14}\text{NH}_3$  and  $^{14}\text{ND}_3$  were performed at 1 K using the external electron beam of the Bonn synchrotron /7/. In these measurements the annealing behaviour of both materials was also examined. All these results demonstrate that we have now a good handling of  $^{14}\text{NH}_3$  and  $^{14}\text{ND}_3$  as target material in high or intermediate energy physics experiments.

One problem however still exists: the uncertainty of the polarization of the nitrogen nuclei ( $^{14}\text{N}$ ), which have spin 1. A direct measurement of the nitrogen polarization by the usual nuclear magnetic resonance (NMR) method is extremely difficult. The magnetic moment of the  $^{14}\text{N}$  nucleus is very small and the quadrupole moment is much larger than that of the deuteron. These facts make the detection of the nitrogen polarization signal very troublesome. However, in the case of an equal spin temperature (EST) among different nuclei species, the nitrogen polarization is calculable. This was checked by measuring the microwave frequency dependence of the polarization of the deuterons and the unsubstituted protons (1%) in  $^{14}\text{ND}_3$  (section 6). In the case of  $^{14}\text{NH}_3$  we compared the results with those obtained in butanol, as our NMR-system was not equipped to detect the nitrogen polarization signal (section 5). First nitrogen polarization measurements in  $^{14}\text{ND}_3$  were performed in a collaboration with the Liverpool polarized target group, which is reported by G. Heyes /8/. More information about the nitrogen polarization in  $^{14}\text{ND}_3$  should be obtained also by polarization measurements in  $^{15}\text{ND}_3$ . First results will be presented (section 7).

Furthermore, these studies were performed in order to gain insight into the prevailing mechanism of the dynamic nuclear polarization (DNP) process in irradiated samples. For calculations the knowledge of the width and shape of the electron paramagnetic resonance (EPR) spectra is important. The results of these measurements will be shown in section 3. Polarization

build-up- and relaxation times in  $^{14}\text{NH}_3$  samples, irradiated with different doses, were examined (section 4). In the course of the deuteron polarization measurements, some strange effects, which cannot be explained completely up to now, were observed (Appendix). All measurements were performed at 1 K in a magnetic field of 25 KG.

## 2. Samples

Shock-frozen beads, produced by dropping liquid ammonia droplets into a liquid nitrogen bath as well as crushed crystalline ammonia fragments were used.  $^{14}\text{ND}_3$ , used for our measurements, has a deuteration of 99% with 1% unsubstituted protons. Detailed information about the ammonia preparation for the DNP measurements can be found in Refs. 9 and 10.

In the ammonia beads or - fragments paramagnetic radicals are produced by irradiation with 20 MeV electrons from the injection linac of the Bonn synchrotron. During the irradiation the ammonia samples are cooled in liquid argon at a temperature of about 90 K ('high temperature' irradiation). The electron beam current is typically  $2 \times 10^{14}$  electrons/s. For most of the irradiations the accumulated flux was  $\sim 10^{17}$  electrons/cm<sup>2</sup>. The irradiation procedure is discussed in detail by S. Brown /11/.

## 3. EPR-Spectra

The first visible result of an irradiation in ammonia is the violet color of the beads. The intensity of this color depends on the irradiation dose and is a scale for the radical (electron spin) density. The EPR measurements in irradiated ammonia ( $^{14}\text{NH}_3$ ,  $^{14}\text{ND}_3$ ,  $^{15}\text{ND}_3$ ) indicated the existence of the radicals  $^{14}\text{NH}_2^*$ ,  $^{14}\text{ND}_2^*$  and  $^{15}\text{ND}_2^*$  respectively. The differential EPR-absorption spectra are shown in fig. 1, obtained at 80 K with a center field of 3.340 KG\*. The broadening of the EPR-lines are due to hyperfine interactions of the electron with the surrounding hydrogen (deuteron) and nitrogen ( $^{14}\text{N}$  and  $^{15}\text{N}$  resp.) nuclei. The corresponding integrated spectra are also shown in fig. 1. The shape and width is used for calculations, which are discussed in section 8. EPR-studies in one fragment of  $^{15}\text{ND}_3$  clearly indicate the crystalline structure of the slowly frozen material /12/.

\* Measured at: Bruker Analytische Meßtechnik GmbH, West-Germany

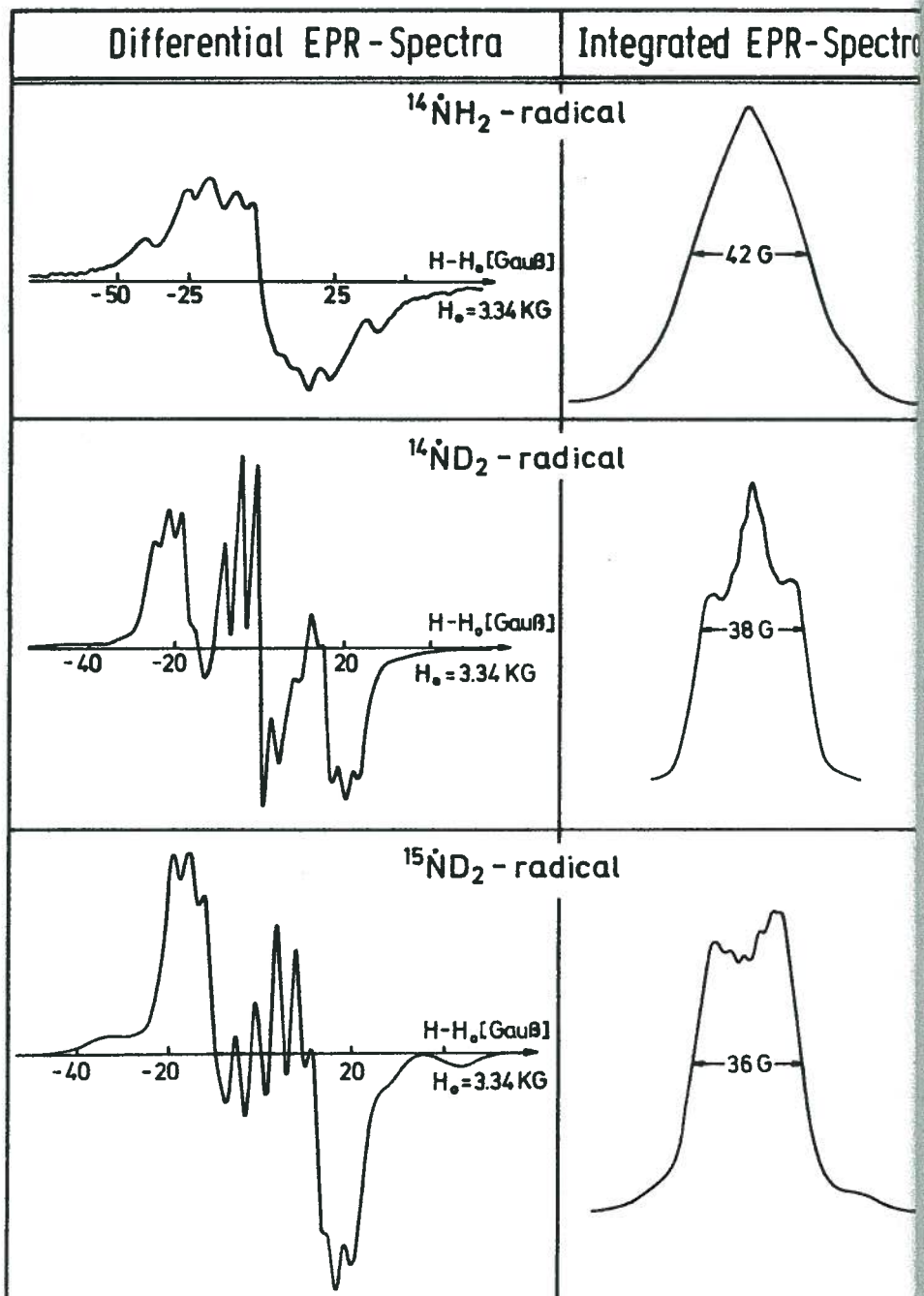


Fig. 1: Differential and integrated EPR absorption spectra of  $^{14}\dot{\text{N}}\text{H}_2$ ,  $^{14}\dot{\text{N}}\text{D}_2$ , and  $^{15}\dot{\text{N}}\text{D}_2$  radicals. The structure of the EPR lines is due to hyperfine interactions of the electron with surrounding nuclei.

#### 4. Lifetime of radicals and radical concentrations

At room temperature radicals have only a volatile existence because they react very rapidly either by themselves or with other molecules. However, at liquid  $\text{N}_2$  temperatures they are more or less chemically stable. After some weeks the  $^{14}\text{NH}_3$  material, kept under liquid  $\text{N}_2$ , became paler thus indicating a loss of radicals. In  $^{14}\text{ND}_3$  this effect could not be observed as clearly as in  $^{14}\text{NH}_3$ . The amine radical  $^{14}\dot{\text{N}}\text{H}_2$  completely disappears at temperatures higher than 117 K. The complete loss of the violet color in  $\text{ND}_3$  occurs at 134 K. Other radicals like  $\dot{\text{H}}$  or the hydrazino radical  $\dot{\text{N}}_2\text{H}_3$  are not stable at the production temperature of 90 K.

The lifetime of the radicals can be checked by measuring the nucleon spin relaxation time  $T_p$  or the polarization build-up time  $\tau$ . The change of the polarization build-up time  $\tau$  and the relaxation time  $T_p$  confirmed also, that the radicals could not be conserved completely at 77 K. However, in the case of  $^{14}\text{ND}_3$   $\tau$  and  $T_p$  increased by only a factor of 2 in a sample kept under liquid  $\text{N}_2$  for 2.5 years. For  $^{14}\text{NH}_3$  some values are given in table 1. With the  $T_p$  value in table 1 the radical spin density  $N_e$  at the beginning was calculated to be  $1.2 \times 10^{20}$  spins/ml, using the relation  $T_p \sim T_e N_e^{-1}$  and comparing  $T_p$  with relaxation measurements in a target material of known radical density (propanediol).

Table 1  
Results in  $^{14}\text{NH}_3$  at 1 K.

Time after irradiation	P [%]	$\tau$ [min]	$T_p$ [min]	$N_e$ [radical spins/ml]
1 day <sup>a)</sup>	31	2	8	$1.2 \times 10^{20}$
5 weeks <sup>a)</sup>	31	2.5	10	$9.6 \times 10^{19}$
1.5 years <sup>b)</sup>	35	6.5	23	$4.2 \times 10^{19}$

a, b) Measurements performed with a  $(3000 \text{ m}^3/\text{h})^{\text{a}}$  and  $(8000 \text{ m}^3/\text{h})^{\text{b}}$  pumping system.

Some samples of  $^{14}\text{NH}_3$  were studied with the purpose to find out the optimal radical density for the DNP. The samples were irradiated for 3, 6 and 10 h, respectively, under the same beam conditions. At that time a faraday cup was not available to measure the accumulated charge. Improvements are in pro-

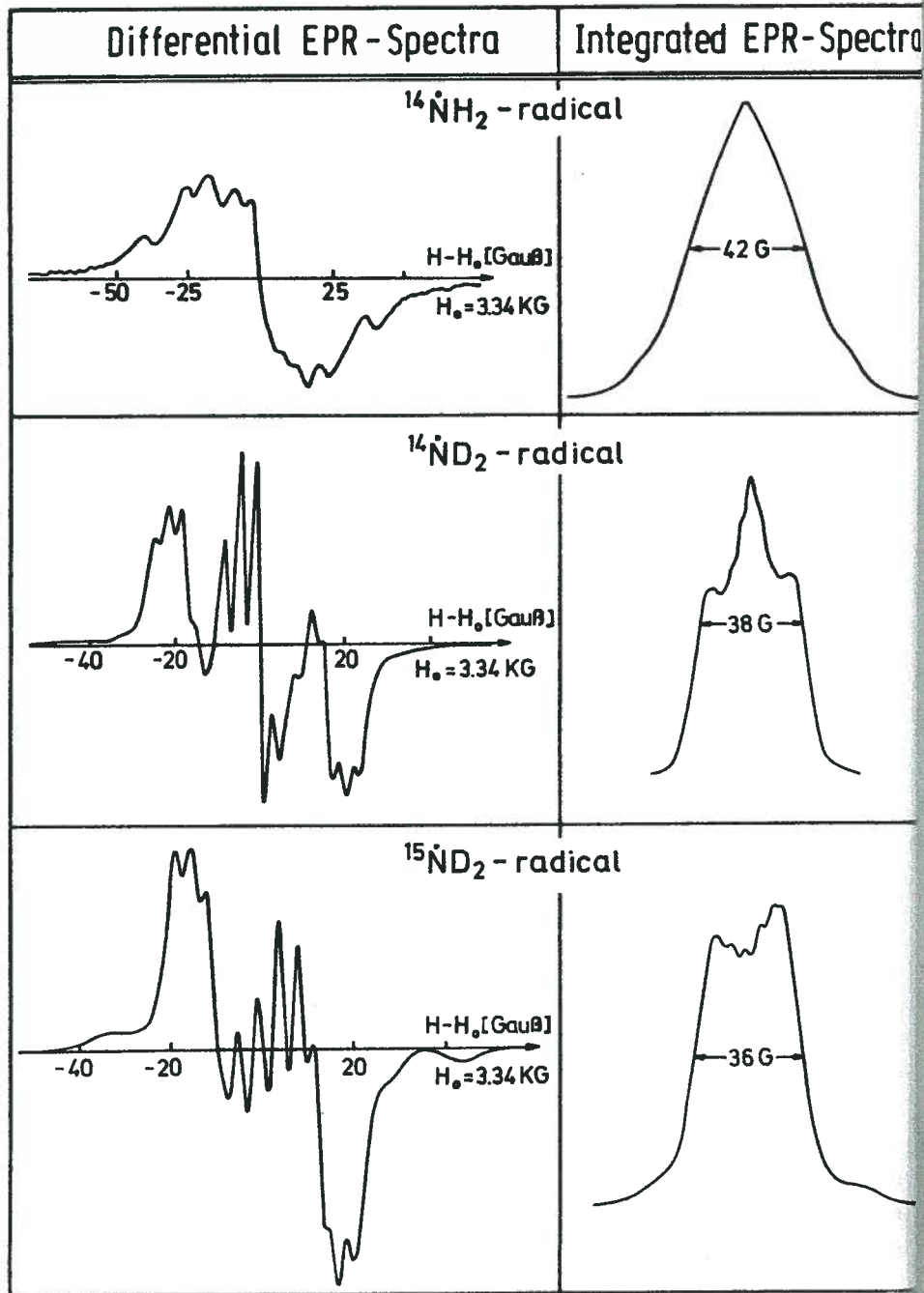


Fig. 1: Differential and integrated EPR absorption spectra of  $^{14}\dot{\text{N}}\text{H}_2$ ,  $^{14}\dot{\text{N}}\text{D}_2$ , and  $^{15}\dot{\text{N}}\text{D}_2$  radicals. The structure of the EPR lines is due to hyperfine interactions of the electron with surrounding nuclei.

#### 4. Lifetime of radicals and radical concentrations

At room temperature radicals have only a volatile existence because they react very rapidly either by themselves or with other molecules. However, at liquid  $\text{N}_2$  temperatures they are more or less chemically stable. After some weeks the  $^{14}\text{NH}_3$  material, kept under liquid  $\text{N}_2$ , became paler thus indicating a loss of radicals. In  $^{14}\text{ND}_3$  this effect could not be observed as clearly as in  $^{14}\text{NH}_3$ . The amine radical  $^{14}\dot{\text{N}}\text{H}_2$  completely disappears at temperatures higher than 117 K. The complete loss of the violet color in  $\text{ND}_3$  occurs at 134 K. Other radicals like  $\dot{\text{H}}$  or the hydrazino radical  $\dot{\text{N}}_2\text{H}_3$  are not stable at the production temperature of 90 K.

The lifetime of the radicals can be checked by measuring the nucleon spin relaxation time  $T_p$  or the polarization build-up time  $\tau$ . The change of the polarization build-up time  $\tau$  and the relaxation time  $T_p$  confirmed also, that the radicals could not be conserved completely at 77 K. However, in the case of  $^{14}\text{ND}_3$   $\tau$  and  $T_p$  increased by only a factor of 2 in a sample kept under liquid  $\text{N}_2$  for 2.5 years. For  $^{14}\text{NH}_3$  some values are given in table 1. With the  $T_p$  value in table 1 the radical spin density  $N_e$  at the beginning was calculated to be  $1.2 \times 10^{20}$  spins/ml, using the relation  $T_p \sim T_e N_e^{-1}$  and comparing  $T_p$  with relaxation measurements in a target material of known radical density (propanediol).

Table 1  
Results in  $^{14}\text{NH}_3$  at 1 K.

Time after irradiation	P [%]	$\tau$ [min]	$T_p$ [min]	$N_e$ [radical spins/ml]
1 day <sup>a)</sup>	31	2	8	$1.2 \times 10^{20}$
5 weeks <sup>a)</sup>	31	2.5	10	$9.6 \times 10^{19}$
1.5 years <sup>b)</sup>	35	6.5	23	$4.2 \times 10^{19}$

a, b) Measurements performed with a  $(3000 \text{ m}^3/\text{h})^{\text{a)}}$  and  $(8000 \text{ m}^3/\text{h})^{\text{b)}}$  pumping system.

Some samples of  $^{14}\text{NH}_3$  were studied with the purpose to find out the optimal radical density for the DNP. The samples were irradiated for 3,6 and 10 h, respectively, under the same beam conditions. At that time a faraday cup was not available to measure the accumulated charge. Improvements are in pro-

gress /5/. The polarization results together with the relaxation time and the polarization build-up time are listed in table 2.

Table 2  
Results in  $^{14}\text{NH}_3$  at 1 K after different irradiation doses.

Sample	P+ [%]	P- [%]	$\tau$ [min]	$T_p$ [min]	$N_e$ [radical spins/ml]
A	36.5	33.5	9.5	23.5	$4.8 \times 10^{19}$
B	38.9	35.0	4.7	18.3	$6.1 \times 10^{19}$
C	37.2	32.6	-	16.5	$6.9 \times 10^{19}$

It can be seen that the optimal radical density is about  $6 \times 10^{19}$  spins/ml and that the positive polarization is always higher than the negative one. To change the radical density, parts of the samples were annealed at 100 K. In all cases the maximum polarization decreased compared to the polarization obtained in the original sample. The chemical reaction  $2 \cdot\text{NH}_2 + \text{N}_2\text{H}_4$  might be responsible for this behaviour.

At 'low temperature' irradiation measurements the following relation between proton relaxation time  $T_p$ , radical density  $N_e$  and irradiation dose was assumed.

$$T_p \sim 1/N_e \sim 1/\text{dose} \quad (I)$$

Seely /13/ specified  $T_p = (\text{dose})^{-0.95 \pm 0.05}$

In our case this linear relation could not be confirmed, as can be seen in fig. 2. In the case of the Slac measurements (Seely) the shortest relaxation time was 24 minutes. However, it is not probable that the relation (I) is only valid up to this value (see table 2). On the contrary, at the 'high temperature' irradiation (90 K), recombination processes, e.g.  $\cdot\text{NH}_2 + \cdot\text{H} \rightarrow \text{NH}_3$  must be considered, which is certainly suppressed at temperatures of 1 K ('low temperature' irradiation). Detailed information about these studies can be found in Ref. 9.

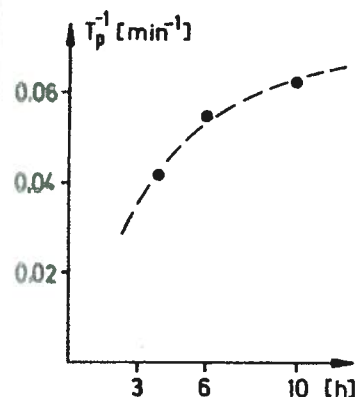


Fig. 2: Inverse proton relaxation time as function of the irradiation time (dose).

### 3. Frequency dependence of the proton polarization in $^{14}\text{NH}_3$

As pointed out by Borghini and Scheffler, different mechanisms of DNP can be distinguished by comparing the polarizations of two (or more) kinds of nuclei in one material /14/. In  $^{14}\text{ND}_3$  this can be done by measuring the  $^{14}\text{N}$ - and the proton polarization. However, our NMR-system was not equipped to detect the nitrogen polarization signal. Therefore we tried to obtain information only from the proton polarization measurement. In the case of EST among the  $^{14}\text{N}$ -nuclei (spin 1) and protons, the  $^{14}\text{N}$ -polarization, which is very difficult to measure (see section 7), can be calculated. The result of the proton polarization measurements is shown in fig. 1. The radical spin density in the sample was  $4.2 \times 10^{19}$  spins/ml. The optimum microwave frequencies were 69.970 GHz for the positive and 70.290 GHz for the negative polarization. The frequency accuracy of  $\pm 2$  MHz is limited by the drift of the microwave generator (carcinotron).

However, it is difficult to distinguish between different DNP mechanisms from the shape of the polarization curve as a function of the microwave frequency unless the EPR-line width is narrow compared to the nuclear Larmor frequency (106 MHz for protons at 25 KG). A fit to the frequency dependence of DNP, assuming a differential solid state effect (DSSE) model, was made /15/. The best fit is also shown in fig. 3. Complete agreement between measured polarization and calculated one could not be reached in this model. Especially the polarization values in the outer parts of the curve could not be fitted without additional assumptions. We believe that in the present sample - as in the case of butanol, chemically doped with porphyrine - the EST-hypothesis must be considered to describe the DNP in irradiated  $^{14}\text{NH}_3$ .

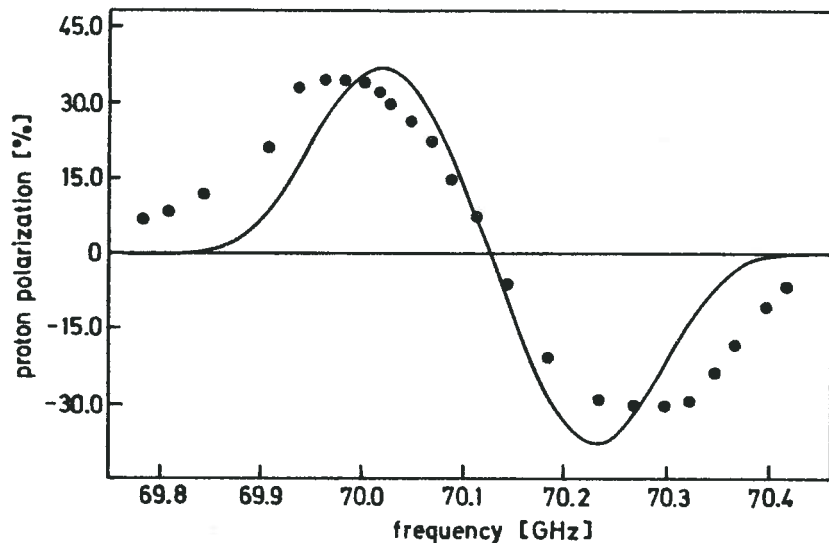


Fig. 3: Measurement of the frequency dependence of DNP in  $^{14}\text{NH}_3$  (solid circles) with a fit (solid line) based on the DSSE, using the measured EPR-spectrum

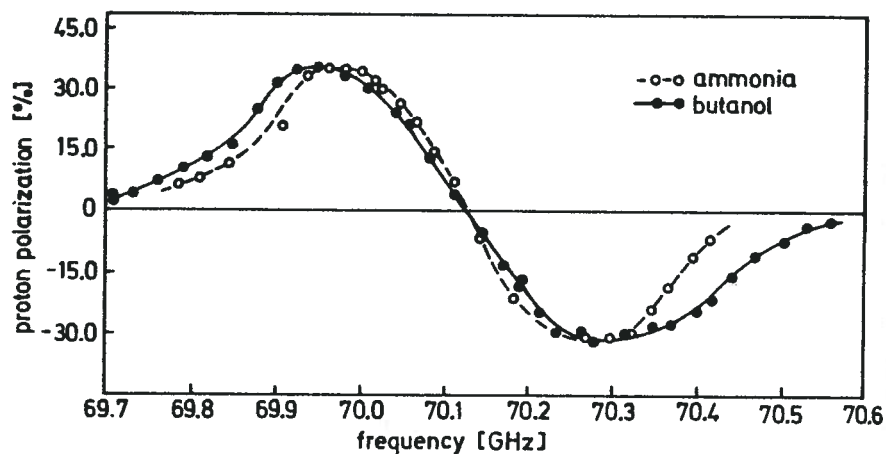


Fig. 4: Measurement of the frequency dependence of DNP in irradiated  $^{14}\text{NH}_3$  (open circles) and in butanol (solid circles). Lines are drawn to guide the eye.

A comparison of the  $^{14}\text{NH}_3$ -polarization with the polarization data of butanol as a function of the microwave frequencies is shown in fig. 4. The butanol data (from Ref. 16) are fitted to the center frequency of the  $^{14}\text{NH}_3$  curve

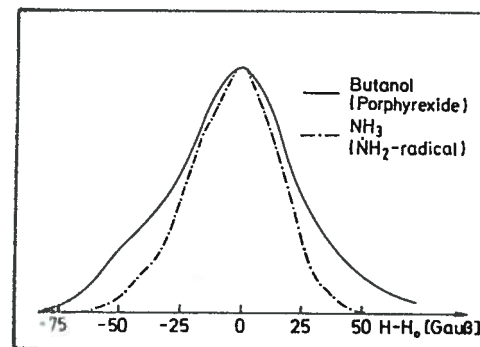


Fig. 5: EPR-spectrum of  $^{14}\text{NH}_2$  radical in  $^{14}\text{NH}_3$  (dashed line). In comparison the EPR-spectrum of porphyraxide (from Ref. 16) dissolved in butanol (solid line).

and normalized to the maximum positive polarization of  $^{14}\text{NH}_3$ . The separation of the polarization maxima are almost equal, 350 MHz for butanol compared to 320 ± 10 MHz for  $^{14}\text{NH}_3$ . The overall shape of the polarization curve in butanol, however, is broader as expected from the broader EPR-line in this material. The EPR-line of the  $^{14}\text{NH}_2$  radical in ammonia is shown in fig. 5 together with the EPR-line from porphyraxide dissolved in butanol. The EPR-spectrum of  $^{14}\text{NH}_2$  was measured at ~80 K and  $H_0 = 3.34$  KG. The EPR-spectrum of porphyraxide was obtained at 1 K in a magnetic field of 25 KG. Here the broadening of the EPR-spectrum is assumed to result from g-factor anisotropy [16], whereas in  $^{14}\text{NH}_3$  we have hfs-broadening (see fig. 1). Even though the two target materials butanol and ammonia seem to be different due to different ways of producing the radicals, they are really very similar under the aspect of DNP-behaviour. More information about the DNP-mechanism in irradiated  $^{14}\text{NH}_3$  was obtained by a direct comparison of the polarization

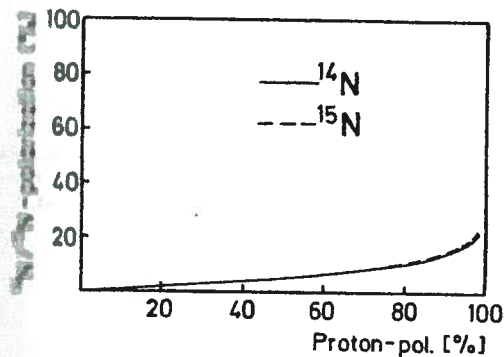


Fig. 6:  $^{14}\text{N}$ - and  $^{15}\text{N}$ -polarization as function of the proton polarization, calculated under the assumption of equal spin temperatures.

(and the corresponding spin temperatures) of protons and nitrogen nuclei in the sample /8/. These measurements confirm that the protons and  $^{14}\text{N}$ -nuclei have equal spin temperatures. In case of 90% proton polarization (obtained in dilution refrigerators) the  $^{14}\text{N}$ -polarization is 15% as can be seen from fig. 6.

#### 6. Frequency dependence of the polarization of deuterons and protons in $^{14}\text{ND}_3$

The nuclear Larmor frequencies of the deuteron (16.34 MHz at 25 KG) and the  $^{14}\text{N}$ -nucleus (7.79 MHz) are both small compared to that of the proton (106.34 MHz). If EST among protons and deuterons in  $\text{ND}_3$  can be established, the same polarization behaviour should be valid also for protons and  $^{14}\text{N}$ -nuclei. In this case, the difficult  $^{14}\text{N}$ -polarization determination could be avoided.

We measured the polarization of the deuterons and unsubstituted protons (1%) in  $^{14}\text{ND}_3$ . The results are shown in figs. 7 and 8. The optimum microwave frequencies are 70.095 GHz for positive and 70.200 GHz for negative deuteron polarization. The magnetic field corresponds to a DMR-frequency of 16.340 MHz for the deuterons.

The curve shown in fig. 7 for the deuterons is asymmetric with respect to the center frequency. More details about this phenomenon is given in the Appendix.

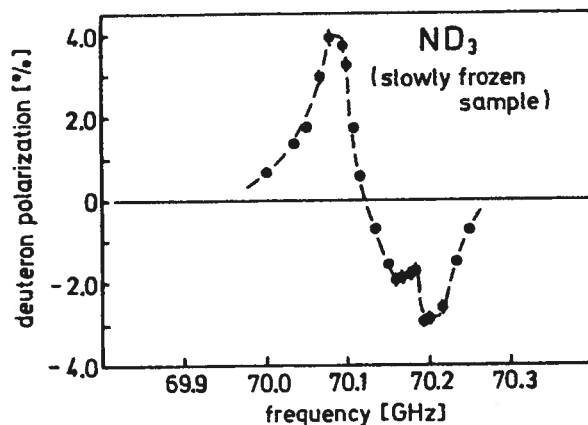


Fig. 7: Frequency dependence of DNP of deuterons in  $^{14}\text{ND}_3$ , measured in a slowly frozen sample at 1 K.

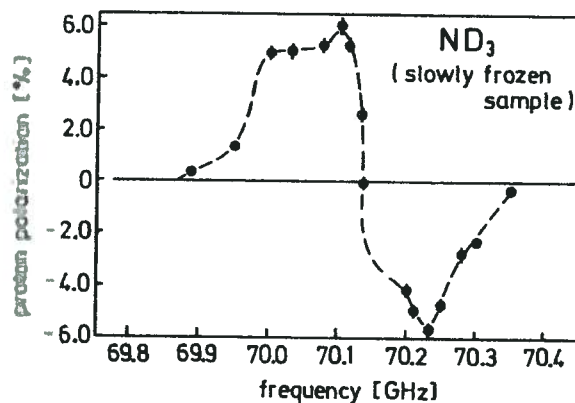


Fig. 8: Frequency dependence of DNP of the unsubstituted protons in  $^{14}\text{ND}_3$  (slowly frozen sample)

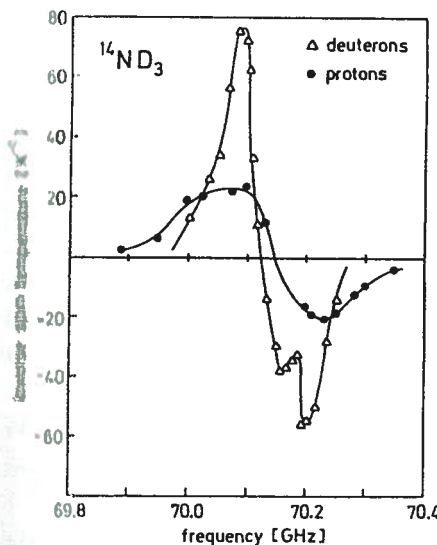


Fig. 9: Inverse spin temperatures of deuterons and protons in  $^{14}\text{ND}_3$ , calculated under the assumption of thermal equilibria in the spin systems.

The frequency dependence of the polarization of the unsubstituted protons (fig. 8) is completely different. There is a broad maximum (especially for positive polarizations) with a small enhancement at about the optimum frequencies for the deuteron polarization. In fig. 9 the inverse spin temperatures of the deuterons and unsubstituted protons are plotted. It becomes obvious that the proton- and the deuteron polarization in  $^{14}\text{ND}_3$  are not governed by equal spin temperatures. This implicates some consequences: (1) The deuteron polarization in  $^{14}\text{ND}_3$  must be calibrated with the thermal equilibrium (T.E.) signal. This is also due to the complicated signal shape (see Appendix). (2) The nitrogen polarization of the  $^{14}\text{N}$ -nuclei must be measured.

### 7. Deuteron and proton polarization in $^{15}\text{ND}_3$

The detection of the NMR-signal of the  $^{14}\text{N}$ -nuclei is extremely difficult as the magnetic moment of the  $^{14}\text{N}$ -nucleus (spin 1) is very small and the quadrupolmoment is much larger than that of the deuteron. At present an absolute polarization calibration by the thermal equilibrium (T.E.) signal is impossible. However, the NMR-detection of the  $^{15}\text{N}$ -nuclei (spin 1/2) should be much easier, because there is no quadrupolmoment, which broadens the NMR-signal. A comparison of the Landé-factor  $g_n$ , the quadrupolmoment  $Q$  and the resonance frequency  $\nu_n$  at 25 KG and 37.9 KG for  $^{14}\text{N}$ ,  $^{15}\text{N}$  and D is made in table 3.

Table 3

Comparison of some values for  $^{14}\text{N}$ ,  $^{15}\text{N}$  and  $^2\text{D}$

	$g_n$	$Q$ [e x $10^{-24}$ cm $^2$ ]	$\nu_n$ [MHz] at 25 KG	$\nu_n$ [MHz] at 37.9 KG
$^2\text{D}$	0.8574	$2.73 \times 10^{-3}$	16.34	24.84
$^{14}\text{N}$	0.4035	$1.6 \times 10^{-2}$	7.69	11.68
$^{15}\text{N}$	-0.566	-	10.79	16.34

Polarization studies in  $^{15}\text{ND}_3$  were performed with the aim to learn more about the  $^{14}\text{N}$ -polarization in  $^{14}\text{ND}_3$ . The material (very expensive) used has a  $^{15}\text{N}$ -enrichment of 95% and a D-enrichment of 98%. The frequency dependence of the polarization of the deuterons and the unsubstituted protons (2%) in  $^{15}\text{ND}_3$  was measured. The results clearly show that the deuterons and protons do not have equal spin temperatures (fig.10) as in the case of  $^{14}\text{ND}_3$ . The similarity to  $^{14}\text{ND}_3$  (see fig.9) is evident. This could be expected, if we compare the EPR-lines of the radicals  $^{14}\text{ND}_2$  and  $^{15}\text{ND}_2$  (see fig.1). The EPR-line width - one important quantity for calculations using different DNP-models - are almost equal.

Also the maximum deuteron polarization, obtained in both materials ('high temperature' irradiated) is comparable:  $-28.5 \pm 1.5\%$  for  $^{15}\text{ND}_3$  and  $-29 \pm 1.5\%$  in the case of  $^{14}\text{ND}_3$  as measured at  $\sim 200$  mK.

First nitrogen polarization studies in  $^{14}\text{ND}_3$ , performed in Liverpool, give hints that - in contrast to the protons - the deuterons and the nitrogen nuclei have equal spin temperatures /8/. If this is also confirmed in

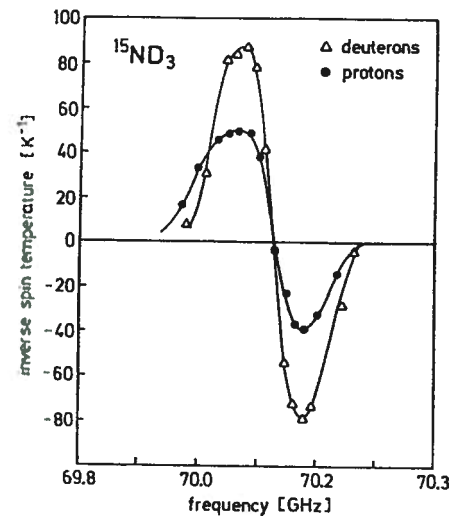


Fig.10: Inverse spin temperatures of deuterons and protons in  $^{15}\text{ND}_3$

$^{15}\text{ND}_3$ , which can be done with better accuracy compared to  $^{14}\text{ND}_3$ , the nitrogen polarization in  $^{14}\text{ND}_3$  and  $^{15}\text{ND}_3$  is almost equal at a given deuteron polarization  $P_D$ . This can be seen in fig. 11, where the deuteron and nitrogen polarization for  $^{14}\text{ND}_3$  and  $^{15}\text{ND}_3$  is plotted assuming EST for the corresponding nuclei. At a deuteron polarization of 30%, achieved in 'high temperature' irradiated material, we have 15% nitrogen polarization.

$^{15}\text{N}$ -polarization measurements are planned in a dilution refrigerator and in a magnetic field of 37.9 KG. Using a frozen spin mode, the deuteron and nitrogen polarization in  $^{15}\text{ND}_3$  can be measured without change of the NMR-equipment (see table 3).

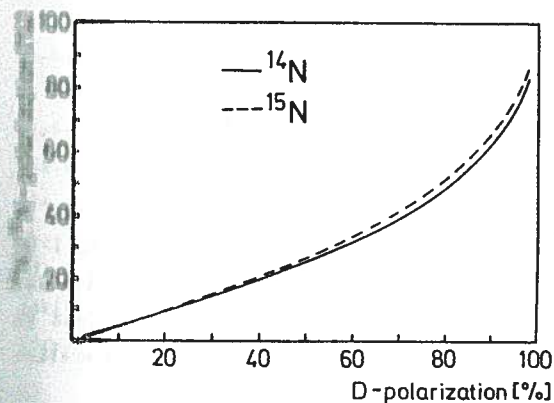


Fig.11:  $^{14}\text{N}$ - and  $^{15}\text{N}$ -polarization as function of the deuteron polarization, calculated under the assumption of equal spin temperatures.

## 8. Polarization mechanism in $^{14}\text{ND}_3$

From fig.9 it can be seen that protons and deuterons in  $^{14}\text{ND}_3$  do not have equal spin temperatures. Also the different microwave frequencies for optimum polarizations disagree with the EST-model. A plot of the two polarizations (protons and deuterons) shows similarity with calculated curves based on the differential solid state effect (DSSE) model /15/. It was therefore attempted to reproduce the measured frequency dependence by fitting the parameters of the model to the data obtained for the shock-frozen sample. For this sample the width and the shape of the EPR-spectrum is known (see fig.1). With the obtained EPR-absorption spectrum inserted into the calculations the width of the polarization curve is well described (fig.12). Various assumptions were made, both for the theoretical model and experimental quantities. Therefore, the comparison with the curves based on the DSSE model should be considered as a qualitative one. However, the qualitative behaviour shows that the DSSE must be considered as one of the possible polarization mechanisms in 'high temperature' irradiated  $^{14}\text{ND}_3$  at 1 K.

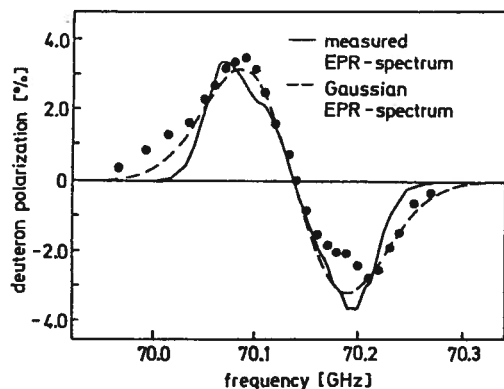


Fig.12: Comparison of the measured and calculated frequency dependence of the deuteron DNP in  $^{14}\text{ND}_3$ , based on the differential solid state effect.

## 9. Conclusion

Some properties of ammonia as improved target material for the use in high or intermediate energy physics experiments have been studied at 1 K. The radical production by irradiation at 90 K ('high temperature' irradiation) is a successful method to reproduce high polarization (obtained in dilution refrigerators) in ammonia. As practical target materials in scatter-

ring experiments  $^{14}\text{NH}_3$  and  $^{14}\text{ND}_3$  are used. A proton polarization in  $^{14}\text{NH}_3$  to 85% /3/ and a deuteron polarization as high as 44% /5/ were measured in dilution refrigerators. However, in some types of experiments the polarization of the N-nuclei may produce difficulties.

Polarization studies in  $^{15}\text{ND}_3$  have been performed to learn more about the nitrogen polarization, which are done easier in this material than in  $^{14}\text{ND}_3$ . However, to use the results for the  $^{14}\text{N}$ -polarization determined from the DNP behaviour in both materials must be studied.

The measurement in  $^{14}\text{NH}_3$  indicates indirectly, that the EST-theory is applicable in this material. Thus the  $^{14}\text{N}$ -polarization is calculable. This was confirmed by measurements of the  $^{14}\text{N}$ -polarization, performed in L. Pool /8/. In  $^{14}\text{ND}_3$  EST between deuterons and unsubstituted protons is observed, whereas  $^{14}\text{N}$ -polarization measurements show /8/, that the deuterons and the  $^{14}\text{N}$ -nuclei have equal spin temperatures. Such a behaviour can be checked with better accuracy in  $^{15}\text{ND}_3$ . First polarization results from  $^{15}\text{ND}_3$  indicate, that both materials are similar under the aspect of DNP behaviour. The polarization results obtained in  $^{15}\text{ND}_3$  can be used for the  $^{14}\text{N}$ -polarization determination.

It should be mentioned, that the conclusions concerning the polarization mechanisms, made at 1 K, must be used with care at lower temperatures. If the EPR-line is broadened by hyperfine interaction a deformation and displacement of the line is predicted, when the nuclear polarization is high /17/.

In any case the EPR line is influenced by further irradiation and by the scattering experiments, where new radicals are produced. In such a case - additional 'low temperature' irradiation - the prevailing polarization mechanism may be different compared to that of 'high temperature' irradiation material.

At low temperatures the polarization obtained in irradiated ammonia is higher than that obtained in butanol and comparable to the polarization values in propanediol. In addition, the content of polarizable nuclei is higher than that of the alcohol materials. As also the polarization resistance to radiation damage in ammonia is excellent /7/,  $^{14}\text{NH}_3$  and  $^{14}\text{ND}_3$  are about to replace the alcohol materials in high and intermediate energy physics experiments /2/ /3/ /5/. For the photodisintegration reaction  $\gamma + \text{pn}$ , using  $^{14}\text{ND}_3$  as target material, the problems with the  $^{14}\text{N}$ -polarization is reduced to a very low level by a subtraction measurement, performed with polarized  $^{14}\text{NH}_3$  /18/.

The strange DMR-signal of deuterated ammonia, discussed in the Appendix, does not affect the accuracy of the polarization determination. Up to now we know of no conclusive theory which can explain all the observed phenomena concerning the DMR-signal without contradiction. Detailed structure studies of ammonia including quadrupole resonance measurements at low temperature (1 K) are needed. As far as we know, such measurements do not exist. In addition, the radiation chemistry at these temperatures is also unknown.

## Appendix

### A. Deuteron polarization signal shape in $\text{ND}_3$

In the course of our polarization studies we observed some effects concerning the DMR-signal, which may be of interest for the interpretation of the structure of ammonia at very low temperatures (<1 K).

The deuteron magnetic resonance (DMR) signal for particles with spin 1 is more complicated than that for protons ( $I = 1/2$ ) because of the additional interaction of the deuteron quadrupole moment with the electric field gradient. A typical DMR-signal of irradiated  $^{14}\text{ND}_3$  is shown in fig. 13. Its clearly deviates from the theoretical signal shape, but can be explained by the simple assumption, that a wide and a narrow signal component are superimposed. At smaller polarization values, as shown in fig. 14, the peaks belonging to the wider component are clearly resolved from the main peaks of the narrow component. The total width of the signal should be given by the width of the wider component. The peak positions of this wider component can thus be determined. They explain the unfamiliar bulges at the outer flanks of the main peaks of the narrow component.

Obviously the two single components must originate from the fact that two groups of deuterons are located in different electric field gradients. However, solid ammonia has one of the simplest molecular structures. The molecules are bound together by rather weak hydrogen (deuterium) bonds involving the lone pair of electrons, which with the three H(D)-atoms make up an almost regular rigid tetrahedron around the N-atom. Since the three deuterons inside the ammonia molecule are equivalent with respect to their bond to the nitrogen atom this effect must be an intermolecular one. During the reversal of the polarization it was observed that the wide component of the signal reverses faster than the narrow one. This means in our simple picture that the group of deuterons seeing a higher field gradient relaxes faster. A relaxation plot of the DNP is shown in fig. 15. The double expo-

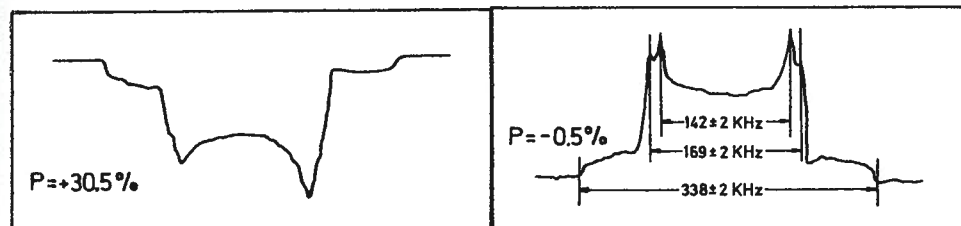


Fig.13: Dynamically enhances DMR-signal in 'high temperature' irradiated  $^{14}\text{ND}_3$ , obtained in a dilution refrigerator at 200 mK.

Fig.14: DMR-signal in  $^{14}\text{ND}_3$ , taken during the build-up of the polarization.

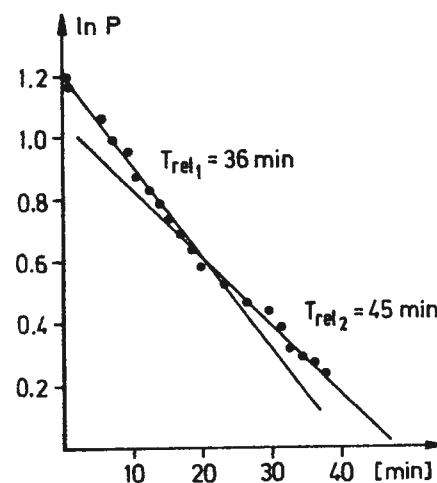


Fig.15: Relaxation measurements of DNP in  $^{14}\text{ND}_3$  at 1 K.

ponential behaviour of the relaxation could be explained by these different relaxations of the deuterons. It should be noted that in  $^{14}\text{NH}_3$  an apparent relaxation behaviour of the proton polarization was observed.

The value of the quadrupole coupling constant,  $e^2qQ/h$ , was calculated from the relation  $\nu_Q = 3e^2qQ \cdot 2I(2I-1)/h$ , where  $\nu_Q/2$  corresponds to the peak-to-peak separation on the DMR-signal. The value of  $e^2qQ/h$  for  $\text{ND}_3$  at 1 K was found to be  $189.3 \pm 2$  KHz (inner peak in fig. 14). This value is much higher than those reported from measurements at 75 K /19/.

Hewat and Riekel examined the structure of  $^{14}\text{ND}_3$  at 2 K and at higher temperatures /20/. The unit cell of ammonia is cubic with 4 molecules per cell. The D-atoms are bonded covalent to their N-atom and build a deuterium bond to the next N-atom. The distance is equal for all 3 deuterons

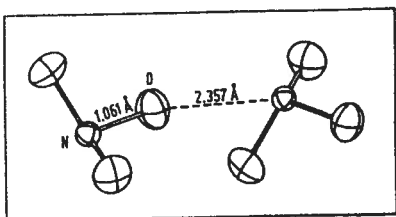


Fig.16: Thermal ellipsoids of  $^{14}\text{ND}_3$  (from Ref.20) showing strong well defined librations even at 2 K (see text)..

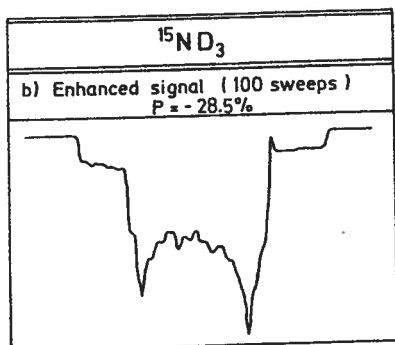


Fig.17: Dynamically enhanced DMR-signal in  $^{15}\text{ND}_3$ , obtained at 200 mK.

( $d = 1.061 \text{ \AA}$ ) and  $d = 2.357 \text{ \AA}$  for the deuterium bond. These values were obtained at 2 K after corrections of the bond length owing to strong librational motion (see fig. 16). How far these results can be transferred to temperatures below 1 K is unknown /21/. Measurements of the crystal structure at that temperature are needed. Nevertheless, the existence of more than two main peaks in the DMR-signal shape suggest two different electric field gradients, which can be produced e.g. by different bond lengths. Another possibility could be an anisotropy of the electric field gradient. The twofold structure of the DMR-signal was also clearly marked in a crystalline  $^{14}\text{ND}_3$  sample, frozen in one block /22/. Calculations, based on the assumption of an anisotropy of the electric field gradient in  $^{14}\text{ND}_3$  are presented in Ref. 23. Typical for DMR-signals obtained from slowly frozen samples are

additional small structures as shown in fig. 17. Since these structures are not seen on the baseline of the DMR-signal they cannot be due to electronic noise. Obviously there are single crystal regions, where some orientations of the electric field gradient are preferred. In contrast to the slowly frozen samples, DMR-signals obtained from shock-frozen samples show a smooth signal form, which points to its polycrystalline structure.

## B. DMR-signals at different microwave frequencies

As can be seen from fig.7, the curve of the frequency dependence of the deuteron polarization is asymmetric.

A double peak structure in the frequency dependence of the polarization was also observed for alcohol materials doped with BDPA, a free radical /24/. However, this effect was symmetric with respect to the center microwave frequency and was explained by the influence of two different polarization mechanisms.

In our case, the double peak structure of the negative polarization values is correlated with a change of the signal shape of the DMR-signal. At the maximum polarization value the narrow component of the DMR-signal is clearly evident (see fig.18), whereas at the smaller peak around 70.165 GHz the contribution of the wider part of the DMR-signal is significantly enlarged, as marked by arrows in fig.18. This change of the polarization signal shape is also observed for the positive polarization values. It seems, however, that here the contribution of the two components of the signal is optimal at about the same frequency. To explain these results a speculative model was made /9/. The basic idea is to assume two different crystal structures in  $^{14}\text{ND}_3$  at 1 K: a unit cell of cubic form, which is known at higher temperatures and another one. At the moment it is also unknown how far other effects like the nitrogen polarization or the molecule spin isomerism must be considered to explain all the observations without contradiction.

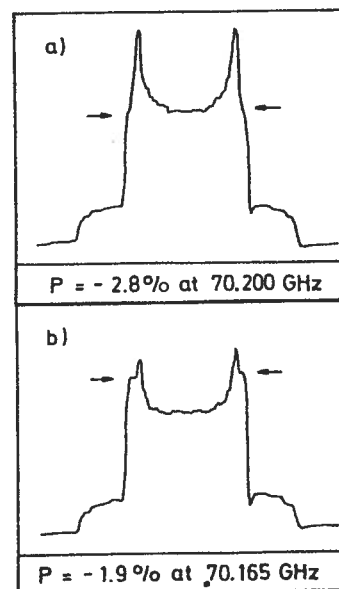


Fig.18: DMR-signals at different microwave frequencies (a) at the maximum negative polarization (b) at the smaller peak around 70.165 GHz (see fig. 7).

## References

- /1/ T.O. Niinikoski and J.M. Rieubland, Phys. Lett. 72A(1979)141
- /2/ D. Crabb, in these Proceedings
- /3/ G. Court, in these Proceedings
- /4/ U. Härtel, O. Kaul, W. Meyer, K. Rennings and E. Schilling, Proc. Conf. on High energy physics with polarized beams and targets, eds., C. Joseph and J. Soffer (Birkhäuser, Basel, 1981) p. 451
- /5/ E. Schilling, in these Proceedings  
W. Meyer et al., Nucl. Instr. and Meth. 227(1984)35
- /6/ M. Seely et al., Proc. Conf. on High energy spin physics, ed., G.M. Bunce, AIP Conf. Proc. no. 95, Part. and Fields Subs. no. 28(1982)  
M. Seely et al., Nucl. Instr. and Meth. 201(1982)303
- /7/ U. Hartfiel, in these Proceedings
- /8/ G. Heyes, in these Proceedings
- /9/ G. Sternal, Staatsexamensarbeit, BONN-IR-84-07
- /10/ W. Havenith, Staatsexamensarbeit, BONN-IR-84-08
- /11/ S. Brown, in these Proceedings
- /12/ W. Thiel, Diplomarbeit, Bonn, in preparation
- /13/ M. Seely, Thesis, Slac
- /14/ M. Borghini und K. Scheffler, Phys. Rev. Lett. 26(1971)1362
- /15/ H. Riechert, Diplomarbeit, BONN-IR-82-23
- /16/ S. Mango, Ö. Runolfsson and M. Borghini, Nucl. Instr. and Meth. 72(1970)45
- /17/ A. Abragam and M. Goldman, Nuclear magnetism: order and disorder (Clarendon Press, Oxford, 1982)
- /18/ E. Schilling, Thesis, Bonn, in preparation
- /19/ S.W. Rabideau and P. Waldstein, J. Chem. Phys. 45(1966)4600
- /20/ A.W. Hewat and C. Riekel, Acta Cryst. A35(1979)569
- /21/ C. Riekel, private communication
- /22/ R. Dostert, Diplomarbeit, Bonn, in preparation
- /23/ E. Kohlgarth, Staatsexamensarbeit, Bonn, in preparation
- /24/ M. Borghini, W. de Boer and K. Morimoto, Phys. Lett. 48A(1974)244

THE DYNAMIC POLARISATION OF THE NITROGEN NUCLEI  
IN  $^{14}\text{NH}_3$ ,  $^{15}\text{NH}_3$  AND  $^{14}\text{ND}_3$ 

G.R. Court, W.G. Heyes.

Department of Physics, University of Liverpool,  
P.O. Box 147, Liverpool, L69 3BX,  
United Kingdom.

W. Meyer, W. Thiel.

Physikalisches Institut, Bonn University,  
D5300 Bonn, West Germany.

## 1. Introduction

For many years the best available polarised proton target materials, in terms of both free hydrogen content and radiation damage resistance have been the chemically doped monohydric alcohols. This situation has recently changed because of the development of irradiated ammonia, which has a better performance on both counts. However, the use of this material does introduce one possible new problem because the spectator nuclei ( $^{14}\text{N}$ ), which have spin 1 can also become polarised. This problem does not exist with the alcohols because both spectator nuclei ( $^{12}\text{C}$  and  $^{16}\text{O}$ ) have spin zero. In experiments where it is not possible to distinguish between the scattering from free protons and bound nucleons, such as the CERN EMC experiment, where deep inelastic polarised muon - polarised proton scattering is being studied, it is necessary to have a precise knowledge of the polarisation of the spectator nuclei as well as the protons in the polarised target material. A similar situation can also exist with polarised deuterons in deuterated ammonia.

The polarisation of nitrogen nuclei in both  $^{14}\text{NH}_3$  and  $^{14}\text{ND}_3$  have therefore been investigated in some detail. The measurement of the  $^{14}\text{N}$  polarisation is relatively much more difficult than the measurement of proton or deuteron polarisations because of the small magnetic moment and large quadrupole moment of this nucleus. The latter factor is particularly important as its consequences is a very large NMR line width.<sup>/1/</sup>

The material  $^{15}\text{NH}_3$  has also been investigated. The  $^{15}\text{N}$  nucleus has spin  $1/2$ , and consequently there is no quadrupole broadening and this makes its polarisation much simpler to measure.

## 2. The Spin Temperature Model

The dynamic polarisation process in the alcohol materials has been well explained by the spin temperature model.<sup>/2/</sup> This model predicts that if two nuclear spin species are present in a system, then the nuclear Zeeman reservoirs may be coupled via the electron spin system in the presence of microwave irradiation. It follows that the two nuclear spin systems will be in thermal equilibrium, that is will have equal spin temperature (EST), so that their polarisations can be related using the Brillouin formula.

These predictions have been precisely confirmed for protons and deuterons in the monohydric alcohols<sup>/3/</sup> and protons deuterons and  $^{13}\text{C}$  in dihydric alcohols.<sup>/4/</sup> However, measurements made on the residual protons in  $^{14}\text{ND}_3$ <sup>/5/</sup> suggest that in this case the EST hypothesis does not apply. It is therefore of great interest to test the applicability of the hypothesis to the nitrogen nuclei in ammonia.

### 3. Experimental Technique

The  $^{14}\text{NH}_3$  and  $^{15}\text{NH}_3$  samples were produced by the slow freezing method and were irradiated at liquid nitrogen temperature (77K) in a reactor. The irradiation time was 26 hours at a reactor power of 100KW in a region which provides a mixture of neutron and gamma flux.<sup>7/6/</sup> The estimated radiation dose was 182 Mrad and the relaxation time for both samples was measured to be 18min at 1K.

The  $^{14}\text{ND}_3$  sample was produced using the shock freezing technique and was irradiated at liquid argon temperature (90K) using the electron beam from the injection linac of the Bonn electron synchrotron.<sup>7/5/</sup> Its relaxation time was measured to be 35min at 1K.

The measurement techniques used in the Liverpool materials development facility are described in detail in reference 1. The maximum polarisations recorded for protons were +71% and -86%, and for deuterons -36%. These values are not necessarily the best possible obtainable with these materials, as in general, because of liquid helium supply limitations, it was not possible to run the experiment for long enough periods to reach equilibrium values.

The polarisation growth times for protons were typically 15min from zero 50% and 80min from zero to 75% while for deuterons growth from zero to 36% required 50min. With the  $^{14}\text{N}$  samples the proton or deuteron polarisation was allowed to rise to a given value and the microwave power was switched off. The refrigerator then cooled the sample rapidly to a temperature in the region of 120mK so that the material was in frozen spin state when the nitrogen polarisation measurements were made.<sup>7/1/</sup> This was not necessary with the  $^{15}\text{N}$  sample and so alternate measurements of nitrogen and proton polarisation were obtained during the growth of polarisation under continuous microwave irradiation.

### 4. Experimental Results

The graph in figure 1 shows the relationship between the measured  $^{14}\text{N}$  polarisation and the proton polarisation in  $^{14}\text{NH}_3$ . The solid line is the calculated relationship based on the EST assumption. Fig. 3 shows the data from  $^{15}\text{NH}_3$  presented in the same way, and in both cases the agreement with the calculated values is good. The data showing the residual proton and  $^{14}\text{N}$  polarisation as a function of deuterons polarisation in  $^{14}\text{ND}_3$  is given in figures 5 and 6 respectively. The residual proton polarisation data confirms the results obtained in reference 5 and the agreement with the EST assumption for the nitrogen nuclei still appears to be good.

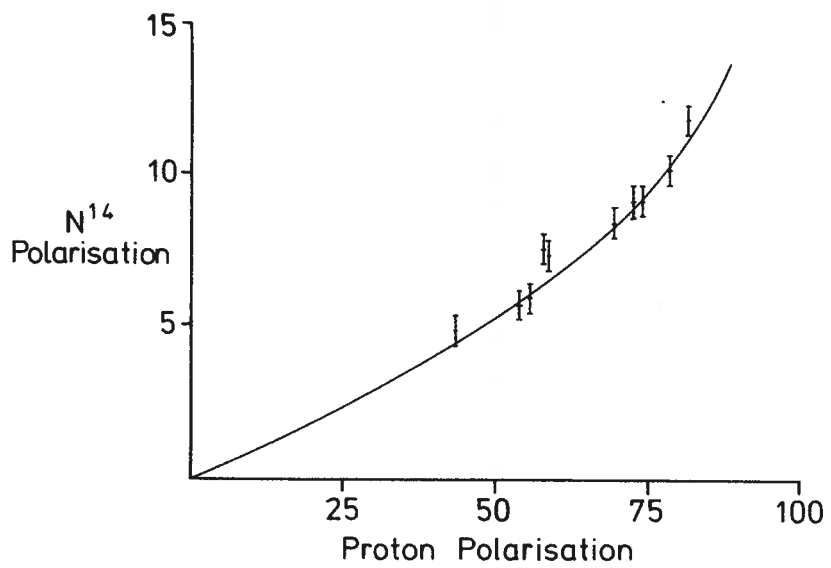
As a further test of the EST assumption the spin coupling relaxation time was measured for the nitrogen nuclei in the three cases. To do this the polarisation of one of the spin species was reduced to a very low value, by saturating its resonance with RF power, when the material was in the frozen spin state. The rate at which the polarisation recovered to its EST equilibrium value in the presence of microwave irradiation, at the optimum frequency and power for normal polarisation growth, was then observed. In principle the polarisation of either species could be destroyed to make this measurement. However because of the very large difference between the energies stored in the two spin reservoirs a much larger and easier to measure effect was obtained by destroying the nitrogen polarisation. No observable coupling between the spins was found in the absence of microwave irradiation at a temperature of 100mK, giving a lower limit on this thermal coupling time constant of 30 hours. The results obtained with microwave irradiation for  $^{14}\text{N}$

and  $^{15}\text{N}$  in  $\text{NH}_3$  and  $^{14}\text{N}$  in  $\text{ND}_3$  are shown in figs. 2,4 and 7 respectively.

As the time constants for both proton cases are very much less than the time constant for polarisation growth the EST assumption fully justified for a proton target. It follows that the nitrogen polarisation can always be calculated from a known proton polarisation. The time constant for the deuterated material is comparable with the growth time constant and so in this case nitrogen polarisation values calculated on the EST assumption can only be used when sufficient time has been allowed for the system to reach equilibrium after any changes in polarisation have been made.

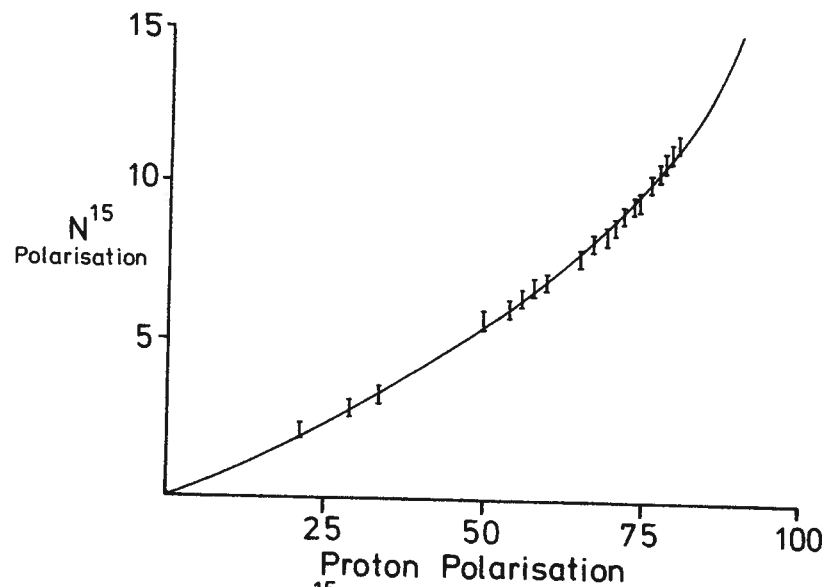
### 5. References

- /1/ G.R. Court, P. Harrison, W.G. Heyes.  
The Liverpool Polarised Target Material Test Facility - these proceeding.
- /2/ M. Borghini. Phys. Lett. 26A 242 (1968).
- /3/ M. Borghini, K. Scheffler. Phys. Rev. Lett. 26 1362 (1971).
- /4/ W. De Boer, M. Borghini, K. Morimoto, R. Niinikoshi, F. Udo.  
J. Low Temp. Phys. 15 249 (1974).
- /5/ W. Meyer, K.M. Al toff, W. Havenith, O. Kaul, H. Riechert, E. Schilling,  
G. Sternal, W. Thiel. Nucl. Inst. Meth. 227 35 (1984).
- /6/ G.R. Court. Proc. of 2nd Workshop on polarised target materials,  
Rutherford Laboratory, 1979, RL80-080, October 1980, p.38.



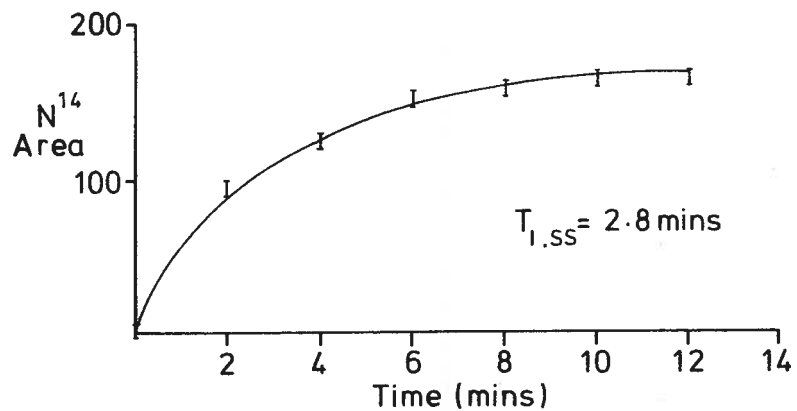
N<sup>14</sup> vs Proton Polarisation

FIGURE 1



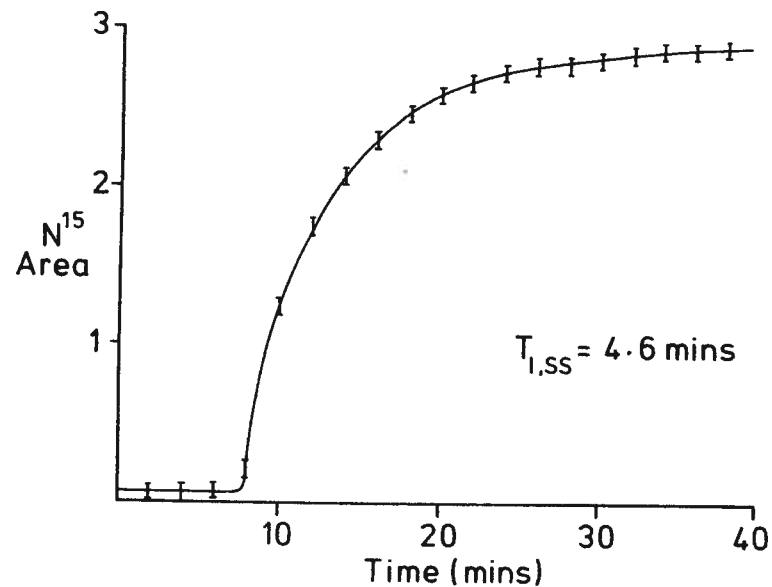
N<sup>15</sup> vs Proton Polarisation

FIGURE 3



Thermal mixing in N<sup>14</sup>H<sub>3</sub>

FIGURE 2



Thermal mixing in N<sup>15</sup>H<sub>3</sub>

FIGURE 4

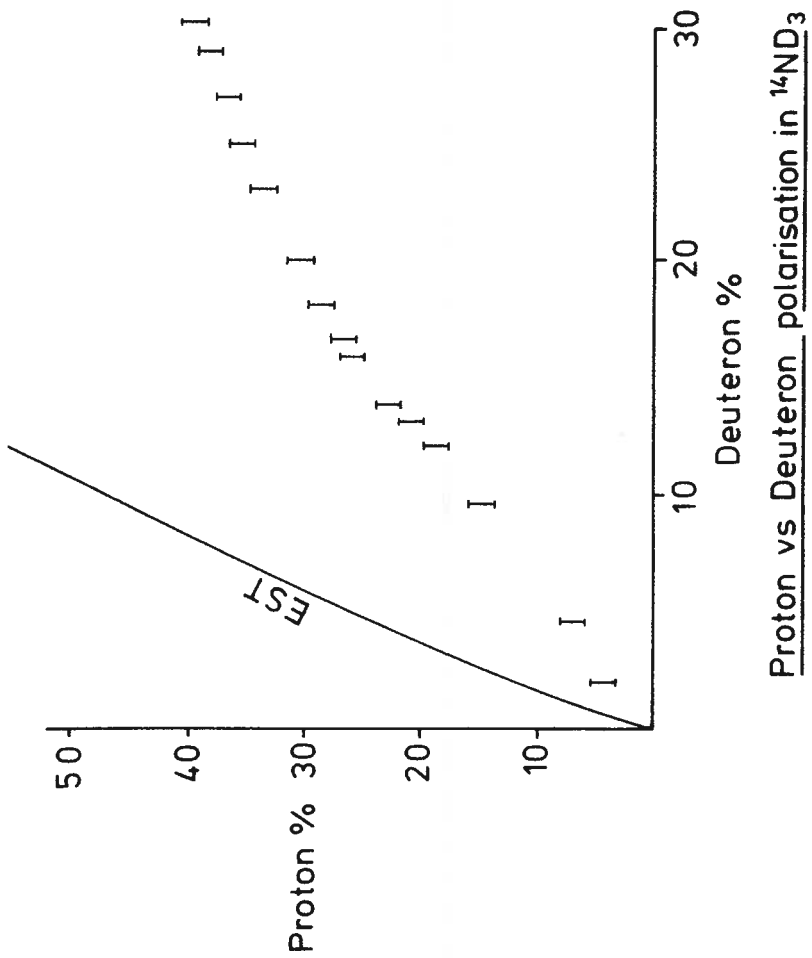


Figure 5

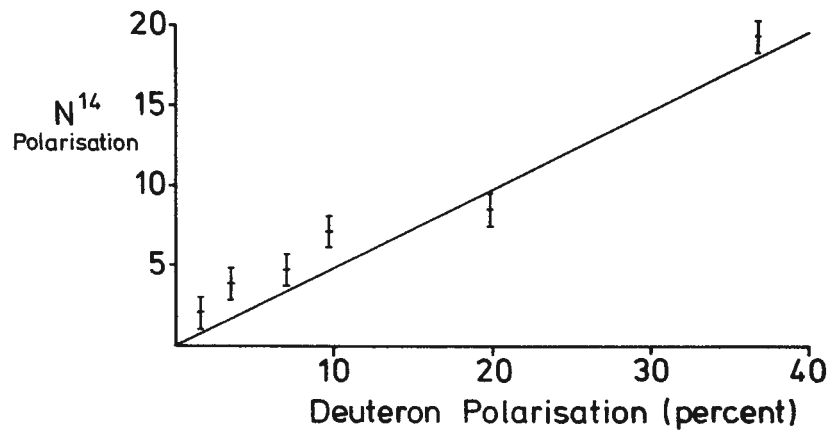


Figure 6

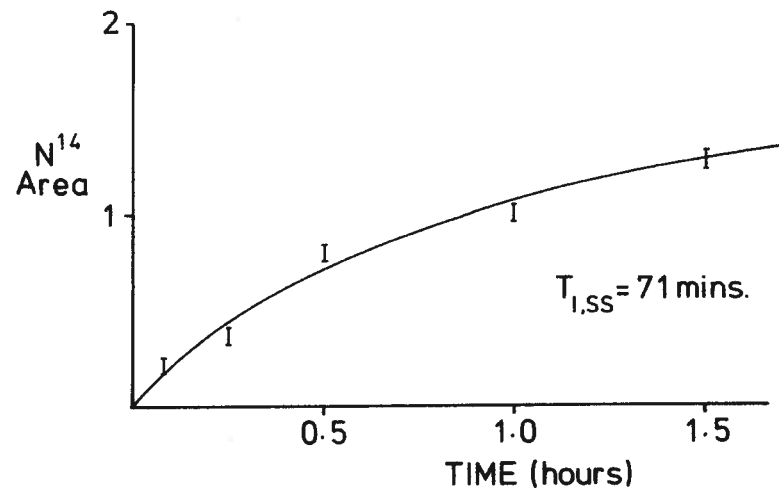


Figure 7

AN INVESTIGATION OF DYNAMIC POLARISATION IN  
IRRADIATED BORANE-AMMONIA AND AMMONIUM BOROHYDRIDE

G.R. Court and W.G. Heyes.

Department of Physics, Liverpool University,  
P.O. Box 147, Liverpool, L69 3BX, U.K.

1. Introduction

The high hydrogen content of the two compounds borane-ammonia ( $\text{NH}_3 \cdot \text{BN}_3$ ) and ammonium borohydride ( $\text{NH}_4 \cdot \text{BH}_4$ ), 19.6% and 24.6% respectively, makes them attractive candidates as polarised proton target materials.<sup>1/2/</sup> High values of proton polarisation have been obtained with these materials in the chemically doped form when they are mixed with ammonia or certain organic amines.<sup>3/</sup> Unfortunately the use of these mixtures reduces the effective hydrogen content and it is therefore of interest to investigate the possibility of obtaining high polarisation values using the pure materials with the necessary electron centres produced by radiation damage. Measurements have been made on borane-ammonia at SLAC using low temperature (1K) "in beam" irradiation.<sup>1/</sup> Up to 30% polarisation was obtained after the material had been annealed. Also it has been shown that high temperature (77K) irradiation of solid ammonia in a reactor produces a material which has excellent dynamic nuclear polarisation properties,<sup>4/</sup> so it was considered that it would be worthwhile to investigate the borohydrides using the same technique.

2. Experimental Technique

Borane-ammonia is a relatively stable white waxy solid at room temperature. The commercially available material was made into a form suitable for test by extruding it as rods approximately 3mm in diameter which were then cut into short lengths. After the irradiation, which was carried out under liquid nitrogen, its colour became dirty brown.

The ammonium borohydride was synthesised in liquid ammonia using the technique originally described by Parry, Schultz and Giradot.<sup>5/</sup> The final stage of this process is the removal of the ammonia by evaporation under reduced pressure. The material is then deposited as a white crystalline powder. As no method could be found to form it into beads or even reasonably sized lumps it was irradiated and loaded into the apparatus in this form. The solid is unstable at room temperature so it was handled using the same techniques as for solid ammonia.

The starting materials for the synthesis are sodium borohydride and ammonium fluoride and it is therefore possible that the final material contains sodium and/or fluoride ions. A chemical analysis was carried out which showed that the concentrations of both these ions in the samples used were less than 1% by weight. The material which was white when manufactured was observed to develop a bright yellow colouration after prolonged storage under liquid nitrogen and a violet colour after irradiation. The irradiation time in the reactor to produce a given electron centre density in both these materials is very much less than for ammonia (by a factor of at least 80) because of the high neutron capture cross section of the  $^{10}\text{B}$  nuclei.

Measurements were made using the Liverpool materials test facility.<sup>6/</sup>

ESR spectra were obtained with both compounds using the bolometric technique at a field of 2.5T and a temperature of 1K. The area under these ESR lines is approximately proportional to the centre density and absolute values were obtained by calibrating with a chemically doped butanol sample having a known centre density. The effect of annealing was studied in borane-ammonia, the anneals being carried out by raising the sample to the required temperature and maintaining it there for five minutes followed by rapid cooling in liquid nitrogen.

3. Experimental Results

(a) Borane-ammonia. An ESR spectrum of the irradiated material is given in figure 1. The g factor is calculated to be  $2.0038 \pm 0.0003$  and the line width (FWHM) is 560MHz. The width and shape of this line is consistent with the dominant radical being  $\text{H}_3\text{N} : \text{BH}_2$ .

The centre densities obtained at three different irradiation doses (specified in terms of integrated reactor power) together with the corresponding proton relaxation times, were as follows:-

Dose (kilowatt-hour)	Centre density ( $\text{cm}^{-3}$ )	Relaxation time (min)
30	$1.2 \times 10^{19}$	$5.6 \pm 0.3$
15	$6 \times 10^{18}$	$6.0 \pm 0.3$
1	$4 \times 10^{17}$	many hours

The variation of centre density with anneal temperature was approximately linear over a the temperature range from 170K to 220K, falling to zero at 240K. This type of behaviour is characteristic of amorphous polymer type materials and so is consistent with the mechanical and chemical properties of this compound.<sup>7/</sup>

A plot of polarisation against microwave frequency measured at a temperature of 1K for the 30 Kilowatt hour sample (with ESR line superimposed) is given in figure 3. The difference between the two optimum microwave frequencies is 460 MHz. The peak polarisations obtained with this sample using the dilution refrigerator were +18% and -13.6%. These polarisation values are somewhat lower than those obtained by the SLAC group. However the two sets of results may not be directly comparable as the SLAC measurements were made with a field of 5T and at a temperature of 1K.

(b) Ammonium borohydride. The ESR spectrum is given in figure 2. The g factor is  $2.0060 \pm 0.0003$  and the line width (FWHM) is 170MHz. The centre density obtained at three different irradiation doses together with the corresponding proton relaxation times were as follows:-

Dose (kilowatt-hour)	Centre Density ( $\text{cm}^{-3}$ )	Relaxation time (min)
10	$1 \times 10^{19}$	$3.0 \pm 0.1$
2	$2 \times 10^{18}$	$2.5 \pm 0.1$
1	$1 \times 10^{18}$	$3.0 \pm 0.1$

The proton relaxation time is essentially independent of centre density which suggests that the predominant relaxation process is via some other spin species, possibly an impurity. The polarisations obtained using the dilution refrigerator were -18% and +6% each after a growth period of approximately 6 hours.

In both cases the equilibrium value had not been reached although the rate of change had become less than 0.2% per hour. The difference between the optimum microwave frequencies for the two directions of polarisation was found to be 215 MHz. It appears that the performance of these particular samples of ammonium borohydride was seriously limited because of the presence of impurities. It is considered that this compound would merit further investigation using this technique if samples of higher purity can be prepared.

#### 4. References

- /1/ M.L. Seely et al.  
Proc. of 1980 Symposium on High Energy Spin Physics with Polarised Beams and Targets. Ed. C. Joseph and J. Soffer, Birkhauser Verlag 1981. p453.
- /2/ M. Krumpolc.  
High Energy Spin Physics 1982.  
AIP conf, proc No.95. p502.
- /3/ D. Hill.  
Polarisation in Chemically Doped Hydrogen Rich Glasses.  
These proceedings.
- /4/ G.R. Court, W.G. Heyes.  
The Dynamic Polarisation of Nitrogen Nuclei in  $^{14}\text{NH}_3$ ,  $^{15}\text{NH}_3$  and  $^{14}\text{ND}_3$ .  
These proceedings.
- /5/ R.W. Parry, D.R. Schultz and P.R. Girardot.  
Journal American Chem. Soc. 80 No1. (1958). 1.
- /6/ G.R. Court, P. Harrison and W.G. Heyes.  
The Liverpool Polarised Target Materials Test Facility.  
These proceedings.
- /7/ S. Ya Pshezhetskii et al.  
EPR of Free Radicals in Radiation Chemistry.  
Wiley 1974, p 300ff.

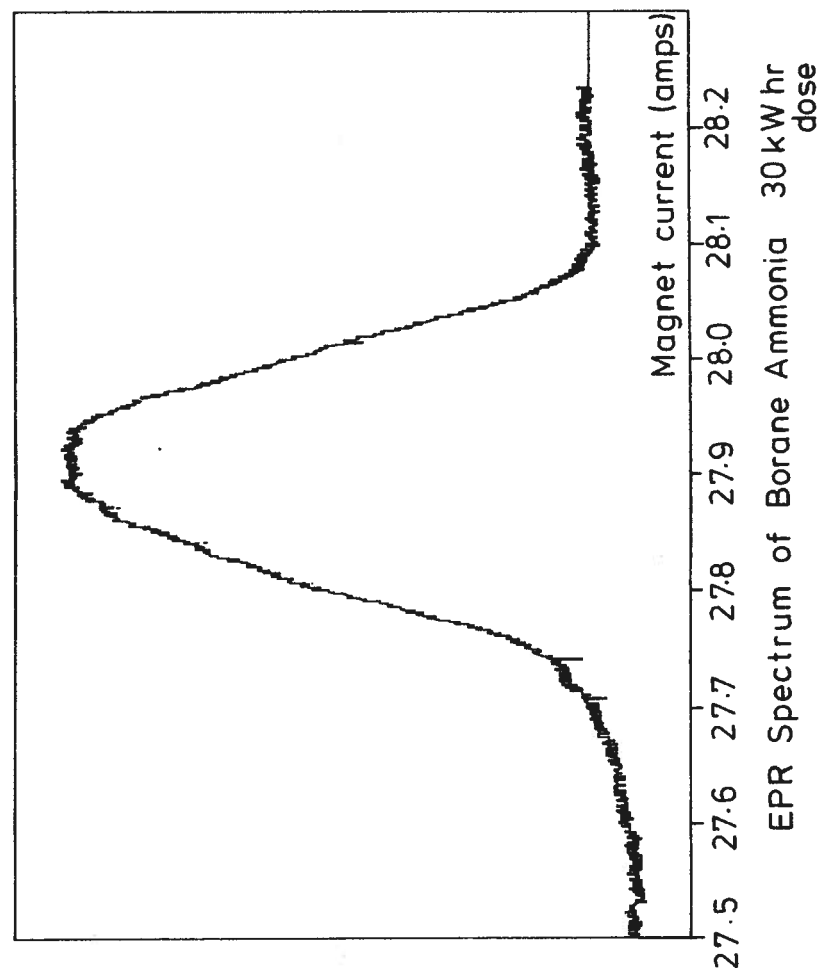


Figure 1

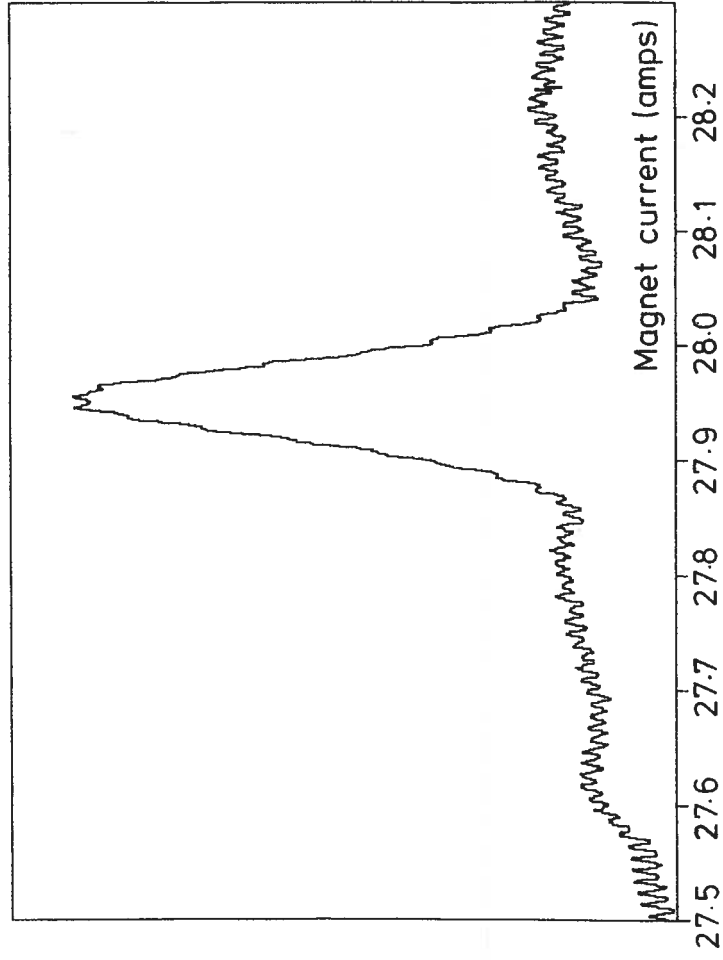
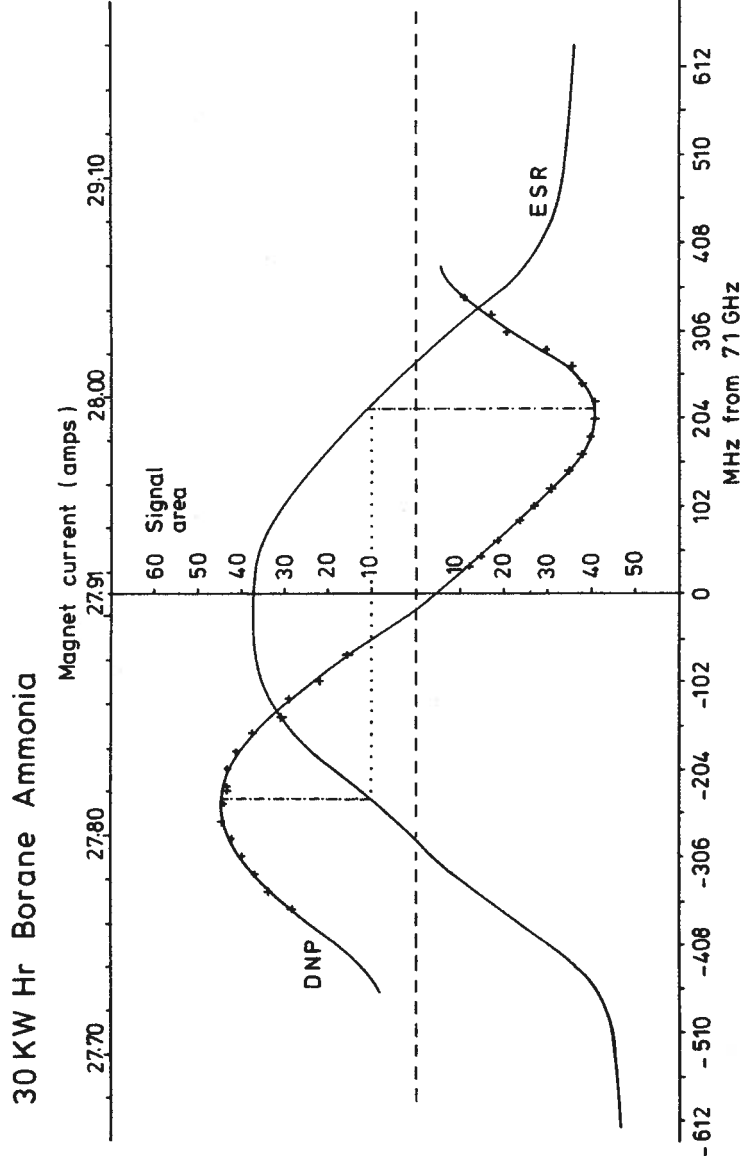


Figure 2



The relationship between ESR lineshape and DNP

Figure 3

THE PRODUCTION OF LARGE QUANTITIES OF IRRADIATED AMMONIA  
FOR USE AS A POLARISED TARGET MATERIAL

S. Brown<sup>3</sup>, G. Court<sup>3</sup>, G. Hayes<sup>3</sup>, W. Meyer<sup>1</sup>  
J. M. Rieubland<sup>2</sup>, A. Rijllart<sup>2</sup>, E. Schilling<sup>1</sup>, D. Williams<sup>3</sup>

Bonn<sup>1</sup>-CERN<sup>2</sup>-Liverpool<sup>3</sup>-Collaboration

Abstract

A report is presented on the production and irradiation procedure used to prepare 3 litres of ammonia beads for the European Muon Collaboration (EMC) polarised target. The initial studies, consisting of a Monte Carlo simulation of the irradiation process and tests using thermoluminescent crystals, are described. The apparatus used and its performance in the LINAC beam at Bonn University will be given along with the problems encountered, such as explosions and beam steering. Tests have been carried out on the first samples of ammonia beads irradiated and the results from polarising small amounts of these samples of differing exposure times is presented.

1. Initial Studies

The irradiation facility used for this work was the 25 MeV electron beam produced by the injection LINAC for the Bonn 2 GeV Electron Synchrotron. In order to try and establish the maximum volume of material which could be irradiated at one go and the optimum position of the irradiation cryostat in the beam line a Monte Carlo simulation of the irradiation process was performed. The Monte Carlo used was an Electron Gamma Shower simulation (EGS) /1/ which enables beam and deposited energy profiles to be produced for a variety of experimental configurations and materials. It was decided that argon should be used as a cooling medium as this largely reduces the explosion hazard experienced in using liquid nitrogen as a coolant /2/. The Monte Carlo was set up with the experimental configuration of Fig. 1. By varying the thickness of ammonia and the distance of the cryostat from the beam window, the maximum dimensions for the ammonia sample were established. The results for the energy deposition in each medium for the optimum condition is shown in Fig. 2. For this configuration, corresponding to the target dimensions and position shown in Fig. 1 nearly 62% of the beam energy is calculated to be deposited in the ammonia. On this basis it was decided to perform further tests with a polythene cube of dimensions 10 x 10 x 10 cm<sup>3</sup> in the LINAC beam.

To determine the energy deposition profile in the cube thermoluminescent crystals of 3 x 3 x 1 mm<sup>3</sup> were uniformly distributed within the polythene. To achieve this the cube was cut into 5 slices, enabling 4 planes, 9 crystals per plane, to be placed in the cube, Fig. 3. The integrated dose absorbed by each crystal may be read out by heating it above a critical temperature and observing the integrated light intensity emitted. For the crystals used this process is linear up to doses of ~ 1000 rads, corresponding to between 5 and 10 LINAC pulses.

A series of 4 test were performed

- TEST 1) Polythene block placed 1m from the beam window, 5 pulses from the LINAC.
- TEST 2) As for 1) but with a sheet of 1.6 mm aluminium placed in front of the block, 5 pulses from the LINAC.
- TEST 3) As for 2) but with 1 mm of lead replacing the aluminium, 7 pulses from the LINAC.
- TEST 4) As for 3) but after 5 pulses the target was reversed, 10 pulses from the LINAC.

The results obtained from 2 of these tests, tests 2 and 4, are shown in Fig. 4. Test 2 agrees well with the Monte Carlo simulation showing almost equal amounts of energy deposited in the first 2 planes and very little in the last plane. Test 4 shows that by reversing the target halfway through the test an almost uniform energy deposition is achieved throughout the target. The conclusions which were drawn were as follows;

- 1) it is possible to irradiate up to 10 cm thick samples of ammonia beads with a uniform deposition of energy provided that the sample is rotated during the irradiation
- 2) that for the cryostat placed 1 m from the beam window the maximum usable height of the sample is 8 cm giving a total volume of 600 cm<sup>3</sup>.

2. Manufacture of Ammonia Beads in Large Quantities

The volume of material required for the EMC polarised target is 2 litres /3/ and it was decided to produce enough target material for 2 full loads. The volume of each bead is, on average, 10mm<sup>3</sup>, therefore 2 loads of the 2 litre target require the production of nearly half a million beads and an automatic or semi-automatic production mechanism is clearly necessary. Several methods of bead making which produce high quality uniform beads have been tested /4/, however none of them easily lend themselves to mass production with little or no supervision. The method chosen therefore is the simple one of dropping liquid ammonia into liquid nitrogen. This produces a wide range of bead sizes and quality and it was necessary to sort the beads using graded sieves before irradiation. The apparatus is shown in Fig. 5 and consists of a small refrigeration unit to provide the coolant for liquifying the ammonia, a double walled condensing syringe through which the coolant circulates and a dewar containing liquid nitrogen. The drop rate of the ammonia into the nitrogen dewar is controlled via a stainless steel valve. By optimising the pressure and size of the hyperdermic needle the required bead volume and uniform drop rate can be achieved. One further refinement to this system could be the use of an electrostatic field to detach and charge the beads to avoid them coalescing on the surface of the nitrogen bath. This method has been used very successfully in the past for pentanol and other materials, but in this case, the ammonia beads did not coalesce on the surface of the liquid nitrogen unless the drop rate was very high. This apparatus is capable of producing about 250 cm<sup>3</sup> of ammonia beads per day (after filtering and sorting). Once the beads have been produced they are stored in glass containers under liquid nitrogen and transported from CERN to Bonn by express freight train (transit time 2 days) in nitrogen dewars specially designed for transporting chemical samples at low temperatures.

### 3. Argon Irradiation Cryostat and Operating Procedure

The technique of using argon as a coolant during the irradiation of ammonia has been used successfully elsewhere /5,6/ without difficulties and the control system for automatic operation of an Argon cryostat already existed at Bonn /2/.

The cryostat is shown in Fig. 6 and consists of 2 parts, a liquifier and an irradiation cell. The argon gas enters from the top and passes through copper tube heat exchangers, mounted inside a liquid nitrogen bath. The argon is liquified in this heat exchanger and passes through the tube and across into the irradiation cell. This cell consists of an aluminium bottom section, used to avoid a high build up of radioactivity during irradiation, in which the target sample sits and a stainless steel upper section to provide good thermal insulation between the liquid argon and the room temperature top plate. The two sections are joined together by a friction welded joint. The target sample holder is suspended at the end of an aluminium shaft, which rotated using a slow speed motor at a rate of between 0.1 and 0.2 RPM. A rod is mounted in the cell to hold a platinum resistance (not shown) used to monitor the height of the liquid argon. The whole system is surrounded by vacuum for thermal isolation.

Fig. 7 shows the layout of the equipment in and near to the LINAC room. As much of the equipment as possible is kept outside the LINAC room to minimise induced radioactivity in the components and also to allow rapid access to the controls should anything go wrong during irradiation. To start the operation the cryostat is first pumped down to remove any traces of air and water vapour which may cause blockages in the tube linking the liquifying section to the irradiation cell. Argon is then let into the system and liquified by manually opening the nitrogen transfer line valve. Care must be taken not to overfill the nitrogen bath with liquid as this causes the argon to freeze in the heat exchanger and eventually blocks the system. Once the correct level of liquid argon has been reached, as detected by the platinum resistance, the argon supply is closed off. Preset high and low limits for the argon pressure within the cryostat control an electrovalve on the nitrogen transfer line and enable automatic filling of the nitrogen bath. The pressure range found to give the best results with this apparatus are;

pressure > 790 torr ..... valve open (start fill)  
 pressure < 770 torr ..... valve close (stop fill)

A 100 litre dewar of nitrogen is sufficient for 10 hours operation with beam on and for more than 16 hours with beam off. A safety valve on the argon circuit is set to 1000 torr in automatic operation so that in the event of vacuum failure or lack of nitrogen, the argon and ammonia is vented to the atmosphere and explosions due to overpressure are avoided.

Once the cryostat is filled with liquid up to the correct level, the sample to be irradiated is transferred from a small dewar of liquid argon to the irradiation cryostat. The pressure levels are set on the argon circuit and the auto-fill system started. The beam is then turned on, focused and steered onto the target. After irradiation it is necessary to wait 30 minutes for the

radiation level near to the LINAC room to die down to a safe level. The 100 litre dewar is then changed and the LINAC room left to 'cool' down for a further 6 to 7 hours. The ammonia is then removed, the argon evaporated and the cryostat pumped down ready for the next irradiation.

### 4. Results of the First Irradiation

The first series of irradiations using this apparatus took place in September, 1982 and were intended to find the optimum irradiation time to produce a good polarisable sample. There were 3 irradiations performed;

- 1) 3 hours of beam producing light violet beads
- 2) 6 hours of beam producing dark violet beads
- 3) 10 hours of beam producing dark violet beads

Small samples from each of the tests were polarised in a helium 3 cryostat at CERN during February, 1983, the results are shown in Table 1.

Table 1

Temperature = 543 mK

Sample	Max Pol + ve	Rise Time	Max Pol - ve	Rise Time	Relaxation Time
NH <sub>3</sub> 3h Sept 82	+69.9%	1h 50% 2h 63%	-64.2%	1h -50% 2h -61.3%	not measured
6h Sept 82	+68%	1h 54% 3h 65%	-68%	1h -57% 2h -68%	67 mins
6h Jan 83*	+63.2%	1h 55% 2h 63%	-66.6%	1h -58% 2h -64%	60 mins
10h Sept 82	+65.2%	1h 56% 2h 61%	-69.2%	1h 56.6% 2h 66.6%	64 mins

\* Stopped before final value reached

As can be seen there is no great difference in the maximum polarisation reached in any of the samples, however, the time for the 3 hour sample to reach 70% of its final value is much longer than for the others. As the requirement of the EMC experiment is for a sample that can be polarised quickly up to 70% it was decided to irradiate all further samples for 6 hours. No further benefit being obtained by an irradiation period of 10 hours.

## 5. Problems Encountered

This section summarises the problems encountered which in part lead to the improvements outlined in the next section. As previously mentioned argon was chosen as a cooling medium due to its apparent stability during irradiation of ammonia. However explosions did occur, the first being a minor discharge after the 10 hour irradiation test in September, 1982. This caused no damage to material only to the nerves of D. Williams who happened to be unloading the sample at the time. The second explosion was more serious, causing the loss of a sample and also the destruction of the aluminium irradiation cell of the cryostat. The explosion occurred during the 4th successive irradiation in the same liquid argon and may be put down to the build up of some unstable compound in the argon circuit. The argon is now changed after each irradiation, as outlined in the operation procedure, since when we have had no further problems. Blockage of the cryostat caused the loss of one sample. The heat exchanger tubes became blocked with debris from the large explosion which did not manifest itself until a later irradiation. There were also problems with the first version of the liquid argon level indicator. The liquid level was found to oscillate within the irradiation cell and due to the improved beam steering and increased heat load on the target this oscillation caused one sample to melt due to insufficient cooling. The problem was caused by a long time constant in the level detection system and was cured when this was reduced.

## 6. Improvements to the System

In the light of experience obtained during the irradiations several improvements were made to the system.

- 1) A long isolated transfer line was built enabling the nitrogen dewar to be placed outside the LINAC room, (Fig. 7), thus making the changing of the dewar safer and quicker.
- 2) The original level detector was replaced by a platinum resistance to improve reliability.
- 3) The use of a fluorescent beam spot monitor inside the vacuum pipe and a beam position monitor just upstream of the target. The former allows the beam size to be optimised at the start of irradiation and the latter to ensure that the beam is focused on the target throughout the irradiation. These improvements alone enabled the irradiation time to be reduced from 6 hours to 3 hours due to better beam positioning.
- 4) The use of a TV camera for continuous monitoring of the argon pressure and vacuum from the LINAC control room. This provides immediate detection of problems due to equipment failure and may enable the sample to be removed from the cryostat before any permanent damage occurs.

## Conclusions

The argon irradiation cryostat described in this report has been successfully operated in the electron beam produced by the Bonn LINAC for the past 2 years. The total amount of ammonia irradiated so far is 3 litres, of which 2 litres are now being used as the target material in the EMC polarised target. The remaining litre is in storage under liquid helium to minimize centre loss due to the recombination. The irradiation cryostat is capable of irradiating 300 cm<sup>3</sup> of ammonia at one time but can also be used with a modified sample holder to irradiate smaller volumes of materials. The maximum irradiation time needed to produce an easily polarised sample is 3 hours.

## References

1. The EGS Code System: Computer Programs for the Monte Carlo Simulation of Electromagnetic Cascade Showers.  
R.L. Ford and W.R. Nelson, SLAC Report No. 210, June 1978.
2. Proceedings of the Second Workshop on Polarised Target Materials.  
Editors: G.R. Court, S.F. Cox, D.A. Cragg, T.O. Niinikoski, Pg. 93-95.
3. Dilution Refrigerator for a Two-Litre Polarised Target.  
T.O. Niinikoski, NIM 192 (1982) 151-156.
4. W. Meyer, A.I.P. Conference Proceedings, No. 95, High Energy Spin Physics - 1982, (Brookhaven National Laboratory), Ed. G.M. Bunce, Pg. 505-511.
5. Proceedings of the Second Workshop on Polarised Target Materials, 1978, Pg. 94.
6. U. Härstel et al., Proceedings of the 1980 International Symposium on "High Energy Physics with Polarised Beams and Polarised Targets", Ed. C. Joseph and J. Soffer, Lausanne 1980, Pg. 447-450.

Experimental configuration used in the Monte-Carlo simulation

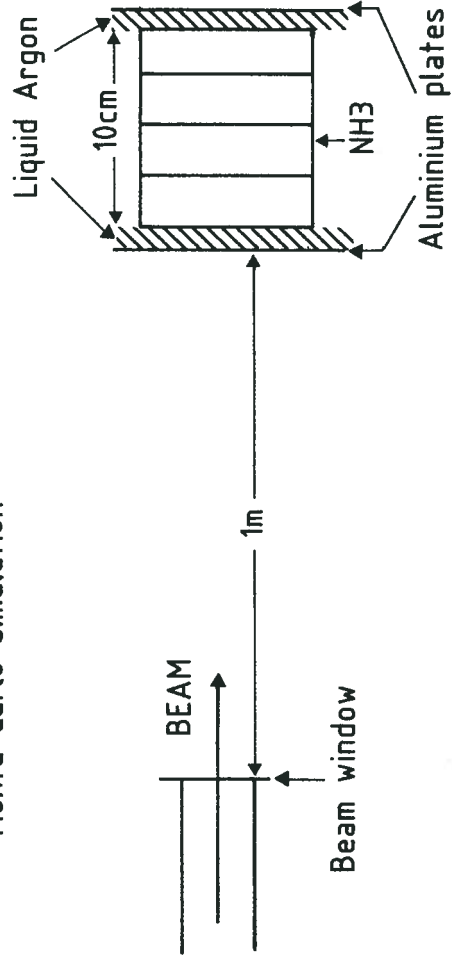


Fig. 1

The amount energy deposited in each material from the Monte-Carlo simulation

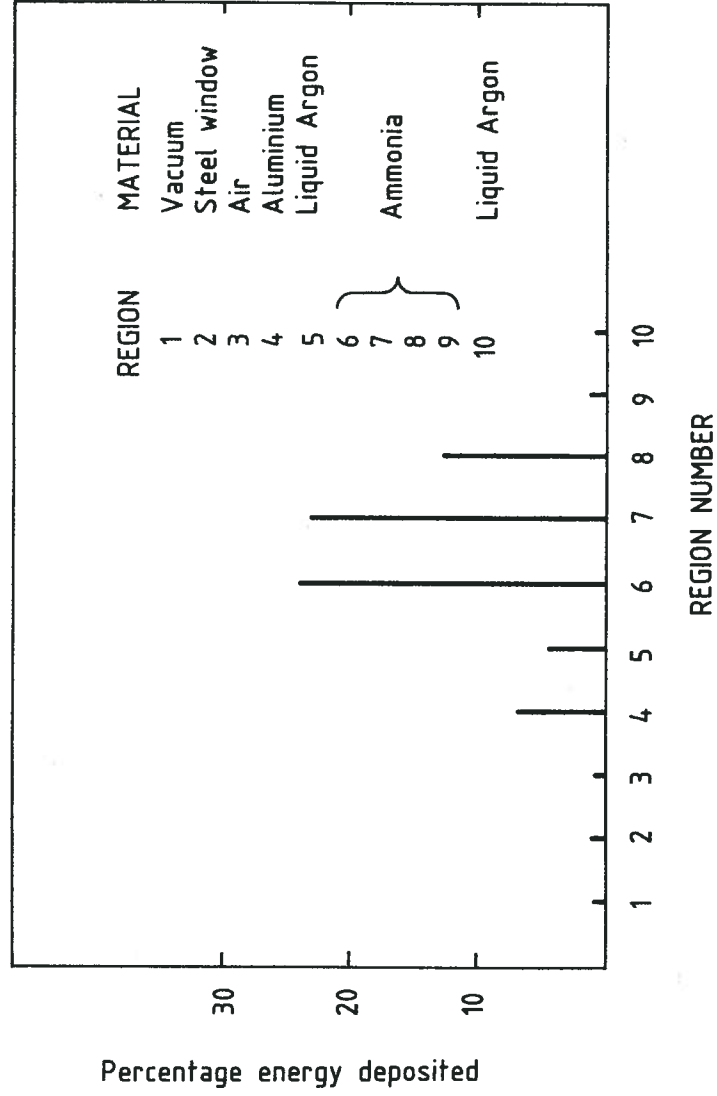


Fig. 2

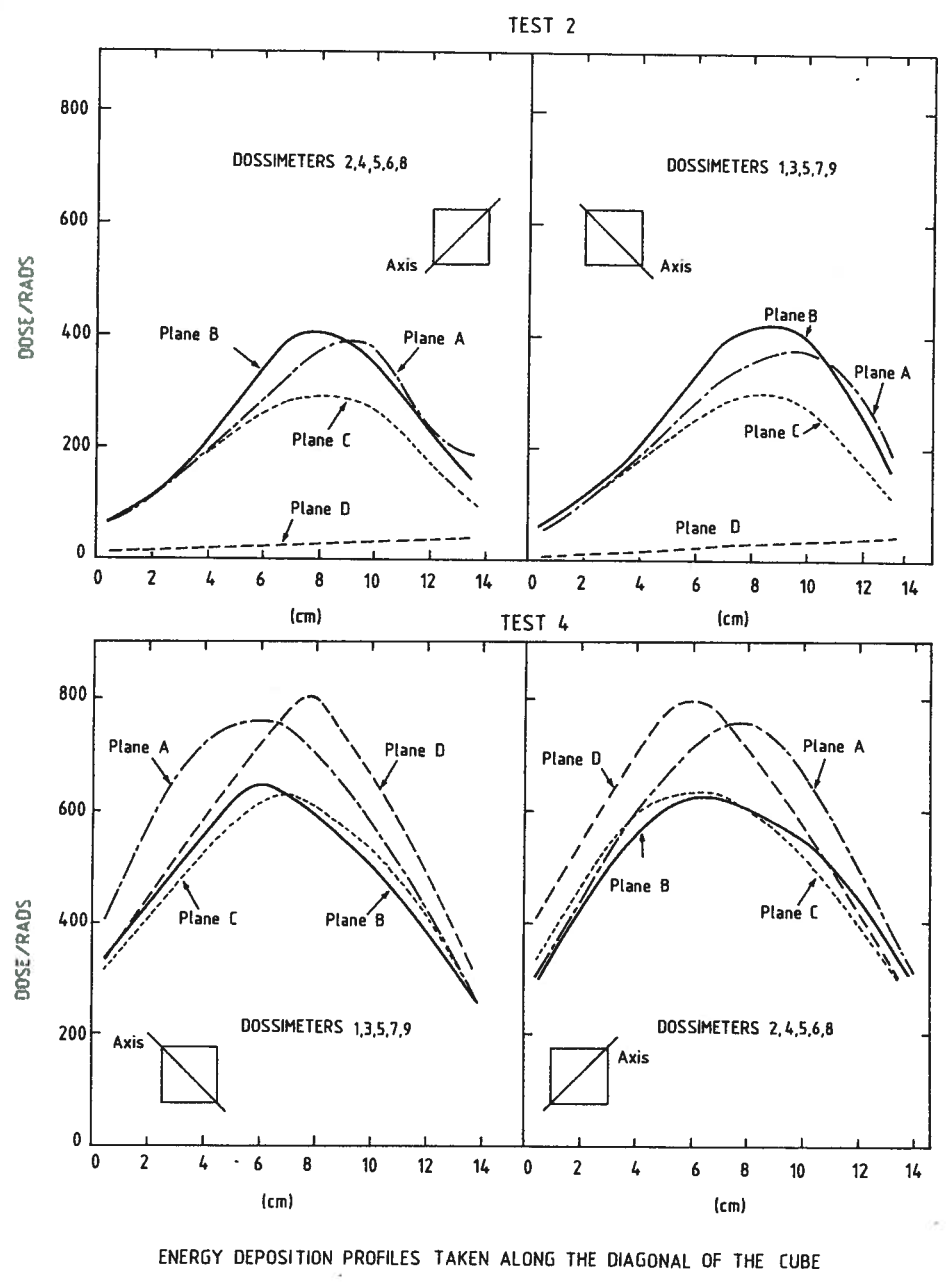
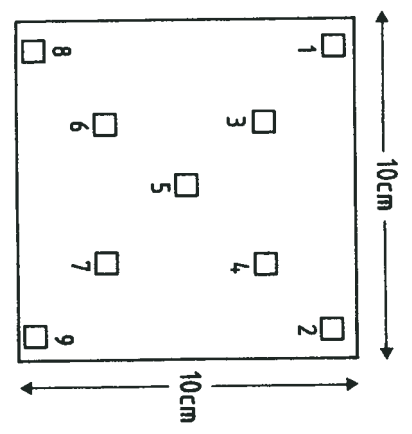
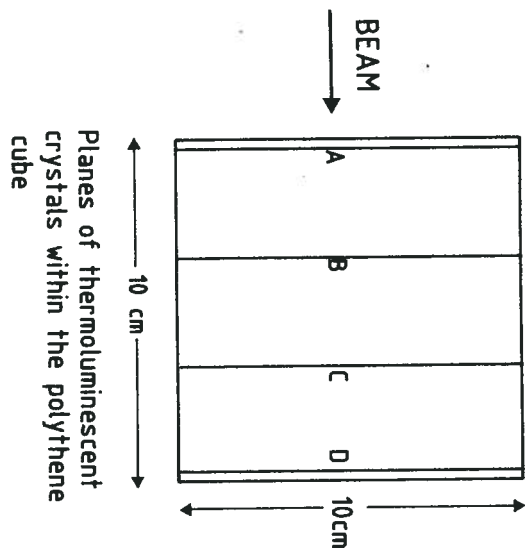
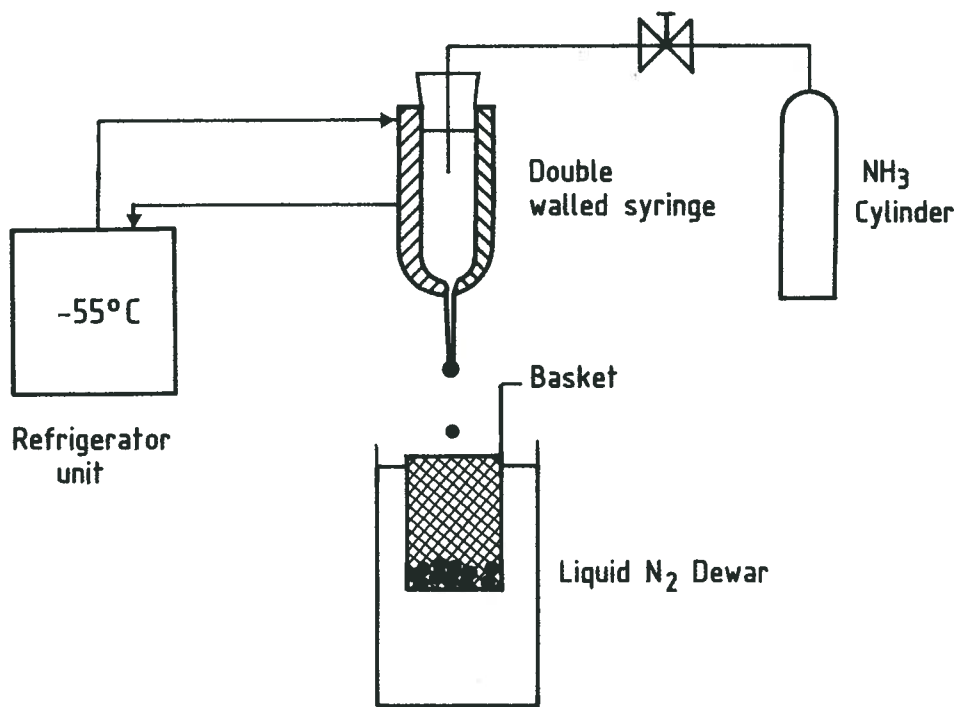


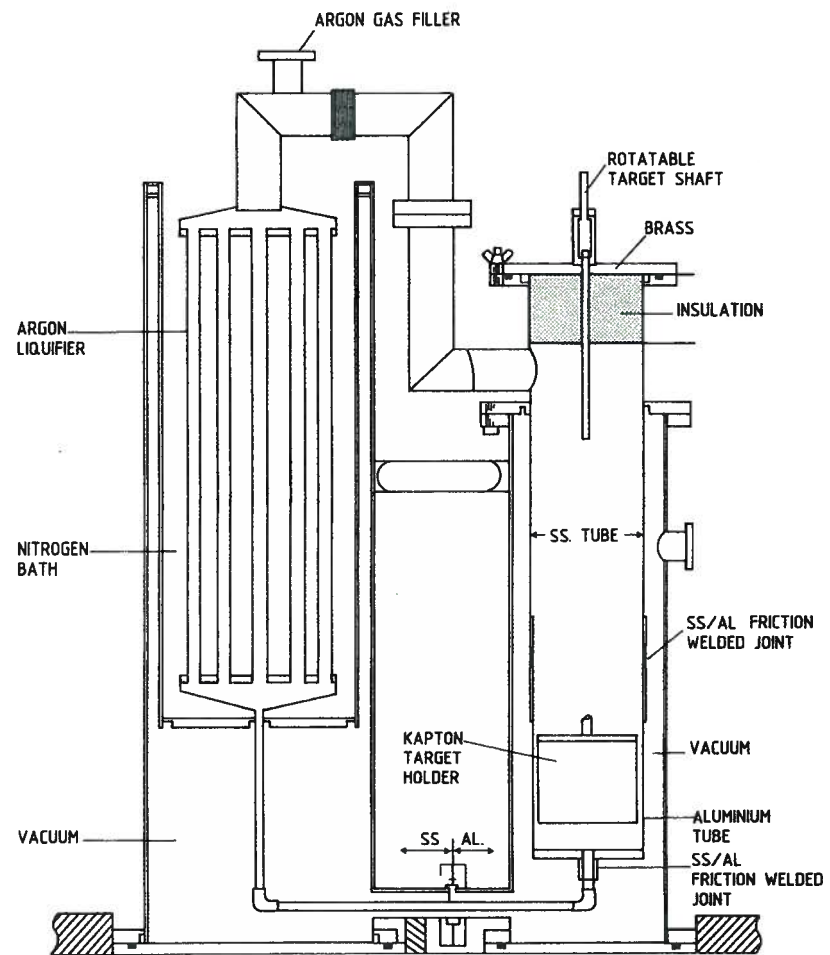
Fig. 4

Fig. 3



APPARATUS FOR AUTOMATIC BEAD PRODUCTION

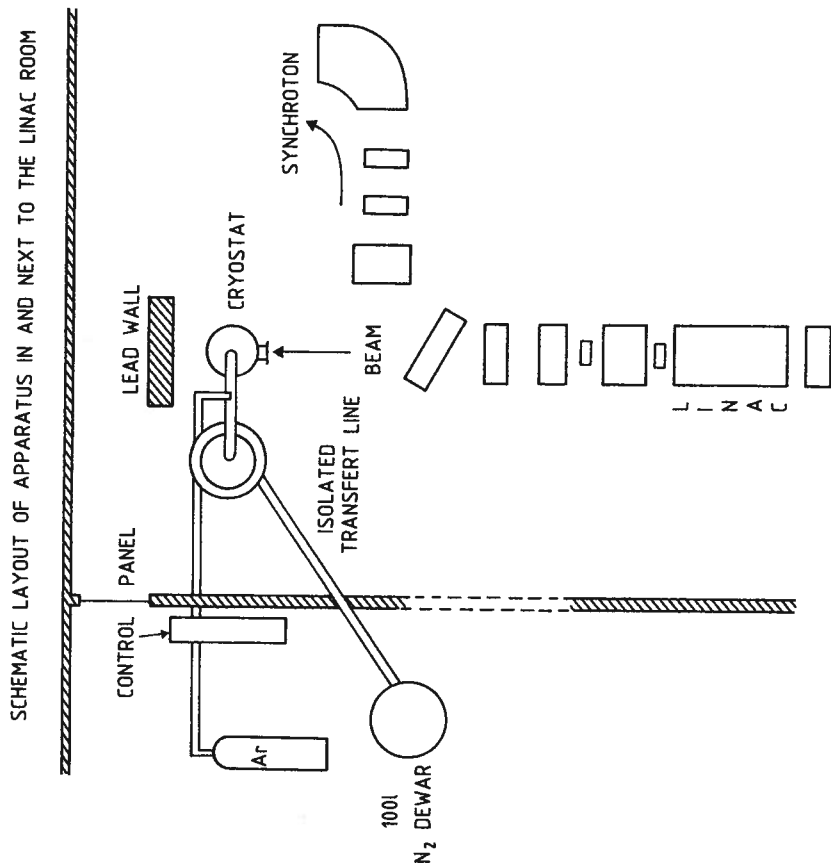
Fig. 5



IRRADIATION CRYOSTAT USING LIQUID ARGON AS THE COOLING MEDIUM

Fig. 6

Fig. 7



## Preparation and Irradiation of Ammonia Target Beads

P.R. Cameron

Harrison M. Randall Laboratory  
Physics Department  
University of Michigan  
Ann Arbor, Michigan 48109-1120

### ABSTRACT

The preparation of Ammonia beads by the 'slow and freeze and crush' method (which results in crystalline beads) is described, as is their irradiation in a 70 MeV electron beam.

#### 1. Preparation

Gaseous Ammonia is liquified in a test tube which is immersed in a dry ice-alcohol bath. After liquification the test tube remains in the bath until the ammonia solidifies into a transparent crystalline solid. The test tube is then transferred to a liquid nitrogen bath and broken. After separating out the glass fragments, the ammonia is crushed through a metal screen and captured in a slightly finer mesh screen./1/

This method has two advantages over the approach of dripping liquid ammonia into a liquid nitrogen bath. The density of the slowly frozen ammonia is somewhat higher, and the material is macrocrystalline rather than microcrystalline, so that the thermal conductivity might also be somewhat higher.

#### 2. Irradiation

The first irradiations were performed at the Cobalt-60 irradiation facility of the Phoenix Memorial Laboratory of the University of Michigan. The Cobalt 60 is configured in a 12 cm diameter cylinder which is 25 cm long. The rate in the 150 cm<sup>3</sup> irradiation volume is about 1 MRad/hr. This method had two advantages over the later electron irradiations. The irradiation was much more uniform, and the problems with activation were essentially nil. The great disadvantage was time. At 1 MRad/hr, about 500 hours of time were required for a reasonable irradiation.

Other beads were subsequently irradiated at the 70 MeV linac of the National Synchrotron Light Source at Brookhaven National Laboratory. The source current was 200 ma, and transmission through the linac was about 50%. The pulse width was 2.5  $\mu$ sec, and the repetition rate was 100 pulses per minute, so that about  $10^{16}$  electrons per hour were incident on the tungsten foil shown in Figure 1. The normal beam spot size at the end of the linac was about .35 cm. It was not convenient to blow the beam up with magnets, to match the 2.5 cm diameter bead holder, so the tungsten foil was used instead. The thickness of the foil was calculated/2/ to give a 2 cm FWHM beam spot at the bead holder. The observed spot diameter just before the bead holder was about 1.7 cm.

The volume of the bead holder was about 70 cm<sup>3</sup>, which was adequate for 3 loads of the Michigan target. The volume of the Argon dewar was slightly less than 5 liters. It was necessary to refill the dewar every 12 hours. Refilling was accomplished manually. The fill tube was 1 cm I.D. and 70 cm long. The lid of the dewar was tightly sealed, and the diameter and length of the fill tube were selected to ensure that boil-off of the argon would prevent back-diffusion of oxygen or water vapor from the atmosphere. Liquid argon was purchased in 160 liter dewars from a local welding supply.

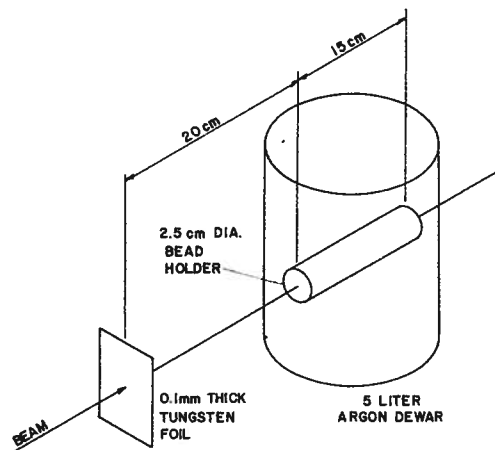


Figure 1

A typical irradiation lasted about 24 hours. During the period from March 1983 to March 1984 four irradiations were accomplished. During an irradiation a total of about  $2 \times 10^{17}$  electrons were incident on the tungsten foil. The bead holder was turned end-for-end midway through each irradiation, so the dose on each end was approximately equal. After irradiation the dewar was allowed to sit about 1/2 hour while short-lived radioactivity partially decayed. It was then necessary to move the dewar so that other experimental programs could proceed. The dewar was about 500 mR/hr on contact, and was moved a few meters, then left to sit overnight. The following day levels were less than a few mR/hr, and the beads were transferred to the storage dewar.

### 3. Conclusion

The method outlined above has been adequate to produce small quantities of beads with a minimum of time and effort. The major limitation has been the flux available for irradiation.

### References

1. T.O. Niinikoski, private communication.
2. Particle Properties Data Booklet, p. 112 (1984).

### ATTEMPT TO POLARIZE A LARGE SAMPLE OF <sup>7</sup>LiH IRRADIATED WITH HIGH ENERGY ELECTRONS

P. Chaumette, J. Deregé, G. Durand, J. Fabre, J. Movchet  
DPHPE, CEN-Saclay, 91191 Gif-sur-Yvette Cedex  
FRANCE

J. Ball  
LNS, CEN-Saclay, 91191 Gif-sur-Yvette Cedex  
FRANCE

### ABSTRACT

Deuteron and lithium polarization of  $P \approx 0.7$  have been obtained for small samples of <sup>6</sup>LiD at 6.5 Tesla. This material is of great interest as polarized neutron target for high energy experiments. We are exploring the procedures for producing large polarizable samples, using a similar material <sup>7</sup>LiH, irradiated by high energy electrons.

### 1. Introduction

Comparison of different materials rich in polarizable neutrons shows that <sup>6</sup>LiD is at present the best material for polarized neutron targets. Both the deuterons and the <sup>6</sup>Li nuclei are polarized. The <sup>6</sup>Li can be assimilated to a polarized deuteron plus an alpha particle, or to <sup>3</sup>H + <sup>3</sup>He /1/. Therefore, the polarizable neutrons represent about 25 percent in weight.

Pr. A. Bragam and his collaborators have successfully polarized small samples of <sup>6</sup>LiD and <sup>7</sup>LiH (0.5 x 5 x 5) mm<sup>3</sup>. The paramagnetic centers were created by irradiation at 150°K with  $10^{17}$  electrons per cm<sup>2</sup> at electron energies from 2 to 3 MeV /2/.

Since it would be impractical to compose large targets for high energy experiments from such small samples irradiated at low energies, we are developing alternate techniques. We started studying <sup>7</sup>LiH which has the same behaviour as <sup>6</sup>LiD /2/ and which is more easily available. We irradiated a sample of 10 cm<sup>3</sup> in liquid Argon with electrons of 200 to 600 MeV. At these energies there is practically no limitation in target thickness.

### 2. Experimental Details

We used <sup>7</sup>LiH crushed in 2 mm pieces from a sintered block, allowing good thermal exchange during irradiation and polarization. The sample is placed in a liquid argon cryostat (Figure 1). The irradiation takes place in one of the beam lines of the Saclay Linear Accelerator (ALS).

The Argon is liquefied by natural convection in thermal contact with liquid nitrogen placed far away from the beam in order to avoid risk of explosion. The entire cryostat can be moved vertically in and out of the beam by remote control. It is inserted into the beam line behind the experimental target just in front of the Faraday cup. The irradiation takes place during normal physics experiments. The number of electrons incident on the sample is known to better than 10 percent from the beam profile and the readings of the Faraday cup.

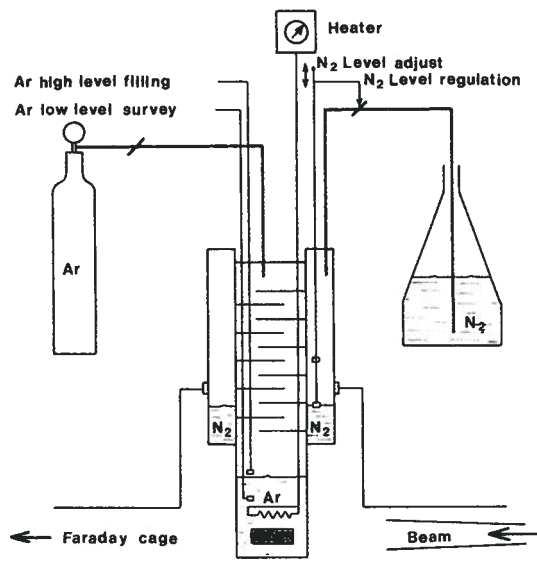


Figure 1. Irradiation apparatus.

### 3. Present Status

We have irradiated three samples of  $\approx 10 \text{ cm}^3$  each with  $0.5 \times 10^{17}$ ,  $1 \times 10^{17}$  and  $2 \times 10^{17}$  electrons/cm<sup>2</sup>, respectively. After exposure the cryostat is maintained in the off-beam position for several hours to let short lived radionuclei decay, especially <sup>37</sup>Cl produced from Argon. The colour of <sup>7</sup>LiH before irradiation is a light grey. It turned into a colour between dark blue and violet for all three samples.

We have tried to polarize these samples in the dilution refrigerator of the "Nucleon-Nucleon" target at SATURNE II in a magnetic field of 2.5 Tesla. We have not been able to reach polarizations better than 3 to 4 percent. The initial growth was relatively rapid but no further increase was observed when polarizing for one hour.

These measurements were repeated in a cryostat of Dr. Roinel's group at 6.5 Tesla with the same unsatisfactory result. An anneal of one of the samples at 120°K did not improve the polarization obtained.

### 4. Conclusion

Our investigations are continuing along the following lines :

- Annealing of already irradiated samples at increasing temperatures with EPR measurements at each step in order to control the densities of different radicals. Comparison with EPR signals from the small samples irradiated by low energy electrons will tell if there exists an optimal anneal temperature.

- New irradiations with 10 and 100 times less electrons/cm<sup>2</sup>. Because of shower development, high energy irradiation may require less incident electrons than low energy exposures.
- If neither annealing temperature nor radiation dose turn out to be the critical parameters, the cryostat will be modified in order to choose any higher temperature during irradiation.

### 6. Acknowledgments

The authors wish to thank P. Leconte for providing excellent conditions for irradiations at the ALS, and the Saclay radiation safety group for their assistance.

We gratefully acknowledge the contributions of P. Bouffard, G. Fournier, J. Jacquinet, Y. Roinel, in many useful discussions and their help in the polarization experiments.

### 6. References

- /1/ A. Abergam 1978, International Symposium on High Energy Physics with Polarized Beams and Polarized targets - Argonne, Illinois AIP Conf.Proc. 51 (1979) 1
- /2/ V. Bouffard, Y. Roinel, P. Roubeau and A. Abergam, in Dynamic Nuclear Polarization in <sup>6</sup>LiD Journal de Physique 41 (1980) 1447

## POLARIZATION IN CHEMICALLY DOPED HYDROGEN-RICH GLASSES

D. Hill and J. Hill\*

Argonne National Laboratory  
Argonne, Illinois 60439

M. Krumpolc

University of Illinois  
Chicago, Illinois 60680

### Abstract

Further results are presented on dynamic polarization in chemically doped glasses consisting of borane complexes dissolved in ammonia and primary amines. Proton polarization > 80% is achieved in a  $^3\text{He}$  cryostat at 2.5T in glasses containing 16 wt.% hydrogen. In addition to details of the sample preparations and the dependence of the polarization on several sample parameters, information is given on calorimetric properties, polarization of the background  $^{11}\text{B}$  spins, and  $^2\text{H}$  polarization in a deuterated analog material.

### Introduction

Since the Brookhaven Workshop we have continued our investigation of DNP in chemically doped glasses, with the aim of finding the best possible combination of hydrogen content and polarization, and also with the hope of clarifying some of the phenomena encountered. After describing the apparatus used to prepare samples, we briefly summarize the results obtained with various glasses. We then single out the best candidate so far found, a combination of ethylamine and borane-ammonia, for a more detailed description. This material compares favorably in several respects to existing target materials. In addition to giving the dependence of the proton DNP on several variables, we present the first data on a partially deuterated analog, including some information on the polarization of the deuteron and of the  $^{11}\text{B}$  "background" spin. Finally, we attempt to cross-correlate some of the DNP results with recent calorimetric data on the same materials.

### Apparatus

Figure 1 shows the sample-preparation apparatus, in scheme. The apparatus is usually used in ambient air, although a few preparations have been done with the apparatus inside a dry box. The purpose of the apparatus is to permit rapid and accurate preparation of sample beads composed of materials which are, variously, solids, liquids, or gases under normal conditions, and to do so at temperatures as low as practicable in order to minimize the possibility of decomposition of the dopant. Normally, the total sample size prepared is 2-3 ml, from which 20-30 beads are taken for the DNP sample. Batches as large as 13 ml have recently been prepared.

The apparatus consists of a cold-bath-type circulator, /1/ a cold Pyrex mixing tube whose contents are measureable via a digital balance, /2/ and a "cold needle" for bead formation. Methyl alcohol is used as the cold-bath fluid as well as the mixing tube immersant. The geometry of the tubular heat exchanger (H.E.) is compensated to eliminate, in first order, changes in buoyant force due to excursions of the temperature of the immersant. The cold needle consists of a stainless steel reservoir fitted with a removable

hypodermic needle, soldered to a tubular heat exchanger. The whole is thermally insulated with foam rubber (not shown). Glass wool is packed in the bottom of the reservoir to intercept any stray particulates which might otherwise obstruct the needle.

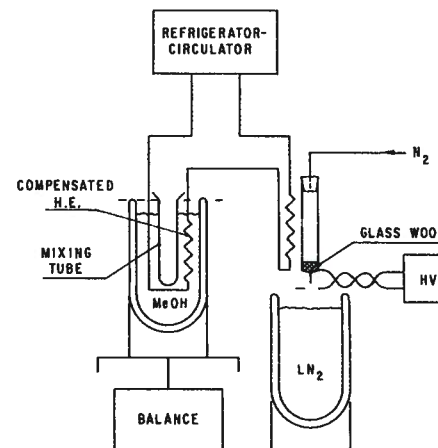


Figure 1 Schematic of the sample preparation apparatus.

A typical sample preparation is as follows: 1) purge the cold needle reservoir with dry  $\text{N}_2$ , 2) circulate coolant, 3) weigh into the mixing tube any constituents (except dopant) that are room-temperature solids or liquids, 4) condense any gaseous constituents into the tube, via a nozzle (not shown) projecting down into the tube, 5) manually mix the contents with a stirring rod, 6) weigh in the dopant and stir for 4 min., 7) pour the mixture into the cold needle reservoir and make beads in the standard way. The rate of droplet formation is controlled by the  $\text{N}_2$  pressure and the bead diameter is set at  $\sim 2$  mm by adjusting the high voltage (HV). The beads are discharged before use.

The samples are tested in a quick-load  $^3\text{He}$  cryostat operating at 0.4K in a 2.5-T-field.

### Summary of the Glasses Tested

Table I shows selected results on the glasses tested so far. All samples in this Table were prepared at 200K (except 16, at 225K) using chemicals as commercially supplied. /3/ None of these samples showed any large sensitivity of the polarization to FM of the microwave source; however, most showed some small (1-5%) improvement with sinusoidal FM at a frequency of 2 kHz and amplitudes in the range of 10-40 MHz peak-to-peak. The polarizations shown are those obtained with FM.

Several of these mixtures show considerable promise, and it is, in fact, not easy to distinguish the "best" sample in this list. In particular, samples 1, 5, and 12 are barely distinguishable if one compares them using some of the standard figures-of-merit. For now we have singled out samples of type 1 for a more extensive examination, mainly on the basis that they give somewhat less asymmetry between the two signs of enhancement.

TABLE I

Selected polarization results for samples prepared at 200K (exception: sample 16 was prepared at 225K). Each result represents a single sample, except for sample 1 which represents an average over eight samples. Meaning of symbols: ammonium borohydride (AB), borane-ammonia (BA), borane-dimethylamine (BDMA), borane-methylamine (BMA), dimethylamine (DMA), ethylamine (EA), methylamine (MA).

Sample No.	Composition By Wt.	EHBA-Cr <sup>V</sup> 10 <sup>19</sup> /ml	Wt.-%-H	Polarization (%)	
				(+)	(-)
1	EA(.85)BA(.15)	4 nom.	16.0	83	77
2	EA(.90)AB(.10)	4 nom.	16.3	68	
3	EA(.88)AB(.12)	4 nom.	16.5	65	
4	DMA(.85)BA(.15)	4 nom.	16.0	74	
5	MA(.85)BA(.15)	5 nom.	16.4	84	72
6	MA(.85)BA(.15)	4 nom.	16.4	79	67
7	MA(.80)BA(.20)	4 nom.	16.6	74	66
8	NH <sub>3</sub> (.55)EA(.25)BA(.20)	4.5	17.2	76	65
9	NH <sub>3</sub> (.44)EA(.18)BA(.38)	4.5 nom.	17.7	66	
10	NH <sub>3</sub> (.17)MA(.56)BA(.27)	5 nom.	17.0	72	
11	NH <sub>3</sub> (.55)MA(.25)BA(.20)	5	17.3	76	66
12	NH <sub>3</sub> (.26)MA(.40)BA(.34)	5 nom.	17.4	79	70
13	NH <sub>3</sub> (.32)MA(.30)BA(.38)	5 nom.	17.6	73	
14	NH <sub>3</sub> (.43)MA(.18)BA(.39)	5 nom.	17.7	77	65
15	NH <sub>3</sub> (.49)MA(.12)BA(.39)	5 nom.	17.9	66	
16	NH <sub>3</sub> (.62)BDMA(.16)BA(.22)	4	17.7	63	53
17	NH <sub>3</sub> (.65)BMA(.15)BA(.20)	6 nom.	17.6	56	
18	NH <sub>3</sub> (.65)BMA(.15)BA(.20)	4 nom.	17.8	58	
19	NH <sub>3</sub> (.50)BMA(.20)BA(.30)	5 nom.	17.9	61	
20	NH <sub>3</sub> (.79)AB(.12)BA(.09)	4 nom.	18.4	39	37
21	NH <sub>3</sub> (.75)AB(.12)BA(.13)	4 nom.	18.4	38	
22	NH <sub>3</sub> (.52)AB(.08)BA(.40)	4 nom.	18.6	49	

**Detailed Studies of Samples of the Type EA + BA + EHBA-Cr<sup>V</sup>**

Figure 2 shows the dependence of the polarization on the temperature of preparation of samples of composition EA(.85)BA(.15)EHBA-Cr<sup>V</sup>(4 x 10<sup>19</sup>/ml). Here, as in later figures, data points lacking tolerance bars correspond to measurements of single samples; tolerance bars indicate the full range of results for multiple samples. Of the eight samples assayed at 200K, two were from a batch size of 2.5 ml and six were from 10-13 ml batches. All subsequent data presented are for samples prepared at ~ 200K, which Fig. 2 indicates is a sufficiently low temperature for practical purposes.

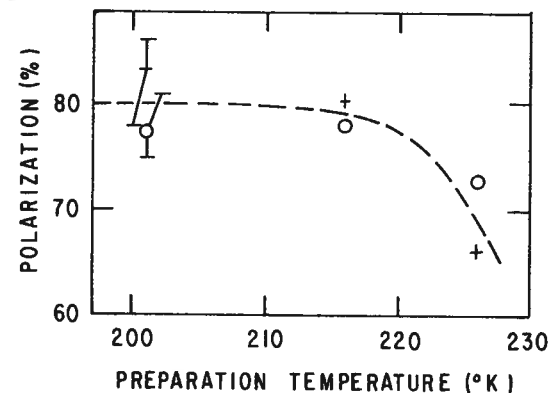


Figure 2 Optimum proton polarization vs. sample preparation temperature for EA(.85)BA(.15)EHBA-Cr<sup>V</sup>(4 x 10<sup>19</sup>/ml). The crosses represent positive enhancement and the open circles, negative enhancement. The dashed curve is a guide for the eye only.

Figure 3 shows the polarization dependence on BA content for EA(1-X)BA(X)EHBA-Cr<sup>V</sup>(4 x 10<sup>19</sup>/ml). Also shown is the behavior of the frequency separation, which is not at all understood. We will refer again to this Figure when we discuss the calorimetric results.

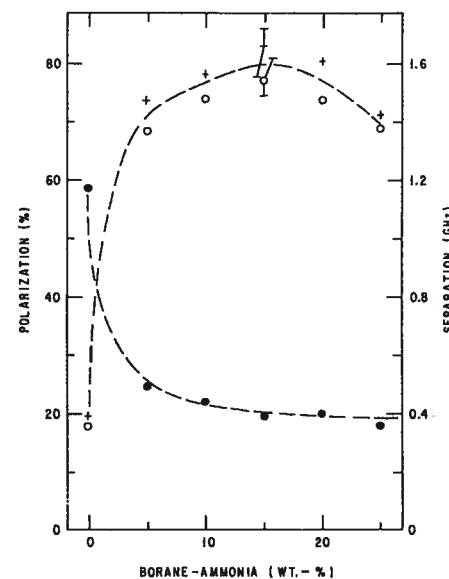


Figure 3 Optimum proton polarization and frequency separation of the positive and negative enhancement maxima vs. BA content, X, for EA(1-X)BA(X)EHBA-Cr<sup>V</sup>(4 x 10<sup>19</sup>/ml). The closed circles represent the separation, the other symbols are as in Fig. 2.

Figure 4 shows the dependence of the polarization and  $T_{1p}$  on the  $Cr^{V}$  content ( $T_{1p}$  is at 1K). The spin concentrations at and above  $4 \times 10^{19}/ml$  are nominal since not all of the dopant dissolves at these levels, in the 4 min. allotted.

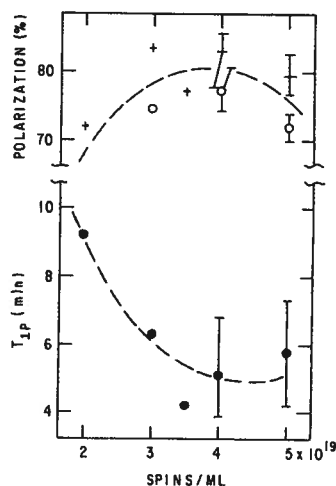


Figure 4 Optimum proton polarization and relaxation time vs.  $Cr^V$  content, for EA(.85)BA(.15)EHBA- $Cr^V$ . The relaxation time is at 1K.

Figure 5 shows polarization reversal, with  $\tau_{.7} = 10$  min.

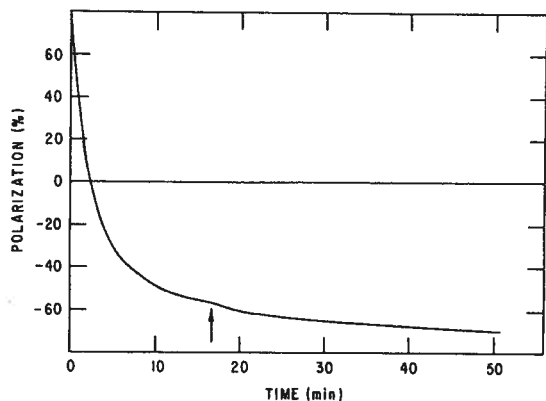


Figure 5 Polarization reversal for EA(.85)BA(.15)EHBA- $Cr^V$  ( $4 \times 10^{19}/ml$ ). At the time marked by the arrow, the microwave power was lowered from twice optimum to optimum.

Figure 6 shows the EPR first-derivative spectra of (a) EA(.85)BA(.15)EHBA- $Cr^V$  ( $4 \times 10^{19}/ml$ ) and (b) "cooked" ethylene glycol, at 2.5T, 0.4K. These were taken by means of a double-modulation NEDOR technique.  $T_{1e}$  was also measured in each case: (a)  $T_{1e} = 170 \pm 20$  ms, (b)  $T_{1e} = 165 \pm 15$  ms.

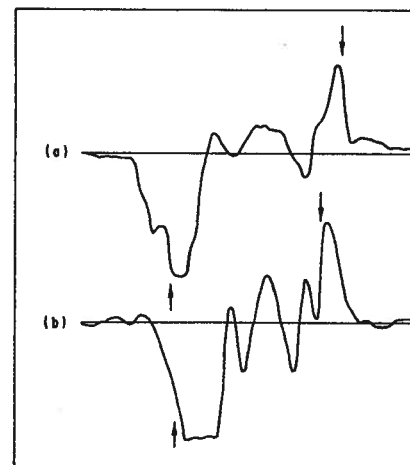


Figure 6 First-derivative EPR spectra taken by the NEDOR technique at 2.5T, 0.4K. (a) is EA(.85)BA(.15)EHBA- $Cr^V$  ( $4 \times 10^{19}/ml$ ) and (b) is dichromate-"cooked" ethylene glycol containing about  $7 \times 10^{19} Cr^V/ml$ . The sweep width is 0.8 GHz. The arrows mark the positions of the DNP maxima.

Figure 7(a) shows a  $^{11}B$  NMR spectrum taken when the proton polarization was + 75%. We have estimated the  $^{11}B$  polarization in two different ways: (a) proton comparison calibration (PCC), that is, lowering the field to obtain the  $^1H$  signal area at the  $^{11}B$  Larmor frequency and using the known  $P(^1H)$  and spectroscopic factors to calibrate  $P(^{11}B)$ , and (b) lineshape (LS), under the assumption that the  $^{11}B$  has a spin-temperature. For  $^{11}B$  ( $I = 3/2$ ), the LS method gives

$$P_{LS}(^{11}B) = (X-1)(3X^2 + 4X + 3)/3(X^3 + X^2 + X+1),$$

where  $X^2$  is the intensity ratio of the outer components. In the case of Fig. 7(a), we obtain

$$\begin{aligned} P_{PCC}(^{11}B) &= 46 \pm 5\%, \\ P_{LS}(^{11}B) &= 48 \pm 3\%. \end{aligned}$$

Equal spin temperature (EST) would give

$$P(^1H) = 75 \pm 2\% \xrightarrow{EST} P(^{11}B) = 47 \pm 2\%.$$

Thus, EST appears to hold in this case.

#### Partially Deuterated Sample

We have made preliminary measurements on a sample in which the ethylamine has been replaced, in an equal number ratio, with perdeuterated ethylamine,  $1/4$  EA d7(.868)BA(.132)EHBA- $Cr^V$  ( $4 \times 10^{19}/ml$ ). The measurements on the remaining  $^1H$  spins give

$$\begin{aligned} P(^1H) &= +89\%, -87\% \\ \Delta\nu_e &= 0.39 \text{ GHz} \\ T_{1p}(1K) &= 7 \text{ min.} \end{aligned}$$

A proton polarization reversal curve is shown in Fig. 8, with  $\tau_{.7} \approx 4.5$  min.

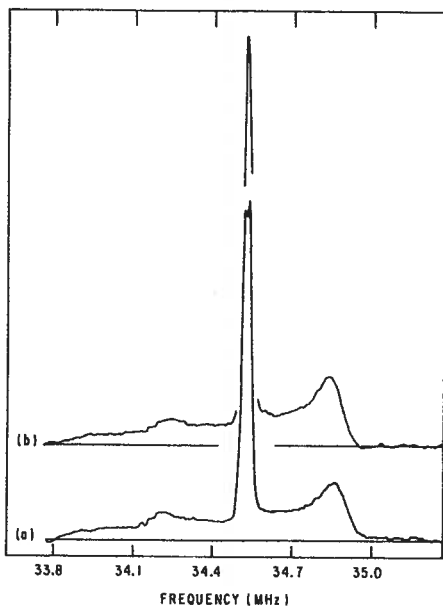


Figure 7 (a) and (b)  $^{11}\text{B}$  NMR spectra for positive enhancement at 2.5T, 0.4K. (a) is for EA(.85)BA(.15)EHBA-Cr $^{\text{V}}$ ( $4 \times 10^{19}/\text{ml}$ ) when  $P(^1\text{H})$  was  $+75 \pm 2\%$ . (b) is for EAd7(.868)BA(.132)EHBA-Cr $^{\text{V}}$ ( $4 \times 10^{10}/\text{ml}$ ) when  $P(^1\text{H})$  was  $+86 \pm 2\%$ .

Figure 7(b) shows a  $^{11}\text{B}$  spectrum taken when the proton polarization was  $+86 \pm 2\%$ , and Fig. 9,  $-82 \pm 2\%$ . In order to estimate polarizations by the "PCC" method the relative numbers of nuclei present must be known. If we use the information provided by the supplier of the EAd7, namely, that the product is 99 atom %D, the fraction of protons remaining in the sample should have been  $\sim .20$ . However, the observed TE area corresponded to a proton fraction of  $\sim .27 \pm .01$ . Evidently either the product was seriously contaminated by our handling or the supplier's specification is in error. We use the fraction indicated by the "TE assay" in the following:

$$P_{\text{PCC}}(^{11}\text{B}) = +57 \pm 3\%, -54 \pm 3\%$$

$$P_{\text{LS}}(^{11}\text{B}) = +57 \pm 3\%, -51 \pm 4\%$$

$$P(^1\text{H}) = +86 \pm 2\%, -82 \pm 2\% \xrightarrow{\text{EST}} +58 \pm 3\%, -54 \pm 2\%.$$

Thus, EST appears to hold between the  $^1\text{H}$  and  $^{11}\text{B}$ .

Figure 10 shows DMR spectra taken when the proton polarization was (a)  $+87 \pm 2\%$ , and (b)  $-86 \pm 2\%$ . Owing to the complexity of the spectrum it appears that the "LS" method cannot be used in this case, at least not without considerable analysis. We have applied the "PCC" method with the result:

$$P_{\text{PCC}}(^2\text{H}) = +36 \pm 4\%, -34 \pm 4\%$$

$$P(^1\text{H}) = +87 \pm 2\%, -86 \pm 2\% \xrightarrow{\text{EST}} +27 \pm 2\%, -26 \pm 2\%.$$

There can be some doubt that EST holds here. In the future we intend to repeat these measurements, and also obtain  $P$  vs.  $v_e$ -curves.

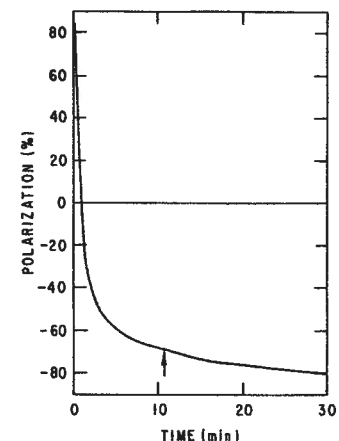


Figure 8 Polarization reversal for the protons in EAd7(.868)BA(.132)EHBA-Cr $^{\text{V}}$ ( $4 \times 10^{19}/\text{ml}$ ). At the time marked by the arrow, the microwave power was lowered from twice optimum to optimum.

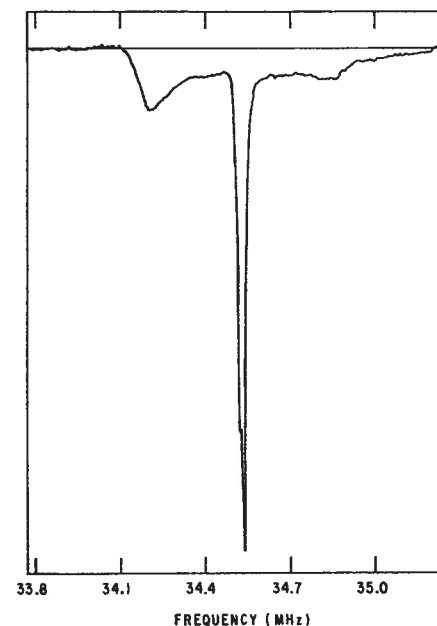


Figure 9  $^{11}\text{B}$  NMR spectrum for negative enhancement when  $P(^1\text{H})$  was  $-82 \pm 2\%$  in the sample of Fig.7(b).

#### Calorimetric Experiments

Figure 11 shows DSC scans /5/ of EHBA-Cr $^{\text{V}}$ -doped beads of EA + BA in (a)-(e), with BA contents of 0, 0.05, 0.10, 0.15, and 0.25, respectively. Figure

11(f) is a scan of EA<sub>7(.868)</sub>BA<sub>(.132)</sub>EHBA-Cr<sup>V</sup>(4 × 10<sup>19</sup>/ml). Exothermic peaks are "up" and time proceeds left-to-right. As the content of BA is increased, a second, low melting-point phase appears, which one would probably identify as a eutectic. This phase appears to dominate in the EA(.85)BA(.15) sample, so that the composition of the eutectic must be close to this. A single phase is maintained in the EA(.75)BA(.25) sample, but the melting point is higher. Samples (c), (d), and (e) appear to be completely glassy, but sample (b) is no more than ~10% glass. The partially deuterated sample (f) appears very similar to the protiated analog (d), although there is a slight doubling of the melting feature.

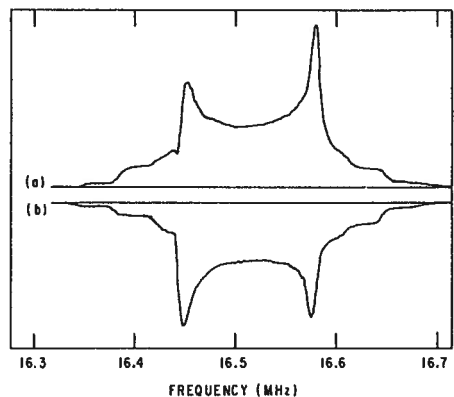


Figure 10 DMR spectra for the sample of Fig. 7(b). In (a),  $P(^1\text{H})$  was  $+87 \pm 2\%$ . In (b),  $P(^1\text{H})$  was  $-86 \pm 2\%$ .

It is interesting to compare these data to the polarization behavior of the same samples in Fig. 3. Two conclusions are indicated: 1) the maximum polarization occurs at or near the eutectic point, reminiscent of alcohol-water mixtures, /6/ and 2) the polarization rises more rapidly than the glass fraction.

#### Safety

If anyone contemplates working with these materials, they should be aware of the possibility of spontaneous combustion. Ammonium borohydride, by itself, can spontaneously ignite upon contact with traces of water, or prolonged contact with humid air. The borane complexes are less susceptible to ignition; however, when mixed with Cr<sup>V</sup> complexes ignition is possible, particularly if large amounts of such a mixture are subjected to room temperature or above.

This work was supported in part by the U.S. Department of Energy.

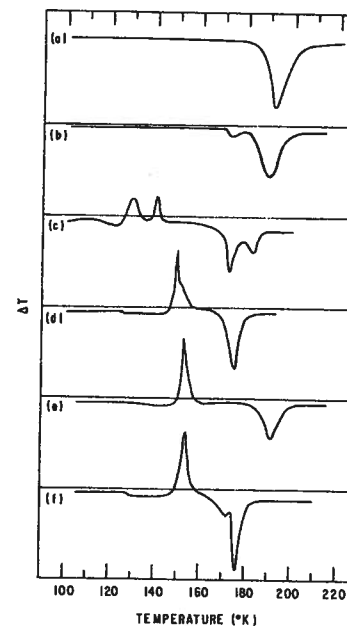


Figure 11 Differential calorimeter scans of (a) EA, (b) EA(.95)BA(.05), (c) EA(.90)BA(.10), (d) EA(.85)BA(.15), (e) EA(.75)BA(.25), and (f) EA<sub>7(.868)</sub>BA<sub>(.132)</sub>, all doped with EHBA-Cr<sup>V</sup>(4 × 10<sup>19</sup>/ml). The scanning rate is  $\dot{T} = 1 \pm 0.1\text{K/min}$ .

#### REFERENCES

- \* Visiting scientist from Rochkurst College, Kansas City, Missouri 64110.
- 1. Neslab Instruments, Inc., Portsmouth, NH; Model CC-80.
- 2. Mettler Instrument, Inc., Hightstown, NJ; Model PC-440.
- 3. All gaseous chemicals were obtained from Matheson Gas Products, Lyndhurst, NJ.  
Borane complexes were obtained from Alfa Products, Danvers, MA.
- 4. MSD Isotopes, Pointe Claire-Dorval, Quebec.
- 5. We have used the calorimeter described in "An Investigation of Polarized Proton Target Materials by Differential Calorimetry -- Preliminary Results", D. A. Hill and J. J. Hill, Argonne Report ANL-HEP-PR-81-05, October, 1980.
- 6. S. Mango, O. Runolfsson, and M. Borghini, Nucl. Instr. and Methods 72, 45 (1969).

STABILITY OF CHROMIUM(V) DOPED TARGET MATERIALS  
CONTAINING BORANE-AMMONIA AND AMINES

M. Krumpolc  
University of Illinois at Chicago  
Chicago, Illinois 60680

D. Hill  
Argonne National Laboratory  
Argonne, Illinois 60439

7 August 1984

ABSTRACT

Stability of the EHBA-Cr(V) complex (sodium bis[2-ethyl-2-hydroxybutanoato-(2-)]oxochromate(V)) in methylamine, ethylamine, propylamine, sec-butylamine and ammonia in the presence of borane-ammonia,  $\text{BH}_3\text{:NH}_3$  (0-20% w/w) has been followed spectrophotometrically between  $-30^\circ$  to  $-65^\circ$  C. It has been observed that even a small amount of  $\text{BH}_3\text{:NH}_3$  (<5% wt) can substantially retard chromium(V) disproportionation (decomposition) into chromium(VI) and chromium(III), and thus enable preparation of chromium(V) doped glasses (targets) within practical temperature ( $-45^\circ$  to  $-50^\circ$  C) and time (30 - 60 min) limits.

1. Introduction

In our effort to prepare polarized targets with a very high hydrogen content (i.e. > 15%), we have extended our search towards borane-ammonia (19.6% H) and several aliphatic amines used as solvents. Preliminary results indicated /1/ that an optimum combination of hydrogen content and polarization can be obtained for a glass containing ethylamine and borane-ammonia. As chromium(V) - used as a dopant in polarized targets - is known to undergo instantaneous decomposition in alkaline media /2/ (e.g. amines) at room temperature, we are searching for the sufficiently low temperature range which would permit preparation of a target material without any significant decomposition.

2. Experimental Section

**Materials.** Methylamine (Matheson), ethylamine (Matheson), propylamine (Aldrich), and ammonia (Matheson) were used as received. Sodium bis[2-ethyl-2-hydroxybutanoato-(2-)]oxochromate(V) was prepared from sodium dichromate and 2-ethyl-2-hydroxybutanoic acid in acetone /2/. Borane-ammonia (Alfa Products, Ventron) was recrystallized from diethyl ether, dried in vacuo and kept in a freezer.

**Stability Measurements.** At  $-30^\circ$  C decomposition of chromium(V) was continuously monitored from decrease in absorbance at 540 nm using a Cary Model 14 recording spectrophotometer equipped with a thermostated cell holder, a thermocouple, and a protective atmosphere of dry air. Low temperature was generated using a Lauda K4R methanol bath circulator. In a typical run 150 mg of

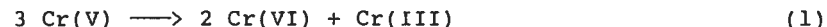
borane-ammonia were dissolved in 850 mg (1.18 mL) of propylamine (15% wt/wt) in a 2 mL, 1 cm-cell, and the solution chilled to  $-70^\circ$  to  $-80^\circ$  C (in dry ice-ethanol bath) under the stream of helium. The chromium(V) complex (6.13 mg;  $10^{19}$  spin/mL) was scooped from a capillary dropper and the cell was shaken for several minutes. The reaction was initiated by warming up the solution briefly to  $-30^\circ$  C in a bath of chilled methanol - dry ice, and then followed spectrophotometrically at the same temperature. In the case of ethylamine (b.p.  $19^\circ$ - $20^\circ$  C), the gas was first condensed and then transferred by a chilled pipet into a cell. Methylamine and ammonia were directly condensed into a cell.

For carrying out experiments at even lower temperatures ( $-50^\circ$  to  $-65^\circ$  C) a cold-bath-cryogenic unit Neslab Cryocool CC-60 II equipped with an immersion cooler was used. The "finger" was placed in a Dewar flask filled with ethanol, and the fluid mechanically stirred. The temperature was maintained with the accuracy of  $\pm 0.5^\circ$  C. The reaction progress was measured by quickly inserting cells (for 5-7 sec) in regular time intervals into a spectrophotometer.

**Spectra Measurements.** Spectra were measured in 2 mL, 1cm-cells (fitted with a stopper) in the range of 460-800 nm where the difference between individual oxidation states of chromium is most noticeable /3/. The initial chromium(V) concentration was  $10^{19}$  spin/mL (0.0166 M).

3. Results and Discussion

Since the objective of this study was the preparation of target materials composed of borane-ammonia dissolved in aliphatic amines, namely ethylamine, it was first necessary to investigate the stability of chromium(V) and determine the temperature range within which this dopant is sufficiently stable. Aliphatic amines are very strong bases and under these conditions chromium(V) at ambient temperature instantaneously disproportionates /4/ into chromium(VI) and chromium(III), eq. 1, (Fig. 1, curve 2a). Figure 1 shows that the same reaction



also proceeds in the presence of borane-ammonia as very similar spectra of the reaction mixture of chromium(VI) and chromium(III) were recorded (curve 2b). However, in this case the chromium(VI) in then slowly over a period of about 1 day reduced to chromium(III) (curve 3). The spectrum of chromium(V) is enclosed for comparison (curve 1). From these data it is thus obvious that the chromium(V) dopant has to be introduced at low temperature.

Further investigation was then conducted at  $-50^\circ$  and  $-65^\circ$  C. The results of our kinetic studies are summarized in Table I. In addition to ethylamine, three other amines and ammonia were used for comparison. Only the initial part of the disproportionation curve could be used for estimating kinetic data, as the absorption of chromium(VI) and chromium(III) in

alkaline media considerably interferes with that of chromium(V) (Fig. 1). Thus, the stability of chromium(V) in individual sol-

Table I. Stability<sup>a</sup> of Chromium(V) ( $10^{19}$  spin/mL) in Aliphatic Amines and Ammonia in the Presence of Borane-Ammonia.

Solvent	Stability at $-50^{\circ}\text{C}$		Stability at $-65^{\circ}\text{C}$	
	Pure	$\text{BH}_3\text{NH}_3$ added (15% w/w)	Pure	$\text{BH}_3\text{NH}_3$ added (15% w/w)
Methylamine	10 min	> 1 hr	45 min	> 1 hr
Ethylamine	2 min	> 1 hr	10 min	> 1 hr
Propylamine	1 min	> 1 hr	5 min	> 1 hr
sec-Butylamine	3 min	> 1 hr	15 min	> 1 hr
Ammonia	>1 hr	> 1 hr	>1 hr	> 1 hr

<sup>a</sup> Stability expressed in terms of the time needed to achieve 15% disproportionation (decomposition) of chromium(V) into chromium(VI) and chromium(III).

vents shown in Table I is given in terms of an initial decrease in absorbance monitored at 540 nm where the difference in absorption between the chromium(V) and its reaction products reaches the maximum. The results show that the stability of chromium(V) in amines is greatly increased in the presence of borane-ammonia. While the data in the first and third columns are kinetically in agreement with the expected disproportionation rate at these temperatures, the unusually high stability of chromium(V) - in the range of about two orders of a magnitude - achieved in the presence of "inert" borane-ammonia (15% w/w) is quite puzzling. It is also obvious that this effect does not occur in ammonia.

In order to gain some further support for this unexpected behavior, the stability of chromium(V) in ethylamine and propylamine was studied at  $-30^{\circ}\text{C}$  at various  $\text{BH}_3\text{NH}_3$ /amine ratios. The results in Figure 2 show that the initial fast disproportionation of chromium(V) is indeed greatly suppressed even by the addition of a small amount of borane-ammonia (<5% wt), as shown by an asymptotic character of both curves. Currently we have no reasonable explanation for this otherwise beneficial behavior.

From the results obtained so far we have been able to identify conditions under which no considerable decomposition of the chromium(V) doped target material of borane-ammonia - amine occurs. Our data indicate that if the target preparation is carried out at the temperature range of  $-45^{\circ}$  to  $-50^{\circ}\text{C}$ , a sufficient amount of time (30-60 min) is available to make it feasible.

This work was supported in part by the U. S. Department of Energy.

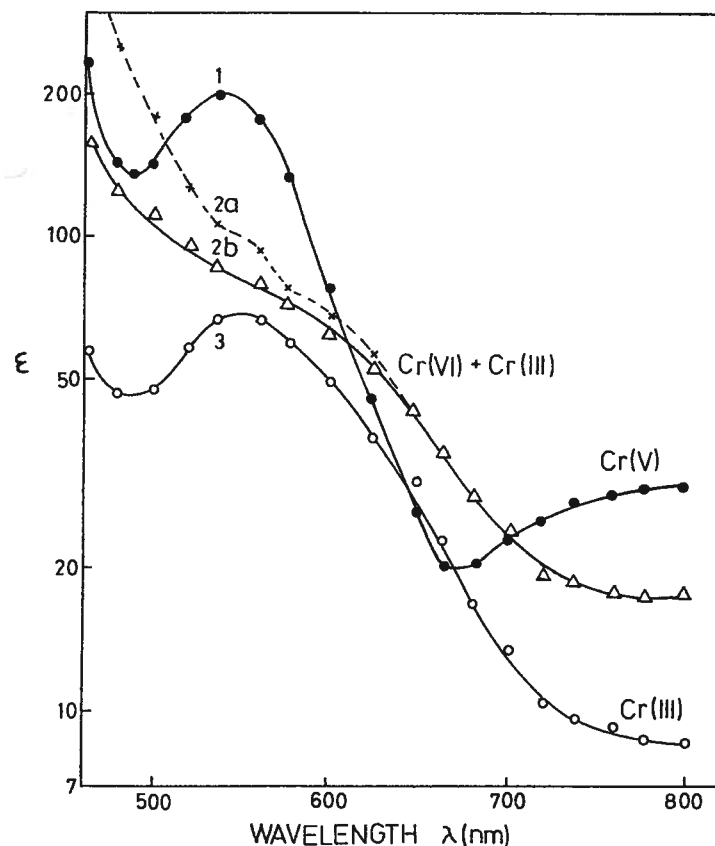


Figure 1. Spectra of the EHBA-Cr(V) complex at  $20^{\circ}\text{C}$ : 1) in acetone; 2a) in ethylamine; 2b) in ethylamine/borane-ammonia (15% w/w); 3) in ethylamine/borane-ammonia (15% w/w) after 24 hr.

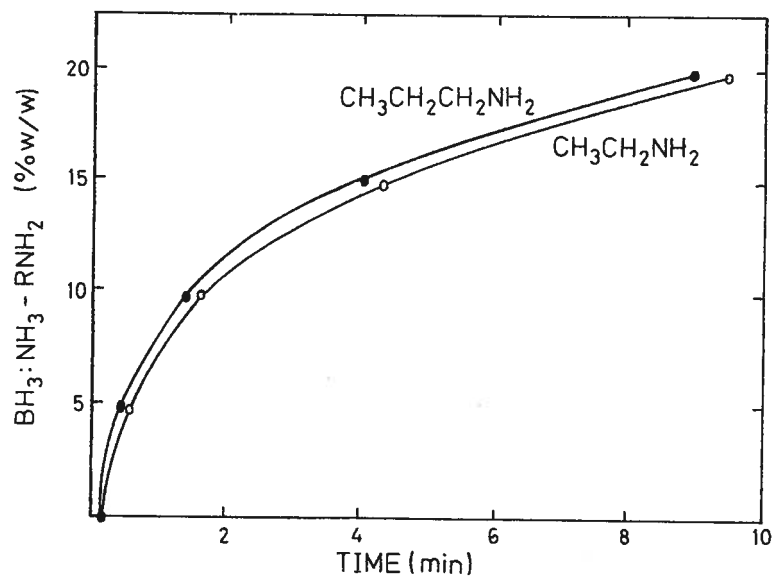


Figure 2. Stability vs. composition of the borane-ammonia/amine target materials at  $-30^{\circ}\text{C}$ . (Stability expressed in terms of the time needed to achieve 15% disproportionation of chromium(V) into chromium(VI) and chromium (III)).

#### 4. References

1. D. Hill and M. Krumpolc, *These Proceedings*.
2. M. Krumpolc and J. Rocek, *Inorg. Synth.*, 1980, 20, 63.
3. M. Krumpolc and J. Rocek, *J. Am. Chem. Soc.*, 1976, 98, 872.
4. M. Krumpolc and J. Rocek, *Inorg. Chem.*, to be published.

# RADIATION DAMAGE IN AN ETHYLAMINE-BORANE:AMMONIA TARGET

D. G. Crabb

University of Michigan  
Ann Arbor, Michigan 48109

D. Hill

Argonne National Laboratory  
Argonne, Illinois 60439

In the course of an experiment at the Brookhaven AGS to measure  $A_{NN}$  in pp elastic scattering at 16 GeV/c, we have subjected a polarized target of ethylamine (85 wt.%) + borane-ammonia (15 wt.%) + EHBA-Cr<sup>v</sup> ( $4 \times 10^{19}/\text{ml}$ ) to an integrated beam flux of  $\sim 10^{14}/\text{cm}^2$ . The target beads were prepared /1/ at Argonne and shipped at LN<sub>2</sub> temperature to BNL. The <sup>3</sup>He refrigerator services a target of  $\sim 25 \text{ cm}^3$  volume, at 2.5T.

Two separate bead loads were used. The first load was polarized at a refrigerant temperature of  $\sim 0.49\text{K}$  with a mixture of <sup>3</sup>He/<sup>4</sup>He as refrigerant, with the results:

$$P = +75\%, -73\% \\ \Delta\nu_e \approx 0.36 \text{ GHz}$$

The second load was initially run with the <sup>3</sup>He/<sup>4</sup>He mixture, and later run at  $\sim 0.47\text{K}$  with pure <sup>3</sup>He as the refrigerant; it gave initial polarizations of

$$P = +74\%, -71\%$$

Frequency modulation of the microwaves was not used in either case. The second load was used for the rest of the results presented here.

Figure 1 shows the evolution of the polarization as a function of irradiation. The break in the curves coincides with the change of refrigerant. The effective cross-sectional area of the target is  $\sim 3.1 \text{ cm}^2$ ; the values on the abscissa should be divided by this number in order to estimate the flux. The slopes of the lines correspond to

$$\phi_0(+)=7 \times 10^{14}/\text{cm}^2 \\ \phi_0(-)=3.5 \times 10^{14}/\text{cm}^2$$

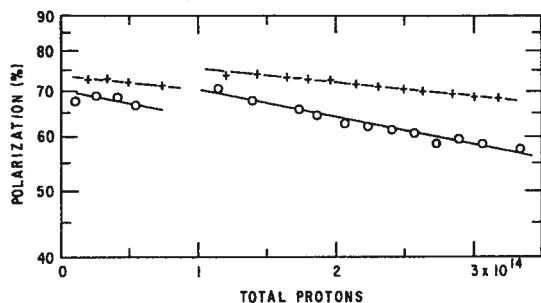


Figure 1 Evolution of the maximum polarization vs. dose. The crosses are for positive enhancement and the open circles, negative. The lines are drawn by eye.

Thus, the radiation tolerance of this material seems to be roughly comparable to that of butanol-porphyraxide, and well below that of irradiated NH<sub>3</sub>.

Figure 2 shows polarization build-up curves at different levels of irradiation. Curves (a) correspond to  $\sim 1.1 \times 10^{14}$  total protons, and curves (b) to  $\sim 3.1 \times 10^{14}$  total protons. We obtain  $\tau_{7(+)} = 20 \text{ min.}$ ,  $\tau_{7(-)} = 14 \text{ min.}$  at either level of dose. These build-up times are substantially shorter than those that we have been able to attain thus far in irradiated NH<sub>3</sub>.

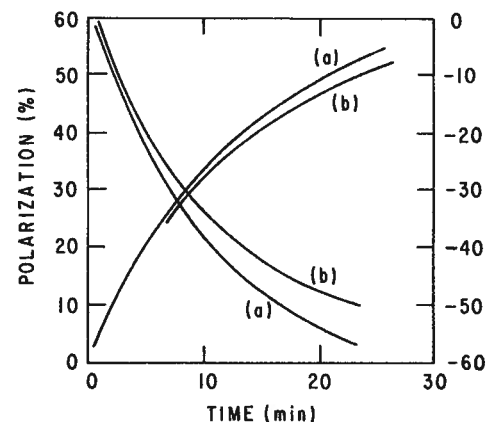


Figure 2 Polarization build-up for two doses (a)  $\sim 1.1 \times 10^{14}$  total protons, (b)  $\sim 3.1 \times 10^{14}$  total protons. The microwave power applied is  $\sim$  twice optimum.

## REFERENCES

1. See D. Hill, J. Hill, and M. Krumpolc, elsewhere in this Workshop.

## THE EMC POLARISED TARGET

S. C. Brown, G. R. Court and R. Gamet  
Department of Physics, University of Liverpool,  
Oliver Lodge Laboratory, Liverpool, L69 3BX, U.K.

O. Hartmann  
University of Uppsala, S75121 Uppsala, Sweden.

T. Niinikoski, J. M. Rieubland and A. Rijllart  
CERN, 1211 Geneva 23, Switzerland.

### 1. Introduction

The EMC polarised target was conceived as part of the programme of experiments being carried out by the European Muon Collaboration to study the nucleon substructure using the CERN SPS muon beam. The specific experiment which is currently in progress aims to measure the proton spin dependent structure function  $G_1(Q^2, \nu)$  for which both the beam and the proton target need to be longitudinally polarised. The experiment exploits the fact that the SPS muon beam has an intrinsic high longitudinal polarisation which arises from its production mechanism. The longitudinal target polarisation requires the polarising magnetic field to be parallel to the beam direction and this is most conveniently provided by means of an iron free superconducting solenoid. The experimental angular access requirements are relatively modest because of the highly relativistic nature of the reaction kinematics at the beam energies involved (100 to 280 GeV). The solenoid was in fact designed so that the angular access for the worst situation (the upstream end of the target) approximately matches the acceptance of the EMC forward spectrometer.

The volume of target material required depends on the beam shape and size as well as the maximum available (or usable) beam intensity. The SPS muon beam has an approximately Gaussian intensity distribution with a FWHM of  $\sim 50$  mm at the target region. The nominal target length was chosen to be 1 m on the basis of a reasonable event rate combined with acceptable cost. The experiment is in fact event rate limited at a level which corresponds quite closely to use of this length of target. The target diameter was chosen to be nominally 60 mm as this allows over 70% of the beam to be intercepted while again keeping the cost within practical limits.

The parameter measured in the experiment is an asymmetry  $A_m$

$$\text{where } A_m = \frac{N_{++} - N_{+-}}{N_{++} + N_{+-}}$$

The physics asymmetry  $A$  is related to  $A_m$  via the expression

$$A_m = P_\mu D_p F D_A$$

where  $P_\mu$  is the beam polarisation,  $P_p$  is the target polarisation,  $D$  is a kinematic factor linking the polarisation of the incident muon to that of the virtual photon and  $F$  is the dilution factor which arises because of the presence of unpolarised protons and neutrons in the nuclei in the target material. Clearly the statistical accuracy of the experiment for a given total number of incident beam particles increase as  $D$  and  $F$  are increased and as consequence of the two materials available, pentanol ( $F = 0.13$ ) and ammonia ( $F = 0.17$ ), ammonia is being used.

If it is assumed that both  $P_\mu$  and  $P_p$  have value of 0.8 then the maximum possible value for  $A_m$  (assuming the factor  $D_A = 1$ ) is 0.1. Systematic errors due to variation in the effective detection efficiency of the apparatus as a function of time become very important when such small asymmetries are being measured. In normal asymmetry experiments these systematic effects are minimised by making frequent reversals of the target (or beam) polarisation direction, combined with very precise monitoring of the beam flux. These techniques are not practicable in the EMC case as the only way the beam polarisation can be reversed, while still maintaining a high intensity and polarisation, is by changing the sign of the beam, while the target polarisation reversal time is relatively long (see section 7). Also it is very difficult to precisely monitor the effective beam flux, firstly because the target has a smaller diameter than the beam so that the effective flux is a function of both beam position and shape, and secondly because of the inherent difficulty in the precise measurement of a flux of high energy muons.

All these difficulties are avoided, or at least reduced to a reasonable level, by splitting the target into two sections in tandem, polarised in opposite directions. The experiment must then be able to identify unambiguously from which half of the target any particular event originates and this necessitates a 200 mm gap between the two sections. The cost of using this arrangement is a loss of 20% of the available event rate and considerable extra complication in the microwave system. Some reversals of the target polarisation are still required as it is necessary to account for the slightly different experimental acceptance for the two halves of the target. However as this effect is small they need to be only at relatively infrequent intervals. The cross section of the target is not, for structural reasons, circular. It is in fact 60 mm high by 50 mm wide (see fig. 1). For the same reasons, the overall section lengths are 380 mm giving a total volume of 2.1 litres.

### 2. Superconducting Magnet (For full description see ref. 1)

The superconducting solenoid has a main coil which is 1600 mm long and has a clear bore of 190 mm. It operates in driven mode at a current of 180 amps for a field of 2.5 T. There are twelve trim coils wound on top of the main coil, each 132 mm long, uniformly distributed along its length. The number of turns and the currents in each trim coil are graded to provide the necessary higher correction field at the ends of the main coil as compared with the middle. The magnet is pool cooled with liquid helium at 4.2 K. The boil off gas is used to cool the radiation shield. The average heat input is approximately 6 watts when the magnet is fully powered. It is automatically filled from a 2000 litres helium storage dewar situated adjacent to the target as necessary. The storage dewar is itself supplied from a Sulzers "Cold Box" liquifier. All the gas is recovered and recirculated through this system. The cryostat is of fully welded construction using only aluminium alloy and titanium.

The main coil and the trim coils each have a separate power supply which give a field stability of  $\pm 5$  parts in  $10^5$  over 24 hours. The energising time to operating field is 10 mins. A computer controlled field shift facility ( $\sim 12.5$  mT) is also included to facilitate automatic measurement of the background levels for the NMR signals. The field uniformity is within  $\pm 8$  parts in  $10^5$  over a volume 1000 mm long and 60 mm diameter. An axial field plot obtained with an NMR probe is given in fig. 2.

### 3. The Dilution Refrigerator (For full description see ref. 2 and 3)

The target material is cooled by a  $^3\text{He}/^4\text{He}$  dilution refrigerator which is integrated with the superconducting magnet but has an independent insulating vacuum. With the currently available target materials, the dynamic polarisation processes requires microwave power of at least 1 mw per gram of material. This corresponds to a total microwave power in this target of 1.1 watt. On test, the refrigerator, which was designed to extract powers up to 2.5 watts at 0.5 K, reached a cooling power of 2 watts at 0.5 K the performance being limited only by the maximum available throughput of the  $^3\text{He}$  circulation pumps. This cooling capability has been found to be adequate for the irradiated ammonia target material being used.

It is impossible to use the conventional technique for target material loading, where the whole low temperature part of the refrigerator is removed, with such a large and complex system. It is therefore necessary to have direct horizontal load access to the mixing chamber for loading. The target material (at 77 K) contained in a special holder is loaded into the access tube and a rapid sealing indium joint makes a superleak tight seal to the mixing chamber<sup>2/</sup>. The holder also acts as beam access tube and carries the beam windows to atmosphere and to the mixing chamber. The region between these two windows is evacuated and contains only thin radiation shields so minimising the material in the beam path. The mixing chamber is 72 mm in diameter and is constructed from 0.25 mm thick mylar film. The only other components situated within the bore of the magnet are the dilute/concentrated  $^3\text{He}/^4\text{He}$  stream heat exchanger and the vacuum isolating tube which also acts as the microwave cavity (fig. 1). Both these are outside a radius of 50 mm so ensuring that even the wings of the beam do not see significant quantities of material. The liquid  $^4\text{He}$  required to operate the dilution refrigerator is supplied from the 2000 litre buffer dewar. The test performance of the refrigerator is given in fig. 3. To the best of our knowledge this is the highest power dilution refrigerator in existence today.

Stable operation at temperatures in the region of 1 K (for NMR polarisation measurement calibration purposes) is possible when nominally pure  $^4\text{He}$  only is circulated. In these circumstances the temperature is measured using a calibrated germanium resistor and three Speer carbon resistors.

The refrigeration system has been designed so that it can be operated for long periods in a standby mode with much reduced consumption of liquid helium, electricity and cooling water. The target material is then maintained at a temperature in the region of 50K which is low enough to ensure that there is negligible decay in the paramagnetic centre density in the target material even over an extended time period. Thus a complete experiment can be carried out without unloading and reloading the target material.

### 4. Microwave System

Each target section is contained within a microwave cavity approximately 400 mm long and 150 mm in diameter. The microwave power is fed into each cavity via a length of rectangular WG22 (8mm) wave guide with a taper slot in the wide wall. Each section is linked to the refrigerator faceplate by a circular 4mm cupro-nickel wave guide which is vacuum sealed at both ends with FEP windows. Two separate microwave power sources, Varian extended interaction oscillators type VKE2401-H3, are used one for each section. These tubes are capable of providing 20 watts which is more than adequate even when transmission losses are taken into account. Each microwave circuit contains a transmission calorimeter to monitor tube power, a directional coupler for

frequency measurement, a specially designed high power blade attenuator, and a three port circulator used as an isolator. The relative frequency is monitored continuously as the beat frequency with a reference klystron which is itself compared against a temperature stabilised cavity wavemeter. The absolute power levels are not measured but power optimisation is carried out using carbon resistor bolometers mounted inside the cavities.

The microwave isolator between the two sections of the target created some design problems as it must not significantly impede the circulation of liquid helium within the mixing chamber as well as allowing mechanical assembly of the mixing chamber and cavity, and target loading. All this must be achieved with minimum extra material as the isolator is in the beam path. The final arrangement involved a series of staggered copper foil baffles and microwave absorbing material mainly in the form of graphite cloth and graphite film painted on the relevant surface. The performance of this isolator is not perfect as it has been observed that if microwave power is fed to only one section the polarisation in the other section rises to a level of a few percent after several hours. However, this does not appear to significantly affect the maximum values of polarisation attainable when both sections are operated at the same time.

### 5. Polarisation Measurement

The polarisation is measured using standard NMR techniques. With such a large amount of material it is not possible to sample the whole volume of one section with one NMR coil. Four NMR channels are therefore used for each section. Each NMR coil is buried in the target material and is in the form of a single turn loop of 2 mm diameter cupro-nickel tube. The loops have an elliptical cross section (30 mm x 80 mm) and an approximate inductance of 0.1  $\mu\text{H}$ . A Teflon sleeve is threaded over the coil tube to reduce the very non-uniform sampling which can occur with material which is in the high RF magnetic field region close to the surface of the coil. The loops are mounted uniformly along each section of the target with their axes perpendicular to the beam direction. They are coupled to the face plate of the load holder via semi-rigid Be-Cu coaxial cables (UG85) which form part of the support structure for the target cells. Each cable is made up to a length of  $3\lambda/2$  before connection to its NMR module. Each coil has its own RF processing module and the eight modules are mounted in a block close to the face plate of the refrigerator.

The coils are operated in series resonance and the system used is a constant current Q meter. With the very large amounts of material sampled by each coil, there are no problems about signal to noise ratio. There are, however, potential difficulties with non-linearity correction because of the high coil filling factor and hence large signal modulation which can occur. The Liverpool RF phase sensitive detection system<sup>4/</sup> is used. This has a very high intrinsic linearity and allows modulation levels in the range 30% to 50% to be used with negligible non-linearity corrections in the integrated signal<sup>5/</sup>. A block diagram of the complete NMR system is given in fig. 4.

The RF power for the NMR system (106.3 MHz swept over a range of 400 KHz) is provided by a signal generator situated in the counting room. All the RF signal processing and the low level NMR signal amplification is carried out in the temperature stabilised modules mounted close to the target. The channels are sampled consecutively at a rate of one measurement per SPS cycle. No RF circuits are switched or interrupted although the RF supply to each coil is removed when it is not being sampled to avoid unnecessary saturation and possible interaction effects.

The high level signals are fed to the counting room where they are digitised and averaged, in a CAMAC based ADC system which also provides the scan waveform for the signal generator. The CAMAC system is controlled by a HP2100A minicomputer which also provides all the control signals for the switching circuits and the signal processing and display facilities. The polarisations and other relevant data is supplied to the main experiment data acquisition computer every SPS cycle. The NMR system is calibrated in the normal way using thermal equilibrium signals at temperatures in the region of 1 K. The statistical uncertainty in the calibration signal areas is typically 1%. The variation of calibration signal for the same target material and coil taken at different times spread over some weeks is in the range 1 to 4%. These larger errors result from uncertainties in the uniformity and absolute determination of the calibration temperature as well as drifts in the NMR electronics.

## 6. Monitoring and Alarm System

The important operational parameters are monitored continuously by a single crate CAMAC system using standard CAMAC modules and an independent crate controller (ICC) with a terminal and a modem connected to the ICC. On power up the ICC automatically loads the last used programme from a RAM file module and this, when combined with battery back up, ensures fail safe operation under all circumstances. The parameters are monitored via a 32 channel ADC used in conjunction with a clock/calendar module. The highest and lowest values which occur for each parameter are recorded over any desired period of time. Limits can be set via the terminal for high value, low value and derivative for any parameter and an alarm signal is generated when any limit is crossed. The system also provides a time record of the seven most important parameters on a colour TV monitor and a printout of all alarms.

The alarm signal starts an audible alarm in the experiment counting room and generates an automatic call on the CERN paging system. The modem is linked to a standard telephone line so that, with the aid of a portable hard copy terminal and an acoustic coupler, a printout of the status of all parameters can be obtained from off site remote locations. These facilities obviate the need for continuous operator attendance

## 7. Performance

The target has been operating in the muon beam in a data taking mode for approximately four months using ammonia beads irradiated at the Bonn Electron Synchrotron<sup>6/</sup>. This material has a proton relaxation time in the range 16-23 mins at 1 K. Average polarisation growth curves for both sections polarised in opposite direction are shown in fig. 5. It appears from this data that the downstream section polarises more efficiently than the upstream one. The reason for this is not clear. It may also be seen that the negative polarisation obtained are consistently higher than positive. This is a property of ammonia and has been observed in small samples under various conditions<sup>7/</sup>. The kinks in the growth curves occur when changes were made to the operational parameters to maximise the rate of polarisation growth. It has been found the separation of the two optimum microwave frequencies becomes greater as the polarisation increases and is approximately 340 MHz at maximum. The optimum power level decreases as the polarisation increases. The very slow rise from 70% to maximum value is also an observed characteristic of irradiated ammonia when polarised in a dilution refrigerator. The maximum mean values so far recorded are -87% and +82%.

A straight average of the polarisation of the individual coils is used

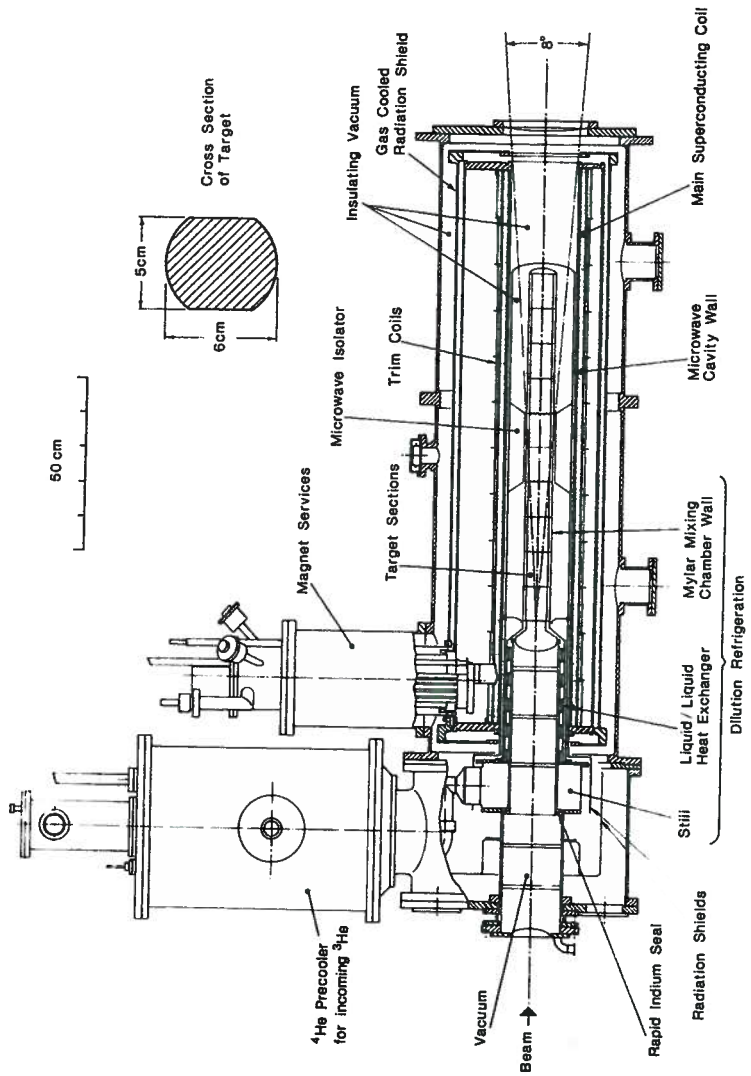
to calculate the mean value. The maximum difference between the values measured by individual coils is in the region of 4% at maximum polarisation. These figures are larger during polarisation growth suggesting that the microwave power distribution within the cavities may be somewhat non-uniform.

The base temperature of the dilution refrigerator is low enough for the target to be operated in frozen spin mode and although this does not alter the experimental situation, it gives some important operational advantages. Firstly the microwave system can be switched off and so does not need to be monitored. Also a partial failure in the magnet power supplies, provided a reasonable value of field can be maintained, or a partial or complete failure of the NMR system does not shut down the experiment. Finally the load on the refrigerator gas circulation pumps is much lower making failure much less probable. A decay rate of polarisation of  $0.78 \pm 0.1\%$  per day has been measured at a nominal mixing chamber temperature of 130 mK.

The target has generally operated very reliably without continuous operator attendance. The most serious problems have arisen as a consequence of power failures. If magnet power is lost and not restarted within approximately 10 mins the field will go to zero and the polarisation is lost, leading to a loss of about 16 hours data taking time. The consequences for the refrigerator of power loss are more serious and it has been necessary to install special back-up systems to ensure that the He<sup>3</sup> can be recompressed into the storage vessels and some cooling maintained for the actual target material to keep it below the electron centre anneal temperature (~ 100 K).

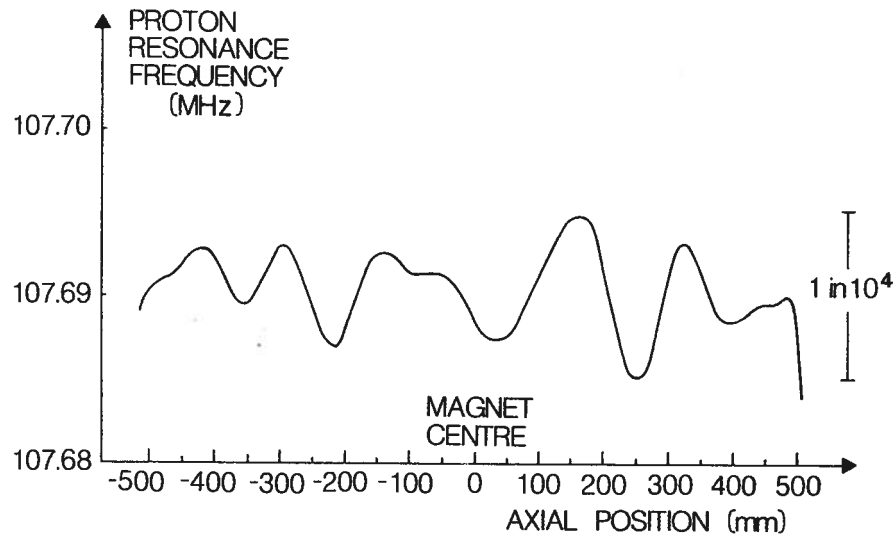
## 8. References

- /1/ N. H. Cuncliffe and R. L. Roberts  
Proc. 7th Int. Conf. on Cryogenic Engineering, London 1978 (IPC Science and Technology Press) p.102.
- /2/ T. O. Niinikoski  
Nucl. Inst. and Methods Vol. 192 1982 p.151
- /3/ T. O. Niinikoski and J. M. Rieubland  
Proc. 9th Int. Conf. on Cryogenic Engineering, Kobe, Japan 1982.
- /4/ D. Gifford  
Proc. of Second Workshop on Polarised Target Materials, Rutherford Laboratory RL80-080 1980 p.85.
- /5/ T. Niinikoski  
Ibid p.80.
- /6/ S. Brown  
Proceedings of this Workshop
- /7/ T. O. Niinikoski and J. M. Rieubland  
Phys. Letts. 72A 1979 p.141.



E.M.C. POLARISED TARGET

FIGURE 1



E.M.C. POLARISED TARGET  
AXIAL MAGNETIC FIELD

FIGURE 2

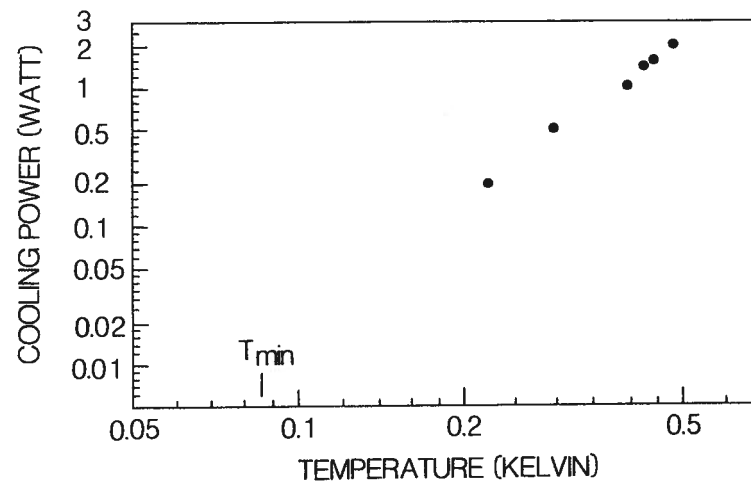
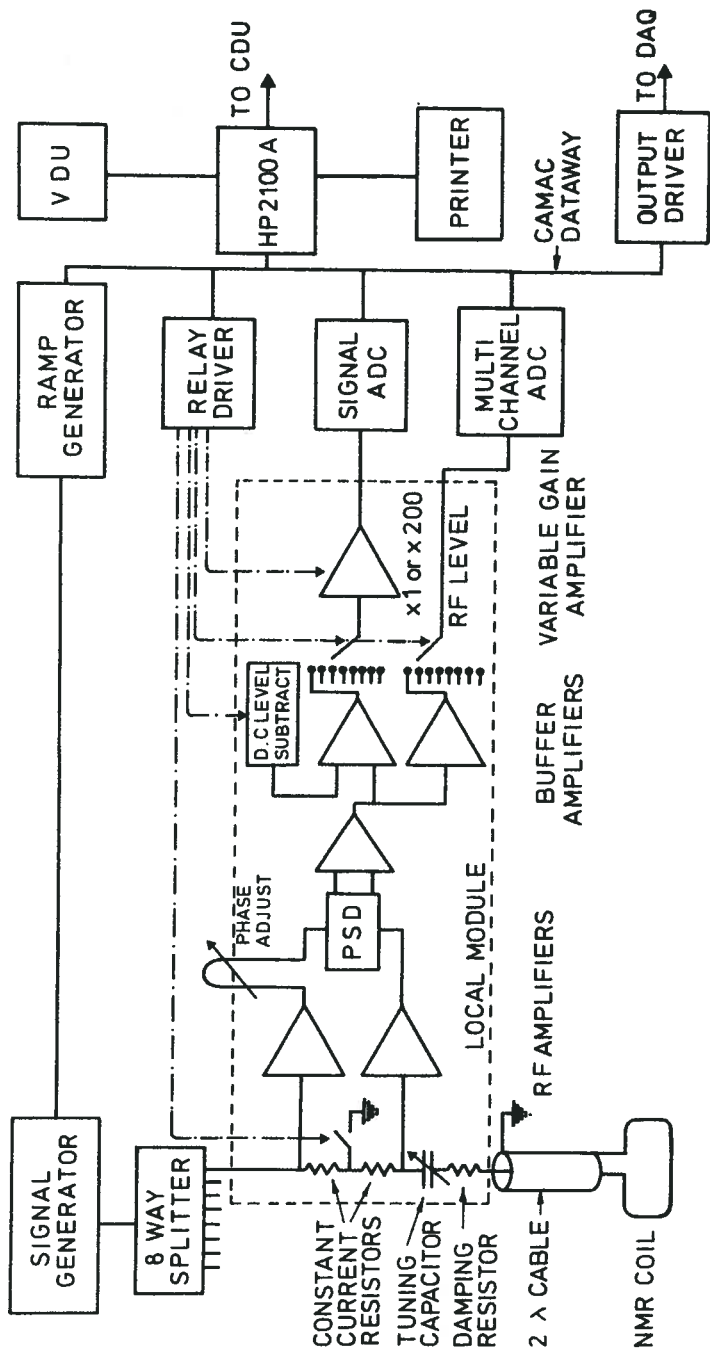
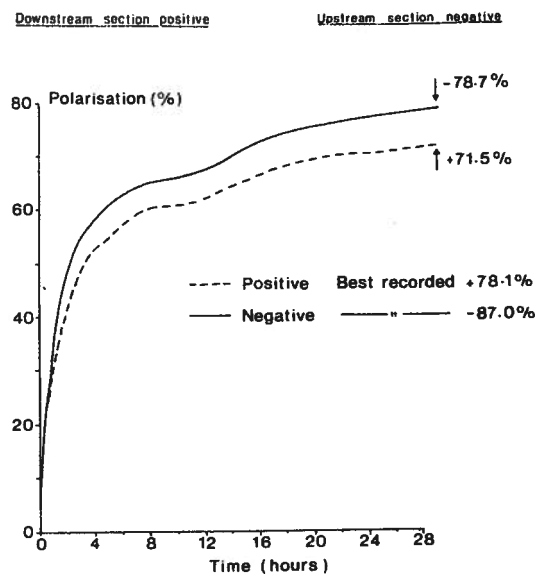
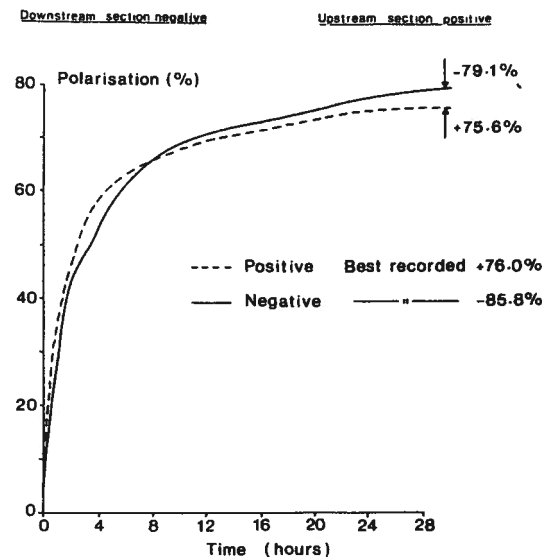


FIGURE 3



BLOCK DIAGRAM OF EMC TARGET NMR SYSTEM

FIGURE 4



EMC Target Polarisation Growth

FIGURE 5

IMPROVEMENTS OF THE POLARIZED TARGET  
FOR NUCLEON NUCLEON EXPERIMENTS AT SATURNE II

J. Ball  
L.N.S. CEN Saclay  
91191 GIF/Yvette CEDEX  
FRANCE

P. Chaumette, J. Derégel, J. Fabre  
DPhPE, CEN-Saclay  
91191 GIF/Yvette CEDEX  
FRANCE

ABSTRACT

The Saturne polarized target system is now currently operating at less than 40 mK in the frozen spin mode, with pentanol polarization of more than 80%. The relaxation time is of the order of one month in the holding field of 0.33 Tesla. The polarization direction can be rotated in about 30 minutes from the vertical to the horizontal (longitudinal or transverse) holding field. For a particular experiment (measurement of  $\Delta\sigma_L$ , axial symmetry of holding field and detectors) this method was successfully used to rapidly reverse the sign of the longitudinal target polarization by rotating the magnet field through 180° instead of repolarizing the target with the opposite sign. During the experiments we have obtained more information on the relaxation time as function of the beam rate in the region of  $10^8$  protons per second.

1. Introduction

The Saturne II polarized target system described in ref. /1//5/ consists of a vertical dilution refrigerator (A), a polarizing solenoid (C), and two holding magnets (D) (longitudinal and vertical, figures 1a and 1b). After the target has been polarized, the holding field is turned on and the polarizing solenoid is moved downwards giving access to the target.

2. Rotation of the polarization by reversing the sign of the holding field

The direction of polarization in the polarizing solenoid is vertical. Horizontal polarization is obtained by 90° rotation of the magnetic field. The same method is now applied to reverse the sign of the target polarization by rotating the magnetic field through 180°. This method is used only in the case of longitudinal polarization where the holding field is parallel or antiparallel to the incident beam. During the field rotation the polarizing solenoid is used to always maintain a non zero field component. The relaxation time is only  $\tau = 8$  min. at 0.05 Tesla, as measured for pentanol doped with EHBA Cr(V) /2/(figure 2). The reversal of target polarization by this method lasts 30 minutes instead of 3 hours for repolarizing with the opposite sign.

This delay includes

- moving the polarizing solenoid into position,

- lowering the field in the holding magnet while rising the solenoid field,
- reversing the power leads on the holding magnet power supply,
- rising the field in the holding magnet while lowering the solenoid field,
- removing the polarizing solenoid

The value of the polarization is checked during this operation using the polarizing solenoid with a field of 0.38 Tesla and the 16 MHz RF circuit originally designed for deuteron polarization.

This method causes no depolarization of the target. It violates the well established principle that the experimental apparatus should remain identical during the two measurements. However it turned out that this is acceptable under the particular conditions of  $\Delta\sigma_L$  measurements using axial detector symmetry. Most of the field integral is seen by the incident beam. Scattered particles are also confined in a small cone around the beam axis and see mostly the longitudinal component.  $\Delta\sigma_L$  measurements performed with target sign reversal by repolarization and by rotation of the holding field gave both the same results /3/.

We have subsequently tried this method also in measurements of Wolfenstein parameters where particles scattered at large angles are studied in coincidence in two detector arms in the horizontal plane (figure 3). After reconstruction and analysis of the events it turns out that the sign of the magnetic field does not introduce systematic errors. This is due to the low value of the field integral seen by the scattered particles (figures 4a and 4b). For similar measurements using a vertical target polarization, to the contrary, the magnetic field has such a strong effect on event configuration that the method of field reversal would be unacceptable.

3. Improvements of the holding field system

The system as described in /1//5/ and shown in figures 1a and 1b has been modified for rapid changeover from vertical to horizontal holding field and vice versa. According to initial estimates of relaxation times as a function of holding field /4/, the system was designed with separated vertical and horizontal holding coils delivering at maximum current a minimum field of 0.5 Tesla in any part of the target volume. Under this condition, simultaneous installation of the vertical and the horizontal holding magnet would have led to excessive size of the coils. Our measurements of relaxation time, presented at Brookhaven /5/(figure 2), showed that it was possible to consider a holding field between 0.3 and 0.4 Tesla. These results enabled us to shift the horizontal coil by 7cm away from the target. This now allows simultaneous installation of both the vertical and the horizontal holding magnet. Both coils are at liquid helium temperature and a switch system connects the power supply to either one of the two magnets (figure 5).

The change from vertical to horizontal (longitudinal or transverse) holding field takes now 30 minutes instead of several days. The operation is similar to field reversal described above, using the polarizing solenoid to check the polarization at 16 MHz. Changing target polarization from vertical to longitudinal direction is now almost as fast as changing the direction of beam polarization with the spin precession solenoid. With this new configuration, it has become considerably faster during physics runs to change the parameters to be measured than to change energy and angles. The effect of holding field on particle trajectories is sufficiently small so that the detectors position can remain unchanged.

#### 4. Relaxation time as a function of beam rate

Different measurements of the relaxation time have been done during data acquisitions (figure 2). Previous data for butanol and pentanol respectively at 55 mK and 45 mK showed little influence of beam rate at  $10^7$  to  $10^8$  protons per burst, every 1.5 second. New measurements with pentanol at 36 mK present no sizeable influence ( $\tau = 50$  days) of beam intensity up to about  $10^8$  protons per burst. Measurements made during nucleon nucleon data taking showed that when the rate reaches  $2 \times 10^7$  protons per burst, the relaxation time drops to  $\tau = 11$  days and the temperature rises to about 50 mK. At both temperatures we observe relaxation times considerably longer than those predicted in 1976 /4/ for propanediol.

#### 5. Conclusion

This target system has been used in nucleon nucleon scattering experiments at Saturne II with polarized proton and deuteron beams in the energy range of 600 to 2800 MeV for a total data taking time of about 5000 hours.

The experience gained with this system has been extremely useful for designing the components, built at Saclay, for a new target to be used in the future polarized proton beam at Fermilab.

The only major problems encountered in the recent past were related to dirty fluids, leading to malfunctioning of the refrigerator after about a week of continuous operation. After having improved filters and traps no such problems had been encountered any more during the last two periods of 13 days and 15 days, respectively.

In the near future a dummy target placed 3 cm below the target cartridge will be installed within the refrigerator. The dummy target will be shifted into the beam by moving the refrigerator system.

We foresee that the target system in its present configuration will be used for future experiments including also polarized neutron beams from polarized deuteron break up where beam heating is 35 times lower than for proton beams. We recall that the refrigerator is designed for a maximum target volume of  $100 \text{ cm}^3$  in order to accommodate the larger size of the neutron beam. Possibly the new experiment will use deuterated target materials as well.

On the other hand target system is used also for the measurements of new target materials irradiated at Saclay linear electron accelerator.

#### 6. References

- /1/ R. Bernard et al., Proc. of the 1980 Int. Symposium, Lausanne, 463.
- /2/ M. Krumpolc and J. Rocek, J. Amer. Chem. Soc. 101, 3206 (1979)
- /3/ J. Bystricky et al., Phys. Lett., 142, 130 (1984)
- /4/ T. O. Niinikoski and F. Udo, Nucl. Inst. Meth. 134, 219 (1976)
- /5/ R. Bernard et al., High Energy spin physics 1982, AIP Conf. Proc. 95, 496 (1983).

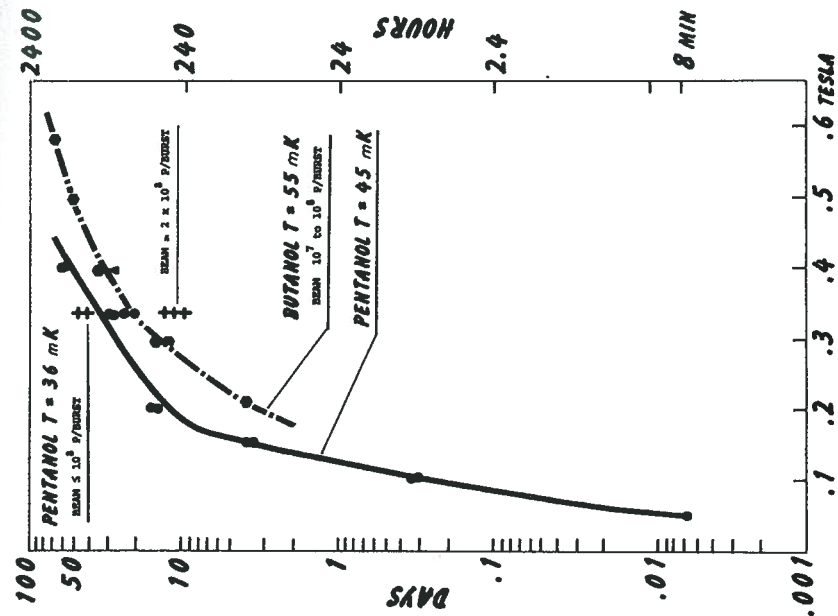


figure 2 Relaxation time as a function of holding field

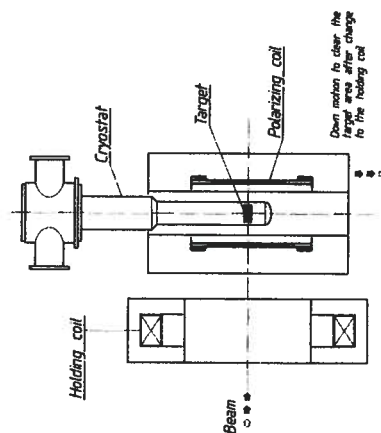


figure 1a Longitudinal holding configuration

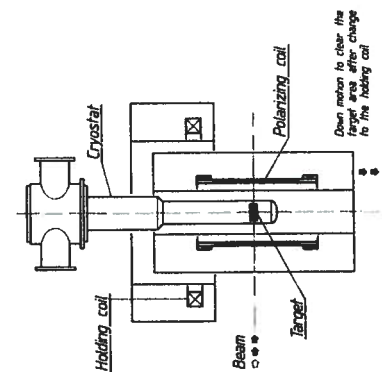


figure 1b Vertical holding configuration

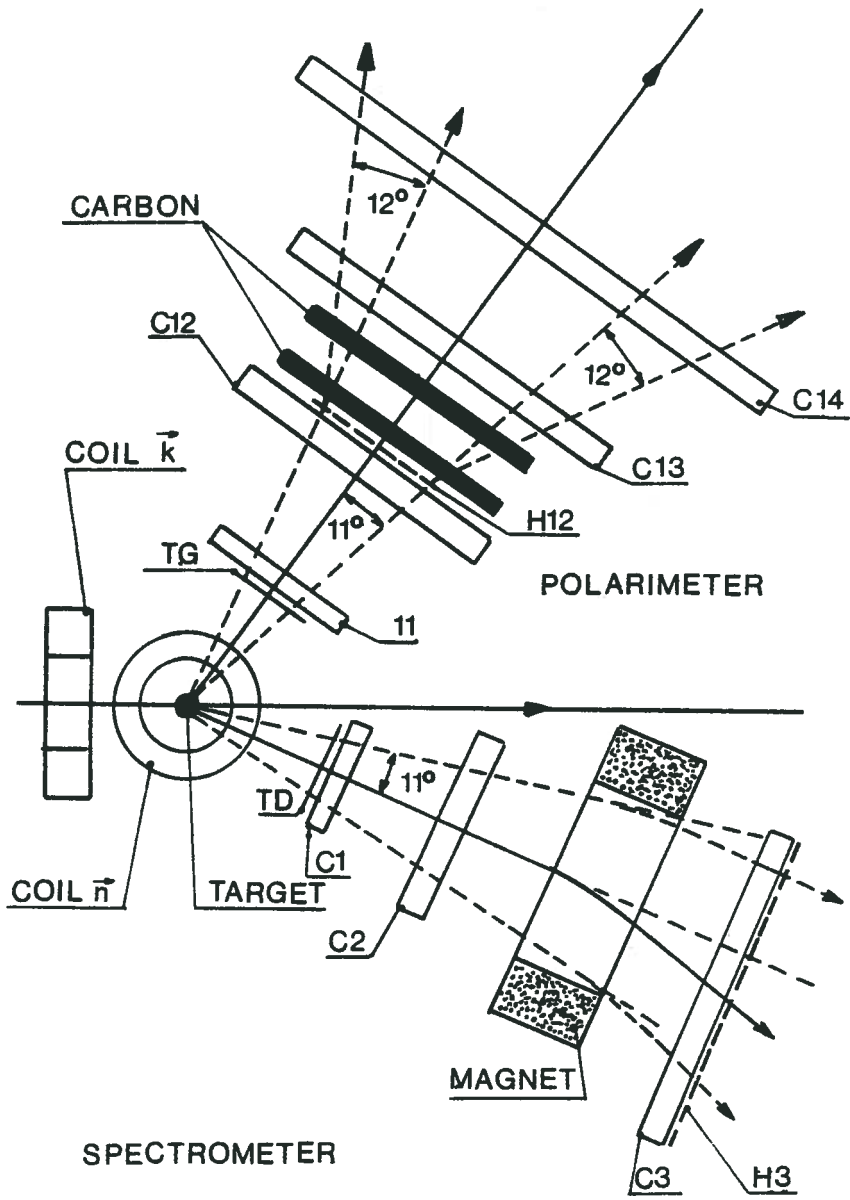
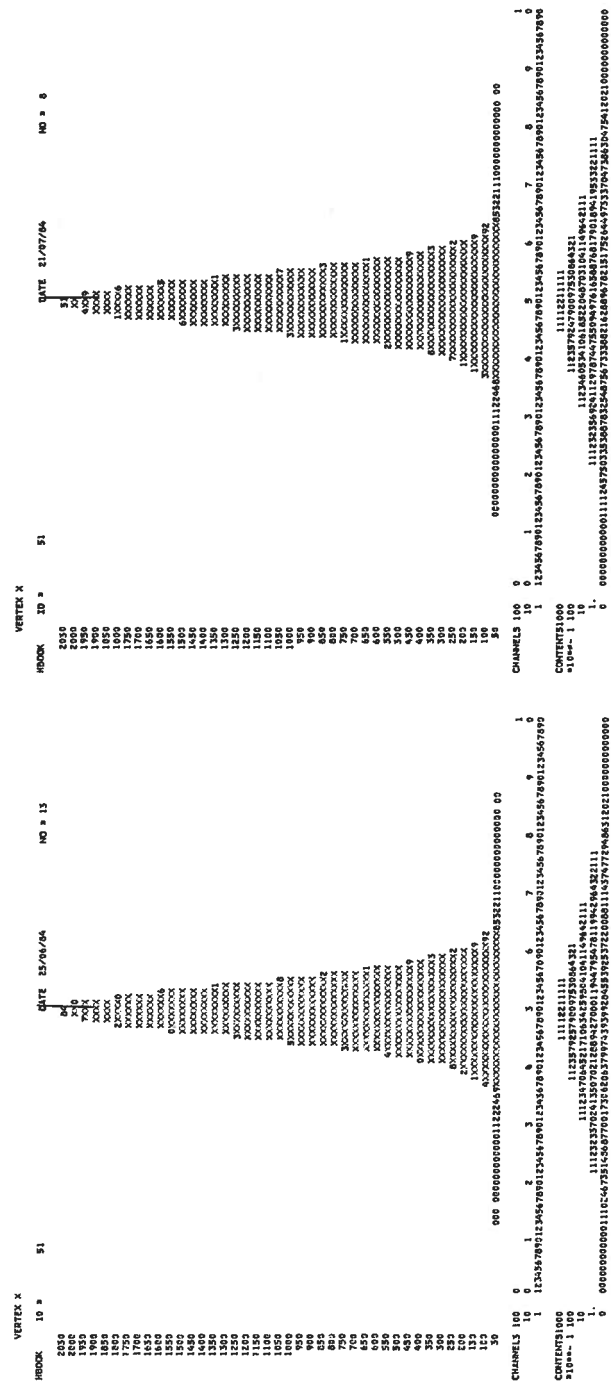


figure 3 Large scattering angle detection system



a) without holding field correction

b) with holding field correction

figure 4 X vertex histograms at 840 MeV

The two histograms are almost similar for a low value of the beam energy

A VERTICAL DILUTION REFRIGERATOR FOR THE LAMPF POLARIZED TARGET

J. J. Jarmer and J. Vaninetti

Los Alamos National Laboratory  
Los Alamos, New Mexico 87545, U.S.A.

ABSTRACT

A vertical dilution refrigerator has been built and tested for use with the LAMPF polarized target. It consists of an outer  $L^4He$  precooler and removable  $^3He/^4He$  dilution insert. The dilution system is capable of 35-mW refrigeration at 0.54 K with a cool-down time of 15-18 minutes to 70 mK and a base operating temperature range of 50-55 mK. Cryogenic test results are presented and the design of a screen-to-tube heat exchanger will be discussed.

1. Introduction

Dilution refrigerators have been used with polarized targets for several years; both horizontal and vertical designs have been discussed in the literature./1-5/ We report here on the design of a vertical dilution refrigerator insert that replaces the normal  $^3He$  insert used in a vertical cryostat./6/ The system consists of two refrigerators, one inside the other. The two are completely separate, the outer being cooled by  $L^4He$  with heat exchange to the inner, accomplished by touch contact through a thin stainless steel tube.

2. Refrigerator Design

A schematic diagram of the dilution refrigerator is shown in Fig. 1. It consists of five different heat exchangers arranged to form a rigid mechanical unit. The assembly fits rather snugly into a SS tube, which separates the outer  $L^4He$  refrigerator (not shown for clarity) from the dilution circuit. Exchanger No. 1 consists of two SS tubes about 8.8 cm diam with wall-to-wall separation of 0.15-0.2 mm. This exchanger is cooled by the outer  $L^4He$  refrigerator. Here the inlet room-temperature gas is cooled (and in some cases may be condensed to liquid) to 2-4 K, depending on cryogenic conditions. Exchanger No. 2 makes use of the cold 1-K gas pumped from the still. It is constructed from twenty-nine 100-mesh copper screens brazed to the inside of a 7.2-cm diam  $\times$  0.015-cm wall  $\times$  15.2-cm-long Cu/Ni cylinder. A 2.5-mm OD  $\times$  2-mm ID  $\times$  670-cm Cu/Ni tube is wrapped around and soldered to the outer surface of the 7.2-cm diam Cu/Ni tube. The warmer inlet  $^3He$  flows inside the smaller tube and then through a flow control valve (run valve) before entering exchanger No. 3. This exchanger consists of 2.5-mm OD  $\times$  2-mm ID  $\times$  466-cm Cu/Ni tubing wrapped in two coils in the still. Exchanger No. 4, 1-mm OD  $\times$  0.8-mm ID  $\times$  610-cm Cu/Ni, has a flow impedance  $Z = \Delta P / \dot{m} V = 5 \times 10^9 \text{ cm}^{-3}$  at its inlet obtained by inserting 3.8 cm of 0.4-mm-diam nichrome wire into a 1.1-mm OD  $\times$  0.41-mm ID  $\times$  122-cm SS tube. Exchanger No. 5 consists of six sintered copper units. Each unit was made by sintering in a hydrogen furnace 325-mesh copper powder to the inside (about half full) and outside of a 2.5-mm OD  $\times$  2-mm ID  $\times$  28-cm Cu/Ni tube as described by Niinikoski./7/ The still and mixing chamber are separated by an evacuated Cu/Ni cylinder 8-cm OD  $\times$  0.05-cm wall, which has a 1.27-cm-diam tube extending down its axis. Through this tube pass 18 instrumentation wires, 3 NMR coaxial cables, a precool line, and a microwave guide. Phenolic plugs are used to fill the extra space and present a high impedance to the flow of  $^3He$  to prevent bypassing exchangers four and five.

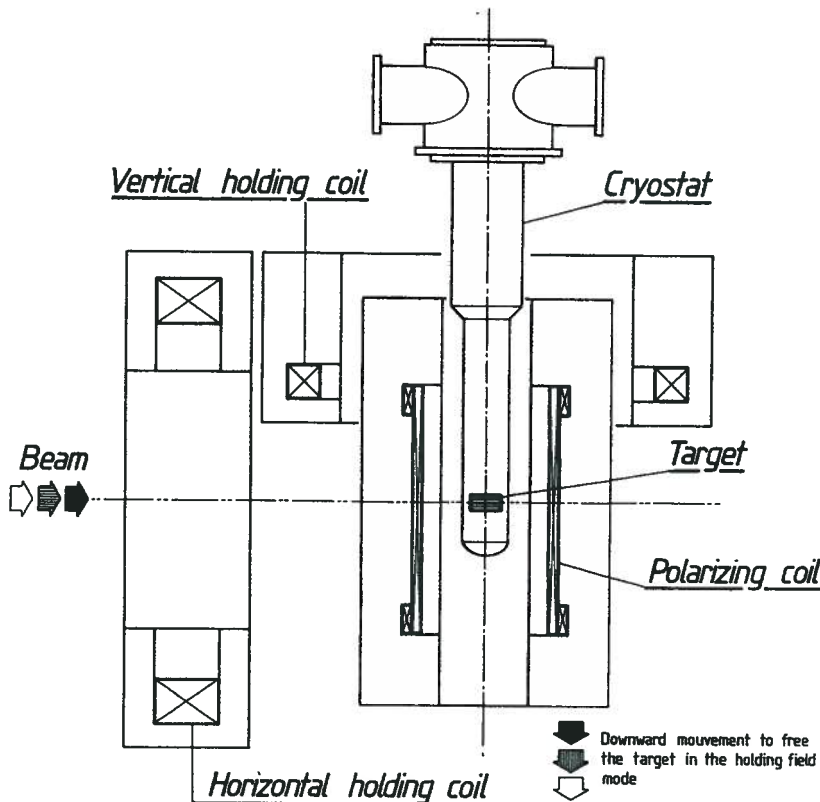


figure 5 New configuration

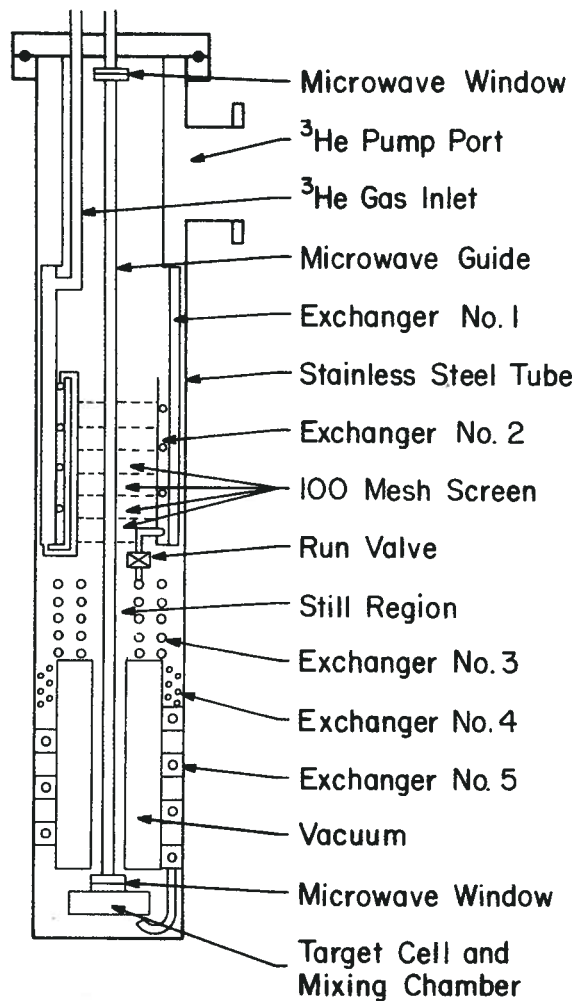


Fig. 1. Schematic diagram of the vertical dilution refrigerator insert.

### 3. Cryogenic Performance

The refrigerator has been tested several times; we indicate here only the range of values typically obtained with various gas mixtures. The gas charge in the storage cylinders was roughly 3.2 moles  $^3\text{He}$  and 22 moles  $^4\text{He}$ . This mixture is too rich in  $^3\text{He}$  and varying amounts (up to 0.8 mole) are removed to obtain the results described below.

The refrigerator has proved capable of absorbing 35 mW of applied heat in the mixing chamber at about 0.54-0.58 K. Under these conditions the circulated gas was 80-85%  $^3\text{He}$  with a flow rate of 12-16 l/m. No heat was applied to the still, the flow being regulated by the run valve between exchangers two and three. Cool-down time from 0.54 K to 70 mK varies from 15-18 min, depending on

when the run valve was adjusted to give reduced flow. A base operating temperature of 50-55 mK, as measured by two calibrated germanium resistors,<sup>/8/</sup> was obtained after about one hour. For these conditions, the circulated gas was about 65-75%  $^3\text{He}$  with a flow of 5-7 l/m. The  $^4\text{He}$  region consumes 1.5-2.5 l/h, depending on the throughput of the dilution stage. It can be operated at 4 K or pumped to obtain 2 K. The lower 2-K operation has only a minor influence on the performance of the dilution stage.

The pressure drop across exchanger No. 2 cannot be measured directly; instead, the still pressure and inlet pressure to the pump system are measured. This pressure drop varies from 150 microns at 5.2-l/m flow to 213 microns at 12 l/m. These data agree reasonably well with calculations<sup>/9/</sup> if we assume the still gas has warmed to 2.5 K.

The refrigerator has been tested as a frozen spin target. A 17-cm<sup>3</sup> sample of propanediol + EHBA ( $6 \times 10^{19}$  spins/cm<sup>3</sup>) was polarized at 25 kG, then held at a reduced field of 5 kG. The polarization decayed with a relaxation time of over 100 hours.

### Acknowledgments

We would like to thank T. O. Niinikoski of CERN for useful discussions of the design of this system. The able assistance of William Coulter and David Yeaman during the frozen spin tests is greatly appreciated.

### References

1. T. O. Niinikoski, "A Horizontal Dilution Refrigerator with Very High Cooling Power," Nucl. Instrum. Methods 97 (1971) 95.
2. T. O. Niinikoski, "Frozen Spin Polarized Target," Nucl. Instrum. Methods 134 (1976) 219.
3. S. Ishimoto, "A Horizontal Dilution Refrigerator with High Cooling Power for A Spin Frozen Target," Nucl. Instrum. Methods 171 (1980) 269.
4. D. Hill, "A Frozen Spin Polarized Target for Use at LAMPF," High Energy Spin Physics--1982 (Brookhaven National Laboratory), AIP Conf. Proc. No. 95 (1982) 485.
5. J. Deregel, "A Frozen Spin Target with Three Orthogonal Polarization Directions," High Energy Spin Physics--1982 (BNL), AIP Conf. Proc. No. 95 (1982) 496.
6. J. J. Jarmer and J. Vaninetti, "A Double Target Cell Cryostat with Quick Interchange of Target Cells," High Energy Spin Physics--1982 (Brookhaven National Laboratory), AIP Conf. Proc. No. 95, (1982) 499.
7. T. O. Niinikoski, "Dilution Refrigeration: New Concepts," Proc. of the Sixth Int. Cryogenic Engineering Conference, Grenoble, France, (1976) 102.
8. Scientific Instruments, Lake Worth, FL, USA.
9. W. A. Steyert and N. J. Stone, "Low Flow Velocity, Fine-Screen Heat Exchangers and Vapor Cooled Cryogenic Current Leads," Los Alamos National Laboratory report LA-7395, 1978.

## THE LIVERPOOL POLARISED TARGET MATERIAL TEST FACILITY

G.R. Court, P. Harrison and W.G. Heyes

Department of Physics, University of Liverpool  
Oliver Lodge Laboratory, Liverpool, L69 3BX  
UNITED KINGDOM

### 1. Introduction

A test facility has been constructed to carry out fundamental measurements and do development work on polarised target materials. It is, in fact, a polarised target without the facility for beam access. It has been designed so that rapid sample changes can be made and also to have maximum flexibility in its operating and measurement conditions.

The apparatus has been used for research in two main areas, firstly an investigation of the general properties and polarisability of the two borohydrides  $\text{NH}_3\text{BH}_3$  and  $\text{NH}_4\text{BH}_4$  when electron centres are produced by irradiation and secondly for the study of the polarisation of the nitrogen nuclei in irradiated ammonia.

### 2. Apparatus

#### a) Magnetic Field

This is generated by a corrected superconducting solenoid which has a 55 mm clear bore. The maximum field is 5T (at a current of 60 amps) and the field uniformity is within 1 part in  $10^4$  over a cylindrical volume 15 mm long (parallel to the axis of the magnet) and 10 mm in diameter. This uniformity is maintained down to a field of at least 250 mT. The magnet is normally operated in the persistent mode but can also be operated continuously in driven mode with field scan when necessary.

#### b) $^3\text{He}/^4\text{He}$ Dilution Refrigerator

The sample material is cooled using a vertical dilution refrigerator. This has direct access to its mixing chamber to facilitate rapid change of samples (fig. 1). The sample is carried on a load tube which is an easy slide fit into the refrigerator and requires no cold seals. It is possible to load samples direct into liquid  $^4\text{He}$  and the time taken to reach stable 1 K operation, using this technique, is less than 30 mins.

Two types of load tube have been used. In the first the wave guide feeding the microwave power to the mixing chamber is the only service within the tube, all other services including an NMR lead being taken through the refrigerator itself. With this load tube, the base temperature is less than 50 mK, but the NMR coil must of necessity be external to and rather weakly coupled to the sample material. An NMR lead is included in the second type of tube allowing the use of a closely coupled NMR coil, but at the cost of an increased heat leak and a consequent rise in the base temperature to between 90 and 110 mK. The maximum power capability of the refrigerator is 9 mW at 400 mK. It can be operated with pure  $^4\text{He}$  to give very stable temperatures in the region of 1 K for calibration purposes.

#### c) Microwave System

The microwave source is a klystron (Varian type VRE 2101A) which covers a frequency band from 70.39 to 71.70 GHz. Its relative frequency is monitored continuously using a temperature stabilised impatt diode source of nominal frequency 71 GHz as a reference. The microwaves are fed into the top of the mixing chamber via a short taper (fig. 1) in which is mounted an 0.05 mm thick Mylar window. The sides of the mixing chamber and the bottom of the vacuum isolation tube are made of copper and form the microwave cavity. The sample holder which is made of FEP film is situated at the centre of the cavity when the load tube is in place. An  $100 \Omega$   $1/8$  watt Allen Bradley resistor is mounted in the centre of the cavity below the sample and is used as a bolometer to sense the microwave power absorbed by the target material. Microwave absorption spectra are obtained with fixed microwave frequency by scanning the magnetic field. If this system is calibrated with a material containing a known concentration of electron centres, it will give semi-quantitative data on electron spin densities.

#### d) Polarisation Measurement

The Liverpool RF phase sensitive detector system<sup>1/</sup> operating in series tune constant current mode is used for all measurements. Its intrinsically good low noise performance combined with the low background signal curvature that it gives are important factors for the measurement with deuterons and nitrogen nuclei. The external coil (2 turns) is tuned at 107 MHz and used exclusively for proton measurements. The coil current used is 0.12 mA which gives an adequate signal to noise ratio but is small enough to ensure that saturation effects can be neglected in all circumstances. Proton polarisations can be measured to an accuracy of better than 2%. The internal coil (5 turns) is usable at frequencies in the range 9 to 16 MHz and is operated with a current of 1.4 mA to improve the signal to noise ratio. Special precautions were necessary in these circumstances to avoid significant errors due to saturation effects. The frequency scan widths used are 400 kHz at 107 MHz and either 100 or 400 kHz at the lower frequencies. Because of signal generator limitation, the use of 400 kHz scan at low frequencies results in a poorer system noise performance and so is only used when maximum sensitivity was not required. Otherwise wide scan measurements are made using a mixture of field and frequency scan, the field being set to a number of values so that a composite signal could be built up from a series of 100 kHz width scans. This technique can clearly only be used with spins in the thermal equilibrium or frozen spin states as the magnetic field must be changed.

### 3. Measurements with $^2\text{H}$ $^{14}\text{N}$ and $^{15}\text{N}$ Nuclei in Ammonia

#### a) Deuterons

The deuteron, which is a spin 1 nucleus, has a resonance frequency of 16 MHz at 2.5 T, and a quadrupole moment. The NMR line shape which is characteristic of all spin 1 nuclei in solids, is made up to a first approximation of two peaks and two pedestals. (fig. 2). The peak separation is in the region of  $140 \text{ kHz}^2$  and so the relative line width is a factor of approximately six greater than for the proton. This lowers the effective signal to noise ratio in a given situation as compared with the proton by a factor of 45 when the lower value of nuclear magnetic moment is also included. However, the thermal equilibrium (TE) polarisation is only 0.05% compared with 0.25% for the proton at 1 K so the signal to noise ratio for TE signals is a factor  $\approx 225$  worse. Deuteron thermal equilibrium signals are

therefore difficult to observe and measure. Using the composite signal technique, we can measure these signals with an uncertainty of  $\pm 8\%$ .

b) Nitrogen 14

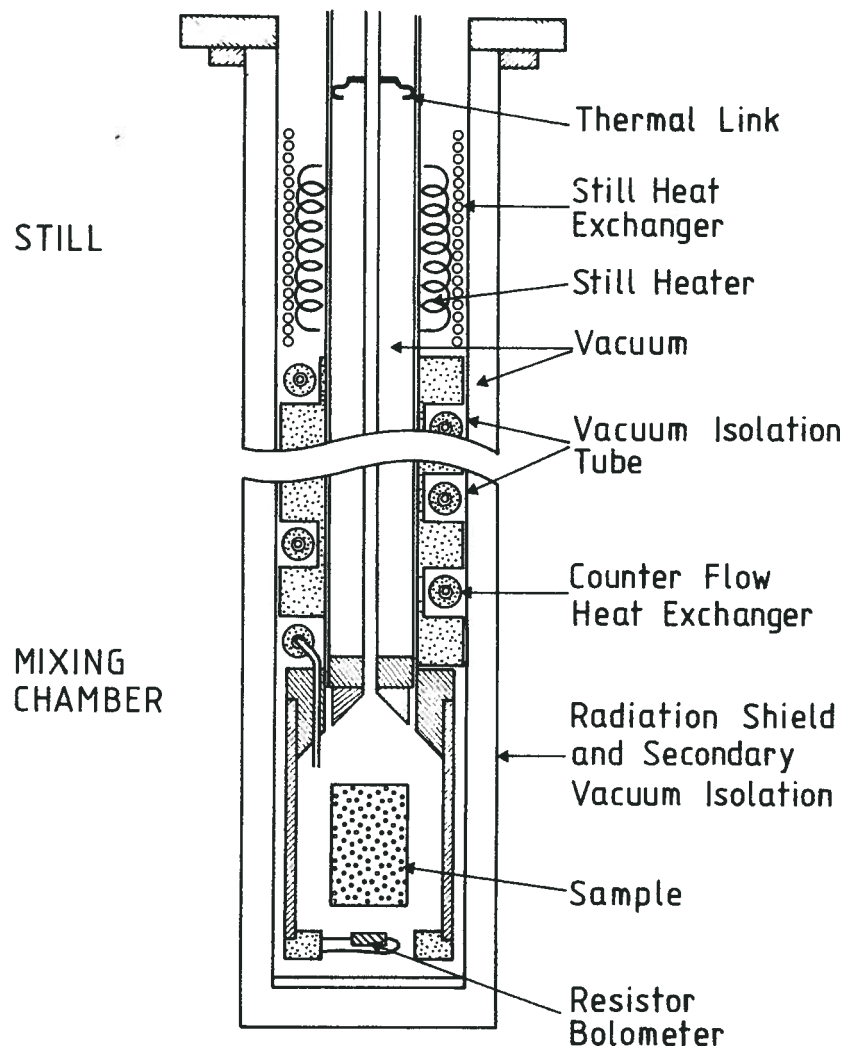
The  $^{14}\text{N}$  nucleus is also spin 1 and its quadrupole moment is a factor of ten larger than the deuteron<sup>3/</sup>. The resonance frequency at 2.5 T is 7.67 MHz and there are one third of the number of nuclei so the signal to noise ratio at a given polarisation is nominally a factor of 60 worse than the deuteron ( $1.3 \times 10^4$  worse compared with the proton). As a consequence, the observation of TE signals in our experimental conditions is impossible and even with polarised signals there is some difficulty. Also, as the peak separation is 2.4 MHz measurements using a single frequency scan are impossible, and even the use of the composite signal technique is impractical. However, when the initial search was made for signals it was found that the widths of the peaks were narrow (in both  $\text{NH}_3$  and  $\text{ND}_3$ ) so making them observable with 100 kHz scan even at low polarisations ( $\sim 2\%$ ) (fig. 3). The shape of the peaks show no evidence for any structure as is observed with the deuteron<sup>2/</sup> and so we believe that the line shape is calculable. The area is then assumed to be a function of three parameters only, the peak height, the peak separation and the dipolar broadening. The peak separation and peak height can be measured from the observed signals and a broadening factor calculated from a fit to the shape of the peak. As a consequence a total signal area, and hence a polarisation, can be calculated provided some means of calibration is available. This method is only practicable if all signal measurements are made at the same centre frequency which again means that the nuclei under study must be in the frozen spin state. The frequency used is 12.2 MHz, the peaks then appearing at field of 3.6 and 4.3 T. Correction have to be made to the measured signal parameters because of this change in field. This frequency was chosen to be as high as possible to maximise both the measurement sensitivity and the relaxation time. The system is calibrated, in the absence of a TE signal, by reducing the magnetic field so that the area of the signal from the protons or deuterons in the frozen spin state and with previously determined polarisation can be measured at 12.2 MHz. The overall uncertainty in the measurement of the  $^{14}\text{N}$  polarisation is  $\pm 10\%$ , this being dominated by the uncertainty in the determination of the measured  $^{14}\text{N}$  signal parameters.

c) Nitrogen 15

This nucleus has spin 1/2 and hence no quadrupole broadening. The resonance frequency at 2.53 T is 10.9 MHz. Its width has been observed to be narrower (3 kHz) than that of the proton (45 kHz) in  $\text{NH}_3$  (fig.4). The signal is therefore relatively easy to observe and measure despite the low magnetic moment. Precise polarisation measurement have been made down to the 1% level. The measurement of TE signals have not been attempted.

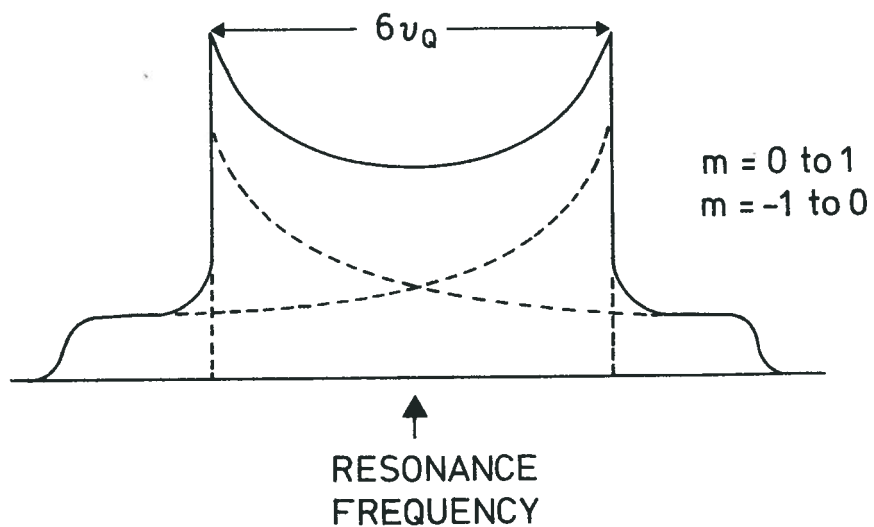
4. References

- /1/ D. Gifford  
Proc. of 2nd Workshop on Polarised Target Materials, Rutherford Laboratory 1979 RL-80-080 October 1980 p.85
- /2/ D. Hartel, O. Kaul, W. Meyer, K. Remming, E. Schilling  
Proc. Int. Symposium on High Energy Physics with Polarised Beams and Polarised Targets, Lausanne 1980 p.451
- /3/ J. M. Lehn and J. P. Kintzinger  
Nitrogen NMR, ed. M. Witanowski and G. A. Web Plenum Press 1973 p.80 ff



Schematic of the still and mixing chamber region of the dilution refrigerator

FIGURE 1



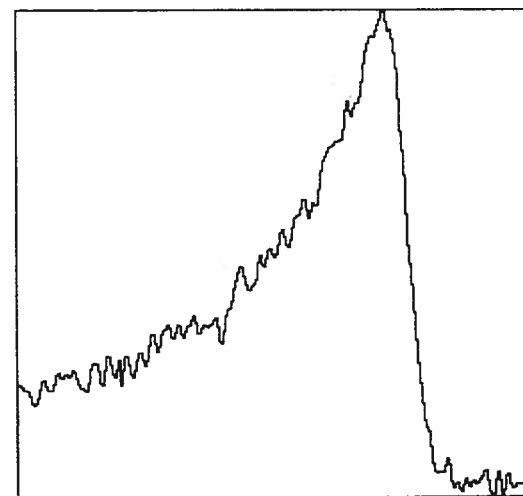
$$\nu_Q = \frac{1}{8} e^2 q Q / h$$

$eq$  = nuclear quadropole moment

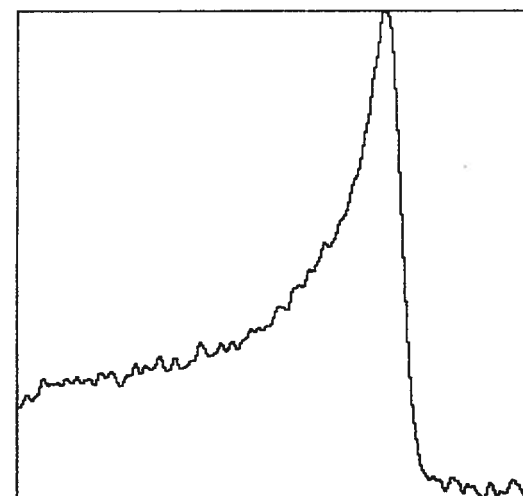
$eQ$  = electric field gradient

THEORETICAL SPIN 1 NUCLEUS LINE  
SHAPE IN A SOLID MATERIAL

FIGURE 2

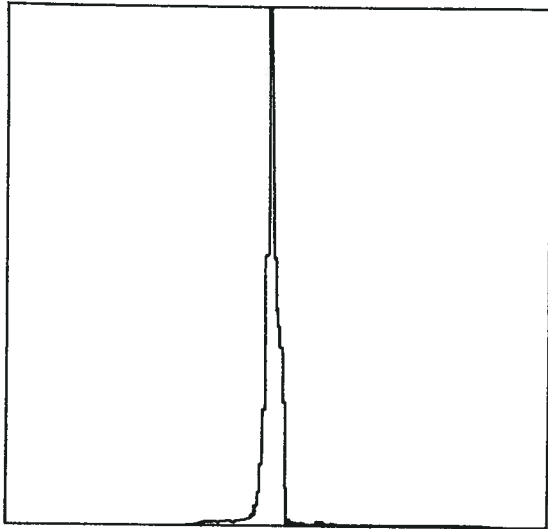


<sup>14</sup>N signal (single peak) in NH<sub>3</sub>  
14 % polarisation 100kHz scan



<sup>14</sup>N signal (single peak) in ND<sub>3</sub>  
18 % polarisation 100 kHz scan

FIGURE 3



$^{15}\text{N}$  signal 10% polarisation 100 kHz scan



$^{15}\text{N}$  signal 10% polarisation 10 kHz scan

FIGURE 4

## A BRUTE-FORCE POLARISED PROTON TARGET

Wabe Heeringa

Kernforschungszentrum Karlsruhe, Institut für Kernphysik 1, Postfach 3640,  
D-7500 Karlsruhe 1, W.-Germany

### ABSTRACT

The advantages and disadvantages of some materials, to produce a brute-force polarised proton target, are discussed. Recently a proton polarisation of 60% was obtained by us with the brute-force method in  $\text{TiH}_2$ . The properties of this target are described.

### 1. Introduction

In brute-force polarisation the nuclei are polarised by the interaction of their magnetic moments  $\mu$  with an externally applied magnetic field  $B$ . Polarisation is achieved by lowering the environmental temperature down to a value, where the thermal energy  $kT$  becomes comparable to the magnetic energy  $\mu B$ . In thermal equilibrium the occupation number  $p(m)$  of the magnetic substate with magnetic quantum number  $m$  is given by

$$p(m) = ce^{-\frac{m\mu B}{kT}}, \quad (1)$$

where  $c$  is a normalization constant and  $I$  denotes the nuclear spin. The nuclear polarisation  $P$  obtained for such a distribution is given by

$$P = \frac{2I+1}{2I} \coth\left(\frac{2I+1}{2} \frac{\mu B}{kT}\right) - \frac{1}{2I} \coth\left(\frac{\mu B}{2kT}\right) \quad (2)$$

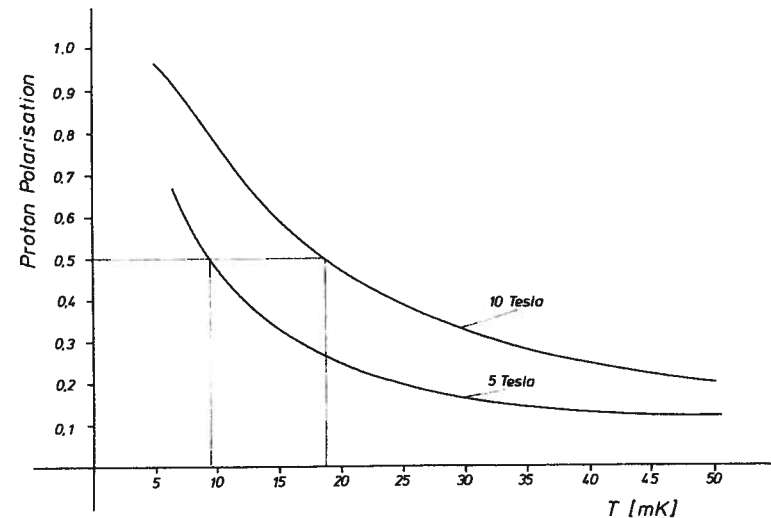


Fig.1: Brute-force polarisation of protons calculated for magnetic fields of 5 and 10 T.

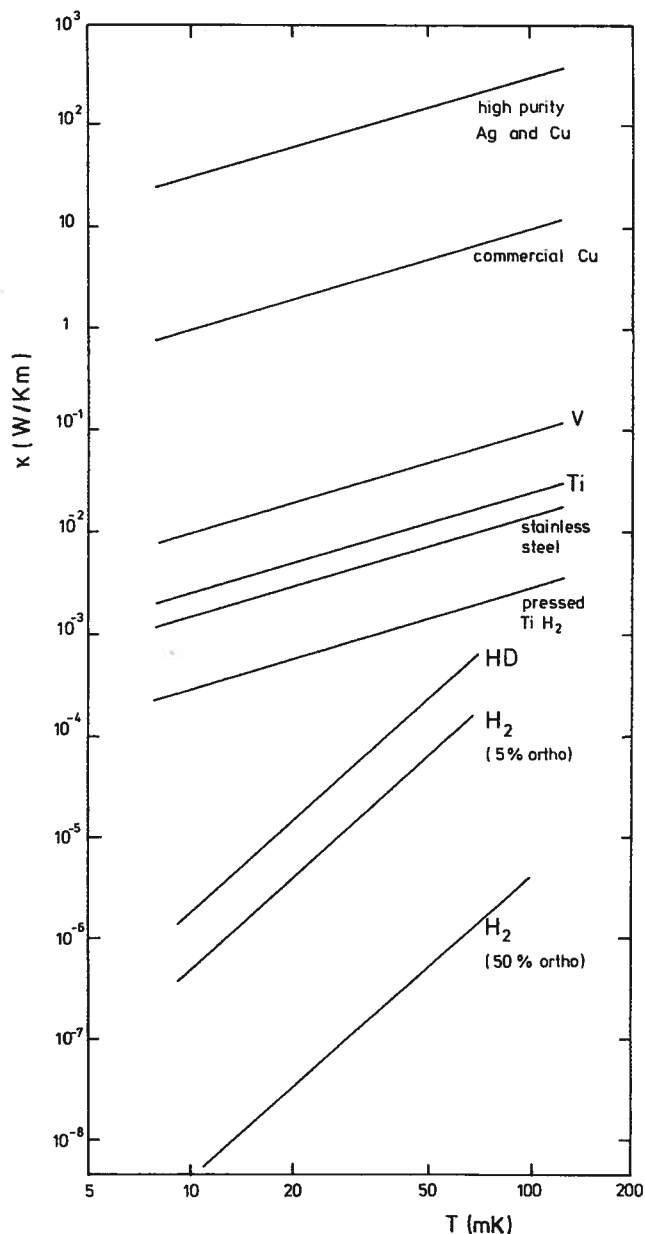


Fig.2: Heat conductivities of several materials in the mK-range. The conductivities of the metals were taken either directly from refs. /1/ and /2/ or are extrapolations with  $\kappa = \lambda T$  from curves given there. The TiH<sub>2</sub> curve is from data measured by our group /3/. The HD and H<sub>2</sub> curves are extrapolations with  $\kappa = \lambda T^3$  from measurements down to 0.2 K or 1 K presented in refs. /4/ - /6/.

The maximum magnetic field, that can be produced by external magnets, is in practical cases limited to about 10 T. Fig.1 shows the equilibrium polarisation of protons in fields of 5 T and 10 T as a function of temperature. It appears that a temperature of 18 mK is necessary in order to obtain a proton polarisation of 50% at 10 T. At such low temperatures the nuclear spin-lattice relaxation time often is very long for electrical insulators, causing an unacceptable polarisation build-up time. Therefore, usually only metals are employed for brute-force polarised targets. Another factor in favour of metals is their relatively good heat conductivity.

## 2. Thermal gradients in target samples

The thermal gradient over the target is an important quantity for the determination of the average polarisation. As heat conductivities generally get worse at lower temperatures, the beam heating, that can be accepted, becomes lower as well. Besides this, also the cooling power of refrigerators goes down towards lower temperatures. The temperature gradient over the sample is determined by the heat load, the target geometry, the thermal conductivity of the target material and the temperature at the outside of the target. The cooling power of the refrigerator and the conductance of the thermal link to it will not be considered here.

Fig.2 shows heat conductivities of several materials in the mK-range. There is a remarkable difference between the highest and the lowest conductivities, which vary by ten orders of magnitude at 10 mK. Therefore, different target geometries are required in different cases.

We consider the following two target geometries:

- a cylindrical thick target, cooled by its cylindrical fitting, see fig.3,
- small beads with radius  $R$ , cooled by the surrounding liquid.

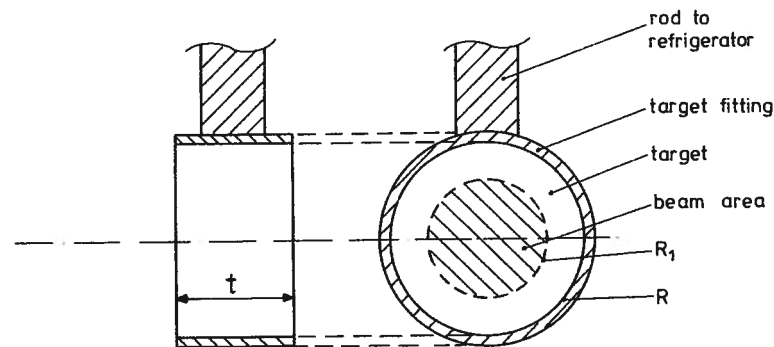


Fig.3: Geometry of a cylindrical target.

If the heat conductivity  $\kappa$  is expressed as  $\kappa = \lambda T^\alpha$ , the following equations can be derived for these cases:

- cylindrical target

$$T_0^{\alpha+1} = T_R^{\alpha+1} + \frac{(\alpha+1)Q}{4\pi\epsilon\lambda} \left(1 + 2 \ln \frac{R}{R_1}\right) \quad (3a)$$

Here  $T_0$  is the temperature at the centre of the target,  $T_R$  the temperature

at its outer radius  $R$ ,  $R_1$  is the radius of the beam and  $t$  is the target thickness.

### b) small beads

$$T_0^{\alpha+1} = T_R^{\alpha+1} + \frac{(\alpha+1)Q}{8\pi RAN} \quad (3b)$$

Here again  $T_0$  is the temperature at the centre and  $T_R$  at the outer radius. In both cases  $Q$  denotes the total heat input of the beam, which is assumed to be deposited homogeneously. In the last case the number of beads is represented by  $N$ . These expressions will be applied for some targets discussed in the next sections.

## 3. Brute-force polarised protons

### 3.1 Solid $H_2$

The properties of solid hydrogen are largely determined by the fact, that hydrogen occurs in the form of two different  $H_2$ -molecules: para-hydrogen with anti-parallel proton spins and ortho-hydrogen with parallel spins. The para-ortho distinction is brought about by the fact, that the protons in the molecule are indistinguishable particles. Hence, the total wave function involving the nuclear coordinates must be antisymmetric with respect to particle exchange. Therefore, the spin-symmetric nuclear state (protons parallel) requires an anti-symmetric rotational wave function with an odd rotational quantum number  $J$ . Conversely, the anti-symmetric nuclear spin state (protons anti-parallel) needs an even rotational quantum number  $J$ .

The  $J = 0$  para-state is the ground state, the first excited state ( $J = 1$ , ortho) has an energy of  $E/k = 172$  K. In thermal equilibrium at  $T < 1$  K one therefore has almost pure para- $H_2$ , which can not be polarised, because the proton spins are anti-parallel. However, spontaneous ortho-to-para decay is forbidden. Therefore it is possible to freeze in a room temperature distribution containing 75% ortho, which converts only slowly into pure para-hydrogen. The solid-state properties of hydrogen, such as nuclear spin-lattice relaxation and heat conductivity, are very strongly dependent on the actual ortho-concentration present in the solid /7,8/.

The ortho-para conversion rate is given by

$$\frac{dx}{dt} = -cx^2, \quad (4)$$

where  $x$  is the ortho-concentration and  $c$  has the value  $c = 1.9 \times 10^{-2} \text{ h}^{-1}$ . Thus at high ortho-concentrations the rate is 1 - 2%/hour, decreasing towards lower  $x$ -values. A considerable heat is released in conversion due to the large energy gap between the states. In table 1 the heat produced in 1 mol of solid  $H_2$  ( $23 \text{ cm}^3$ ) has been calculated for various ortho-concentrations. The ortho-concentration simultaneously represents the maximum proton polarisation  $P_{\text{max}}$ , that can be achieved in the sample. At  $x = 5\%$  the heat load still amounts to 18  $\mu\text{W}$ .

Table 1: Conversion heat produced in a solid sample of 1 mol  $H_2$

x = ortho-concentration	conversion heat
75%	3.15 mW
25%	0.35 mW
10%	0.07 mW
5%	0.018 mW

At such a heat load the most powerful dilution refrigerators nowadays can reach a temperature of 15 - 20 mK. Fig.1 shows that at 10 T a proton polarisation around 50% is achieved in this temperature range. Hence, the overall polarisation of the sample in this case amounts to  $5\% \times 50\% = 2.5\%$ . The overall polarisation obtained at the higher  $x$ -values is even worse. This shows that the conversion heat is too large for present-day dilution refrigerators, apart from very small samples.

Very small samples would still suffer, however, from the very low conductivity of solid hydrogen. Suppose we have solid hydrogen with 5% ortho in the form of beads with a radius of 1 mm. The heat load due to conversion released in one bead would be about 3 nW in this case. Assuming an outside temperature  $T_R = 10$  mK for the beads, employing eq. (3b) and the heat conductivity given in fig.2, we find for the central temperature  $T_0 \approx 33$  mK. It seems to be almost impossible, therefore, to employ solid  $H_2$  as target material for a brute-force polarised proton target.

### 3.2 Solid HD

The para-ortho distinction does not apply for HD-molecules, because proton and deuteron are distinguishable particles. Thus protons and deuterons in HD can be polarised independently. A proton polarisation of 40% has been achieved by Bozler et al. /9/ at  $T = 23$  mK and  $B = 10$  T. A small amount of ortho- $H_2$  had been added to the HD in order to decrease the proton spin-lattice relaxation time, which otherwise would have been on the order of many days.

By the subsequent conversion of the ortho- $H_2$  the spin-lattice relaxation time will increase steadily in such a polarised target, because the proton-lattice coupling in para- $H_2$  is very weak. This decoupling of the protons from the lattice opens up the possibility to operate this target at moderate fields and higher temperatures, e.g. 4.2 K, where relaxation times exceeding a day are expected if one has waited long enough /10/. At such temperatures the thermodynamic properties of HD (such as heat capacity and heat conductivity) are much less troublesome than at 10 mK. The heat conductivity of HD at 4.2 K is in between that of stainless steel and copper, whereas at 10 mK it is three orders of magnitude below that of stainless steel, see fig.2.

However, also at higher temperatures polarised proton samples employing HD have not been utilized as targets up to now. A difficulty, to be encountered at higher temperatures, will be the increase in relaxation rate, due to radiation damage caused by the beam.

### 3.3 Metal hydrides

Large quantities of hydrogen can be absorbed by many metals, yielding metal hydrides with a very high free proton density. Table 2 shows free proton densities for several materials at  $T = 0$  K. As metal hydrides have metallic

Table 2: Free proton densities for several materials, calculated at  $T = 0$  K.

Material	free protons/cm <sup>3</sup>	Material	free protons/cm <sup>3</sup>
$H_2$	$5.3 \times 10^{22}$	TiH	$4.9 \times 10^{22}$
$H_2O$	6.1	TiH <sub>2</sub>	9.0
CH <sub>4</sub>	6.2	ZrH <sub>2</sub>	7.3
C <sub>4</sub> H <sub>10</sub> O	6.6	YH <sub>2</sub>	5.7
NH <sub>3</sub>	8.2	YH <sub>3</sub>	7.7

properties they are supposed to have fairly good heat conductivity and spin-

lattice relaxation. The highest proton density is found for TiH<sub>2</sub>. We have employed this material to produce a polarised proton target. Its properties are described in the next section.

#### 4. Proton polarisation in TiH<sub>2</sub>

Titanium hydride was produced by heating titanium sponge in an evacuated quartz tube and hydrogenating it with known amounts of hydrogen gas. Details can be found in refs. /3, 11/. The H/Ti-ratio of the hydride that was produced is  $1.96 \pm 0.02$ . At ratio's larger than one the titanium falls apart into a powder, which has to be pressed in order to obtain a solid sample of high density. For this purpose a pressing tool was built, which can withstand a pressure of  $2 \times 10^5$  N/cm<sup>2</sup> on a surface of 5 cm<sup>2</sup>. The powder was pressed into a copper cylinder with 25 mm inner diameter and 1 mm wall thickness. The sample finally obtained has a length of 35 mm.

The density of the pressed powder was determined by mass-volume measurements and also by means of the absorption of a collimated beam of  $\gamma$ -rays from a <sup>137</sup>Cs source. The result is  $\rho = 3.78 \pm 0.04$  g/cm<sup>3</sup>, which agrees with the density found for solid crystals /12/. Thus the pressure employed was sufficient to press the powder to its highest possible density. The resulting proton density is  $8.95 \times 10^{22}$  protons/cm<sup>3</sup>. The hydrogen content of the target is 1.3 mol H<sub>2</sub>.

A similar sample was produced with a 6 mm diameter copper rod at the position of the cylinder axis. This sample has been employed for thermodynamical experiments /3/. The heat conductivity of the pressed powder measured with this sample is shown in fig.2. It appears to be about one order of magnitude below that of massive titanium. An upper limit of 5 min was measured for the proton spin-lattice relaxation time at T = 3 mK. Hence the proton relaxation is no limiting factor in polarising the sample.

A proton polarisation of 60% has been measured in the sample without central rod in a field of 8.2 T at a temperature around 12 mK. The measurement was carried out by transmitting 1.2 MeV polarised neutrons through the sample and determining the difference in count rate for parallel and anti-parallel spin orientations. This is a useful method because at low energies the neutron-proton spin-spin cross section is large and it is accurately known. Fig.4 shows the results of this experiment.

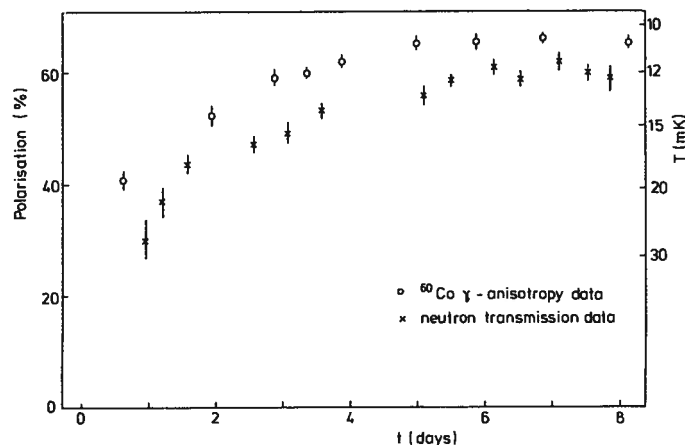


Fig.4: Results of the polarisation measurement of protons in TiH<sub>2</sub>.

Besides the polarisation data from the transmission experiment also the temperature measurements of a <sup>60</sup>Co Co thermometer are shown, which was attached to the outside of the sample. The slight discrepancy between both data sets that remains towards the end of the experiment might be attributed to a small radial temperature gradient existing over the sample, or to a small systematic error in the quantities involved in the deduction of the polarisation. The polarisation build-up time is several days. This is partly due to the poor heat conductivity of the pressed TiH<sub>2</sub> powder, and partly to the relatively low heat conductance of the copper rod connecting the target to the mixing chamber of the dilution refrigerator. This was kept low deliberately in order to have an indication for the heat flow through the rod. Thus faster polarisation times are possible.

The heat load that can be absorbed by this target can be calculated employing eq. (3a) and the heat conductivity shown in fig.2. The results are displayed in Table 3 for two values of the heat load  $\dot{Q}$ , assuming  $R_1 = 2 R/3$ . It appears that only heat loads on the order of some tenths of a microwatt can be

Table 3: Heat gradient over the TiH<sub>2</sub> sample and average proton polarisation for two values of the heat load  $\dot{Q}$  induced by the beam.  $T_R$  and  $T_0$  are the temperatures at the outside and the centre of the target, respectively.

$T_R$	$\dot{Q}$	$T_0$	Pol. at 10 T
10 mK	0.1 $\mu$ W	11.2 mK	$75 \pm 2\%$
20 mK	0.5 $\mu$ W	23 mK	$44 \pm 2\%$

accepted. The target is presently being used in a scattering experiment with 20 - 50 MeV polarised neutrons.

#### 5. References

- / 1/ O.V. Lounasmaa, Experimental Principles and Methods below 1 K, Academic Press, London 1974
- / 2/ G.E.Childs, L.J.Ericks and R.L.Powell, Thermal conductivity of solids at room temperature and below, NBS Monograph 131, 1973
- / 3/ W.Heeringa, R.Aures, R.Maschuw, H.Postma and F.K.Schmidt, to be published
- / 4/ J.H.Constable and J.R.Gaines, Phys.Rev. B8 (1973) 3966
- / 5/ R.G.Bohn and C.F.Mate, Phys.Rev. B2 (1970) 2121
- / 6/ J.E.Huebler and R.G.Bohn, Phys.Rev. B17 (1978) 1991
- / 7/ Isaac F.Silvera, Rev.Mod.Phys. 52 (1980) 393
- / 8/ H.Ishimoto, K.Nagamine and Y.Kimura, J.Phys.Soc. Japan 35 (1973) 300
- / 9/ H.M.Bozler, J.A.Brown and E.H.Graf, Bull.Am.Phys.Soc. 18 (1973) 545
- / 10/ A.Honig, Proc. IInd. Intern. Conf. on Polarized Targets, Ed. G.Shapiro, LBL-500, Berkeley 1971, p.99
- / 11/ R.Aures, W.Heeringa, H.O.Klages, R.Maschuw, F.K.Schmidt and B.Zeitnitz, Nucl. Instr. and Meth. 224 (1984) 347
- / 12/ W.M.Mueller, J.P.Blackledge and G.G.Libowitz, Metal Hydrides, Academic Press, New York 1968

## A Simple Model of Bead Cooling

P.R. Cameron

Harrison M. Randall Laboratory  
Physics Department  
University of Michigan  
Ann Arbor, Michigan 48109-1120

### ABSTRACT

A simple model of bead cooling is presented, which analyzes the thermal behavior of a  $\text{He}^3/\text{He}^4$  mixture-charged Polarized Proton Target operated in an intense proton beam. It is suggested that the observed improvement results because the beads are coated with a film of superfluid mixture, so that the relevant thermal resistance at the bead-fluid interface looks more like the Kapitza resistance than the nucleate boiling resistance. Transport of  $\text{He}^3$  to the region of beam heating is probably greatly enhanced by the action of osmotic pressure. The effect of heat flush in purifying the mixture is considered to be negligible.

### 1. Introduction

It has recently been shown<sup>/1/</sup> that operation of a  $\text{He}^3$  evaporation-type Polarized Proton Target with the pure  $\text{He}^3$  gas charge replaced by a  $\text{He}^3/\text{He}^4$  mixture increases the maximum operational beam intensity by at least a factor of three. It is possible to develop a simple model which seems to reasonably account for this improvement.

The factors which must be considered in removing large amounts of heat from the target beads include the thermal resistances of the beads, the bead-fluid interface, and the fluid surrounding the beads, and the pressure drop of this fluid as it flows through the interbead openings. This consideration is complicated by the fact that none of the relevant heat transfer coefficients have been measured in the temperature range of interest, by the fact that these coefficients have differing dependences upon bead size and beam heating, and by the fact that the mechanism of transport is some form of forced convective two-phase flow of a mixture of isotopes, which might also exhibit superfluidity.

### 2. Forced Convection

A comparison of the forced convection and pool boiling curves <sup>/2/</sup> is shown in Figure 1. The nucleate boiling curve is insensitive to fluid velocity, whereas the forced convection curves are not. The characteristic flow patterns and regimes <sup>/2/</sup> corresponding to the forced convection curves of Figure 1 are shown in Figure 2, where the duct can be considered an idealization of the interconnecting openings between the ammonia beads. The largest heat transfer coefficients are observed in the spray liquid dispersed region of the flow, where the beads are "...coated with a thin film of liquid in which nucleation is suppressed by the high velocity of the mist-laden vapor, and heat transfer is due to convection or conduction through the thin liquid film with evaporation at the liquid-vapor interface."<sup>/2/</sup> As the heat flux increases the liquid film eventually evaporates off the surface of the

beads, a condition often called 'burnout', although the term 'dryout' would be more accurate. At burnout the temperature rises very quickly and the heat transfer coefficient drops sharply.

### 3. Heat Flush

Before considering the thermal resistances, it is useful to deal with heat flush, which is an incredibly effective method<sup>/3/</sup> for producing ultra-pure  $\text{He}^4$  at temperatures above about 1.1 K. The mechanism of heat flush is easily understood in terms of the two fluid theory. At temperatures above about 1.1 K the two fluid theory suggests that superfluid in the vicinity of a heat source is converted into normal fluid (raised out the quantum mechanical ground state) and experiences an osmotic pressure which drives it out to regions of greater superfluid concentration, carrying entropy (and energy) as it goes. It is replaced by superfluid (carrying no entropy, being all in one quantum mechanical state) which rushes in under the influence of the same osmotic pressure, seeking to reduce the normal fluid concentration near the heat source. The outrushing normal fluid arrives at the heat sink, is converted to superfluid, and rushes in to replace the intrushing superfluid, which arrived at the heat source and became outrushing normal fluid. And so forth. This is by far the most efficient mechanism of heat transport yet found. It is limited by the generation of turbulence in the counterflowing liquids. As the velocities increase a point is reached where the entropy generated by the turbulence is greater than the entropy being transported away from the heat source.

Heat flush occurs because the  $\text{He}^3$  atoms do not experience frictional forces with the intrushing superfluid component, whereas they do with the outrushing normal component, and are flushed by the heat into the cooler region. In this way a concentration gradient is set up which opposes the temperature gradient.

At lower temperatures the situation is more complicated. Thermal counterflow ceases to be of importance in the transport of heat, which is handled by phonons and rotons. Below about 0.6 K the rotons cease to contribute, and the phonons carry the heat. Phonon propagation in  $\text{He}^4$  is very sensitive to impurities. The thermal conductivity in solutions at these temperatures is limited by phonon- $\text{He}^3$  scattering,<sup>/4/</sup> and varies approximately as  $1/X$ , as can be seen in Figure 3. In very dilute solutions

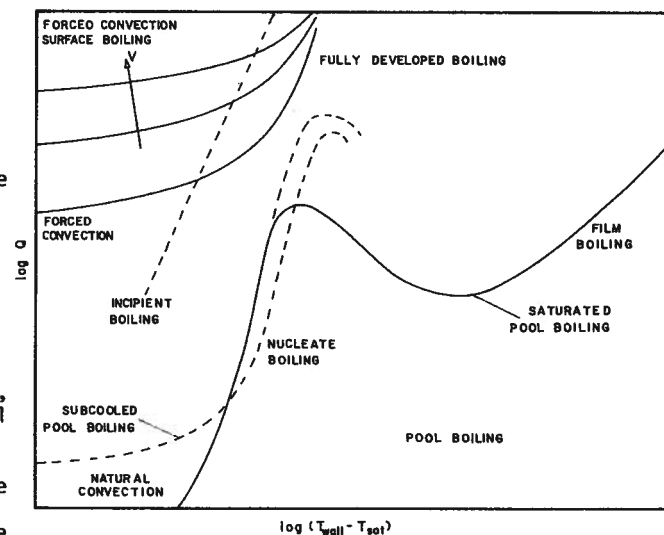


Figure 1  
Forced Convection and Pool Boiling Curves

the mean free path between phonon-He<sup>3</sup> collisions becomes greater than the phonon wavelength. The resistance to phonon propagation then arises primarily from wall collisions in the enclosure,<sup>5/</sup> and the thermal conductivity varies approximately linearly with the diameter, as we see again in Figure 3.

Given that thermal counterflow is not an effective mechanism for heat transport at the temperatures of interest, the question is then whether it also ceases to be an effective mechanism for mass transport. The pressures generated by the opposing concentration and temperature gradients can be described by<sup>6/</sup>

$$(kT/m_3)\nabla X + S_4\nabla T = 0 \quad (1)$$

where the first term is the osmotic pressure due to the concentration gradient and the second is the osmotic (fountain) pressure due to the temperature gradient. The second term is constrained to be small by the very small value of S<sub>4</sub>, the entropy of pure He<sup>4</sup> at about 0.5 K, and because the magnitude of the temperature gradient  $\nabla T$  is limited by the fact that the total temperature rise is experimentally determined to be less than a few hundred millikelvin. Therefore the concentration gradient must also be small, and the effect of heat flush is negligible. A numerical evaluation of these pressures is given by Radebaugh<sup>7/</sup>. The fountain pressure P<sub>f</sub> is equal to the osmotic pressure only at low values of X. At the values of X and T found in the target cavity of our PPT the osmotic pressure is seen to be about three orders of magnitude greater than the fountain pressure, and the He<sup>3</sup> atoms diffuse easily into the warm region. The experimental validity of this conclusion is seen in the operation of the ubiquitous dilution refrigerator. If heat flush were effective at these temperatures, the flush from the still into the lower temperature heat exchangers would interrupt the He<sup>3</sup> circulation and render the refrigerator inoperable.

#### 4. The Thermal Resistances

The heat which is deposited in the beads must pass through a series of thermal resistances before being removed by the refrigerator. These thermal resistances are listed in Table I, along with simplified expressions which give the temperature rise which occurs when the heat passes through each of the thermal resistances. The heating due to the beam is<sup>8/</sup>

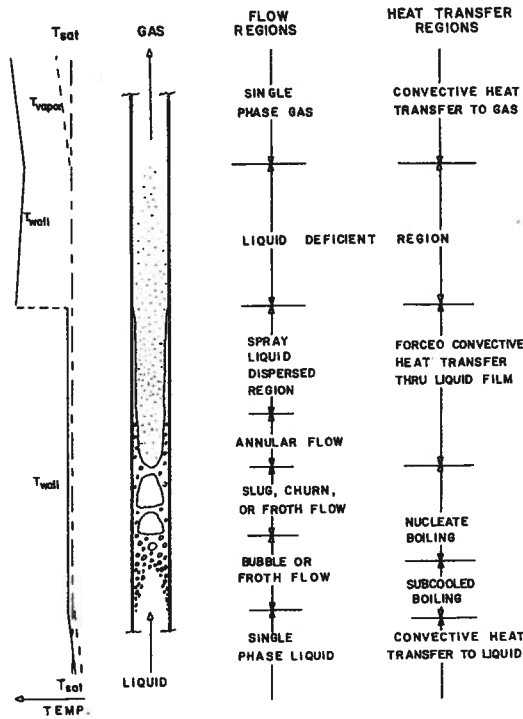


Figure 2  
Forced Convection Flow Patterns and Regimes

$$\dot{Q}_{\text{beam}} = \dot{n}\rho \frac{dE}{dx} \quad (2)$$

where the density  $\rho$  is about 0.82 g/cm<sup>3</sup> for ammonia, and the effective length  $l$  of the target is about 2.9 cm. The greatest heat flux will be at the center of the 1.0 cm FWHM beam spot. It is convenient to express this heat load in terms of the heat supplied to each individual bead:

$$\dot{Q}_{\text{bead}}^{\text{FWHM}} = (1.2\dot{n} + 0.4) d^3 \text{ mwatt} \quad (3)$$

Here the bead diameter  $d$  is in centimeters, and the microwave heating is also included. Substitution of equation (3) into the expressions of the second column of Table I gives the results shown in the third column. The relation between bead diameter and temperature rise is shown explicitly there.

TABLE I

bead conductivity	$T_1 - T_2 = \int_{r=0}^{d/2} \frac{\dot{Q}}{kA} dr$	$T_1 - T_2 = (.07\dot{n} + .025) \frac{d^2}{k}$
bead-liquid interface		
a. nucleate boiling	$T_2 - T_3 = \frac{\dot{Q}}{cA}$	$T_2 - T_3 = (1.2\dot{n} + 0.4) \frac{d}{\pi c}$
b. Kapitza	$T_2^4 - T_3^4 = \frac{\dot{Q}}{SA}$	$T_2 - T_3 = ((.38\dot{n} + .13) \frac{d}{S} + T_3^4)^{1/4} - T_3$
liquid conductivity	$T_3 - T_4 = \frac{L\dot{Q}}{kA}$	$T_3 - T_4 = (1.2\dot{n} + 0.4) \frac{Ld}{k}$
pressure drop	$p - p_0 = \frac{32\eta l v}{\epsilon^4 d^2}$	$p - p_0 = \frac{3.1\dot{n} + 1.0}{\epsilon^4 d^2} \times 10^{-4} \mu$

The temperature rise due to the thermal resistance of the beads varies as the square of the bead diameter, and inversely with the thermal conductivity  $k$ . Beads which are formed by quickly freezing the liquid ammonia in liquid nitrogen are tough and opaque when frozen without voids, and have a microcrystalline structure. Beads which are formed by crushing the slowly grown crystals<sup>9/</sup> are transparent and brittle. It is possible that there is a significant difference between the thermal conductivities of beads made in these different ways.

The temperature rise at the bead-fluid interface is perhaps of greatest interest here. If boiling occurs at the bead surface, then the relevant thermal resistance is the nucleate boiling resistance. The temperature rise is then directly proportional to bead diameter, and inversely proportional to the conductance coefficient  $c$  for nucleate boiling. If the bead is surrounded by liquid in which nucleation is somehow suppressed, then heat flow is limited by the much smaller Kapitza resistance. The dependence on bead diameter and Kapitza surface conductivity  $S$  is then much weaker, going as the one-fourth power.<sup>10/</sup>

The temperature rise through the liquid surrounding the beads is dependent on the thermal conductivity, which may be found from Figure 3. Substitution of an appropriate value of  $k$  into the expression in the third

column of Table I shows that for values of  $X$  on the lambda curve of the phase separation diagram, the liquid thickness  $L$  must be less than about 0.1 mm. The heat which is generated within the beads cannot be transported by conduction to some surface a few centimeters away, where cooling occurs. Convection is also of little help, as the heat capacity of the mixture is small enough in comparison with the heat loads under consideration to rule out convective heat transport over such a distance./11/ Some form of local cooling must then occur: perhaps nucleate boiling at the surface, or evaporation from the surface of a liquid film which surrounds the beads.

The last item in Table I is the pressure drop in the vapor which flows through the interbead openings. The effective diameter of the opening between the beads has been defined to be the product of a parameter  $\epsilon$  and the actual bead diameter  $d$ . The value of  $\epsilon$  is probably somewhere between .10 and .15 for our irregular shaped beads, which can pack closer than the HCP structure of spheres. In the third column we see that the pressure drop is extremely sensitive to this parameter  $\epsilon$ . The velocity  $v$  of the vapor is determined from the mass which must be converted from liquid to gas to absorb the given heat load. The length  $l$  of the passageway between the center of the beads and the exit is taken to be about 5 cm, which is somewhat greater than the nominal 2 cm to compensate for the many bends in flow path. The pressure  $p_0$  at the exit of the target cavity is about 100 microns. Knowing the vapor pressure curve of  $He^3$ , the pressure drop can then be converted to a temperature difference. It is interesting to note that all of the thermal resistances in Table I vary directly with some power of the bead diameter except the pressure drop, which varies inversely with the square of the bead diameter. Results presented at this conference/12/ then suggest that pressure drop is the dominant thermal resistance in the range of bead sizes (0.4-2.5mm) that have been investigated.

#### 5. The Model

A simple model of the dynamics of the bead cooling might now be constructed, although it must be stressed that the actual situation is exceedingly complicated and perhaps very much unrelated to the model we present here. It seems quite certain that the target cavity fills with phase-separated mixture when no heat is applied. It is not clear what fraction of liquid remains after microwave power is turned on. Vapor is generated, which escapes through the top of the cavity, and which is replaced by liquid flowing in through the perforations in the teflon bead liner. When

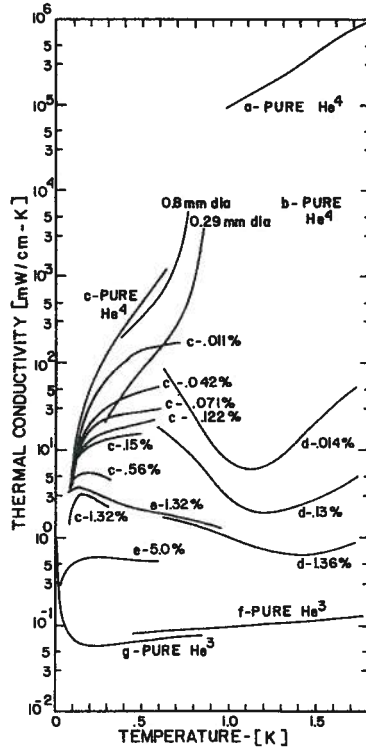


Figure 3  
Thermal conductivity of Mixtures  
letters refer to ref /13/

the beam is turned on the rate of vaporization increases greatly-5  $10^{10}$  ppp supplies about 15 times more power to the beads in the FWHM beam spot. The pressure gradient developed as this vapor flows out through the interbead openings then becomes appreciable, and further displaces liquid from the center of the cavity. The pressure which is available to drive the flow of liquid in to the center of the cavity is the hydraulic (gravitational) head of the liquid surrounding the central region, or about 1 cm of mixture, which corresponds to about 100  $\mu$  of mercury. When the volume of vapor generated in evaporatively cooling the beads is sufficient to cause pressure gradients of this order, then dryout will begin (if it has not already set in as a result of some other more local limit to the heat flux). The situation is complicated by the AGS duty cycle, which provides a 1 second beam spill every 3 seconds. During beam spill the pressure in the pumping line rises about 20 microns, recovering quickly between spills. This corresponds to about .03  $cm^3$  of liquid removed from the cavity, or if the beads are coated with film, to a change in film thickness of about 1 micron. During the time between beam spills the film (which is probably superfluid) must then replenish itself via a driving pressure of about 100 microns. While this does not seem unreasonable, it is possible to think of a much more powerful mechanism to replenish the liquid evaporated by the beam pulse. The  $He^3$  in the mixture which coats the beads has a much higher vapor pressure than the  $He^4$ , and is preferentially evaporated when the beam pulse supplies heat. This region is depleted of  $He^3$ , and an osmotic pressure is set up which tries to drive in  $He^3$  from the unheated outer regions of the cavity. This osmotic pressure was identified in the discussion on heat flush as being adequate to prevent the development of any significant concentration gradients resulting from heating without evaporation. The heated region in the center of the cavity then corresponds to the still in a dilution refrigerator, the cooler outer regions correspond to the dilute phase, and the beam heating corresponds to the still heater. Characteristic values of osmotic pressure in the concentration and temperature range found here are of the order of 1 to 100 torr, which is comparatively a very large pressure./7/

#### 6. Conclusion

The behavior of the mixture-charged evaporation-type PPT is probably dominated by two factors. The  $He^4$  promotes the formation and maintenance of a liquid film on the surface of the beads, which reduces the thermal resistance between the bead and the surrounding fluid. And osmotic pressure very effectively drives the  $He^3$  into the warm region, where it is preferentially evaporated. The observed relation between bead size and polarization is problematic, and merits further attention.

## References

1. P.R. Cameron et al., "Operation of a Polarized Proton Target in an Intense Beam: Cooling the Beads", this workshop.
2. W. Frost and W.L. Harper, "Terminology and Physical Description of Two-Phase Flow", in *Heat Transfer at Low Temperatures*, Plenum (1975).
3. P.V.E. McClintock, "An Apparatus for Preparing Isotopically Pure He<sup>4</sup>", *Cryogenics*, p. 201 (Apr. 1978).
4. I.M. Khalatnikov and V.N. Zharkov, "Theory of Diffusion and Thermal Conductivity for Dilute Solutions of He<sup>3</sup> in Helium II", *JETP* 5, 5 (1957).
5. H.A. Fairbanks and J. Wilks, "Heat Transfer in Liquid Helium Below 1 K", *Proc. Roy. Soc.* A231, p. 545 (1955).
6. T.P. Ptukha, "Thermal Conductivity and Diffusion in Weak He<sup>3</sup>-He<sup>4</sup> Solutions in the Temperature Range from the Lambda Point to 0.6 K," *JETP* 13, 6 (1961).
7. R. Radebaugh, "Thermodynamic Properties of He<sup>3</sup>-He<sup>4</sup> Solutions with Applications to the Dilution Refrigerator", NBS Tech. Note 362 p. 41 (1967).
8. T.O. Niinikoski and F. Udo, "Frozen Spin Polarized Target", *NIM* 134, p. 219 (1976).
9. P.R. Cameron, "Preparation and Irradiation of Ammonia Target Beads", this workshop.
10. T.O. Niinikoski, "Dilution Refrigerators: New Concepts", *Proc. ICEC 6*, Grenoble, 104 (1976).  
T.O. Niinikoski, "Polarized Targets at CERN", *High Energy Physics with Polarized Beams and Targets*, Argonne, AIP 51 (1978).
11. J.C. Wheatley, private communication (Mar. 1984).
12. D.G. Crabb et al., "Operational Characteristics of Radiation-Doped Ammonia Target Beads", this workshop.
13. a W.H. Keesom et al., *Physica* 7, p. 817 (1940).  
b H.A. Fairbank and J. Wilks, *Proc. Roy. Soc.* A231, p. 545 (1955).  
c R.L. Rosenbaum et al., *JLTP* 16, 1/2, p. 131 (1974).  
d T.P. Ptukha, *JETP* 13, 6, p. 1112 (1961).  
e W.R. Abel and J.C. Wheatley, *PRL* 21, 17, p. 1231 (1968).  
f J. Wilkes, *The Properties of Liquid and Solid Helium*, Clarendon Press, Oxford (1967) p. 432.  
g A.C. Anderson et al., *Phys. Rev.* 147, 1, p. 86 (1966).

## OPERATION OF A POLARIZED PROTON TARGET IN AN INTENSE BEAM: COOLING THE BEADS

Peter R. Cameron, Donald G. Crabb,  
Ali M.T. Lin, Richard S. Raymond

Harrison M. Randall Laboratory  
Physics Department  
University of Michigan  
Ann Arbor, Michigan 48109-1120

## ABSTRACT

A simple modification to the operation of an existing He<sup>3</sup> evaporation-type Polarized Proton Target is described, which results in substantial improvement in the maximum operational beam intensity. The pure He<sup>3</sup> gas charge is replaced with a He<sup>3</sup>/He<sup>4</sup> mixture, which improves heat transfer from the ammonia target beads. Data accumulated while operating this target in a high energy physics experiment is presented. Suggestions for further improvements are offered.

## 1. Introduction

The discovery of large spin effects in the strong interaction/1/ has been a major impetus in the development of polarized proton capabilities at the Brookhaven AGS/2/. The recent measurement/3/ of the largest analyzing power ever recorded in high energy p-p scattering has heightened the interest in these unexplained spin forces. With significant improvements in polarized sources already realized/4/, and with several schemes for further improvement/5/ being implemented, there is a real possibility that in the near future the polarized high energy experimenter will be confronted with the pleasant prospect of more polarized beam than he knows what to do with.

The operation of a Polarized Proton Target in an intense beam requires that large amounts of heat be removed from the target beads at low temperatures, and that the beads retain their enhanced polarization characteristics while absorbing gigarad radiation doses. The emergence of ammonia as a radiation-doped target material/6/ has shifted the limit in beam intensity from radiation resistance to bead cooling.

It has been found/7/ that using a He<sup>3</sup>/He<sup>4</sup> mixture in a He<sup>3</sup> evaporation-type PPT greatly increases the tolerable beam intensity, as a result of improved bead cooling. We present here a description of the operation of our PPT when charged with a mixture, and some of the data accumulated while using this target in a high energy physics experiment. The details of the cooling of the ammonia beads is discussed elsewhere/8/, as are the radiation-dependent characteristics of the beads/9/.

## 2. Apparatus and Results

The University of Michigan PPT employs a Roubeau-type/10/ evaporation refrigerator. In our target the amount of beam which can be directed onto the cavity is probably limited by the density of heat flux which is tolerable in the target cavity, rather than the characteristics of the heat exchangers or the pumping system. The target cavity is shown in Figure 1.

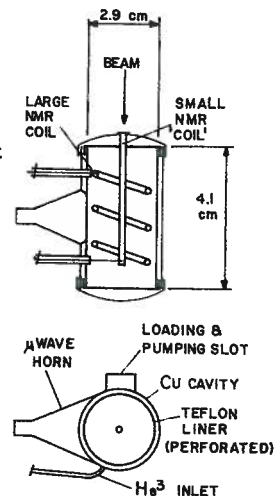


Figure 1  
The Target Cavity

The 25 liter STP gas charge of pure  $\text{He}^3$  normally used in the refrigerator was replaced with a 45 liter STP mixture of  $\text{He}^3$  and  $\text{He}^4$  with  $X=0.4$ , where  $X$  is the  $\text{He}^3$  fraction of the total mixture. This mixture had previously been used in our dilution refrigerator/11/. The difference in volumes is consistent with higher temperature regions of the condenser containing liquid when operating with the mixture, and with the ratio of gas to liquid volume being 745 to 1 for  $\text{He}^4$  but only 460 to 1 for  $\text{He}^3$ .

During cooldown the refrigerator performed in its usual manner until about 0.8 K. It stalled there briefly while phase separation occurred, then cooled rapidly to about 0.5 K. Cooling power measurements were made. Power was supplied to the annealing heater, which is several turns of resistance wire wrapped around the outside of the copper target cavity. These results are plotted in Figure 2, along with the results from a similar measurement made while using a pure  $\text{He}^3$  gas charge. Equal cooling power is obtained at a higher temperature with the mixture charged refrigerator, probably because of the additional burden on the heat exchangers. The  $\text{He}^3$  fraction of the circulating stream was measured to be  $X = 0.6$ . This fraction is somewhat independent of flow rate, decreasing only slightly as flow is increased up to a limit of about 5 mmole/sec, where phase separation is lost (as determined by temperature measurements).

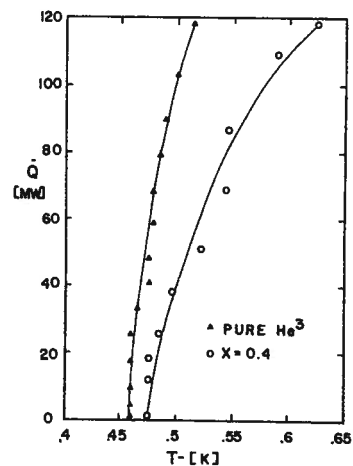


Figure 2  
Cooling Power  
Lines are drawn to guide the eye

A plot of target polarization for various beam intensities is shown in Figure 3. Each circle represents a data run of about 2.5 hours. The decrease in polarization with increasing intensity is clearly visible. The straight line in the figure is a fit by eye to the data. The curved line is a typical 'isoerrorbar', a plot of the equation  $Pn^{1/2} = \text{constant}$ . If the efficiency of the data taking apparatus used in the high energy physics experiment is insensitive to beam intensity, then any combination of polarization and intensity on this curve will give equally

small error bars in the high energy results. Our experience indicates that the optimum intensity is slightly less than  $5 \cdot 10^{10}$  protons per pulse.

Unfortunately, the correlation between intensity and polarization is not so obvious in much of the data. A more typical plot is shown in Figure 4. This data was accumulated in about one month. The large scatter can be attributed to several causes. The beads themselves change as the beam creates new polarizing (and depolarizing) centers. The depolarizing radiation damage is removed at regular intervals by annealing. The effect of the annealing procedure is very sensitive to temperature and the time spent at a particular temperature/9/. The optimization of the PPT (helium flows, microwave frequencies and power levels) varies somewhat. And finally (and most significantly), it has been remarked /12/ that the half life of a PPT is about ten years. The Michigan PPT was born in 1975, and a large fraction of the variation in polarization can be attributed to locating and giving remedy to the creaks and quirks of her aging. Also shown on the left side of Figure 4 is data accumulated while operating with pure  $\text{He}^3$ . The polarization decreases rapidly as the beam intensity becomes greater than about  $3 \cdot 10^{10}$  pp.

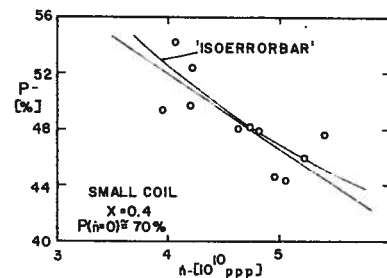


Figure 3  
Target Polarization vs.  
Beam Intensity

The data of the two previous figures was measured with the small NMR 'coil', (see Figure 1), which is simply a copper-nickel tube running the length of the cavity.

The large coil is a tube wound into a three turn helix whose diameter is about 1.5 cm. The proton beam diameter is typically about 1 cm FWHM. When the beam is turned on, the resulting difference between the two coils becomes an obvious measure of the relation between polarization and intensity, whose advantage lies in the subtraction of some of the effects of the variations mentioned above. Figure 5 shows this difference as measured while operating with pure  $\text{He}^3$  and with the mixture. For the case of pure  $\text{He}^3$  the difference increases rapidly as the intensity approaches  $4 \cdot 10^{10}$  pp. Higher intensities resulted in a very rapid loss of polarization.

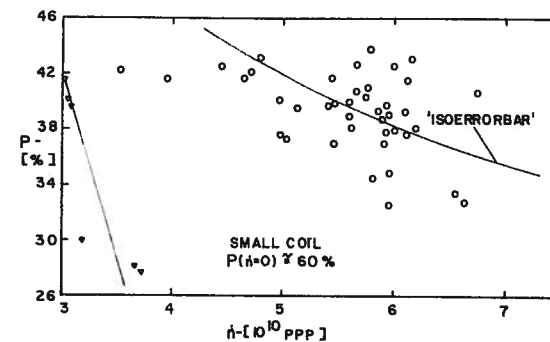


Figure 4  
Target Polarization vs. Beam Intensity  
triangles - pure  $\text{He}^3$   
circles - mixture  $X=0.4$

For the mixture this difference increases up to about  $5 \cdot 10^{10}$  ppp, then remains approximately constant or decreases slightly.

Having observed that the pure  $\text{He}^3$  charged PPT behaved in a manner that might be described by the term 'burnout' as intensity increased, we looked for similar effects in the mixture charged case. These results are shown in Figure 6. The target beads used were somewhat deficient in centers, and the maximum polarization with no beam was less than 50%. No effects which might be described as 'burnout' were seen at  $3 \cdot 10^{11}$  ppp (however, the increase in beam spot size is ignored in these results). The cryogenics collapsed at this point because flows in the  $\text{He}^4$  cryostat could not be set high enough to accommodate the unusually high  $\text{He}^3$  flow and its resulting condensation heat load, due to a broken pump. It is clear that the polarization quickly falls below the isoerrorbar as intensity approaches about  $10^{11}$  ppp.

The relation between bead size and polarization is shown in Figure 7. The point with the large horizontal bar was a mixture of beads ranging from about 1 mm to 2.5 mm diameter. The 0.4 mm beads were made by crushing and sorting this mixture of larger beads. The beam intensity in the 'with beam' results was typically about  $5 \cdot 10^{10}$  ppp. The figure refers to the beads as 'fragments', which is a more descriptively accurate term. Our beads are manufactured by slow freezing and crushing, rather than by dripping liquid ammonia into a  $\text{LN}_2$  bath, and their shape is quite irregular. Beads used in polarized targets are usually about 1 mm diameter. Our data indicates that larger diameters are favored when operating with mixtures in intense beams.

### 3. Improvements

There are several possibilities for improvement now being considered. First, it has been suggested that the benefits which result from adding  $\text{He}^4$  to the  $\text{He}^3$  gas charge are caused by the presence of a tenacious film on the surface of the beads, and might persist when only a small amount of  $\text{He}^4$  is

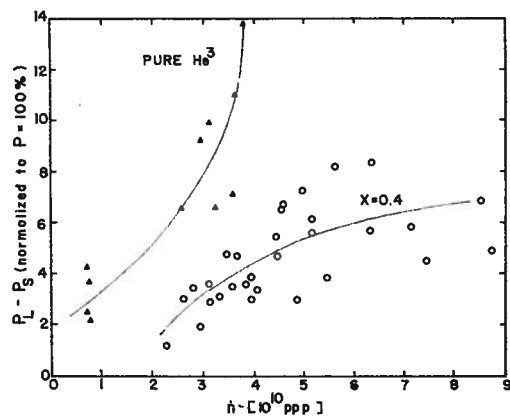


Figure 5  
Polarization Difference vs. Intensity  
triangles - pure  $\text{He}^3$   
circles - mixture  $X=0.4$   
Lines are drawn to guide the eye.

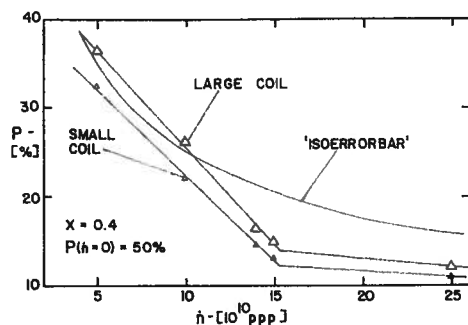


Figure 6  
Looking for Burnout

added/13/. The mixture used in our PPT was recently increased from  $X=0.4$  to  $X=0.6$  with no apparent change in performance. We are interested in trying mixtures in the range  $X=0.9$ .

Second, the heat flux can be lowered by increasing the effective volume. This can be done by increasing the diameter of the FWHM beam spot, or by increasing the target length. Increasing the diameter of the beam spot decreases both heat flux and the efficiency of the spectrometer being used in the high energy physics. However, the heat flux decrease varies as the square of the diameter, whereas the efficiency decrease is some linear fraction of the diameter increase, so that improvement might be possible here. The target length is limited by the size of the homogenous magnetic field region needed for dynamic nuclear polarization. A gain of about 1.5 might be had by replacing the present pole tips with samarium colbalt/14/.

Third, the geometry of the target cavity might be changed. The present geometry dates from the early days of organic target materials, when beam intensity was limited by radiation damage. It has been suggested/13/ that osmotic pressure drives the  $\text{He}^3$  into the central region of beam heating. If this is in fact what is happening, then changes in the inlet location probably will not result in significant improvement. It was also pointed out/8/ that the data of Figure 7 suggests that the inefficiency of the process whereby the generated vapor is removed from the center of the cavity limits the polarization which can be gotten at a given heat load. This might be improved by drilling a series of small holes along the length of the small NMR 'coil', which would result in direct pumping on the central region.

Finally, we intend to give more thought to the possibility that improvements in our refrigerator could be helpful. We are presently limited by the amount of mixture we can circulate. While the  $\text{He}^3$  insert is easily removable for bead changes, it is so at the cost of good thermal contact with the  $\text{He}^4$  section. To improve this would require a new refrigerator. There are two possibilities which should be considered in addition to the technique of operating an evaporation refrigerator with a mixture. These are the dilution refrigerator/15/, and the subcooled  $\text{He}^4$  bath/16/. It is not obvious which of these three approaches is the best.

### 4. Conclusions

Operation of our evaporation-type PPT with the pure  $\text{He}^3$  gas charge replaced by a mixture has tripled the maximum tolerable beam intensity, as a result of improved bead cooling. The target is also much more resistant to burnout, and therefore less vulnerable to unanticipated variations in beam intensity.

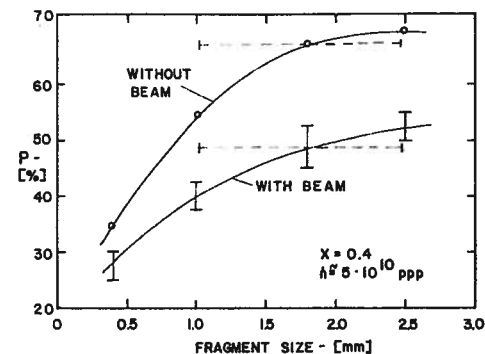


Figure 7  
Polarization vs. Bead Size  
Lines are drawn to guide the eye.

## References

1. For a review, see R.C. Fernow and A.D. Krisch, "High Energy Physics with Polarized Proton Beams", Ann. Rev. Nucl. Part. Sci. 31 (1981).
2. see papers in Proc. 1982 Symp. on High Energy Spin Physics, AIP 95, Brookhaven (1982). Proc. 6th Int. Symp. on High Energy Spin Physics, Marseilles (1984).
3. R.S. Raymond et al., "Analyzing Power Measurements in High  $P_{\perp}^2$  Elastic p-p Scattering", Proc. Conf. on Intersections of High Energy and Nuclear Physics, Steamboat springs, CO (1984).
4. Proc. Conf. on Polarized Proton Ion Sources, AIP 117, Vancouver (1983).
5. see ref. 2 and 4 above, and also Y.Y. Lee, "The Accumulator-Booster Proposal", BNL 32949R (1984). J. Alessi et al., "A Ring Magnetron Ionizer for Polarized Negative Ion Sources", BNL33272 (1983). A. Hershcovitch, "Generation of Intense Polarized Beams by Selective Neutralization of Negative Ions", BNL 34239 (1983). Th. Sluyters, "Liquid Helium Cooled Atomic Hydrogen Beam Research", Adv. Source Dev. Grp. Tech Note 1, BNL (1983). T. Niinikoski, "CERN Workshop on Cold Atomic H", (1984) (unpublished). R.S. Raymond et al., "Plans for an Ultracold Polarized Atomic Hydrogen Jet", Proc. Argonne Workshop on Pol. Targets in Storage Rings, Argonne (May 1984). L.W. Anderson et al., "Polarization of Fast Atomic Beams by Collisional Pumping: A Proposal for Production of Intense Polarized Beams", Phys. Rev. Lett. 52, 8, p. 609 (1984).
6. T.O. Niinikoski and J.M. Rieubland, "Dynamic Nuclear Polarization in Irradiated Ammonia Below 0.5 K", Phys. Lett. 72A, 141 (1979).
7. D.C. Peaslee et al., "Large- $P_{\perp}^2$  Spin Effects in  $p + p + p + p$ ", PRL 51, 26, p. 2359 (1983).
8. P.R. Cameron, "A Simple Model of Bead Cooling", this workshop.
9. D.G. Crabb et al., "Operational Characteristics of Ammonia Beads in an Intense Proton Beam", this workshop.
10. P. Robeau and J. Vermeulen, "Continuous Flow Horizontal  $\text{He}^3$  Cryostat for Organic Polarized Proton Targets", Cryogenics, Dec. 1971, p. 478.
11. P.R. Cameron et al., "Horizontal Dilution Refrigerator for Use in Intense Proton Beams", Proc. BNL Spin Symp., AIP 95 (1982).
12. S. Mango, private communication.
13. J.C. Wheatley, private communication.
14. G. Danby, private communication.
15. T.O. Niinikoski, "Dilution Refrigerators: New Concepts", Proc. ICEC 6, Grenoble, 104 (1976).
16. T.O. Niinikoski, "Polarized Targets at CERN", Argonne, AIP 51 (1978). R.C. Niemann, "Heat Transfer Surface Requirements for the PPT-III  $\text{He}^3$  Evaporator", Argonne HEF/MME Tech Note 52.D.19 (1969). V.W. Hughes and K.P. Schuler, SLAC Proposal "Son of E130" (1982).

## First Experience with a $^3\text{He}/^4\text{He}$ Mixture in a $^3\text{He}$ -Refrigerator in High Intensity Electron Beams

K.H. Althoff, B. Boden, V. Burkert, U. Hartfiel, T. Hewel, G. Knop, M. Leenen, W. Mehnert, W. Meyer, H.D. Schablitzky, E.P. Schilling, H.H. Schmitz, W. Thiel

Physikalisches Institut der Universität Bonn,  
Nussallee 12  
D-5300 Bonn 1  
Fed. Rep. of Germany

presented by T. Hewel

### ABSTRACT

The performance of dynamic deuteron polarization of a  $\text{ND}_3$  sample in an intense electron beam was studied using a  $^3\text{He}/^4\text{He}$  mixture as coolant (volume ratio 300/200). The results are compared to measurements performed with pure  $^3\text{He}$ .

### 1. Motivation

Measurements with a tensor polarized deuteron target in elastic electron-deuteron-scattering enable a separation of the three electromagnetic deuteron form factors  $F_C(q^2)$ ,  $F_M(q^2)$ ,  $F_Q(q^2)$ . Such measurements are in preparation at the Bonn 2.5 GeV Synchrotron /1/. Therefore, studies have been made whether the  $^3\text{He}$ -refrigerator available in Bonn could give sufficient cooling power in order to maintain a high deuteron polarization in an electron beam. With a  $^4\text{He}$ -refrigerator the target operates at 1 Kelvin /2/ where the tensor component is very small (<1%). To achieve higher tensor polarization values it is necessary to decrease the target temperature.

### 2. Experimental Set-up

The experimental set-up shown in fig. 1 was basically identical to the one described in a previous talk /2/. The main difference was the use of a  $^3\text{He}$ -refrigerator (figure 2) instead of the  $^4\text{He}$ -system. This refrigerator is capable of working in two modes with  $^3\text{He}$  and  $^4\text{He}$  as coolants, respectively /3/. The electron beam current was up to 35 nA at an energy of 1.5 GeV and with a duty cycle of about 5%.

As target material  $\text{ND}_3$  was used. Its performance under high irradiation doses in an intense electron beam has been discussed in ref. /2/. The  $\text{ND}_3$ -fragments were placed in a capton cell and kept in a helium bath. The target volume was about  $6 \text{ cm}^3$ .

The calibration of the deuteron polarization was performed at 1 Kelvin to make use of the shorter polarization build-up time at this temperature. The electron beam was scanned across the target front face in  $256 \times 256$  steps to achieve a uniform irradiation of the target volume. The scanning speed was proportional to the beam current.

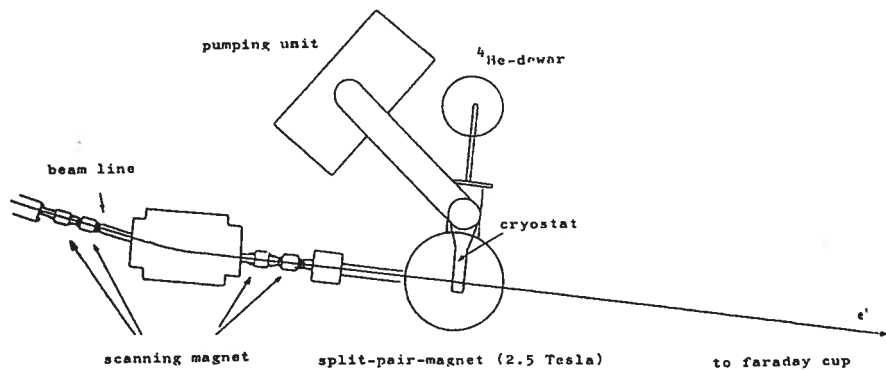


figure 1: Layout of the Experiment

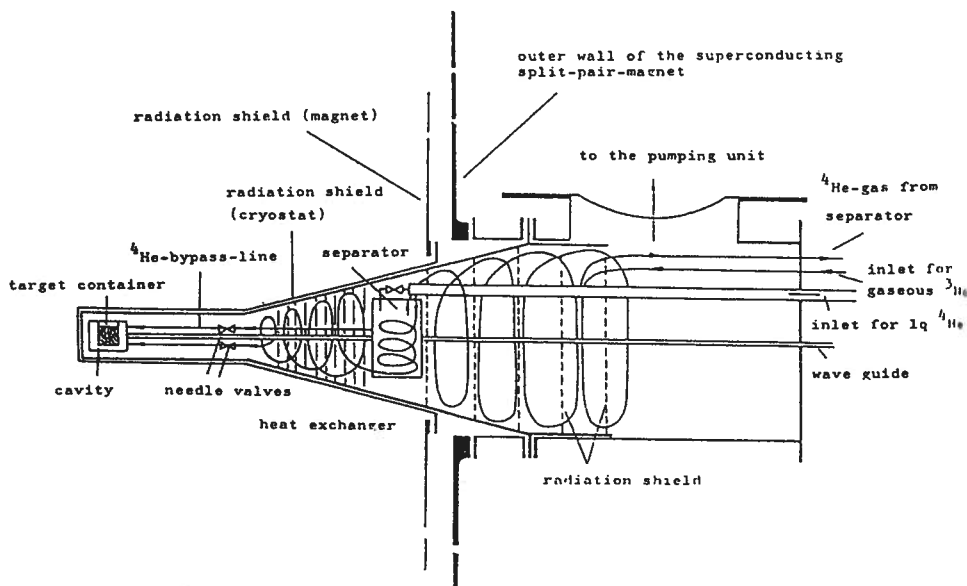
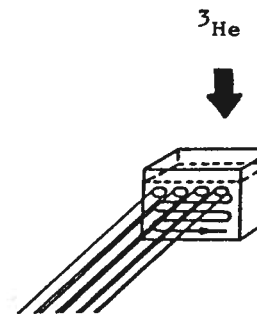


figure 2:  $^3\text{He}$ -Cryostat /3/



target front face =  $3.0 \text{ cm}^2$   
 beam profile =  $0.3 \text{ cm}^2$

### 3. Measurements

To ensure that the expected loss in polarization was not due to radiation damage the target material was irradiated up to a range where the deuteron polarization approached an asymptotic value as described in ref. /2/ and shown in fig. 3.

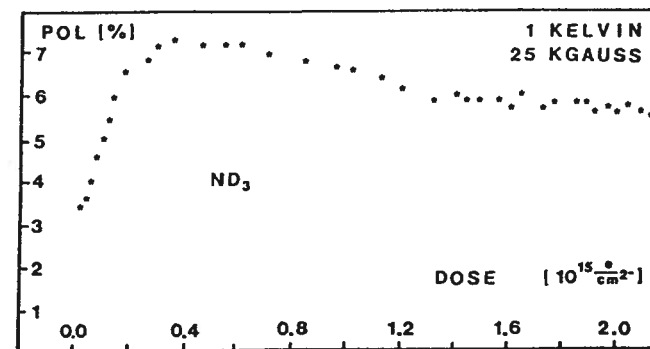


figure 3: Irradiation dependence of  $\text{ND}_3$  (at 1 K) /2/.

The initial polarization  $P_{\text{max}} = P(I_b = 0)$  was in the range of 13% to 15%. The first measurements were performed with pure  $^3\text{He}$ . The  $^3\text{He}$  flow rates were 2, 4, 6 and 8 mmole/sec. At a flow rate of 2 mmole/sec we achieved stable performance of the  $^3\text{He}$ -refrigerator only with zero beam current. At a higher flow rate the polarization was less affected by changes of the beam current, as visible in fig. 3(a) - c). Finally  $^4\text{He}$  was added to the  $^3\text{He}$  cooling circuit up to a volume ratio  $^3\text{He}/^4\text{He} \approx 300/200$ . This mixture was used at a flow rate of 6 mmole/sec. From fig. 4d) it is evident that the decrease in polarization is smaller than the one measured with pure  $^3\text{He}$  and a flow rate of 6 mmole/sec and also smaller than the one with 8 mmole/sec and pure  $^3\text{He}$ .

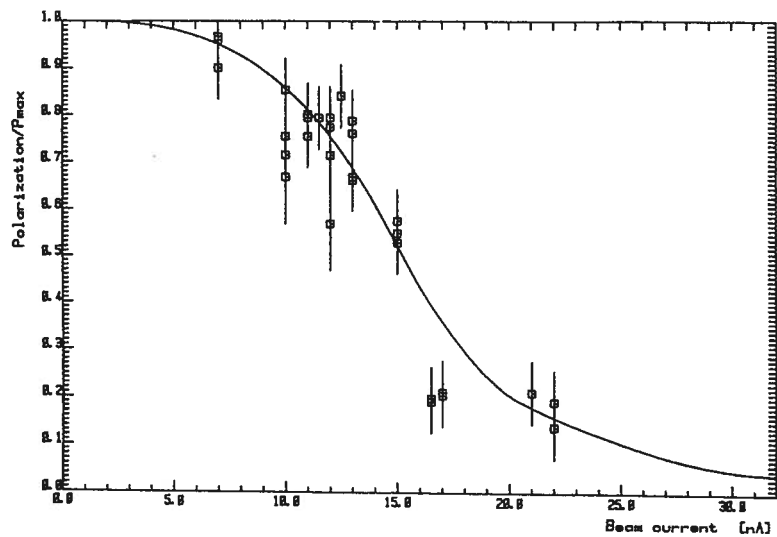


figure 4a: Flow rate: 4 mmole/sec. pure He-3  
(The lines 4a-d are drawn to guide the eye.)

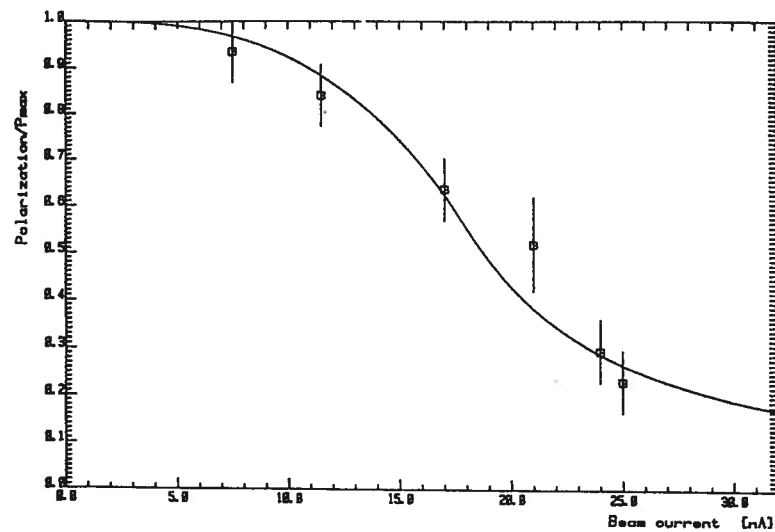


figure 4c: Flow rate: 8 mmole/sec. pure He-3

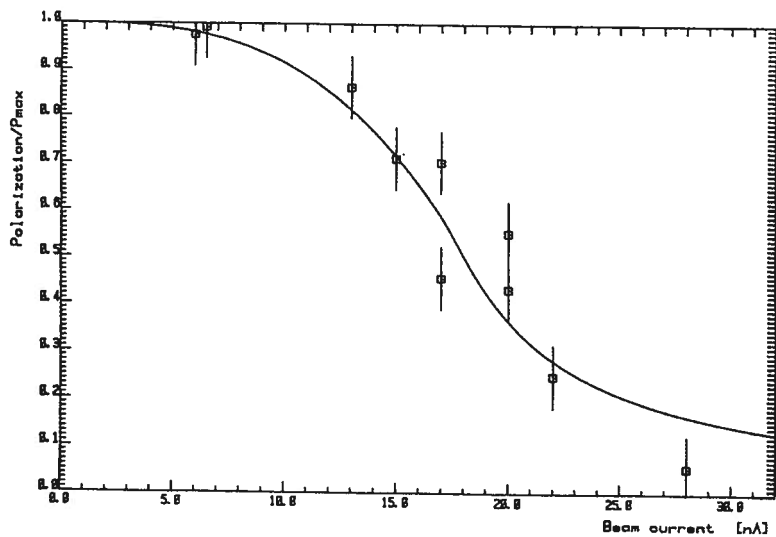


figure 4b: Flow rate: 6 mmole/sec. pure He-3

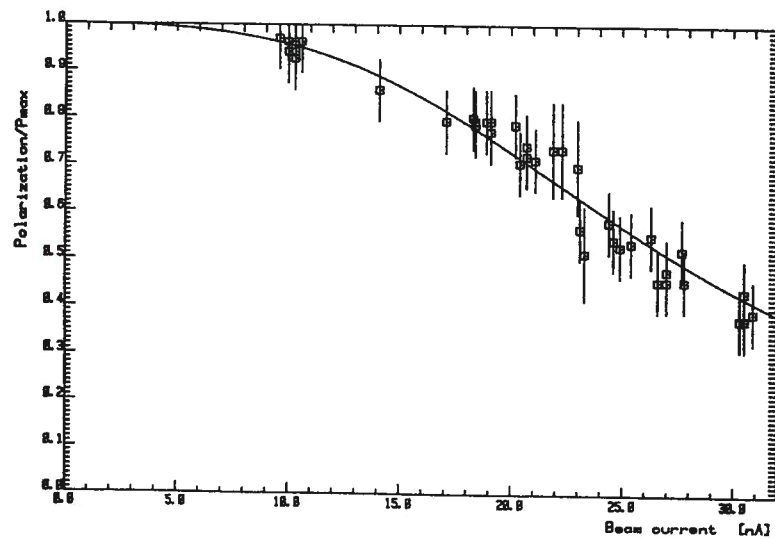


figure 4d: Flow rate: 6 mmole/sec. He-3/He-4 mix.

From these studies conclusions for the use of a coolant of minor cooling capability have to be drawn with care, for the following reasons:

1.) In the experiment it was observed that the increase of the helium bath temperature due to beam heating was negligible. This indicates that a local heating of the  $\text{ND}_3$ -fragments is responsible for the decrease in polarization.

2.) Calculations on the power deposited by the electron beam confirm that the power is mainly dissipated in the  $\text{ND}_3$  material. Thus it should be investigated whether the polarization is the same everywhere in the target sample or whether there is a local depolarization where the beam hits the target. The interpretation of our data gives hints that - in dependence of the beam current - the local depolarization is considerably larger than the measured one (the NMR-coil integrates over the full target volume) /4/.

More work is needed to find an optimal  $^3\text{He}/^4\text{He}$  mixture (may be in dependence of a given beam current) to minimize the local polarization loss.

- /1/ H.D. Schablitzky, V. Burkert, Internal Report (1984), unpublished.
- /2/ U. Hartfiel, Radiation Resistance Studies of  $\text{NH}_3$  and  $\text{ND}_3$  at 1 K, these proceedings.
- /3/ H. Herr and V. Kadansky, Nucl. Instr. and Meth. 121 (1974) 1.
- /4/ T. Hewel, Diploma thesis, BONN-IR-84-43.

## Microprocessorized NMR measurement

A. Rijllart

CERN  
CH-1211 Geneva 23  
SWITZERLAND

### ABSTRACT

An MC68000 CAMAC microprocessor system for fast and accurate NMR signal measurement will be presented. A stand-alone CAMAC microprocessor system (MC68000 STAC) with a special purpose interface sweeps a digital frequency synthesizer and digitizes the NMR signal with a 16-bit ADC of 17  $\mu\text{s}$  conversion time. It averages the NMR signal data over many sweeps and then transfers it through CAMAC to a computer for calculation of the signal parameters. The computer has full software control over the timing and sweep settings of this signal averager, and thus allows optimization of noise suppression. Several of these processor systems can be installed in the same crate for parallel processing, and the flexibility of the STAC also allows easy adaptation to other applications such as transient recording or phase-sensitive detection.

### 1. Introduction

The polarization in polarized targets can be determined from the absorption part of the RF susceptibility

$$\chi(\omega) = \chi'(\omega) + i\chi''(\omega) \quad (1)$$

by integrating over the frequency domain

$$P_1 \propto \int_0^\infty \chi''(\omega) d\omega. \quad (2)$$

This is valid when the RF excitation causes negligible saturation. The RF absorption signal can be conveniently measured with a series

resonant Q-meter, of which the output responds linearly to  $\chi''(\omega)$  when  $\chi(\omega)$  causes a relatively small change (<10%) impedance change in the resonant circuit. The integration over the frequency domain, using the continuous NMR technique, is done by sweeping an RF oscillator through the absorption region, digitizing the Q-meter output with an ADC, and calculating the surface area of the signal. The averaging technique is used to obtain higher precision, especially on small signals.

## 2. The NMR set-up

The NMR set-up/1/, shown schematically in fig. 1, consists of an RF synthesizer, a Q-meter circuit followed by post-detection amplifiers and filters, the MC68000 STAC/2/ with the NMR-interface, and a mini-micro computer. The NMR-interface gives the MC68000 STAC the control of the frequency synthesizer, the sample-and-hold and ADC circuits, and several DAC and logic outputs.

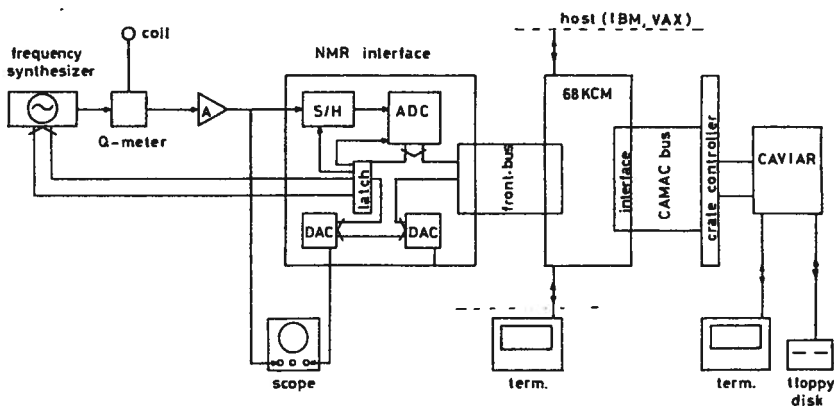


Fig.1. Block diagram of NMR set-up.

The operation of the set-up is as follows: after having received the parameters about the sweeps to do from the computer the STAC steps the frequency synthesizer through the desired frequency range; at each step the signal is digitized and the value accumulated in a corresponding memory location. After the programmed number of

sweeps, the STAC sends a LAM (Look-At-Me) signal to the computer, which can then read-out the accumulated signal in a block-transfer. The averaged signal is then treated in the computer to get the polarization and other relevant parameters. During the analysis of the signal the STAC is accumulating data on the next one.

For tuning the RF circuits the STAC can sweep the frequency continuously without sending LAM signals, and the NMR signal can be displayed on an oscilloscope. The horizontal sweep can be taken from a DAC which is incremented and decremented synchronously with the frequency steps by the STAC. Alternatively, the scope can be triggered by a signal from the control logic of the NMR-interface to have a time display of the NMR signal.

## 3. The MC68000 STAC and NMR-interface

The MC68000 STAC is single width CAMAC module based on an 8 MHz MC68000, and is commercially available. It further consists of:

- i) 16 kbyte RAM, 150ns access time
- ii) 32 kbyte EPROM, 450ns access time
- iii) a CAMAC interface
- iv) 2 V24 interfaces
- v) a hardware break-point register
- vi) a simple programmable timer
- vii) a 60-pin 3M front-panel connector carrying the processor bus

The NMR-interface is a single CAMAC circuit board, 3 slots wide, made with wire-wrap technique. This interface is connected to the front-panel connector of the STAC and has no connection to CAMAC. On the circuit board are:

- i) a sample and hold amplifier, 5  $\mu$ s settling time
- ii) a 16-bit ADC, 17  $\mu$ s conversion time
- iii) a 12-bit DAC, 1.5  $\mu$ s settling time
- iv) a 10-bit DAC, 250 ns settling time
- v) a 32-bit digital frequency synthesizer interface
- vi) an 8-bit buffer/latch for device control and logic I/O
- vii) a 60-pin 3M front-panel connector to interface to the STAC

#### 4. Signal averaging performance

The STAC executes 200 frequency sweeps of 200 steps, with 16  $\mu$ s for the signal to settle, in 2.6 s. So each step takes 66  $\mu$ s. Minimum step time for the software is therefore about 50  $\mu$ s. The surface area of an NMR signal of 0.25% polarization can be determined with about 0.2% statistical accuracy, using the settings above. Fig. 2 shows two typical NMR signals measured using a 250 nH coil with about 50% filling factor in a pentanol target.

Proton TE NMR signals have been observed in different polarized target materials at liquid nitrogen temperature using 2000 sweeps.

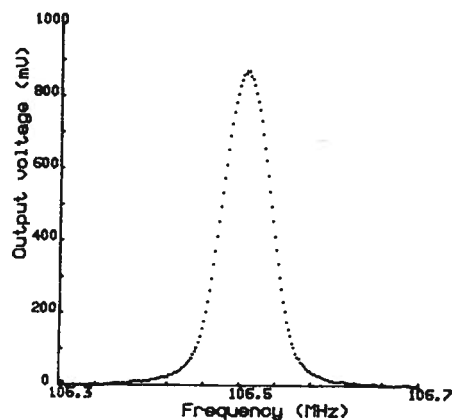


Fig.2a. Proton NMR spectrum at 0.8 K.

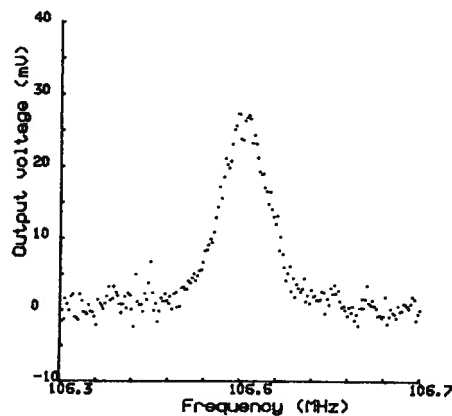


Fig.2b. Proton NMR spectrum at 20 K.

#### 5. Q-meter circuits

The Q-meter circuits used in this NMR set-up are:

- i) The Liverpool Q-meter/3/. This Q-meter has been developed by a CERN-Liverpool university collaboration and consists of a series resonant circuit with a resonant cable in between the tuning capacitor and the NMR coil, RF amplifiers, and a phase-sensitive detector followed by LF amplifiers. Its frequency range is from 5-200 MHz aimed at proton and deuteron NMR signal detection.
- ii) The CERN 1 GHz Q-meter. This Q-meter was made at CERN of connectorized components. It uses 2 coils, each at the end of a resonant cable mounted in the cryostat, which connect to a 180° hybrid for maximum Q-curve compensation at the input of the RF amplifiers. One coil is to measure the NMR signal, the other serves as a reference. In this way, and with selective intermediate filtering, the total RF gain could be as much as 70 dB before the mixer. It was purpose built for stable atomic hydrogen (H) NMR signal measurement at 4.8 T field.
- iii) The CERN 5-32 MHz Q-meter. Another Q-meter circuit was made with connectorized components for lower frequency NMR signal detection. With the good experience from the differential method with the hybrid at 1 GHz, a similar input circuit was used for Q-curve compensation. RF gain of more than 60 dB could be used before mixing. This Q-meter, shown in fig. 3, is particularly suited for deuteron and metal NMR signal measurement.

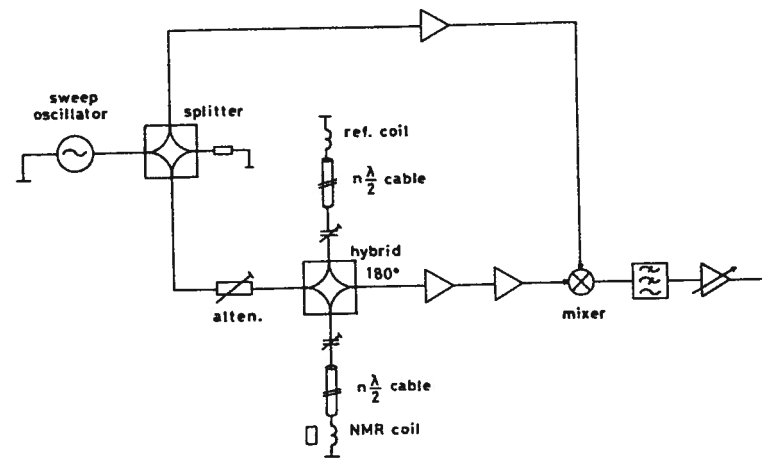


Fig.3. Q-meter circuit with hybrid.

## 6. Measured NMR signals

Table 1 shows the NMR signals which have been measured with the described microprocessorized NMR set-up, at which frequency and field, and which Q-meter was used.

Table 1. NMR signals measured with the described set-up.

NMR signal	Frequency (MHz)	Field (T)	Q-meter
proton	106.5	2.5	Liverpool
<sup>3</sup> He	158	4.8	Liverpool
HI	965	4.8	CERN HF comp.
<sup>65</sup> Cu	32.5	2.6	CERN RF comp.
<sup>63</sup> Cu	32.5	2.8	CERN RF comp.
<sup>27</sup> Al	32.5	2.9	CERN RF comp.

In all set-ups the Rockland model 5600 direct digital frequency synthesizer was used, except in the HI NMR signal measurement where the Wavetek model 3001 was used with a frequency doubler. The Wavetek was swept by applying the DAC triangle wave from the NMR-interface to the external FM input, as its digital frequency control response time is very slow due to the PLL based frequency synthesis.

In case of the <sup>3</sup>He NMR signal the Rockland was used with a doubler, as at 158 MHz frequency, close to the upper limit, the output level was not very constant over the used frequency scan.

## 7. Multi-processor NMR set-up

In large targets the polarization has to be measured in different parts. The largest system at CERN has 8 channels. The STAC could control, for example, a four channel NMR interface, which would simultaneously measure the polarization in different coils. Multiplexing could be done in between the sample-and-hold and the ADC. This would not slow down the measurement cycle too much. Two of such four channel systems would be needed in case of our largest target. Other STAC systems could be added to control, for instance, a microwave source or a colour monitor display memory, either

programmed in assembler or high-level language. The software in the controlling computer would be able to handle such a multi-processor system easily as it remains within the CAMAC definition.

## 8. Adaptation to other applications

With only small changes in the STAC software, this signal averager has been used successfully as:

- Transient recorder for bolometric measurements detecting HI. The signal averager can take data on a trigger, without sweeping an oscillator, with a programmable delay time between the steps. Single shot events, like the recombination of HI, can be recorded this way with a maximum of 4000 steps in length and a minimum of 25  $\mu$ s interval between steps.
- Phase-sensitive detector for H beam intensity measurements. Using an external synchronization pulse the STAC can be commanded to take data over 360° of a modulation signal. Many of these records can be averaged, like with the NMR signals, for optimum noise suppression. The averaged data is sent to a computer for demodulation and further filtering. With such a lock-in detector the measured signal shape can be studied, the optimum phase angle for detection calculated by the computer, and background correction can be done similar to the baseline subtraction with NMR signals, if necessary. The highest lock-in frequency which can be used depends on the desired number of points in the record, for 20 points this is 2 kHz. There is no low frequency limit.

With a multi-channel NMR interface different signals could be digitized in time simultaneously and correlations calculated.

## 9. Conclusion

The introduction of an MC68000 microprocessor system sweeping a digital frequency synthesizer and digitizing the NMR signal with a 16-bit ADC has the following advantages:

- Continuous signal measurement. The NMR signal is continuously being measured with only very small deadtime during data

transfer.

2. High accuracy and dynamic range. The 16-bit ADC data is accumulated with 32-bit precision by the MC68000.
3. High spectral stability and purity. The direct digital frequency synthesizer has excellent stability ( $\pm 2 \cdot 10^{-9}$ /day) in centre frequency and the sweep is determined by binary codes. Harmonics are 40 dB below the fundamental.
4. High flexibility. All relevant parameters such as centre frequency, sweep width, number of sweeps to average etc., are controlled by software.
5. Easily expandable to multi-system due to modular structure of both hardware and software.

#### References

- [1] T.O. Niinikoski and A. Rijllart, An MC68000 microprocessor CAMAC system for NMR measurement of polarization, Nucl. Instrum. Methods 199, 485 (1982).
- [2] A. Rijllart, An MC68000 Stand-Alone CAMAC Microprocessor System, Microprocessing and Microprogramming 12, 291 (1983).
- [3] G. Court, D.W. Gifford and T.O. Niinikoski, Proc. 2nd Workshop on Polarized Target Materials, 76 (1980).

#### HYDROGEN NMR SIGNAL ASSOCIATED WITH SILVER

J. J. Jarmer and J. Vaninetti

Los Alamos National Laboratory  
Los Alamos, New Mexico 87545, U.S.A.

and

D. Hill

Argonne National Laboratory  
Argonne, Illinois 60439, U.S.A.

#### ABSTRACT

We have observed a small hydrogen NMR signal associated with the silver plating on a copper microwave cavity and silver wire of an NMR coil. Limits on the size of the signal and its possible effect on the calibration of target polarization are discussed.

#### Discussion

We have measured a background hydrogen NMR signal which appears to be associated with silver plating on the surrounding copper microwave cavity. The circumstances that led to this conclusion are described.

A low-beam-intensity experiment at the Clinton P. Anderson Meson Physics Facility (LAMPF) required as large a target as possible. Consequently a cylindrical teflon target cell 3.8 cm diam  $\times$  6 cm long was constructed. The limitation on size was the field deviation over the volume (less than 12 G). The cell was instrumented with three NMR coils that were sensitive to the polarization of different parts. For discussion purposes the coils are called 1, 2, and 3. Their locations were as follows: coil 1, a saddle coil sensing a major portion of the periphery of the target; coil 2, a series-wound, dual-hair pin around the circumference at each end of the cylinder; coil 3, a hair pin along the axis.

The target was contained in an internally silver-plated copper cavity with about 2 mm clearance. In this configuration, coils 1 and 2 were close (about 1 mm) to the walls of the cavity, coil 3 farther removed (about 1.8 cm). For one phase of the experiment, carbon beads were substituted for the normal material (propanediol + EHBA) and cooled with liquid  $^3\text{He}$ . NMR measurements were made on all three coils to check for possible hydrogen contamination in the carbon. To minimize this possibility, the beads had been previously heated at elevated temperature under vacuum, then stored in a dry gas environment. A small hydrogen signal was measured on coils 1 and 2; none was observed on coil 3. The signal size was about 2-3% of the 1-K thermal-equilibrium (TE) signal obtained with the propanediol. When the carbon was removed, a careful visual inspection was made of all three coils. Our first suspicion was that water, alcohol, or some other material containing hydrogen was on the coils; none was found. We note that the normal procedure before loading requires the target to be pumped for several hours while at room temperature in order to minimize such problems. After several discussions, it was concluded that the only significant difference between the coils was that 1 and 2 were close to the silver-plated copper. The microwave cavity was replaced with a new copper cavity that was not silver plated. The measurements with carbon beads were

repeated. The hydrogen signal observed previously was largely absent. From this we conclude that the silver plating was the source.

A similar conclusion was drawn when empty-target measurements were made on a completely different cell at Argonne National Laboratory. In this case a silver wire was used for the NMR measuring coil. The empty-target measurements consistently exhibited a background-hydrogen signal about 3% of a typical T<sub>1</sub> signal. When the silver wire was replaced with copper, the background signal was not present.

From these observations we conclude that a hydrogen NMR signal can be associated with silver. The chemical mechanism of this phenomenon has not been explored. We recommend caution when silver or silver plating is used near NMR coils in polarized proton targets.

## Tensor Polarized Deuteron Targets for Intermediate Energy Physics Experiments

W. Meyer and E. Schilling  
Physikalisches Institut der Universität Bonn  
Nussallee 12  
D-5300 Bonn 1  
Fed. Rep. of Germany

### 1. Introduction

One of the basic problems in particle physics is the investigation of the nucleon-nucleon interaction. At low energies it is well described by the one pion exchange picture, whereas at high energies the interaction is understood on the quark level.

However, the simplest properties of few-nucleon systems such as their binding energies, density distributions, quadrupole and magnetic moments cannot be accurately determined by considering only the interactions between the nucleons in the framework of a potential theory. In models improvement is achieved by including the exchange of more and heavier mesons like  $\rho$ ,  $\omega$ ...and isobar configurations. An open question is also the possible configuration of exotic states such as dibaryons (six quark configurations).

The deuteron is a two-nucleon system, where all these aspects are relevant. There are no problems with the many particle approximation as exists with other heavier nuclei. The deuteron is the simplest of all nuclear systems and its properties are as important in nuclear physics as the hydrogen atom was in atomic physics. However, both the theoretical and the experimental situation at intermediate energies are unsatisfactory. It is obvious that a thorough understanding of the deuteron is extremely necessary for all other nuclei.

At intermediate energies measurements from a tensor polarized deuteron target are being prepared for the following reactions: the photodisintegration of the deuteron, the elastic pion-deuteron scattering and the elastic electron-deuteron scattering. The experimental situation of the polarization experiments for these reactions is briefly discussed in section 2. In section 3 the definitions of the deuteron polarization and the possibilities to determine the vector and tensor polarization are given. Present tensor polarization values and further improvements in this field are reported in section 4.

### 2. Deuteron polarization experiments

#### 2.1 Deuteron photodisintegration

The motivation for recent measurements of the deuteron photodisintegration reaction  $\gamma d \rightarrow pn$  at intermediate energies has been the possible existence of exotic states, such as dibaryons.

Due to the complicated spin structure of the deuteron photodisintegration reaction, 12 complex helicity amplitudes are required to characterize completely the  $\gamma d \rightarrow pn$  process; hence 23 different observables have to be measured as a function of the photon energy and the proton c.m.s. angle. Only few experiments have been performed to investigate single polarization quantities like target asymmetry T (using a vector polarized deuteron target), beam asymmetry  $\Sigma$  (using linearly polarized photons) and recoil nucleon polarization P /1/.

Recently some data from double polarization experiments, performed with linearly polarized photons combined with a recoil nucleon polarization

measurement, has become available. Compared to the number of observables the number of experiments is still deplorably small, too small to allow reliable analyses.

It is unlikely that a complete measurement of the 23 observables will ever be made. However, the number of measured polarization observables can be increased in the near future with improved experimental techniques, e.g. tagged polarized photon beam and high vector polarized deuteron target. In addition, experiments with a tensor polarized deuteron target are possible (see section 4). Such measurements are now being planned /2/.

## 2.2 Elastic pion-deuteron scattering

There are two different spin observables measured for this reaction: the vector polarization  $T_{11}$  /3/ and the tensor polarization  $T_{20}$  of the recoil deuteron, which has been measured by two groups /4/ /5/. However, the experimental results for  $T_{20}$  are very different. Both groups used a double scattering technique where the tensor polarization of the recoiling deuteron in the  $\pi$ -d scattering reaction is determined from the cross section of the  $d^3\text{He} \rightarrow p^4\text{He}$  reaction.

In view of the present discrepancy in the  $T_{20}$  data it is difficult to interpret the results. Therefore, an independent experiment - the  $\pi$ -d elastic scattering from a tensor polarized deuteron target - is planned to resolve this discrepancy /6/.

## 2.3 Electron-deuteron elastic scattering

Polarization experiments are expected to play a central role in studies of the electric form factors of the nucleons. For the deuteron three form factors are required to specify completely its electromagnetic current: The charge monopole  $F_c$ , the charge quadrupole  $F_Q$  and the magnetic dipole  $F_M$ . Measurements of the differential cross section  $\sigma_Q$  have provided a sum of all three form factors and by means of a Rosenbluth separation  $F_M$  can be obtained. The separation of  $F_c$  and  $F_Q$  requires the measurement of at least one polarization observable. To achieve the separation of  $F_c$  and  $F_Q$ , work has been started at the MIT-Bates Linear Accelerator Center by measuring the recoil tensor polarization in electron-deuteron elastic scattering /7/. One main problem of this experiment is the low analysing efficiency of the polarimeter.

Contrary to this external beam experiment, the deuteron form factors could be studied by the use of polarized internal targets in an electron storage ring. However, a considerable increase of the atomic beam density (about a factor of 100) is needed to achieve high enough luminosities. New techniques are under development and a new generation of atomic beams is expected /8/.

A further possibility to separate  $F_c$  from  $F_Q$  can be obtained by elastic scattering of the electrons from a tensor polarized deuteron target. This experiment is being prepared in Bonn. The advantage of this type of experiment is, that 'conventional' polarized target techniques can be used. However, a large solid angle detection and of course a deuteron target with high tensor polarization are decisive for the success of the measurements/9/.

## 3. The deuteron as a polarized target

The deuteron as a target in scattering experiments introduces some additional problems compared to the proton. Fermi motion between the nucleons and final state interaction must be considered. In the case of polarized deuteron target experiments, the measurements are lengthy, as the

polarization is relatively small (in comparison to the proton). Furthermore, the detection of the polarization signal and the polarization determination is difficult.

### 3.1 Definitions of the deuteron polarization

The orientation of the deuteron spin system ( $I=1$ ) along an axis  $O_z$  can be described by the vector polarization

$$P = \langle I_z / I \rangle \quad (1)$$

and the tensor polarization or alignment, defined as

$$A = \langle 3I_z^2 - I(I+1) \rangle / I^2 \quad (2)$$

If a deuteron is subjected to a magnetic field  $H$  in the direction  $O_z$ , the Zeeman interaction gives a set of 3 sublevels. The polarization of the deuteron can be calculated from Eqs. (1) and (2) to be

$$P = (p_+ - p_0) + (p_0 - p_-) = p_+ - p_- \quad (3)$$

and

$$A = (p_+ - p_0) - (p_0 - p_-) = 1 - 3p_0 \quad (4)$$

where  $p_+$ ,  $p_0$  and  $p_-$  are the fraction of the spins in the magnetic sublevels  $m = I_z = +1, 0$  and  $-1$ , respectively. The sum of  $p_m$  is normalized to 1. The vector polarization varies between  $-1$  and  $+1$ , whereas  $A$  has values between  $-2$  and  $+1$ .

### 3.2 Determination of the deuteron polarization

The polarization is normally measured by the nuclear magnetic resonance (NMR) method. If the deuteron spins are in thermal equilibrium (T.E.) with the solid lattice at a known temperature  $T$  in a known magnetic field  $H$ , the deuteron polarization is calculable using the Eq.

$$P = \frac{4 \tanh \frac{\mu H}{2kT}}{3 + \tanh^2 \frac{\mu H}{2kT}} \quad (5)$$

where  $\mu$  is the magnetic moment and  $k$  is the Boltzmann constant. The vector polarization  $P$  of the target is obtained by comparing the T.E. signal ( $P=0.05\%$  at 1 K and 2.5T) with that of the enhanced signal (T.E. method). If we neglect the small quadrupole interaction, the tensor polarization  $A$  is given by

$$A = \frac{4 \tanh^2 \frac{\mu H}{2kT}}{3 + \tanh^2 \frac{\mu H}{2kT}} \quad (6)$$

From these definitions it follows that under thermal equilibrium  $A$  and  $P$  are related by

$$A = 2 - \sqrt{4 - 3P^2} \quad (7)$$

In practice, the tensor polarization  $A$  is calculated from the measured vector polarization  $P$ .

The shape of the deuteron magnetic resonance (DMR) signal offers another possibility to measure the polarization. In an external magnetic field the energies of the three magnetic sublevels can be written as

$$E_m = -h\nu_D m + h\nu_Q \left[ (3\cos^2(\theta) - 1) \right] \left[ 3m^2 - (I(I+1)) \right]$$

where  $\nu_D$  is the deuteron Larmor frequency and  $\nu_Q = 1/8(eq\psi_{zz}/h)$ ,  $eq$  is the deuteron quadrupole moment and  $\psi_{zz}$  is the value of electrical field gradient along the principal axis of the  $\mathbb{E}$  field gradient tensor.  $\theta$  is the angle between this axis and the direction of the magnetic field.

The quadrupole interaction shifts the levels depending on the angle between the magnetic field  $H$  and the electrical field gradient  $\psi_{zz}$ , as shown in fig. 1. This gives rise to two transitions. The corresponding lines are smeared out, since we do not have a single crystal. The two lines partially overlap each other, and the observed DMR signal is a superposition of them, as indicated in fig. 2. The two peaks correspond to  $\theta=90^\circ$ , the pedestals to  $\theta=0^\circ$ . The right peak and the left pedestal correspond to the  $m=+1$  to  $m=0$  transition with an intensity  $I_+$ , and the other peak and pedestal to the  $m=0$  to  $m=-1$  transition with an intensity  $I_-$ . At high polarization the intensities, which are proportional to the difference in the populations  $p_m$  of the corresponding states become different and the DMR signal shows an asymmetry. If we define  $R=I_+/I_-$  and assume a Boltzman distribution among the sublevels the vector polarization is given by

$$P = (R^2 - 1)/(R^2 + R + 1) \quad (8)$$

and the tensor polarization by

$$A = (R^2 - 2R + 1)/(R^2 + R + 1) \quad (9)$$

as follows from the definitions.

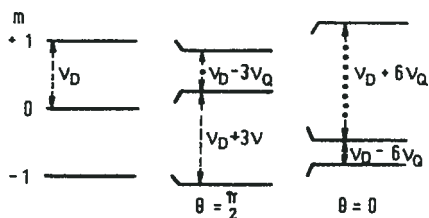


Fig. 1: Energy level diagram of the deuteron spin system. The quadrupole interaction shifts the levels depending on the angle  $\theta$  between the magnetic field  $H$  and the electrical field gradient  $\psi_{zz}$ .

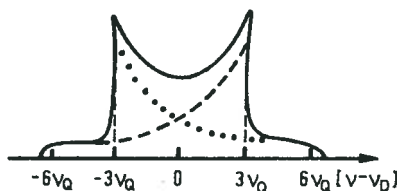


Fig. 2: Theoretical deuteron line shape, which is the sum of the two possible transitions  $m=-1$  to  $m=0$  (dashed line) and  $m=0$  to  $m=1$  (dotted line). Some line broadening has been taken into account. Otherwise the peaks would tend to infinity.

An alternative method for the determination of the deuteron polarization can be used, if different kinds of nuclei in one material have an equal spin temperature. Consequently the temperature  $T$  in Eqs. (5) and (6) can be replaced by the spin temperature  $T_s$ , which can be calculated from the proton polarization measurements performed in the deuterated sample (normally the target materials are not fully deuterated).

It is obvious that in all cases very precise NMR-measurements must be done, to obtain the tensor polarization value with sufficient accuracy. An accuracy for  $P$  of  $\pm 5\%$  is reported [10/11], using the T.E. calibration method. This gives an accuracy for  $A$  of about  $\pm 10$ - $\pm 12\%$ , depending on the degree of the polarization ( $A=12$ - $25\%$ ). A T.E. signal of deuterated ammonia taken at 1 K and 2.5 T and the dynamically enhanced signal corresponding to 44% vector polarization and 15% tensor polarization are shown in fig. 3.

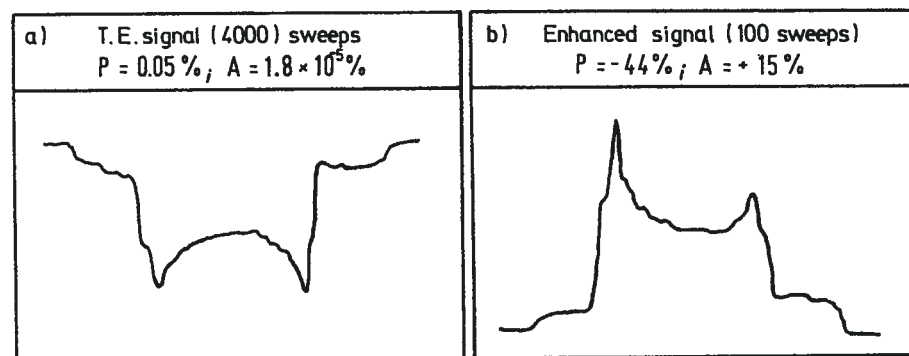


Fig. 3: Deuteron magnetic resonance signals of deuterated ammonia. (a) T.E. signal taken at 1 K and 2.5 T - plotted after 4000 sweeps. (b) Dynamically enhanced signal taken at 200 mK - plotted after 100 sweeps. From the vector polarization of -44% the tensor polarization of 15% is calculated using eq. (7). The small structures in the enhanced signal are typical for slowly frozen samples.

#### 4. Values of the tensor polarization

In the normal case a vector polarized deuteron target is automatically tensor polarized. As can be seen from fig. 4, noticeable tensor polarization  $A$  demands high vector polarization  $P$ , which can be obtained in dilution refrigerators. Typical values for  $P$  are 35-45%, from which  $A$  is calculated to be 10-15%. Of course, higher tensor polarization values are desirable to perform experiments with good efficiency.

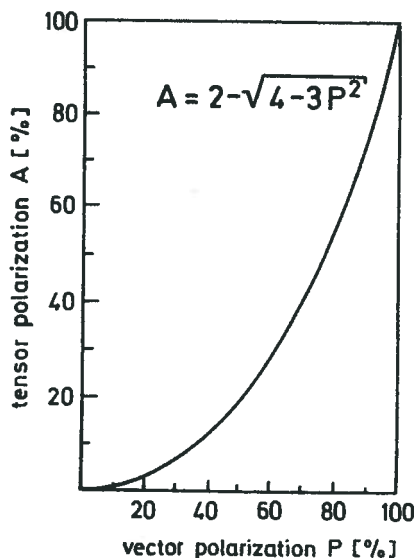


Fig. 4:  
Tensor polarization versus vector polarization of the deuteron assuming a Boltzman distribution among the magnetic levels

The highest deuteron polarization was measured in  ${}^6\text{LiD}$  in a dilution refrigerator at a very high magnetic field of 6.5 T /12/. The polarization results are shown in fig. 5. As a comparison the maximum value obtained in  $\text{ND}_3$  is plotted. In both materials the radicals were produced by irradiation /13/. It is expected, that at higher magnetic fields (>2.5 T) an increase of the tensor polarization can also be obtained in the currently used target material  $\text{ND}_3$ . Measurement at 3.5 T are under investigation.

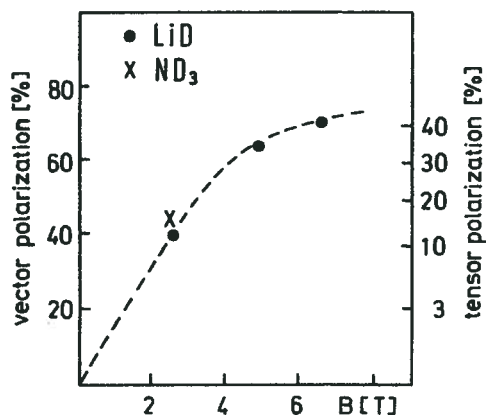


Fig. 5:  
Polarization of LiD in dependence of the magnetic field. For comparison the maximum polarization of  $\text{ND}_3$ , obtained at 2.5 T is also shown.

Another method of enhancing the tensor polarization consists of disturbing the thermal equilibrium of the deuteron spin system. The inhomogeneous behaviour (see section 3.2) of the deuteron spin system makes it possible to 'burn holes' in the DMR line with a saturating RF field /14/. This always changes the population  $p_0$  of the level  $m=0$ , thus changing  $A=1-p_0$ . From fig. 6 it can be seen that if the deuteron spin system saturated at a frequency  $\nu = \nu_D - \delta$  this decreases  $p_0$  of the corresponding deuterons, thus enhancing the line at  $\nu = \nu_D + \delta$ .

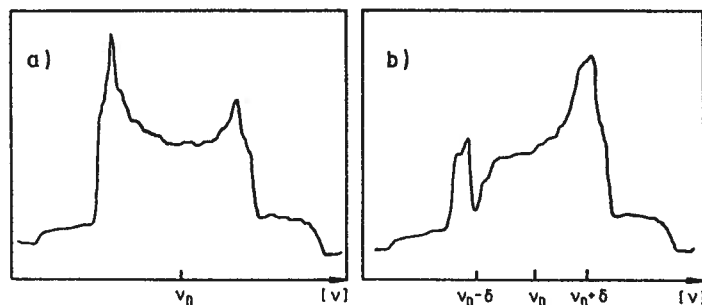


Fig. 6:  
(a) DMR signal of deuterated ammonia corresponding to  $P=37\%$ .  
(b) This DMR signal was obtained from the original signal after application of a saturating RF field at a frequency  $\nu_D - \delta$  (see text).

Of course, the tensor polarization cannot be changed independently of the vector polarization by this method. It is clear, that best results are obtained in a frozen spin target starting with a high deuteron polarization.

First measurements of the tensor polarization in  $\text{ND}_3$  gave values up to 20%. This was achieved by irradiating the sample with a frequency-modulated RF field around the peak position on the right and around the pedestal position at the left side of the DMR signal (fig. 7).

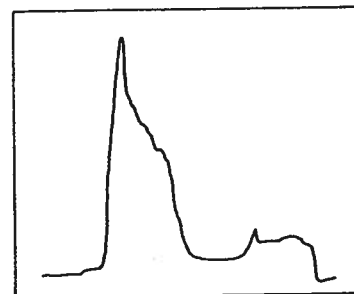


Fig. 7:  
DMR signal of deuterated ammonia obtained after irradiating the sample with a frequency-modulated RF field (see text).

Contrary to these methods, which prepare a mixture of vector and tensor polarization, a pure tensor polarization of the deuteron spin system can also be obtained under special conditions. This could be demonstrated in samples, in which a strong thermal contact between a proton spin-spin interaction reservoir and the deuteron quadrupole interaction reservoir exist /15/. A DMR signal of pure tensor polarization is shown in fig. 8.

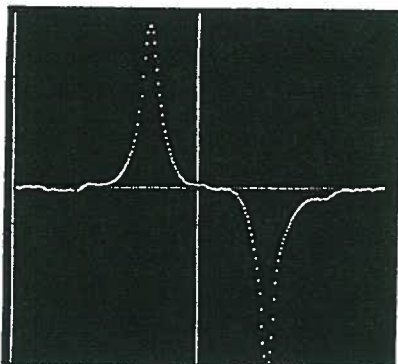


Fig. 8:  
DMR-signal under 'RF field induced alignment':  $P = 0$ ,  
 $A = -0.20$  (from Ref. 15).

## 5. Summary

In the last few years the study of polarization phenomena at intermediate energies has become of great interest. The motivation for recent deuteron polarization experiments in photon induced reactions as well as in the elastic pion-deuteron scattering has been the possible existence of exotic states.

Looking at polarized target experiments only measurements with a vector polarized deuteron target have been performed. These measurements became possible after the development of  $^3\text{He}$ -refrigerators in the early seventies. In the meantime dilution refrigerators have become more and more the standard equipment of a polarized target system, as in dilution refrigerators the highest deuteron polarization values can be obtained. Measurements with a tensor polarized target are now being prepared.

Further developments in the field of polarized target materials allow improved experiments with intense beams such as electrons. Form factor measurements of the deuteron by means of electron scattering from a tensor polarized deuteron target are under preparation. It is expected that in addition to recoil tensor polarization measurements independent results are accessible. Furthermore, experiments at higher  $q^2$  values of the virtual photon are planned, where the sensitivity to the differences between theoretical models becomes higher. Although in future there will be other possibilities for electron scattering experiments, such as internal targets, the polarized target will be with us for some time to come. This is certainly the case for experiments on photon induced reactions.

We would like to thank K.H. Althoff for many stimulating discussions and his steady help. The help during the measurements of R. Dostert, E. Kohlgarth and W. Thiel is gratefully acknowledged.

## References

- / 1/ W. Meyer, Proc. of the 6th Int. Symp. on High Energy Spin Physics, Marseille 1984, to be published
- / 2/ W. Meyer, Proc. of the 1984 Workshop on Electron and Photon Interactions at Intermediate Energies, Bonn-Bad Honnef, to be published
- / 3/ J. Bolger et al., Phys. Rev. Lett. 48(1982)1667
- / 4/ R.J. Holt et al., Phys. Rev. Lett. 47(1981)472
- / 5/ W. Gruebler et al., Phys. Rev. Lett. 49(1982)444
- / 6/ E. Boschitz, private communication
- / 7/ M. E. Schulze et al., Phys. Rev. Lett. 52(1984)597
- / 8/ W. Gruebler, Proc. of the Workshop on Polarized Targets in Storage Rings, Argonne 1984, to be published
- / 9/ V. Burkert and H.D. Schablitzky, Bonn Proposal 1984
- /10/ W. Meyer et al., Nucl. Instr. and Meth. 204(1982)59
- /11/ H. Hayashii et al., Nagoya-Preprint, DPNU-17-81
- /12/ Y. Roinel, Proc. of 'High Energy Physics with Polarized Beams and Polarized Targets, Eds. C. Joseph and J. Soffer (Birkhäuser Verlag, Basel, 1981)p. 458
- /13/ W. Meyer et al., Nucl. Instr. and Meth. 227(1984)35
- /14/ W. de Boer, CERN-Report, 74-11
- /15/ W. de Boer et al., Phys. Lett. 46A(1973)143

Lecture at the Workshop on Polarized Target Materials and Techniques  
Bad Honnef, West Germany - September 3-6, 1984

### POLARIZED PROTON PHYSICS AT THE AGS

A.D. Krisch  
Randall Lab of Physics  
The University of Michigan  
Ann Arbor, Michigan 48109-1120

Since a similar lecture<sup>1</sup> will be published in the Proceedings of the 1984 Marseille Symposium on High Energy Spin Physics, I will only give a brief summary of my lecture.

To accelerate polarized protons in the AGS it was necessary to make major hardware modifications in almost every part of the accelerator complex, which is shown in Figure 1. A new polarized H<sup>-</sup> ion source was constructed, which now operates at a world record 25  $\mu$ A. Dr. Alessi described this source in some detail at this conference. A team led by S. Giardano constructed a 200 MHz Radio Frequency Quadrupole (RFQ) to replace the Cockcroft-Walton 760 KeV preaccelerator. We believe that this was the first RFQ successfully used with an operating accelerator.

To maintain polarization during the acceleration cycle in the main ring it was necessary to pass more than 30 strong depolarizing resonances without serious depolarization. The 3 strong intrinsic depolarizing resonances were jumped using 8 fast pulsed quadrupole magnets installed around the AGS ring. These quadrupoles shifted the vertical betatron tune with a 1.6  $\mu$ sec risetime and thus passed very rapidly through the resonances. Almost 30 strong imperfection resonances were corrected with the appropriate  $n$ th harmonic ( $\sin n\theta$  where  $G\gamma = n$ ) produced by the 96 correction dipole magnets in the AGS ring. A new type of strong depolarizing resonance (intrinsic/imperfection) was discovered and overcome near 15 GeV/c.

The 200 MeV polarimeter constructed by Rice measured the polarization at the end of the LINAC. The fast internal polarimeter constructed by Michigan measured the relative polarization during the acceleration cycle. The high energy polarimeter shown in Fig. 2 measured the absolute polarization by observing the left-right asymmetry in proton-proton elastic scattering at  $P_{\perp}^2 = 0.3$  (GeV/c)<sup>2</sup> where the Analyzing Power, A, was taken to be  $4.6 \pm 0.4\%$ .

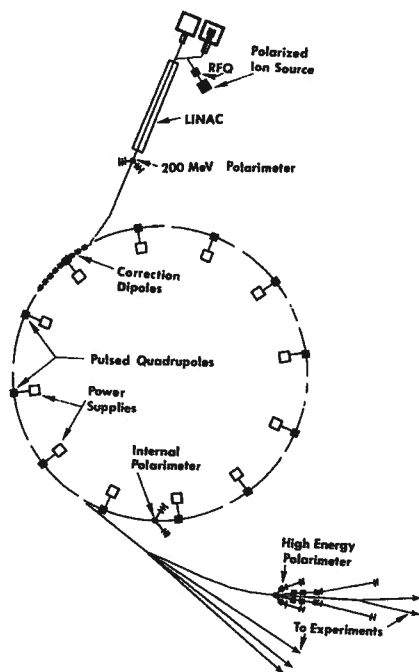


Fig. 1 Diagram of the AGS showing those areas where modifications were made to allow the acceleration of polarized protons.

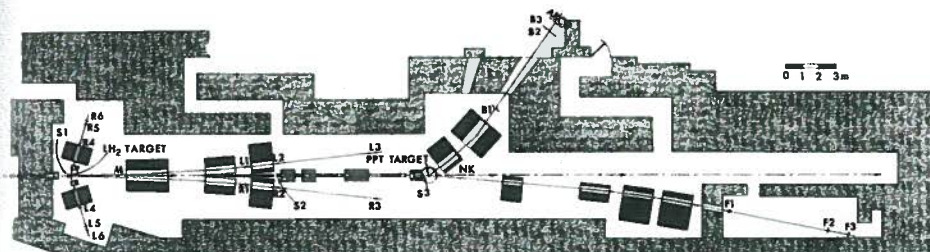


Fig. 2 The Michigan high energy polarimeter is shown on the left. It uses a liquid hydrogen target to measure the left-right asymmetry in p-p elastic scattering. The polarized beam is then scattered in the Michigan polarized proton target and p-p elastic events are detected by the spectrometer which contains magnets for momentum analysis and the F and B scintillation counter hodoscopes.

In July we reached a momentum of 16.5 GeV/c with a polarization of 40% and an intensity of  $10^{10}$  protons per pulse. We expect to increase the momentum, polarization, and intensity during 1985. A detailed paper on the AGS Polarized Proton Beam is being prepared by the Argonne, Brookhaven, Michigan, Rice, Yale polarized beam collaboration.

I will briefly discuss the one-spin experiments which we have been doing at the AGS during the last two years. We have studied spin effects in p-p elastic scattering at 28 GeV/c with an unpolarized beam scattering from our polarized proton target shown in Figure 2 along with the layout of our AGS experiment. A high intensity beam of almost  $10^{11}$  protons per pulse is extracted from the AGS and scatters from the polarized proton target. We have 2 magnets for momentum analysis in the large-angle recoil arm and 4 magnets in the forward arm. The forward and recoil protons are each detected by an 8-channel 3-fold scintillator hodoscope telescope. The target protons can be polarized in either the up(+) or down(-) spin state, while the beam is unpolarized. Thus we can measure one-spin effects such as A, the analyzing power, which is related to the spin-orbit interaction.

In Figure 3 the analyzing power, A, is plotted against  $P_{\perp}^2$  for  $p + p \rightarrow p + p$  at 28 GeV/c. In Spring 1984 we improved our statistics at  $P_{\perp}^2 = 5.95$  (GeV/c)<sup>2</sup> and measured another point at  $P_{\perp}^2 = 6.56$  (GeV/c)<sup>2</sup>. The rather surprising new data is shown. I have no idea what this rising A at high  $P_{\perp}^2$  might mean. No one has ever before looked at such high- $P_{\perp}^2$  spin effects, and this sharp rise is quite unexpected. Most QCD models predict that  $A = 0$  at high- $P_{\perp}^2$ . Perhaps this strange result is a continuation of the historical trend that, whenever spin effects are studied in an unexplored region, there are surprises.

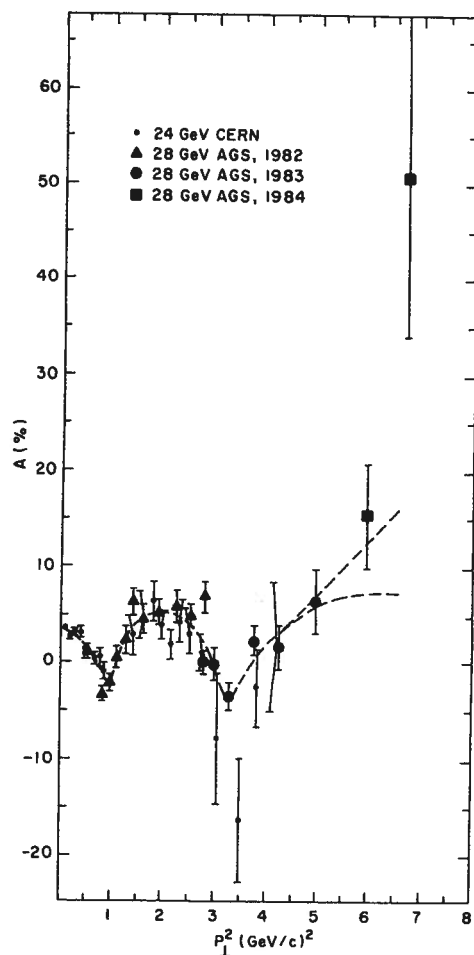


Figure 3. New Data on  $A$  vs.  $P_{\perp}^2$

This research was supported by the U.S. Department of Energy.

1. A.D. Krisch, Polarized Protons at the AGS and High- $P_{\perp}^2$  Spin Experiments, Proc. of the 6<sup>th</sup> International Symposium on High Energy Spin Physics, Marseille, Sept. 12-19, 1984, J. Soffer, Ed. (to be published).

## THE EXPERIMENTS AT KEK WITH POLARIZED BEAM AND POLARIZED TARGET

Naoaki Horikawa

Department of Physics, Nagoya University  
Chikusa-Ku, Nagoya 464  
JAPAN

### ABSTRACT

We report the experimental plans to use the polarized target and/or the polarized beam facility which is presently under construction at KEK, especially, focusing on an experiment which is formally accepted.

### I. Introduction

Presently, KEK has the following 3 kinds of facilities,

- 1) 12 GeV Proton Synchrotron (PS),
- 2) Photon Factory ..... 2.5 GeV Electron Storage Ring for Solid State Physics,
- 3) TRISTAN .....  $e^+e^-$  colliding machine with the energy of  $30 \times 30$  GeV.

The construction of TRISTAN is now in progress, aiming at the start of the measurement in 1986. The Photon Factory has been constructed for the study of the solid state physics by the X ray from the synchrotron radiation. As for PS, after the decision of the construction of TRISTAN, the future plan of PS has been discussed and then the following three items were proposed.

- i) Acceleration of Polarized Beam,
- ii) Construction of High Intensity K-Beam and
- iii) Acceleration of Nuclei.

After some discussions, the latter two subjects were delayed to the later chance, because it associates the improvements of the machine and the beam channels and the item i) was accepted. At that time, to push the construction of the polarized beam facility, the following 3 theme were proposed.

- (i) The Measurement of Spin Correlation Parameter  $A_{nn}$  and large  $P_T$  Region in  $p^{\uparrow}n^{\uparrow} \rightarrow pn$  Scattering (by Nagoya, Kyoto, Hiroshima, Tokyo, INS, KEK and UCLA).
- (ii) The Measurement of Spin Transfer in  $P^{\uparrow}A \rightarrow \Lambda^{\uparrow}X$  Reaction (by Tsukuba).
- (iii) The Acceleration of Polarized Deuteron and Measurement of Physical Quantities in  $n^{\uparrow}p$  Process, Aiming at Dibaryon Research in  $I=0$  State (by Kyoto, Hiroshima, Nagoya, Tokyo, INS and KEK).

Among these proposals, the first one was approved by KEK PAC, and others were shifted to the later opportunity from some reasons. The experimental study of the acceleration of the polarized beam has just started after the approval of this experiment. We would like to mention here a little bit about the present status of the polarized beam and next go to the introduction of the approved experiment.

## II. The Study of the Polarized Proton Beam

As a polarized proton source, the new ECR (Electron Cyclotron Resonance) type ion source has already been developed. The study of the acceleration has started at last October. However, the further research is forced to stop nearly one year due to the construction of the TRISTAN tunnel. The following result was obtained from the first acceleration test of two weeks in the 500 MeV Booster ring.

Table 1 The results from the 1st acceleration test without the special tuning apparatus. The ratio of polarization between Booster and LINAC was changed by selecting a suitable  $v_z$  of the Booster.

	Beam Intensity	Polarization (%)
ion source	$\sim 10 \mu\text{A}$	$\leq 80$
after LINAC (20 MeV)	$\sim (0.5 \sim 1) \mu\text{A}$	$(47 \pm 6) \leq P \leq (56 \pm 8)$
after Booster (500 MeV)	$(1 \sim 3) \times 10^8$ ppp	$(12 \pm 2) \leq P \leq (15 \pm 2)$
		$\frac{P(\text{Booster})}{P(\text{LINAC})} = (25 \sim 40) \%$

From this study, the characteristics of the resonance in the Booster were made clear, and the methods to jump over the resonances are being prepared.

## III. The Experimental Plan of "The Measurement of the Spin Correlation Parameter $A_{nn}$ at Large $P_T$ Region in $p \uparrow n \uparrow \rightarrow pn$ Scattering"

### 1) Motivation

The motivation of this experiment is following.

- What behavior will be seen in  $A_{nn}$  at large  $P_T$  in  $pn \rightarrow pn$  process?
- Does new data of  $A_{nn}$  in  $pn$  process be able to select the scattering model at the large  $P_T$  region in the hadron collision?

The spin correlation parameter  $A_{nn}$  in  $pp$  elastic process showed an extraordinary behavior in the large  $P_T$  region /1/. That is, the value of  $A_{nn}$  starts to increase at  $P_T^2 \sim 3.2$  ( $\text{GeV}/c$ )<sup>2</sup> and reaches to 0.6 at  $P_T^2 = 5$  ( $\text{GeV}/c$ )<sup>2</sup>. This feature depends only on the  $P_T^2$ , but on the incident momentum or angle. The  $A$  parameter which was recently reported /2/ shows also a dip structure at  $P_T^2 \sim 3.2$  ( $\text{GeV}/c$ )<sup>2</sup> and increases with  $P_T$ , as shown in Fig. 1.

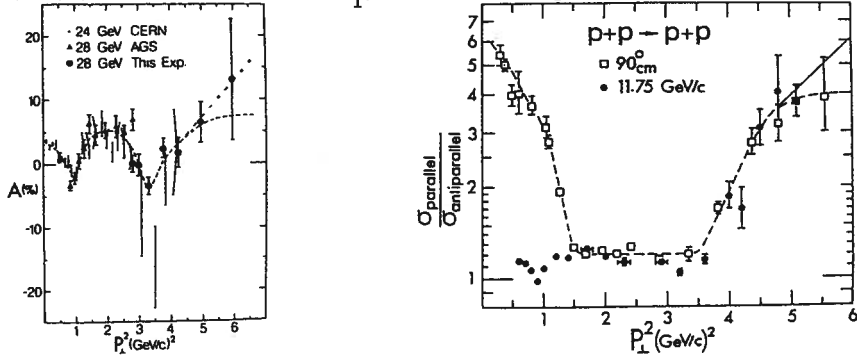


Fig. 1 Asymmetry and spin correlation parameters in  $pp$  elastic scattering. A remarkable change at  $P_T^2 = 3.2$  ( $\text{GeV}/c$ )<sup>2</sup> is seen in both parameters.  $\sigma^{\uparrow\uparrow}/\sigma^{\uparrow\downarrow} = 4$  corresponds to the value of  $A_{nn} = 0.6$ .

To explain the anomalous  $A_{nn}$  at large  $P_T$ , theoretists proposed various predictions based on some models, that is, the optical model, and some kinds of quark models /3,4,5,6,7,8/. Nevertheless, the common understanding of the reaction mechanism is not yet been established, due to mainly lack of data. Quark model predictions of  $A_{nn}$  for  $pp$  and  $pn$  elastic processes are listed in Table 2.

Table 2 The predictions of  $A_{nn}$  by several quark models.

Model	p-p	p-n	$(d\sigma/dt)^{np}/(d\sigma/dt)^{pp}$
QIM (Farrar et al.) (Brodsky et al.)	$A_{nn} = -A_{\ell\ell} = -A_{ss}$ $A_{nn}(90^\circ) = 1/3$	$A_{nn} = -A_{\ell\ell} = -A_{ss}$ $A_{nn}(90^\circ) = -0.44$	$\sim 0.6$
Diquark spectator model (Wolters)		$A_{nn} = -0.22 \pm 0.22$	
Q-Q scattering model (Chen)	$A_{nn} = \begin{cases} 1/9 & \text{with color} \\ -1/11 & \text{without color} \end{cases}$	$A_{nn} = 0$	

It seems to be two ways to get a new development from this stage. One is to go to higher energies, and another is to investigate other processes at large  $P_T$ . Motivated by this situation, we planned the measurement of  $A_{nn}$  in  $pn$  elastic process at large  $P_T$  region, using polarized proton beam facility being developed at KEK and polarized deuteron target.

### 2) Experimental procedure

The experiment will be performed under the conditions presented in Table 3.

Table 3 Experimental conditions presently set.

Counting rate (N) = $I_b \cdot I_L \cdot d\sigma/dt \cdot \Delta t \cdot \Delta\phi/2\pi \cdot \eta$	
Measurement region;	$P_p = 6.0 \sim 13 \text{ GeV}/c$
	$\theta_{CM} = 90^\circ$
Beam intensity;	$I_b = 10^8$ pps
Beam polarization;	$P_b \geq 50 \%$
Target material;	ND <sub>3</sub>
Target polarization;	$P_t \geq 40 \%$
Target thickness;	7 cm in length
Width of data bin;	$\Delta t = 3.0$ ( $\text{GeV}/c$ ) <sup>2</sup>
Acceptable aperture;	$\Delta\phi/2\pi = 4 \times 10^{-2}$
Neutron detection efficiency; $\eta = 0.4$	

The beam line at KEK and the experimental layout is shown in Fig. 2.

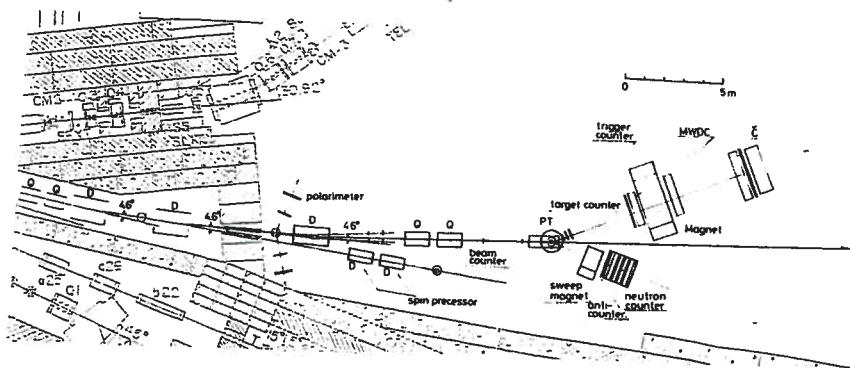


Fig. 2 The beam line and schematic layout of the apparatus.

To perform this experiment with a good statistics, the following difficulties are expected.

- (1) The low counting rate due to the low beam intensity and the small  $d\sigma/dt$ , and the low detection efficiency of neutron counter.
- (2) The real events selection from the background events caused by the polarized deuteron target which includes other nuclei.

The beam intensity is limited by the radiation level. Therefore, to overcome the problem (1), one must prepare (i) a large polarized target, (ii) a neutron counter with higher detection efficiency, (iii) higher polarization of the beam and target. As for the problem (2), it is essential to use the polarized target which includes less background nuclei, such as  $ND_3$ . Moreover, the precise determination of the kinematics of events is also inevitable for the event selection in the software stage. From such necessity, we are developing and testing the following special apparatus; (1) polarized  $ND_3$  target with dilution cryostat, (2) a beam defining hodoscope counter with high counting rate, (3) Si-strip detector for scattered charged particles around the polarized target and (4) position sensitive neutron counter consisted of Fe plates and streamer tube array. In Fig. 3 and Fig. 4 the prototype Si-strip detector and the schematic view of the neutron counter are shown.

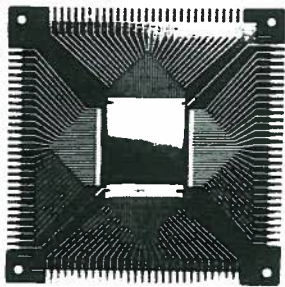


Fig. 3 The prototype Si-strip detector. The size is  $30 \times 30 \text{ mm}^2$  with a channel separation of 0.5 mm.

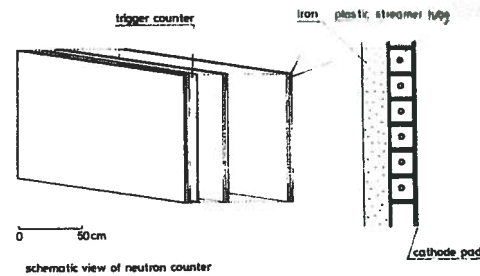


Fig. 4 The planned neutron counter which is composed of Pb and Fe plates and the array of the plastic streamer tube.

For the event selection, it has been clear that the coplanarity cut due to the difference of Fermi momentum of neutron in free deuteron and in nucleus is most effective in our case. In Figs. 5(a) and (b), the coplanarity distribution by simulation is shown.

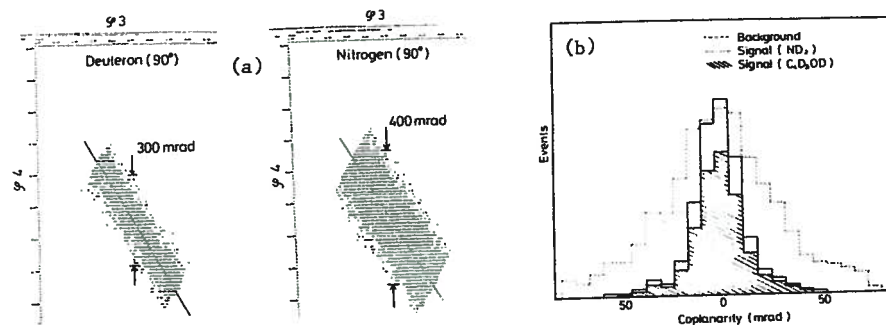


Fig.5 The coplanarity relation between proton and neutron. (a) shows the neutron distribution in the perpendicular plane to the incident direction, when the production angle of proton in the same plane is determined. The events from the free deuteron and the quasi-free event from N-nucleus is compared. (b) shows the event distribution from 2 kinds of targets. The background events are normalized.

We aim to take the  $A_{nn}$  data at 13 GeV/c with the statistical error less than  $\pm 15 \%$ .

#### References

1. Crabb D.G. et al., Phys. Rev. Letters 41(1978)1257
2. Peaslee D.C. et al., Phys. Rev. Letters 51(1983)2359
3. Chen C.K., Phys. Rev. Letters 41(1978)1440
4. Farrar G.R. et al., Phys. Rev. D20(1979)202
5. Brodsky S.J. et al., Phys. Rev. D20(1979)2278
6. Wolters G.F., Phys. Rev. Letters 45(1980)776
7. Hendry A.W., Phys. Rev. D23(1981)2075
8. Collins P.D.B. and Kearney P.J., Z. Phys. C22(1984)278

PLAN FOR A POLARIZED TARGET FOR THE FERMILAB POLARIZED BEAM

J. Dall<sup>a</sup>, P. Chaumette, J. Deregél, H. Desportes, G. Durand and L. van Rossum

CEN-Saclay, Laboratoire National Saturne\*,  
CEN-Saclay, Département des Particules Élémentaires

D. Hill

Argonne National Laboratory  
Argonne, Illinois 60439

G. Shapiro

Lawrence Berkeley Laboratory  
Berkeley, California 94720

In July, 1984, Fermilab granted Stage II approval for the first round of experiments using the Polarized Beam Facility. These experiments are being planned by a collaboration of physicists from Argonne, Fermilab, KEK, Kyoto, LAPP Annecy, LBL Berkeley, Northwestern, Rice, Saclay, Serpukhov, and Trieste. The first experiments are scheduled to begin January, 1987.

The two-spin experiments will require a polarized target, which is being built by Saclay, Argonne, and Berkeley. The planned target dimensions are 3 cm dia. x 20 cm length; the diameter is set by the rather large spot size of the lambda-decay-derived beam. The polarizing solenoid and dilution refrigerator, shown in Figure 1, are being built by Saclay. The superconducting solenoid has a warm bore of 9.5 cm and a field capability of 6.5 T. The high field capability should be useful for polarizing LiD and, perhaps, other materials. The main winding of the magnet has recently been successfully tested to > 6.5 T.

The first experiment to use the target will be a measurement of  $\Delta\sigma_L$  (pp) at 200 GeV/c, so at first only longitudinal target polarization is needed. The polarizing solenoid has been designed so as to allow the later addition of a large aperture holding magnet which will give the capability of other spin orientations in the frozen-spin mode. Meanwhile, if we use frozen-spin mode in the longitudinal field of the polarizing solenoid, the refrigerator has been designed so that the solenoid can be shifted 15 cm upstream. The aperture of the longitudinally-polarized target is then  $\pm 150$  mrad ( $90^\circ$  c.m. at 200 GeV/c), which is enough for unrestricted access near  $X_{F=0}$ .

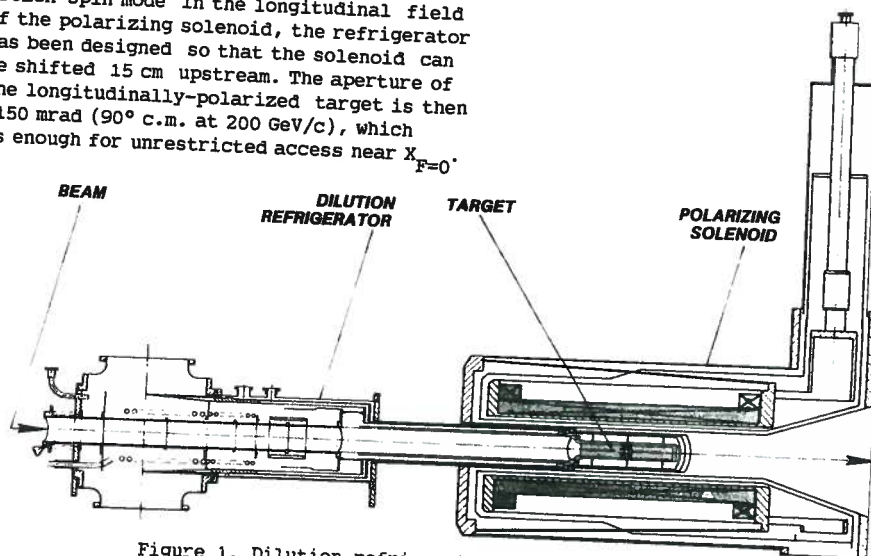


Figure 1. Dilution refrigerator and polarizing solenoid.

STABLE ATOMIC HYDROGEN: POLARIZED ATOMIC BEAM SOURCE

T.O. Niinikoski, S. Penttilä<sup>a</sup>), J.-M. Rieubland and A. Rijllart

CERN,  
Geneva, Switzerland

ABSTRACT

We have carried out experiments with stable atomic hydrogen with a view to possible applications in polarized targets or polarized atomic beam sources. Recent results from the stabilization apparatus are described. The first stable atomic hydrogen beam source based on the microwave extraction method (which is being tested) is presented. The effect of the stabilized hydrogen gas density on the properties of the source is discussed.

1. INTRODUCTION

It has been pointed out on several occasions [1-3] that spin-polarized atomic hydrogen gas ( $H\downarrow$ ) has suitable properties for potential applications in fundamental physics research. In this rather dense gas we have electron and nuclear polarizations, the temperature of the gas is low, and the properties of the hydrogen atoms can be accurately calculated to the relativistic limit. Also, we have a rather good understanding of the physical parameters of the  $H\downarrow$  system. The feasibilities and uses of stable atomic hydrogen have already been discussed [1-4] but until now no experimental applications have been attempted. At CERN, a study of stable atomic hydrogen has been carried out with a view to possible applications in polarized targets or polarized atomic beam sources.

The electron-spin polarized atomic hydrogen gas has been predicted to stay in a gaseous state down to absolute zero temperature, because of the light atomic mass and because the triplet pair-interaction potential has only a very weak attractive part with no possibility of bound states. At low temperatures a scattering of two hydrogen atoms in the triplet state is predominantly s-wave and the scattering length is  $a_t = +0.72 \text{ \AA}$ . In the spin-polarized atomic hydrogen gas,  $a_t$  represents an effective hard-core diameter of an atom, and the atoms should then form a close-to-ideal gas.

The principal goal in the recent development of stabilization techniques for atomic hydrogen has been to reach the degenerate gas regime where, according to statistics, the gas might show dramatic behaviour. In this quantum regime the mean thermal de Broglie wavelength  $\lambda = h/\sqrt{2\pi mk_B T}$ , which is a measure of the average spatial extent of the wave packet of a hydrogen atom, begins to be the size of the mean spacing  $d = n^{-1/3}$  between particles; here  $n$  is the density of the atoms. Lhuillier and Laloë [5] have predicted that already in a non-degenerate and nuclear spin-polarized gas, when  $\lambda \geq a_t$ , there exist exchange processes which have effects on the nuclear-spin transport properties. When the mean free path of atoms is large enough, it is possible to observe collective nuclear spin oscillations—spins waves. At a temperature of 0.3 K the thermal wavelength is 32  $\text{\AA}$ , and with a density of  $10^{17} \text{ cm}^{-3}$  the mean spacing is 220  $\text{\AA}$ . We are now in the classical regime.

The  $H\downarrow$  gas is stabilized against very reactive recombination processes by making the electron-spin Boltzmann factor,  $\exp(\mu_B/k_B T)$ , very large, which guarantees that the two upper hyperfine states  $|c\rangle$  and  $|d\rangle$  are not thermally populated. For this we need low temperatures (0.2-0.6 K) and a high magnetic

<sup>a</sup>) Present address: University of Turku, 20500 Turku, Finland.

field ( $\geq 5$  T). The walls of a stabilization cell and the magnetic field gradients will confine hydrogen atoms. Condensation on the walls is reduced by means of superfluid  $^4\text{He}$  and  $^3\text{He}/^4\text{He}$  linings, which have absorption energies much below those of ordinary solid materials such as metals or solidified gases. On superfluid  $^4\text{He}$  the absorption energy is about 1 K, and on a  $^3\text{He}$ -coated wall it is 0.3 K.

The highest densities of  $\text{H}\downarrow$  at present exceed  $10^{18} \text{ cm}^{-3}$ , observed in bubbles of 100  $\mu\text{m}$  diameter after compression [6-8].

## 2. STABILIZATION APPARATUS

The CERN stabilization apparatus shown in Fig. 1 consists of a powerful horizontal dilution refrigerator [9], a warm-bore superconducting solenoid of 5 T, and installations for electron paramagnetic resonance (EPR) experiments at 140 GHz and continuous-wave nuclear magnetic resonance (CW-NMR) at 1 GHz. At room temperature, dissociated hydrogen atoms are fed into the cryostat through the heated PTFE transport tube, which is 6 mm in diameter and 90 cm in length. In the transport tube the atoms thermalize through wall collisions. The gradient of the solenoid field spin selects and confines the atoms. The cold part of the transport tube is lined with helium film. The apparatus has a loading rate of over  $10^{16}$  stabilized atoms per second into the sample cell. At a magnetic field of 5 T and a temperature of below 0.5 K we have measured densities up to  $10^{17} \text{ cm}^{-3}$ . The sample cell area arrangement inside the mixing chamber is shown schematically in more detail in Fig. 2. The copper parts have been fixed to the accommodator shown in Ref. [10]. However, Fig. 2 does not show the  $^3\text{He}$ -NMR coil in the  $^3\text{He}$ - $^4\text{He}$  mixture for tuning the magnetic field.

Total pressure of the  $\text{H}\downarrow$  gas was determined by means of a 10 mm diameter, capacitive Mylar membrane pressure gauge, which was part of a 53 MHz tunnel-diode oscillator circuit. In the measurements the third harmonic was counted. Calibration, which was done with the helium vapour, gave a sensitivity of  $\Delta f/\Delta p = 3 \times 10^6 \text{ Hz/Torr}$ .

The 1 GHz resonator was made from a copper wire, 50  $\mu\text{m}$  in diameter and 6 mm long. The wire was mounted to the end of a coaxial line and was located within a cylindrical sample volume, 15 mm long and 5 mm in diameter as shown in Fig. 2. The CW-NMR measurements were performed by sweeping the frequency. The circuit uses a hybrid bridge and a double balanced mixer for coherent homodyne detection [11].

The volume of the EPR cavity is about  $7 \text{ mm}^3$ ; compared with the previous experiments [10], we expected a significant reduction in the observed EPR linewidth. The  $\text{H}\downarrow$  atoms are confined between two windows in the ends of the cylindrical-shaped cavity, which communicates through a narrow channel with the load and stabilization volume. The 0.8 mm diameter and 10 mm length of this channel were chosen in order to attenuate the 140 GHz microwave field strongly in this structure well below the cut-off of propagation. The magnetic field was swept slowly across the resonance line, and the density decay, caused by recombination of flipped atoms, was monitored by means of the pressure sensor. A bolometer, weakly coupled to the microwave field, allowed the intensity of the microwave field to be monitored. From an I-V curve the responsivity of the bolometer was calculated to be  $\Delta R/\Delta P \approx 5 \times 10^{10} \Omega/\text{W}$  at 0.3 K.

## 3. RESULTS

Resonance measurements were done in the magnetic field around 5 T, limited by the band of our carcinotron microwave source. A higher field would reduce recombination and relaxation rates. In our configuration the volume/surface ratio is constant, because the volume of the  $\text{H}\downarrow$  gas is limited by the field gradients and helium-coated walls. Such a quantity of helium gas was condensed onto the surfaces that the moving helium film did not cause any significant pressure oscillations in the loading tube. Such oscillations were seen to affect the loading speed.

Figure 3 shows the time evolutions of the pressure and the CW-NMR absorption signal at a temperature of 0.28 K and a magnetic field of 4.9 T during and after a fast loading. The upper part shows the pressure on logarithmic scale and demonstrates the density decay according to the rate equation

$$-\dot{n}/n^2 \approx K + 2G, \quad (1)$$

where K is the surface recombination rate constant and G is the rate constant for nuclear relaxation from the state  $|b\rangle$  to the state  $|a\rangle$ . In the case of Fig. 3, G includes also relaxations induced by the RF field.

The ground hyperfine state  $|a\rangle$  is the mixed spin state, which has a small electron spin-up admixture. The state  $|b\rangle$  is the pure spin state. Thus collisions involving an  $|a\rangle$ -state atom can result in recombination to molecular hydrogen at a rate which is higher than the nuclear relaxation rate. After closing a valve in the filling tube, recombination on the surfaces reduces the density rapidly as long as there are enough  $|a\rangle$ -state atoms. The surface recombination rate constant of  $K \approx 3 \times 10^{-18} \text{ cm}^3/\text{s}$  is obtained from the fast part of the decay. After depletion of the  $|a\rangle$  atoms, the nuclear relaxation rate constant G starts to control the decay. The fitting to the linear part of the curve gives the relaxation rate constant of  $G \approx 8 \times 10^{-20} \text{ cm}^3/\text{s}$ ; the corresponding nuclear polarization is  $P \equiv -[1 - (G/K)] \equiv -97\%$  during that part of the time evolution.

In Fig. 4 we see a typical averaged NMR absorption signal at a temperature of 0.3 K, and at the field of 5.065 T which corresponds to the resonance frequency of 929 MHz. The sweep width of the frequency was 320 kHz and the density of the sample about  $10^{16} \text{ cm}^{-3}$ . To average one signal we needed about 15 s. The homogeneity of the field in the NMR volume was determined and tuned by condensing  $^3\text{He}$  gas to the volume and measuring the frequency of the  $^3\text{He}$  NMR. The  $^3\text{He}$  NMR linewidth gives an effective homogeneity of  $1 \times 10^{-4}$ . The  $\text{H}\downarrow$  NMR signal width from Fig. 4 gives  $\Delta B/B = 4 \times 10^{-4}$ , which is about four times larger than that of the  $^3\text{He}$  signal. This is caused by the nuclear-spin transport phenomena in the NMR volume [12]. This is also supported by the clearly observable fine structure on the top of the absorption signal, persisting over long averaging periods. Details of the fine structure can be better seen by averaging the sweeps in only one direction instead of averaging them in both directions.

The spin waves split the nuclear magnetic resonance into peaks spaced at

$$\omega - \omega_0 = \mu P D_1 k^2 \quad (2)$$

from the Larmor frequency  $\omega_0$ ; here k is the wave number of the mode in the spin wave resonator,  $\mu$  is the 'identical spin rotation' parameter [5], and  $D_1$  the diffusion coefficient for the transverse magnetization [5]:

$$D_1 = D_0/[1 + (\mu P)^2]. \quad (3)$$

The longitudinal (ordinary) spin diffusion coefficient  $D_0$  is given by [5]

$$D_0 = (3/8)(k_B T/nm)(1/\Omega_v^{1,1}), \quad (4)$$

where  $n = n_a + n_b$ , m is the mass of the H atom, and  $\Omega_v^{1,1}$  the relevant collision integral [5]. Our observed line shapes depend on the polarization qualitatively according to Eq. (2), although the spin wave modes k cannot be clearly resolved. A more complete account will be published elsewhere.

In the absence of long-range spin-spin interactions, the longitudinal nuclear polarization of the two level system, defined by  $P = (n_a - n_b)/(n_a + n_b)$ , is proportional to the area of the CW-NMR

absorption signal which depends on the microscopic complex susceptibility  $\chi = \chi' + i\chi''$  of the sample. The absorption signal area in a linear system should be  $s = \int \chi''(\omega) d\omega \propto P \cdot n$ . The requirement that  $|P|$  should stabilize at 0.97, when the density decay becomes controlled by the nuclear relaxation, is clearly violated by our data shown by the dots representing  $s/n$ , the signal surface scaled by the atomic density (given by the pressure signal).

The effects of the transverse spin diffusion on the signal surface  $S$  are very small in the absence of losses of transverse magnetization, although the height and width of the spin wave peaks <sup>depend</sup> on  $D_{\perp}$  in first order. The losses of transverse magnetization result from dephasing in the gradient of the external field or on the surfaces, from magnetic relaxation on surfaces, and from exchange of atoms through the filling hole. In the simplest picture we may assume that the transverse magnetization in the rotating frame is inversely proportional to the diffusion coefficient:  $\chi''(\omega) \propto D_{\perp}^{-1}$ . This gives immediately

$$S \propto P \cdot n \cdot D_{\perp}^{-1} \propto P \cdot n \cdot D_0^{-1} \propto P \cdot n^2 \quad (5)$$

using Eqs. (3) and (4). Figure 3 shows also the polarization evolution  $P \propto S/n^2$ , which gives a much better fit to the required asymptotic saturation of  $P$  towards the value  $-0.97$ .

A more complete discussion on the NMR signal surface area will be published elsewhere [13].

The EPR detection of the  $H\downarrow$  atoms was based on the deduction of a part of the sample through recombination during partial saturation. One advantage of the small cavity, which was about 10 mm away from the axis of the solenoid field, was that the resonances ( $|a\rangle \rightarrow |d\rangle$  and  $|b\rangle \rightarrow |c\rangle$ ) can be approached from the high- or the low-field side. The pressure sensor was used to measure the line width, which was about 20 G, and the calculated gradient of the field within the EPR cavity at 5 T was about 100 G/cm. The resonance absorption was not strong enough for detection by the bolometer. Only weak EPR-induced recombination heat was observed. With the estimated microwave power level of 50 nW,  $5 \times 10^{15}$  spin flips per second could be monitored when the field was swept at 2 G/s over the resonance.

#### 4. STABLE ATOMIC HYDROGEN BEAM SOURCE

It has been shown that the most promising use of stable atomic hydrogen can be as a polarized atomic beam source [10]. Stabilized atoms are extracted by flipping the magnetic dipole moments of polarized hydrogen atoms by means of the EPR microwave field. Because of the topology of the solenoid field, a large fraction of the atoms will flow out of the magnet without recombining during collisions. At a high density the motion of the flipped atoms is diffusion—or drift—driven by the gradients of the solenoid field. The collisions which limit the motion cause relaxation, recombination, and nuclear depolarization due to spin exchange.

##### 4.1 CERN source

The source under construction and tests consists of a loading tube and storage volume, surrounded by the dilution refrigerator and the storage magnet. Additional solenoid, or hexapole magnet optics can be installed to increase the beam density in the beam detectors, which include a compression tube and ion gauge, and a quadrupole mass-spectrometer with crossed-beam ionizer. The source will be pulsed by microwave power modulation.

Figure 5 shows the polarized atomic hydrogen source which is being tested at CERN. The basic apparatus is the same as in the stabilization experiments. The accommodator and stabilization assembly has been replaced by a large copper tube traversing the mixing chamber. The open end of the tube forms an extraction orifice. The short PTFE tube ends at the still, where warm ( $\sim 30$  K) hydrogen atoms will thermalize on the cold surfaces coated by superfluid helium. A loading rate of  $10^{18}$  per second has been achieved so far. Before the storage volume there is a low-density buffer of unpolarized atomic hydrogen

gas. Because of the open configuration, special care has been given to the helium film. Burning and condensing of the film are carried out in the still and the heat exchange region where most of the cooling power is available.

The position of the extraction orifice can be changed with respect to the field of the 5 T solenoid. The length of the solenoid is 180 mm. The inner diameter of the storage cell is 25 mm. The effective storage volume is about  $130 \text{ cm}^3$ , and if the density in the middle of the 5 T field is  $n_0 = 10^{16} \text{ cm}^{-3}$  there are  $3 \times 10^{17}$  trapped  $H\downarrow$  atoms.

##### 4.2 Microwave extraction

The electron spin of the  $H\downarrow$  atom is reversed adiabatically when an atom crosses the resonance surface. The time which the flipped atom then needs to get out of the magnet (and then also the flux of atoms) depends strongly on the density and the gradients in the resonance region. In low densities,  $n < 10^{15} \text{ cm}^{-3}$ , when the mean free path is approximately equal to the diameter of the storage volume, the beam quality is determined by the source temperature and focusing solenoid optics. At higher density the motion of the flipped atoms is limited by interatomic collisions. In a field gradient the motion is directional and is characterized by a drift constant. In constant field the flipped atoms move randomly obeying the law of thermal diffusion. For the purpose of the following simplified discussion, we shall ignore interatomic collisions at a density below  $10^{15} \text{ cm}^{-3}$ ; only wall collisions are then limiting the number of atoms emerging into the beam tube. Track-tracing simulations have been performed [14] to follow the free motion of the atoms in this low-density limit.

In order to find an optimum working density and the resonance region for a required pulse length  $\tau_p$  and duty cycle, we have estimated the drift speed  $v_D$  of a flipped atom along the symmetry axis of our magnet. The  $v_D$  is a function of the field gradient  $(\nabla|\vec{B}|)_z$ , of the temperature, and of the diffusion coefficient  $D_0$  [5] which depends inversely on the density. The origin is in the middle of the solenoid magnet, where the field was 5 T and the temperature of the  $H\downarrow$  gas was 0.3 K. In Fig. 6 is shown the flow time  $t_F$  of flipped atoms as a function of the  $z$  coordinate for various densities  $n_0$  in the centre of the solenoid (where  $z = 0$ ). Also, the field dependence of the mean free path of  $H\downarrow$  atoms,  $\ell \propto 1/(n\sqrt{T})$ , is shown by the dashed curve when  $n_0$  is  $10^{16} \text{ cm}^{-3}$ . The resonance (spin-flip) points on the axis are  $z = 20$  mm and  $z = 40$  mm. When  $z = 20$  mm the field and the corresponding axial gradient are  $B = 4.949$  T and  $(\nabla|\vec{B}|)_z = -460$  G/cm, respectively. When  $z = 40$  mm the values are  $B = 4.823$  T and  $(\nabla|\vec{B}|)_z = -920$  G/cm. Figure 6 clearly shows how sensitive  $t_F$  is to the density and the field gradients. When  $n_0 = 10^{16} \text{ cm}^{-3}$  an atom which leaves from  $z = 20$  mm spends 80 ms reaching point  $z = 60$  mm, whilst an atom leaving  $z = 40$  mm needs only 17 ms to get to the same point.

In the pulsed operation, if the length of the microwave pulse is  $\tau_p \approx 2$  ms and the duty cycle is 10%, the working density should be about  $3 \times 10^{15} \text{ cm}^{-3}$  so that  $t_F$  would be smaller than  $10 \times \tau_p$  when the leaving area is  $z = 20$  mm.

The model can also be used to estimate the probability for an atom in the hyperfine state  $|d\rangle$  or  $|c\rangle$  to leave the magnet in its original state when it is moving in the  $H\downarrow$  gas.

A contribution of the three-body recombination was calculated with the rate constant estimated by Bell et al. [15]. There is a 97% probability that the atom will survive when the density is  $n_0 = 10^{16} \text{ cm}^{-3}$  and it has left from the resonance point  $z = 20$  mm.

The two-body collision of two atoms in different electron-spin states on a superfluid helium-coated surface is very destructive. Owing to the topology of the solenoid field, the two-body recombination rate is insignificant. When  $z = 20$  mm and we are 12 mm from the axis, the radial gradient is  $(\nabla|\vec{B}|)_r = +57$  G/cm, which will drive the atoms toward the axis.

The effect of the electron-spin dipole relaxation was estimated by using the result of Kagan et al. [16]. In the above conditions the probability is about 95% that the atom will drift to the lower density area without the electron-spin relaxation.

From an earlier discussion on the electron-spin exchange [10], the exchange cross-section  $\sigma_{ex}^*$  can be used. This gives the same spin-exchange-rate constant ( $T_1^{-1} \approx 0.54 \times 10^{-12} \cdot n$  as has been calculated by Morrow and Berlinsky [17]). The spin-exchange rate is so large that the nuclear polarization of the beam will be close to zero even at low energies.

In the following we consider a flux to an interaction channel, of diameter 10 mm, to build up a density of  $10^{13} \text{ cm}^{-3}$ . When the source temperature is 0.3 K the average velocity after acceleration of the 5 T field is 250 m/s. This gives the required current density of  $3 \times 10^{17} \text{ s}^{-1} \cdot \text{cm}^{-2}$ . In a pulse of 2 ms we then have a total of  $6 \times 10^{14}$  atoms, and if the duty cycle is 10% then the average flux is  $3 \times 10^{16} \text{ s}^{-1}$ . If now the efficiency of our source is 10% (including focusing of atoms, recombinations, relaxations) we need the flipping rate of  $3 \times 10^{17}$  atoms per second.

To reach this time-scale the resonance surface has to be in a region of strong field gradient. To produce so many adiabatic reversals of electron spins at the resonance surface, the microwave field strength must be high enough [10]. The microwave power level now depends on a field gradient  $\nabla|B|$ , an amplitude of an alternating field  $B_1$ , and the thermal speed of the atoms. Input power is related to the size and the quality factor of the EPR volume.

## 5. CONCLUSION

The stable atomic hydrogen experiments have supported and also more precisely limited the concepts of applications discussed here, most of which are based on the pulsed neutral beams available with microwave extraction.

With the stabilization apparatus, we have achieved a high loading speed of  $10^{16} \text{ H}\downarrow$  per second into the storage cell and, after the modification, up to  $10^{18} \text{ H}$  per second have been detected. This is required for a large throughput of hydrogen atoms in a source.

The CW-NMR experiments on  $\text{H}\downarrow$  gas have shown that during high-speed loading the  $|a\rangle$  state is more populated than it would be in thermal equilibrium. The NMR signals have also shown the existence of the nuclear-spin transport in  $\text{H}\downarrow$  gas. The EPR experiments—at least in a small cavity—have proved that in a field gradient of 60 G/cm without any high microwave field strength, large adiabatic spin-flip rates are possible.

The first working refrigerator suitable for a stable atomic hydrogen source experiment with the open storage cell configuration is ready and is being tested.

The properties of the source depend very much on the working density. When the density is higher than  $10^{15} \text{ cm}^{-3}$ , a diffusional motion determines the minimum length and maximum duty cycle of the beam. By placing the resonance region in a strong gradient ( $\nabla|B|$ )  $\approx 600 \text{ G/cm}$ , and working at a density under  $10^{16} \text{ cm}^{-3}$ , it seems possible to form pulses of a few milliseconds length with a 10% duty cycle and to obtain beam densities of more than  $10^{13} \text{ cm}^{-3}$  at the focusing point.

The electron spin-exchange cross-section is so large that the nuclear polarization in the beam will be almost zero and a RF transition is needed downstream in the beam in order to convert the electron polarization into nuclear polarization.

## REFERENCES

- [1] Proc. Workshop on Polarized Proton Ion Sources, Ann Arbor, 1980 (AIP Conference Proceedings No. 80, New York, 1981).
- [2] Proc. 5th Int. Symposium on High-Energy Spin Physics, Brookhaven, 1982 (AIP Conference Proceedings No. 95, New York, 1983).
- [3] Proc. Workshop on Polarized Proton Sources, TRIUMF Vancouver, 1983 (AIP Conference Proceedings No. 117, New York, 1984).
- [4] T.O. Niinikoski, Proc. Int. Symp. on High-Energy Physics with Polarized Beams and Polarized Targets, Lausanne, 1980 (Birkhäuser EXS38, Basle, 1981), p. 191.
- [5] C. Lhuillier and F. Laloë, J. Phys. (France) **43**, 197 and 225 (1982); C.L. Lhuillier, J. Phys. (France) **44**, 1 (1983).
- [6] H.F. Hess, D.A. Bell, G.P. Kochanski, R.W. Cline, D. Kleppner and T.J. Greytak, Phys. Rev. Lett. **51**, 483 (1983).
- [7] R. Sprik, J.T. M. Walraven and I.F. Silvera, Phys. Rev. Lett. **51**, 479 (1983).
- [8] T. Tommila, S. Jaakkola, M. Krusius, K. Salonen and E. Tjukanov, Proc. 17th Int. Conf. on Low-Temperature Physics LT-17, Karlsruhe, 1984 (Elsevier Science Publishing Company, Inc., New York, 1984), p. 453.
- [9] T.O. Niinikoski and J.-M. Rieubland, Proc. ICEC 9, Kobe, Japan (Butterworth & Co, London, 1982), p. 580.
- [10] T.O. Niinikoski et al., *in* Ref. 3, p. 139.
- [11] A. Rijllart, *in* these proceedings.
- [12] B.R. Johnson, J.S. Denker, N. Bigelow, L.P. Lévy, J.H. Freed and D.M. Lee, Phys. Rev. Lett. **52**, 1508 (1984).
- [13] T.O. Niinikoski, S. Penttilä, J.-M. Rieubland and A. Rijllart, Molecular field effects on spin-polarized atomic hydrogen, to be published.
- [14] M. Ellilä, T.O. Niinikoski and S. Penttilä, Solenoid optics for slow atomic beams, to be published.
- [15] D.A. Bell, G.P. Kochanski, L. Pollack, H.F. Hess, D. Kleppner and T.J. Greytak, Proc. 17th Int. Conf. on Low-temperature Physics LT-17, Karlsruhe, 1984 (Elsevier Science Publishing Company, Inc., New York, 1981), p. 449.
- [16] Yu. Kagan, I.A. Vartanyants and G.V. Shlyapnikov, Sov. Phys.-JETP **54**, 590 (1981).
- [17] M. Morrow and A. Berlinsky, Can. J. Phys. **61**, 1042 (1983).

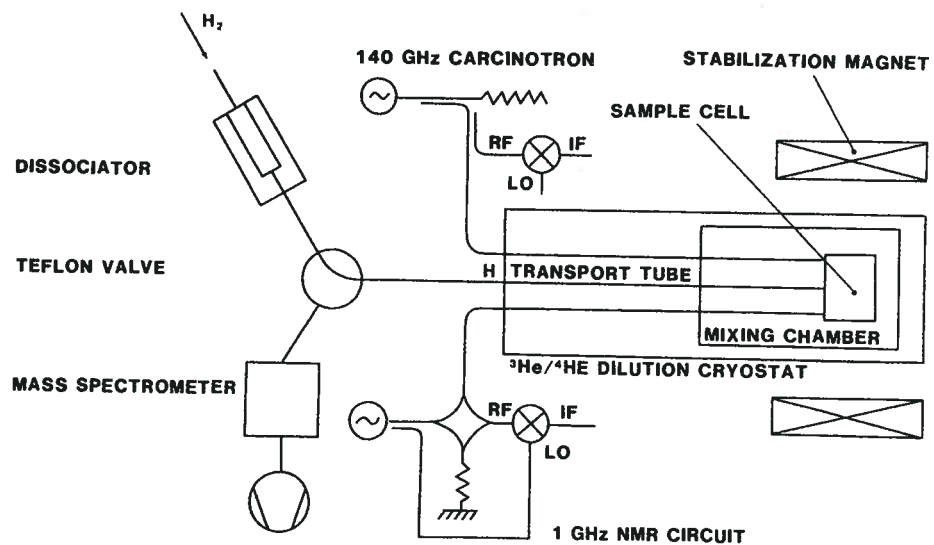


Fig. 1 CERN stabilization apparatus. The main parts are a dissociator, a powerful horizontal dilution refrigerator, and a superconducting solenoid of 5 T with a warm bore.

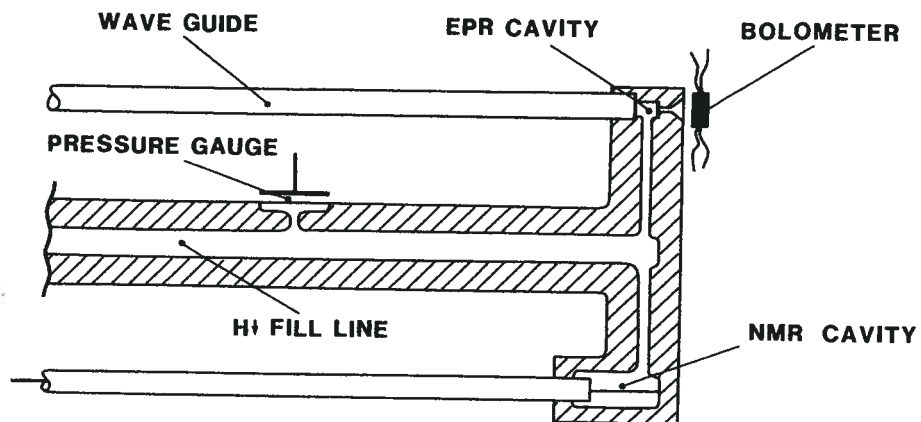


Fig. 2 Schematic of the sample cell configuration inside the mixing chamber.

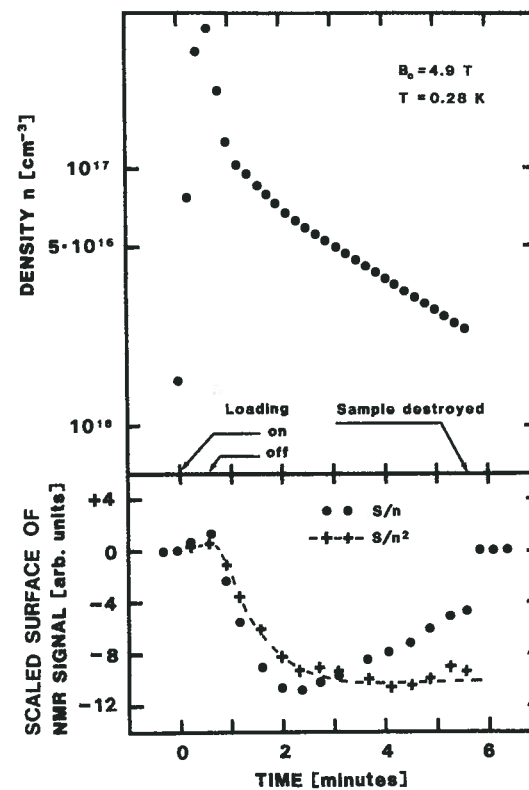


Fig. 3 Time evolutions of the total density, probed by the pressure gauge, and of the NMR absorption signal area.

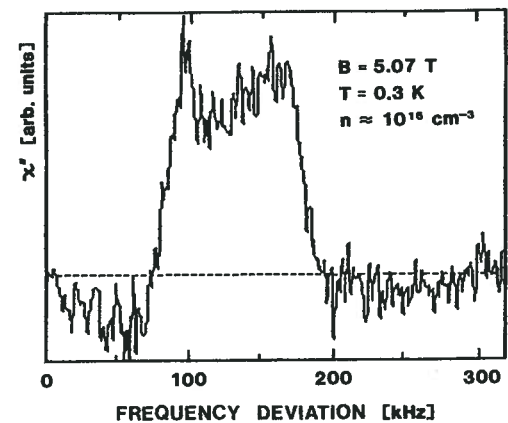


Fig. 4 Typical CW-NMR absorption signal, after averaging 800 sweeps, at a field of 5 T and temperature of 0.3 K. The density of the sample was about  $10^{16} \text{ cm}^{-3}$ .

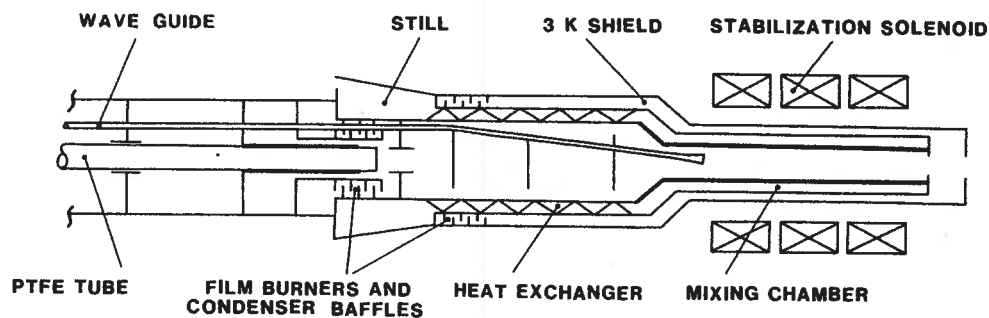


Fig. 5 CERN H<sup>↑</sup> source.

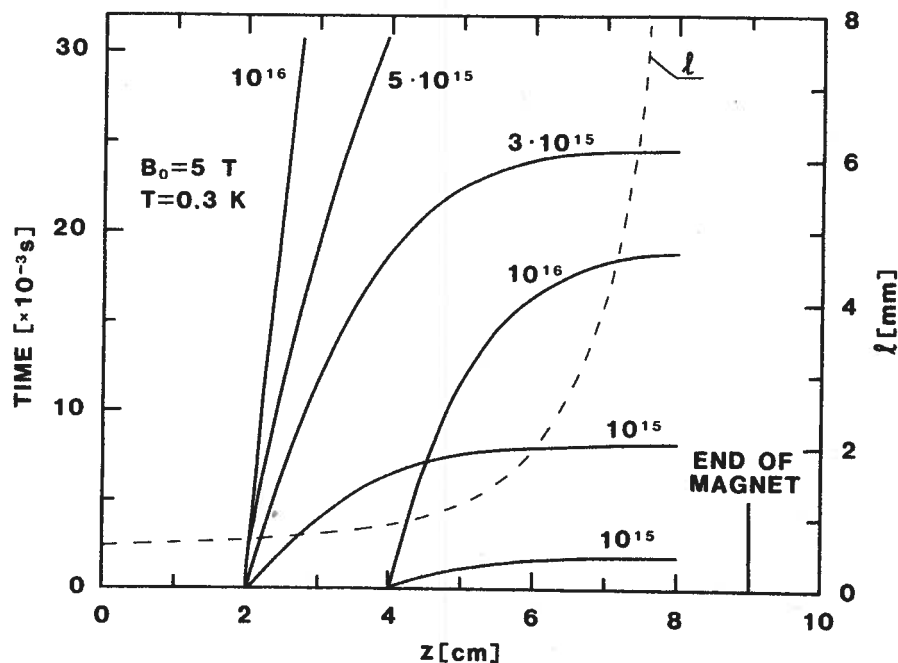


Fig. 6 Mean flow-time of H<sup>↑</sup> atoms along the symmetry axis of the solenoid field in dense H<sup>↑</sup> gas. The two resonance regions  $z = 2$  cm and  $z = 4$  cm are in the field gradient area. The density in the middle of the magnet is a parameter. Also, the field dependence of the collision mean free path on the field is shown as the dashed line when  $n_0 = 10^{16}$  cm<sup>-3</sup> at the origin.

## POLARIZED ATOMIC BEAMS FOR TARGETS

W. Gruebler, P.A. Schmelzbach, D. Singy and W.Z. Zhang  
 Institut für Mittelenergiephysik, Eidg. Technische Hochschule  
 CH-8093 Zürich, Switzerland

### ABSTRACT

It is proposed that polarized atomic beams can be used to produce polarized gas targets with high polarization and greatly improved density. The status of the present available polarization, density and intensity are presented. The improvement of atomic beam density by cooling the hydrogen atoms to low velocity is discussed. The possible use of polarized atomic beams as target in storage rings is shown.

### 1. INTRODUCTION

The production of polarized hydrogen and deuterium atoms by the atomic beam methods has a long history. One of the outstanding application of polarized atoms is the use in polarized ion sources, where the atomic beam is ionized to polarized positive or negative hydrogen ions, which are injected in all types of accelerators. The status of the ground state atomic beam polarized ion sources has periodically been reviewed over the past twentyfive years<sup>1-8</sup> and much can be learned from these review papers about the basic principles, the technical problems and the present state-of-the art. This work lays a firm base for the application of polarized atomic beams in polarized targets. In the past this application has suffered from the low density of polarized atomic hydrogen beams and therefore has only been used in a few experiments. Recently important progress for higher beam density and intensity has been achieved by cooling the atomic beams to low temperature and store the compressed beam in a storage vessel. This makes the production of polarized targets interesting not only in experiments in storage rings but also in experiments using extracted high energy or secondary beams. Besides the very high polarization - nearly 100% of the theoretical values -, the flexibility to choose easily the polarization direction at the target and the possibility to produce tensor polarized deuterons make such targets very attractive. While at present well established methods and techniques

can be used for conventional atomic beams, new promising techniques are under investigation and further new methods to be tested for targets with even higher density are proposed in the present work. This paper first presents the basic principles for the production of polarized atomic beams, then discusses the polarization and density which can be achieved and will finish with an outlook to possible improvements which may be achieved in the near future.

## 2. PRODUCTION OF POLARIZED ATOMIC BEAMS

The basic scheme of an atomic beam apparatus for polarized targets using a thermal atomic beam is shown in Fig. 1. Hydrogen atoms are generated by

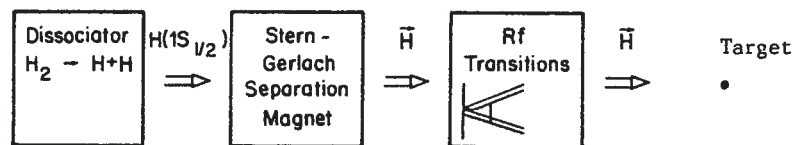


Fig. 1. Schematic diagram for the production of a polarized atomic beam for the use in polarized targets.

dissociating molecules at low pressure in a rf discharge. An atomic beam of thermal velocity is formed by a nozzle. This beam is polarized in passing through an inhomogeneous magnetic field (usually either a quadrupole or a sextupole field). This Stern-Gerlach separation of magnetic substates of the hydrogen atoms delivers an electron polarized atomic beam. Rf transitions are induced between hyperfine states of the atoms in order to select different nuclear polarization states and to provide rapid spin reversal.

The different combinations of necessary target B-field, rf transitions, Stern-Gerlach separation magnets (S-G) as well as the relative intensity  $I$ , the maximum polarization  $p_{\max}$  and the figure of merit  $I p^2$  are summarized in Table 1 for hydrogen atoms and in Table 2 for deuterium atoms.

Table 1

Production of polarized hydrogen targets

Mode	Target B-field	Stern-Gerlach separation (S-G) and rf-transitions	Substates	$P_{\max}$	$I$	$I^2 p^2$
a	weak	S-G	1 + 2	+1/2	1	1/4
b	weak	S-G, 1+3 (WF)	2 + 3	-1/2	1	1/4
c	strong	S-G, 2+4	1 + 4	+1.0	1	1.0
d	strong	S-G, 1+3 (WF)	2 + 3	-1.0	1	1.0
e	any	S-G, 2+4, S-G	1	+1.0	1/2	1/2
f	any	S-G, 2+4, S-G, 1+3 (WF)	3	-1.0	1/2	1/2

strong B-field: >> 507 Gauss

Table 2  
Production of polarized Jeterium targets

Mode	Target B-field	Production scheme	Substates	Vector pol. $p_z$	Tensor pol. $p_{zz}$	Relative intensity $I$	Figure of merit	
							$I p_z^2$	$I p_{zz}^2$
a	strong	S-G	1 + 2 + 3	0	0	1	0	0
b	strong	S-G, 1 → 4 (WF)	2 + 3 + 4	- 2/3	0	1	4/9	0
c	strong	S-G, 2 → 6, 3 → 5	1 + 5 + 6	+ 2/3	0	1	4/9	0
d	strong	S-G, 3 → 5	1 + 2 + 5	+ 1/3	-1	1	1/9	1
e	strong	S-G, 3 → 5 2+3 } (WF) 1+4 } 5+6 }	3 + 4 + 6	- 1/3	+1	1	1/9	1
f	strong	S-G, 2 → 6	1 + 3 + 6	+ 1/3	+1	1	1/9	1
g	strong	S-G, 2 → 6 3+2 } (WF) 1+4 } 6+5 }	2 + 4 + 5	- 1/3	-1	1	1/9	1
h	strong	S-G, 1 → 4(WF), S-G, 3 → 5	2 + 5	0	-2	2/3	0	2 2/3
i	any	S-G, 2 → 6, S-G, 3 → 4	1 + 4	0	+1	2/3	0	2/3
k	any	S-G, 3 → 5, 2 → 6, S-G	1	+ 1	+1	1/3	1/3	1/3
l	any	S-G, 3 → 5, 2 → 6, S-G, 1 → 4 (WF)	4	- 1	+1	1/3	1/3	1/3

strong B-field: >> 117 Gauss

### 3. DENSITY OF POLARIZED ATOMIC BEAMS

While the polarization of an atomic beam reaches nearly ideal values coupled with a great flexibility, the low density of conventional polarized atomic beams is a serious drawback for the use for polarized targets. Large improvements is required in order to make this type of target competitive with other methods. Since some time intensive investigations for the increase of the density of atomic beams are performed successfully in different laboratories. The status of the development of a high density atomic beam for a polarized ion source is discussed in an accompanying contributed paper to this conference<sup>9)</sup>. There, the use of a beam cooled down to 15 - 30 K and of a two-magnet system especially designed for a low velocity beam leads to a one order of magnitude increase of the beam density. In this case, the gain is mainly limited by the reduced phase space accepted by the ioniser of the source. In a geometry suitable for a target, a gain of at least 20 may be expected.

In summary, the improvements obtained by an atomic beam cooled to a temperature of 30 K and the new design of separation magnet systems will result in a beam intensity of several  $10^{17}$  atoms per second with a density over  $10^{13}$  atoms  $\text{cm}^{-3}$ . Further increase of these values can be gained by cooling to lower temperature. One has to keep in mind, however, that the very short focal length of septupole magnets will then make it increasingly difficult to conciliate high density and beam transportation over longer distances.

### 4. USE OF POLARIZED BEAMS FOR TARGETS

The improvements in the density of the atomic beams discussed in the preceding chapter make the direct use of an atomic beam as a target attractive for internal polarized target. In this application the crossed beam technique can be used. With a small angle ( $\sim 10^0$ ) between the crossing

beams, an intersection region of about 10 cm can easily be obtained. This results in a windowless target with a thickness of  $\sim 10^{14}$  atom  $\text{cm}^{-2}$ . The atomic beam can be caught in a beam dump which is differentially pumped by several stages. Titanium- and Cryogetter-pumps have a high pumping speed for hydrogen and are therefore interesting for this application. Since the loss of particles along the path of the atomic beam through the accelerator or storage ring is low the vacuum problems in the intersecting region can be solved.

Higher target density can be obtained by storing the polarized atoms in a target vessel. In this technique the atomic beam enters through a opening of the size of the beam diameter into a target container. The directional movement of the atoms is transformed to a stagnant atomic gas. The conductance of the beam entering the vessel is infinite, whereas the conductance of the atomic gas for leaving the container has a finite value. For this reason the atomic hydrogen is accumulated in the target cell. Precaution has to be taken that recombination and depolarization on the wall surface is low. At room temperature teflon has a low surface recombination coefficient  $\gamma = 2 \cdot 10^{-6}$  compared with a  $\gamma = 2 \cdot 10^{-3}$  for Pyrex or quartz. This value for teflon, however, increases substantially with decreasing temperature. For the temperature around 10 K a molecular  $\text{H}_2$  surface provides a low recombination and at very low temperature liquid  $^4\text{He}$  is a suitable surface in order to prevent rapid recombination. A molecular hydrogen surface is quickly formed by recombination of atomic hydrogen on a cold surface with high recombination rate.

The particle density of such a gas depends on the number of particles  $I_0$  entering the target cell, the conductance of the entrance tube and the temperature  $T$  of the target cell.

Assuming a target temperature of 10 K, a multicapillary aperture with an  $l/r$  ratio of 100 and a beam intensity of  $3 \cdot 10^{17}$  atoms  $\text{s}^{-1}$ , the equilibrium density will be  $\rho = 2.2 \cdot 10^{15}$  atoms  $\text{cm}^{-3}$ .

Decreasing the temperature of the target cell to below 1 K (with target cell surface covered with  $\text{L}^4\text{He}$ ) would increase the density by another factor 5. The flux of atoms flowing out of the target cell, can also be reduced by systems with pumping effects. A heat pipe system working with liquid helium has been tried by Silvera et al.<sup>10</sup>. A reduced conductance in the entrance tube of a factor 79 has been reported by these authors<sup>10</sup>. A similar device may be possible at higher temperature using Ne as a working fluid.

Finally the possibility to pump stable atomic hydrogen gas with a diffusion pump should be investigated. Helium or molecular hydrogen could be used as working fluid. The recombined unpolarized molecular hydrogen gas would be separated by cryo-pumping. If such a diffusion pump would work large pressure ratios could be obtained. Even with a substantial loss of atomic gas by recombination a target cell could be filled to a high density.

## 5. CONCLUSIONS

The use of polarized atomic hydrogen beams as internal targets in accelerators or storage rings has many interesting advantages:

- High polarization. The nuclear polarization of the atomic beam is larger than 95 %. This feature is particularly interesting for tensor polarized deuteron targets.
- High flexibility of the polarization. The direction of the polarization can be changed easily by weak or moderate magnetic fields at the target position. In a deuteron target pure vector or tensor polarization or a combination of both can easily be achieved. The orientation of the polarization in any direction with respect to the accelerated beam allows to investigate the effect of all three tensor components  $t_{20}$ ,  $t_{21}$  and  $t_{22}$  of the deuteron.

- Polarization reversal. The sign of the polarization can be reversed by rf transition in the neutral beam with kHz rate. This method prevents shifts of the atomic beam position and since no change of the magnetic field at the target position is involved there is also no change of the charged particle trajectories of the stored beam.
- Moderate magnetic field. The target requires only weak or moderate magnetic fields at the target position in order to define the direction of the polarization.
- High purity. The atomic beam contains pure hydrogen or deuterium and no other atoms like carbon or oxygen.
- Open geometry. The moderate magnetic fields can be produced by Helmholtz coils, which allow to detect the product particles of a nuclear reaction practically in any direction.
- Density and thickness of internal targets. The new generation of atomic beams will have densities in the order of  $10^{13}$  atoms  $\text{cm}^{-3}$ . Target thickness of  $\sim 10^{14}$  atoms  $\text{cm}^{-2}$  can be produced.
- Moderate cooling technique. The cooling of the atomic beams requires only conventional cooling techniques.
- Stored polarized atomic gas. If needed, the target density can be increased by accumulating the atomic gas in a target cell. Density of  $10^{16}$  atoms  $\text{cm}^{-3}$  can be obtained, ultimate density in the  $10^{17}$  atom  $\text{cm}^{-3}$  range may be possible. This technique allows the production of target thickness of  $10^{17}$  to  $10^{18}$  atoms  $\text{cm}^{-2}$ . In this case, however, the flexibility in changing the polarization is reduced by the probable necessity to use pure states only in order to avoid fast recombination.

#### REFERENCES

- 1) R. Fleischmann, 2nd Int. Symp. on Polarization Phenomena of Nucleons, Karlsruhe, P. Huber and H. Schopper, eds. (Birkhäuser Verlag Basel and Stuttgart 1966) p. 21
- 2) H.F. Glavish, Third Int. Symp. on Polarization Phenomena in Nuclear Reactions, Madison, H.H. Barschall and W. Haeberli eds. (The University of Wisconsin Press Madison 1971) p. 267
- 3) T.B. Clegg, Fourth Int. Symp. on Polarization Phenomena in Nuclear Reactions, Zürich, W. Grüebler and V. König eds. (Birkhäuser Verlag Basel and Stuttgart 1976) p. 111
- 4) H.F. Glavish, Conf. on Higher Energy Polarized Proton Beams, A.D. Krisch, A.J. Salthaise, eds. AIP Conf. No 42 (AIP New York 1976) p. 136
- 5) W. Grüebler, Proc. Fifth Int. Symp. on Polarization Phenomena in Nuclear Physics, Santa Fe, G.G. Ohlsen et al., eds. AIP Proc. No. 69 (AIP New York 1981) p. 848
- 6) W. Haeberli, Proc. Int. Symp. High Energy Physics with Polarized Beams and Polarized Targets, Lausanne, C. Joseph and J. Soffer, eds. (Birkhäuser Basel 1981) p. 199
- 7) W. Grüebler, Proc. Polarized Proton Ion Sources, Ann Arbor, A.D. Krisch and A.T.M. Lin eds., AIP Conf. Proc. No. 80 (AIP New York 1982) p. 53 and p. 69
- 8) W. Grüebler, Proc. High Intensity Polarized Proton Sources, Vancouver 1983, AIP Conf. Proc., in press
- 9) P.A. Schmelzbach et al., Contribution to this Conference
- 10) I.F. Silvera and J.T.M. Walraven, Phys. Rev. Lett. 44 (1980) 164

PLANS AND PROGRESS TOWARD AN ULTRA-COLD  
POLARIZED PROTON JET

R.S. Raymond, P.R. Cameron, D.G. Crabb  
Randall Laboratory of Physics  
The University of Michigan  
Ann Arbor, Michigan 48109

ABSTRACT

Plans for the construction of a jet of polarized protons are discussed. Electron-polarized hydrogen atoms will be stored at 0.5 K in an 8 T magnetic field and extracted to form a jet by driving hyperfine transitions with microwaves.

The principles behind the ultra-cold polarized jet have already been discussed at this meeting/1/. This paper describes equipment being designed and built by our group from The University of Michigan to test the possibility of a jet useful for high-energy physics. We are receiving considerable assistance from the atomic physics group at MIT lead by D. Kleppner and cryogenic advice from T. Niinikoski. Brookhaven National Laboratory is providing space and liquid helium and we are borrowing a pumping system from Rice University.

Our philosophy is that we want to understand in reasonable detail hydrogen transport, microwave-induced transitions, and beam formation, so we have tried to design a system for which changes are as painless as possible and instrumentation is as complete as possible. This equipment may never be used in a high-energy physics experiment, but with it we hope to learn how to build a jet that can be.

PLANS

An assembly drawing of the apparatus is shown in the figure. The upper canister holds the  $^4\text{He}$  section, still, and heat exchangers of a dilution refrigerator, surrounding the hydrogen feed tube and dissociator. The  $^4\text{He}$ -coated mixing chamber surrounds the atomic hydrogen storage volume and is inside of a superconducting solenoid. Atomic hydrogen is produced from molecules in a liquid-nitrogen temperature discharge in the dissociator. The atoms then pass quickly from liquid-nitrogen temperature to the  $^4\text{He}$ -coated walls of the still, and are further cooled in going down to the fringe field of the solenoid, where selection by electron spin occurs. Those atoms with spin antiparallel to the field are drawn into the magnet, thermalize by striking the mixing-chamber walls, and are trapped. Microwaves will shine into the storage cell from the left and flipped atoms emerging to the right will form the jet. Inside the storage cell we will have pressure transducers and a bolometer to measure stored density, temperature sensors, a resonant structure to increase microwave field strength, and perhaps a heater.

Wall temperatures around the storage volume will affect performance and the question of optimum wall temperatures is typical of the problems to be considered. The ends of the

storage volume should be very cold (0.3 K), the inlet end to encourage trapping and the outlet end for the sake of beam quality. The walls of the central region must be cold enough (0.5 K) that  $^4\text{He}$  vapor does not interfere with extraction, but recombination on the walls increases with decreasing temperature and for the densities at which we must run, wall temperatures much below 0.5 K would result in unacceptable recombination losses. Kleppner has estimated/2/ that for a wall temperature of 0.45 K and a stored atomic density of  $10^{16}/\text{cm}^3$  12% of the atoms would be lost to recombination. Despite simplifying assumptions, this calculation does indicate the regions of temperature and density in which we will operate and the sort of problems to be overcome for a successful design.

In the same spirit, calculations by Kleppner/2/ indicate that the following parameters should be reasonable for our apparatus:

Magnetic field - 6 T  
Stored atomic density -  $10^{16}/\text{cm}^3$   
Extraction pulse length -  $0.25 \mu\text{s}$   
Focussed target thickness -  $10^{14}/\text{cm}^2$   
Duty cycle - 10%

Progress

A superconducting solenoid has been built for us by American Magnetics and, at 7.6 T, the field along the axis has been measured at MIT/3/ to be uniform to better than one part in  $10^5$  over 5 cm.

A liquid-nitrogen cooled dissociator has been built and is being tested at MIT/3/.

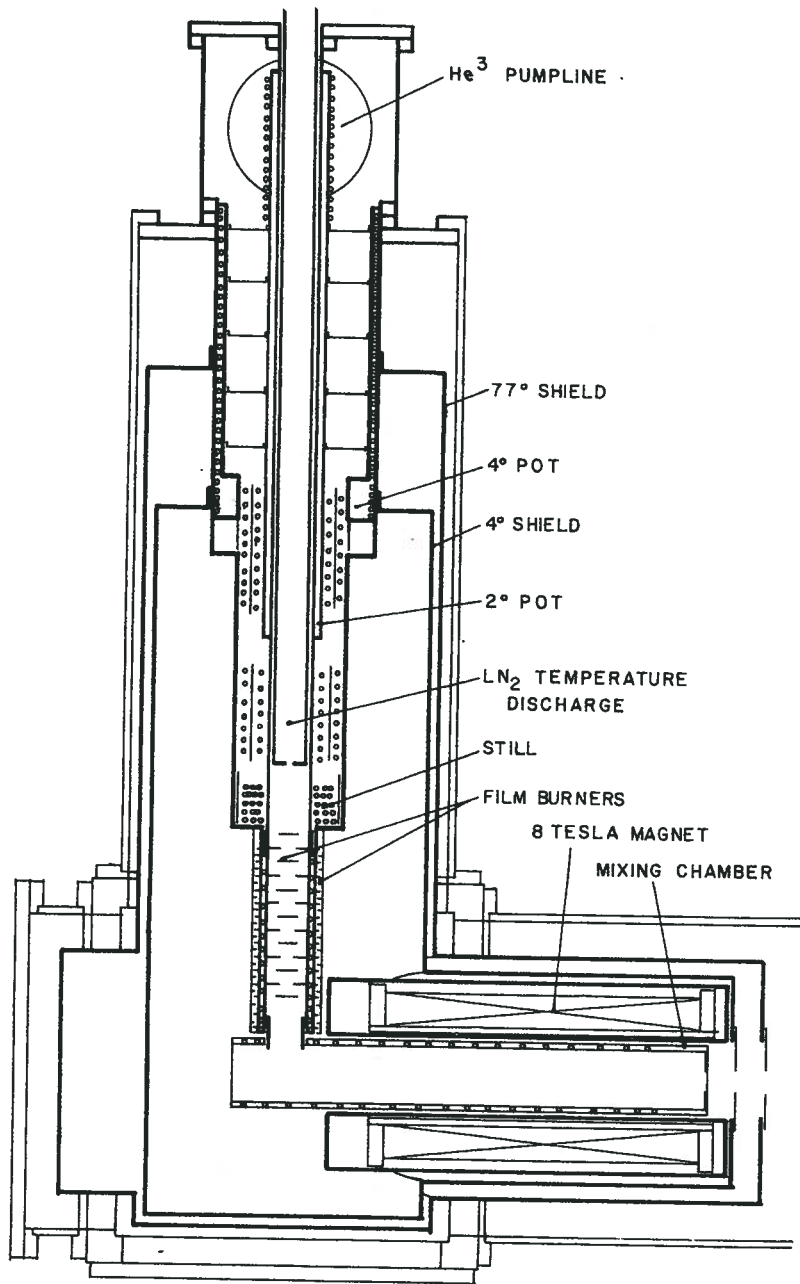
The vacuum housing has been built and is ready for leak checking. Heat shields are being fabricated and the basic design of the dilution refrigerator is complete.

A  $^3\text{He}$  pumping system consisting of sealed Roots blowers and a mechanical pump has been borrowed from Rice University.

We expect to begin assembly and testing shortly and hope in the next few months to learn more about the problems and possibilities involved in using this type of jet for high-energy physics.

REFERENCES

- /1/ - S. Pentilla et al.
- /2/ - D. Kleppner, private communication.
- /3/ - S. Buchman, H. Hess, private communication.



MICHIGAN-MIT-BROOKHAVEN  
POLARIZED COLD ATOMIC HYDROGEN JET

## AUTHOR INDEX

- |                |                       |                    |                              |
|----------------|-----------------------|--------------------|------------------------------|
| Althoff, K.H., | 13, 23, 33, 149       | Knop, G.,          | 23, 149                      |
| Ball, J.,      | 81, 112, 182          | Kohlgarth, E.,     | 13, 33                       |
| Boden, B.,     | 149                   | Krisch, A.D.,      | 174                          |
| Brown, S.,     | 66, 102               | Krumpolz, M.,      | 84, 94                       |
| Burkert, V.,   | 23, 149               | Leenen, M.,        | 23, 149                      |
| Cameron, P.R., | 7, 79, 136, 143, 202  | Lin, A.M.T.,       | 7, 143                       |
| Chaumette, P., | 81, 112, 182          | Mehnert, W.,       | 23, 149                      |
| Court, G.R.,   | 53, 60, 66, 102, 122  | Meyer, W.,         | 13, 23, 33, 53, 66, 149, 165 |
| Crabb, D.G.,   | 7, 100, 143, 202      | Movchet, J.,       | 81                           |
| Deregel, J.,   | 81, 112, 182          | Niinikoski, T.,    | 102, 183                     |
| Desportes, H., | 182                   | Penttila, S.,      | 183                          |
| Dostert, R.,   | 13, 33                | Raymond, R.S.,     | 7, 143, 202                  |
| Durand, G.,    | 81, 182               | Riechert, H.,      | 33                           |
| Fabre, J.,     | 81, 112               | Rieubland, J.M.,   | 66, 102, 183                 |
| Gamet, R.,     | 102                   | Rijllart, A.,      | 66, 102, 155, 183            |
| Grüebler, W.,  | 193                   | Van Rossum, L.,    | 182                          |
| de Haas, L.J., | 1                     | Schablitzky, H.D., | 23, 149                      |
| Harrison, P.,  | 122                   | Schilling, E.,     | 13, 23, 33, 66, 149, 165     |
| Hartfiel, U.,  | 23, 149               | Schmelzbach, P.A., | 193                          |
| Hartmann, O.,  | 102                   | Schmitz, H.H.,     | 149                          |
| Havenith, W.,  | 13, 33                | Shapiro, G.,       | 182                          |
| Heeringa, W.,  | 129                   | Singy, D.,         | 193                          |
| Hewel, T.,     | 23, 149               | Sternal, G.,       | 13, 33                       |
| Heyes, W.G.,   | 53, 60, 66, 122       | Thiel, W.,         | 13, 23, 33, 53, 149          |
| Hill, D.,      | 84, 94, 100, 163, 182 | Vaninetti, J.,     | 119, 163                     |
| Hill, J.,      | 84                    | Wenckebach, W.Th., | 1                            |
| Horikawa, N.,  | 177                   | Williams, D.,      | 66                           |
| Jarmer, J.J.,  | 119, 163              | Zhang, W.Z.,       | 193                          |
| Kaul, O.,      | 13, 33                |                    |                              |

## LIST OF PARTICIPANTS

Ball, J.	Saclay
Brown, S.	CERN
Burkert, V.	University of Bonn
Cameron, P.R.	University of Michigan
Court, G.R.	University of Liverpool
Crabb, D.G.	University of Michigan
Durand, G.	Saclay
Grüebler, W.	Eidg. Techn. Hochschule Zürich
Hartfiel, U.	University of Bonn
Healey, D.	TRIUMF
Heeringa, W.	Kernforschungszentrum Karlsruhe
Heyes, W.G.	University of Liverpool
Hewel, T.	University of Bonn
Hill, D.	Argonne National Laboratory
Horikawa, N.	Nagoya University
Jarmer, J.J.	Los Alamos National Laboratory
Kaul, O.	University of Bonn
Konter, J.	SIN
Krisch, A.D.	University of Michigan
Krumpolz, M.	University of Illinois
Mango, S.	SIN
Meyer, W.	University of Bonn
Nakanishi, T.	Nagoya University
Niinikoski, T.	CERN
Penttila, S.	University of Turku
Raymond, R.S.	University of Michigan
Rieubland, J.M.	CERN
Rijllart, A.	CERN
Schilling, E.	University of Bonn
Thiel, W.	University of Bonn
Van Rossum, L.	Saclay
Wenckebach, W.Th.	Kamerlingh Onnes Laboratory Leiden

## ACKNOWLEDGMENTS

The Editor would like to thank all involved in the effort to produce these proceedings. My first thanks go to the authors for their excellent work in preparing camera-ready copies under the pressure of the deadline.

Mrs. M. Hölzmann and Mrs. A. Machtemes deserve my thanks for typing numerous lists and manuscripts. Especially I would like to thank Mrs. A. Machtemes for her assistance during the workshop and D. Sundermann for his efforts during the visit to Bonn.

I wish to thank Dr. D. Menze for allowing me to use his drawing of the Physikalisches Institut and Dr. J. Debrus for his advice and help in organisational problems during the workshop.

Particular thanks go to Prof. K.H. Althoff and the members of the Bonn Polarized Target Group Elkelind Kohlgarth, Rainer Dostert, Ernst Schilling and Werner Thiel.

W. Meyer

## INSIDE COVERS

The inside front cover shows the building of the Elly-Hölterhoff-Böcking Stiftung built around 1900. Since 1976 this building is the residence of the Physikzentrum. The office of the Deutsche Physikalische Gesellschaft (DPG) was opened there one year later.

The inside back cover shows the Physikalisches Institut built in 1913 and inaugurated with an international congress held by the Solar Union honouring Heinrich Kayser, successor to Heinrich Hertz on the professorial chair for experimental physics at Bonn.

